QUEEN MARY UNIVERSITY OF LONDON

Quantitative Measurements of the Demineralisation Rates and Mineral Masses of Deciduous and Permanent Enamel

Author:
Linda Hassanali

Supervised by:
Professor Paul Anderson
Professor Ferranti S. Wong
Professor Richard J. M. Lynch

Thesis submitted to the University of London for the Degree of Doctor of Philosophy

10/20/2017

Dental Physical Sciences Unit, Institute of Dentistry, Barts and the London School of Medicine and Dentistry, Queen Mary University of London

I, Linda Hassanali, confirm that the research included within this thesis is my own work or that where it has been carried out in collaboration with, or supported by others, that this is duly acknowledged below and my contribution indicated. Previously published material is also acknowledged below.

I attest that I have exercised reasonable care to ensure that the work is original, and does not to the best of my knowledge break any UK law, infringe any third party's copyright or other Intellectual Property Right, or contain any confidential material.

I accept that the College has the right to use plagiarism detection software to check the electronic version of the thesis.

I confirm that this thesis has not been previously submitted for the award of a degree by this or any other university.

Signature: 
Date:19.10.2017

Details of collaboration and publications:
Collaborations:
LH is the recipient of a GSK and BBSRC grant award.
Publications:
Hassanali, L., Wong, F.S.L., Lynch, R. J. M. and Anderson, P. (2017) A novel kinetic method to measure apparent solubility product of bulk human enamel. *Front. Physiol.* 8: 714. doi: 10.3389/fphys.2017.00714.

Contents

Figure index

Table index

Acknowledgements

The completion of this work could not have been possible without the participation and assistance of my primary supervisor Professor Paul Anderson. His contribution is sincerely appreciated and gratefully acknowledged. I would also like to express my deep appreciation and indebtedness to my second supervisor Professor Ferranti Wong and industrial supervisor Professor Richard Lynch for their support and contributions.

My thanks and appreciation go to Professor Graham R. Davis and Dr David Mills for their contribution to the X-ray microtomography study.

To the members of the Dental Physical Sciences Unit, I am forever grateful for all your uplifting messages and unconditional support.

To GlaxoSmithKline and Biotechnology and Biological Sciences Research Council for providing the financial sponsorship over the last four years.

Finally, to my parents Sameera and Mazhar Hassanali and my family, for all the unconditional love and care. I dedicate this work to them.

Abstract

Human deciduous and permanent enamel samples were simultaneously exposed to 0.1 M acetic acid pH 4.0 solution with an increasing calcium and phosphate concentration. Demineralisation rates at each calcium and phosphate increment were measured by scanning microradiography (SMR) to monitor in real-time the demineralisation trend. No significant differences ($p > 0.05$) were observed between baseline demineralisation rates of each enamel type. Similarities in the demineralisation trend as a function of increasing calcium and phosphate concentration were also observed. SMR detected a halt in demineralisation rate at 30 mM and 32.5 mM calcium concentration for permanent and deciduous enamel equilibrium between the solution and enamel samples had been achieved. Comparisons of the SMR data with a speciation software program indicated the solubility product of deciduous and permanent enamel is 121 in pH 4.0 and 25 ^{o}C conditions. X-ray Microtomography (XMT) results of the mineral concentrations of each enamel type showed no significant differences ($p >0.05$) and Confocal laser scanning microscopy (CLSM) image analysis of rhodamine B dye infiltration showed no significant differences between the interprismatic regions of each enamel type ($p >0.05$), complementing the SMR data. Permanent enamel exhibited significantly larger prism head diameters near to the surface of enamel compared to near the EDJ, whereas prism head diameters in deciduous enamel remained relatively constant throughout enamel.

Thus the high caries incidence rates amongst children may be due to a lower level of protection offered by saliva and the oral environment of a child compared to an adult rather than the structure and the physical chemistry of the tissue itself.

Chapter 1 Introduction

Previous research on the demineralisation rates of deciduous enamel (DE) suggest deciduous teeth are exposed to a higher risk of caries than their permanent successors (Amaechi et al., 1999; Featherstone and Mellberg, 1981; Wang et al., 2006). Further, reports from clinics show higher caries incidence rates and hospital admissions rates amongst children than adults (LGA, 2016; PHE, 2015). In this study, microstructural features and demineralisation characteristics of human DE and permanent enamel (PE) samples were compared simultaneously using three quantitative techniques; X-ray microtomography (XMT), Confocal Laser Scanning Microscopy (CLSM) and Scanning Microradiography (SMR) in order to quantitatively measure the similarities and differences between the two enamel types and shed light on the reasons behind the differences observed in the clinic.

Previous reports comparing the microstructure and demineralisation rates of DE and PE are contradictory (Oliveira et al., 2010; Fosse, 1968). Uncertainties may be due to differences in methodologies and extrapolating data from one experiment, often based on PE, to explain the other. Such practices have led to under/overestimations in terms of each enamel types mineral composition, mineralisation level, demineralisation rates and microstructural features.

In this study, the techniques were strategically chosen to complement each other to provide a balanced overview on how the structural features within each enamel type - measured by XMT and CLSM, may affect the demineralisation characteristics - measured by SMR, and to substantiate or invalidate claims that certain microstructural features are associated with faster demineralisation rates. For

example, that faster demineralisation rates in DE are associated with wider interprismatic regions in DE and a lower mineral concentration (Shellis, 1984b).

It is important to investigate the similarities and differences between DE and PE using accurate and quantitative measuring techniques and to ensure each enamel type is exposed to the same conditions and where possible that they are measured simultaneously to ensure comparisons are fair and reliable. Information provided from highly controlled and fair investigations will not only limit confounding variables associated with separate investigations on DE and PE but can also be used to explain differences observed in the clinic and furthermore, may be used to create accurate screening techniques for anti caries agents.

1.1 Aims and Objectives

The aim of this study was to:

Compare the microstructural features within DE and PE and relate the microstructural features within both enamel types to their respective demineralisation characteristics.

The objectives of this study were to:

- Quantitatively measure and compare the mean mineral concentration within DE and PE and measure mineral gradients from the outer surface towards the EDJ, using X-ray microtomography.
- Quantitatively measure the solubility and compare the demineralisation rates within DE and PE, using scanning microradiography.
- Monitor and compare the trends in the demineralisation rates of DE and PE during demineralisation within a solution with an increasing calcium and phosphate concentration.
- Identify the solubility product of DE and PE.
- Identify, quantitatively measure and compare microstructural features within DE and PE, using confocal scanning laser microscopy.

SECTION 1: LITERATURE REVIEW

Chapter 2 : Enamel

Human dental enamel is a non-innervated, avascular, and highly mineralised outer covering of the dental crown. It acts as a barrier to protect the tooth from degradation by external sources such as food, drink and pollution (Berkovitz et al., 2011).

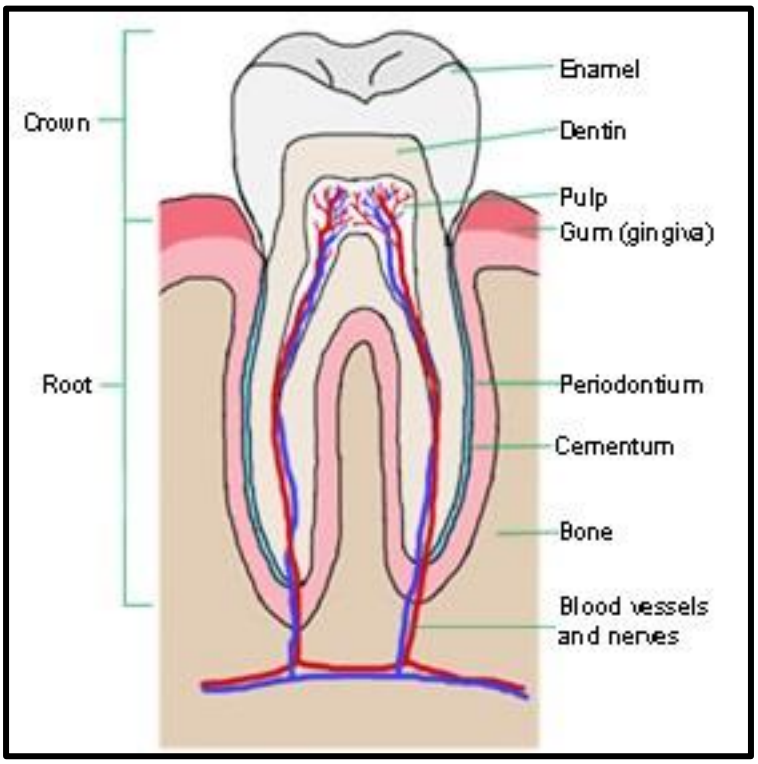

Figure 2.1 Cross sectional diagram of a human tooth showing the different layers and components. Blood vessels and nerves enter through the apex of the roots; extend along the root canals and into the pulp (image from https://www.myvmc.com/anatomy/teeth-adult-permanent-dentition/)

The inner layers of a tooth, dentine and the pulp are innervated; therefore, damage or loss of enamel can lead to sensitivity and pain from hot and cold stimuli. The pulp is also vascularised; therefore, if caries progression extends through to the

pulp, this may lead to additional health problems such as coronary heart disease (DeStefano et al., 1993).

While the pulp can be regenerated, a lack of nerve and blood supply to enamel means it cannot, however, enamel is continuously exposed to ions within saliva which remineralise enamel mineral as part of a dynamic equilibrium that exists between demineralisation and remineralisation. In addition, saliva protects enamel from demineralisation by being a source of proteins, antifungal and antibacterial agents (for a review on the role of saliva see section 3.2.8).

Enamel is composed of substituted calcium hydroxyapatite (~ 85 % in volume), water (~12% in volume) and an organic component mainly comprising of proteins (~ 12% in volume) (West and Joiner, 2014) and is heterogeneous in regard to the distribution of its components (Robinson et al., 1971; Theuns et al., 1983; Wong et al., 2004). For example, the tips of cusps appear to be more mineralised and are thicker than cervical regions that are exposed to less wear, suggesting that the distribution of components is related to tooth morphology and function (Cuy, et al., 2002, Simmons et al., 2011).

Enamel is made predominantly of hydroxyapatite crystals arranged into prisms where bundles of crystallites are arranged parallel to one another and are orientated perpendicular to the enamel dentine junction (EDJ). Interprismatic enamel crystallites are less ordered. Enamel also contains some protein remnants, constituting around 1% of the overall weight with approximately 90% being Amelogenin. This isotropic structure gives enamel the strength and fracture

toughness it requires to withstand the stresses and strains it experiences throughout its lifetime.

At an ultrastructural level, prisms approximately 4-5 microns in diameter and composed of bundles of long calcium deficient hydroxyapatite crystallites span the entire width of the enamel crown running from the enamel dentine junction to the surface; in some instances, extending over approximately 1 mm in length (West and Joiner, 2014). The crystallites are approximately 50 nm wide by 25 nm thick and are arranged primarily with their long axis parallel to the prisms. At the prism peripheries, these crystallites deviate to produce an interface between prisms creating a distinct key-hole characteristic feature of prismatic enamel. The characteristic type 2 pattern observed in scanning electron microscope (SEM) images of prismatic enamel after exposure to acid is thought to be due to a greater porosity in interprismatic regions leading to preferential demineralisation as shown in **Figure 3.7b**.

Previously published demineralisation rates of DE and the high caries incidence rates recorded suggest that demineralisation in PE is slower (LGA, 2016; Wang et al., 2006). Larger interprismatic regions in DE compared to PE are assumed to be responsible for the faster demineralisation rates observed (Shellis, 1984b). In addition, DE appears whiter, which is assumed to be due to its greater porosity (Goldberg, 2017).

However, quantitative research focused on comparing DE and PE is scarce. Additionally, research often focuses on each enamel type independently of the other, and frequently the results obtained from research on PE is extrapolated to

DE (Oliveira et al., 2010). The analysis of DE and PE in the same research is therefore an important step towards providing reliable comparisons between substrates through methodological standardisation. An understanding of the similarities and differences of each enamel type that is based on accurate and reliable data obtained from quantitative and qualitative research techniques will contribute to the development and establishment of preventative and restorative protocols within the clinic.

2.1 Calcium orthophosphates

The mineral component of bones and teeth is composed of calcium orthophosphates in the form of calcium deficient hydroxyapatite. The application of calcium orthophosphates covers a wide range of areas from healthcare to agriculture making them a topic of considerable interest to researchers. For example, they are involved in mineralisation processes; pathological calcifications; are used as biocompatible materials for bone replacement and as coatings on bone prosthetics; are a source of phosphorus in fertilisers, and are used as phosphors in fluorescent lighting (Smets, 1987).

Calcium orthophosphate versatility stems from an ability to accept a large variety of substitutional ions which alter their properties. For example, the incorporation of carbonate and magnesium into hydroxyapatite appears to increase its solubility whereas the incorporation of fluoride reduces solubility.

Biological apatites exhibit nonstoichiometry, with vacant lattice sites. This complicates their crystal chemistry.

2.2 Hydroxyapatite

Each unit cell of a hydroxyapatite crystallite consists of a central hydroxyl group surrounded by three calcium ions which are surrounded by three phosphate ions. Six calcium ions enclose the unit in a hexagonal formation.

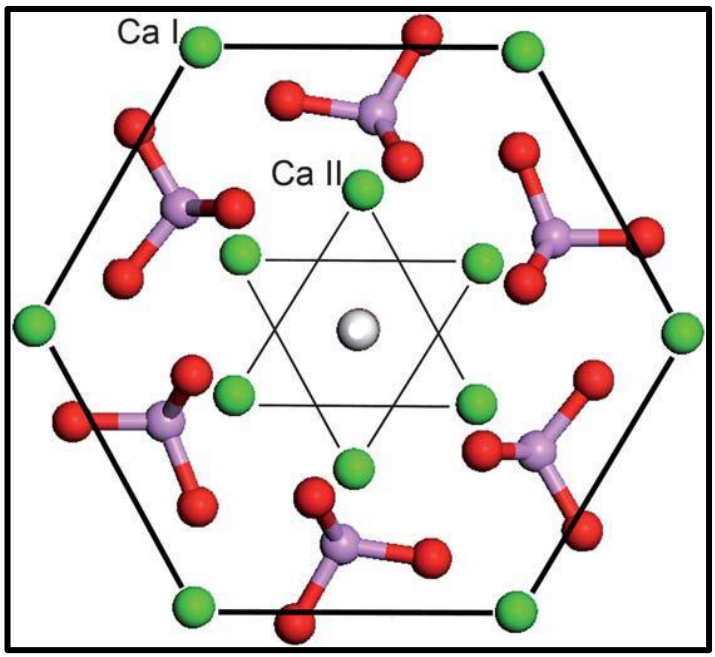

Figure 2.2 schematic diagram of the unit cell of a hydroxyapatite crystallite. (Image taken from Lu et al., 2011)

Though hydroxyapatite is a highly uniform, regular and organised crystal, biological hydroxyapatite found in bones and teeth commonly undergoes ionic substitutions. For example, carbonate may substitute phosphate or hydroxyl ions (Elliott et al., 1985 and Ferguson, 1999). This depends on local carbon dioxide concentrations and occurs during tooth development, and is attributed to the supposedly higher solubility of enamel compared to HAp (Berkovitz et al., 2011).

2.3 Dental enamel formation

The beginning stages of tooth development involves the interaction of an ectodermal tissue (the external layer of germ cells of the gastrula which develop into the epidermis) known as the enamel organ with mesenchymal tissue known as the dental papilla. Studies have shown mesenchymal tissue to be the determining feature in onset of tooth development rather than ectodermal tissue (Berkovitz et al., 2011). When dental papilla mesenchymal cells were cultured with epithelium cells from a developing foot pad, tooth development commenced whereas when enamel organ cells were cultured with developing foot pad cells results were negative (Berkovitz et al., 2011). A condensation of mesenchymal cells of neural crest origin beneath the dental epithelium of the primitive oral cavity results in thickening of the dental epithelium which then invaginates into the mesenchyme dental papilla forming two processes: the vestibular lamina forms the vestibule of the mouth, demarcating the lips and cheeks from the tooth bearing regions and the dental lamina which contributes to tooth germ development within the dental lamina.

Odontogenesis has been classified into 3 main stages according to the degree of morphodifferentiation and histodifferentiation of the epithelial components: bud, cap and bell stages.

During the bud stage, the enamel organ is composed of a simple, spherical condensation of epithelial cells that is surrounded by mesenchyme that is separated by a basement membrane. At the cap stage, a cap shaped structure is formed by invagination of the inner surface of the enamel organ. Cells within the

central portion of the enamel organ are rounded compared to peripheral cells which begin to form the external and internal enamel epithelia. By the late cap stage, external enamel epithelial cells are cuboidal and internal enamel epithelial cells become more columnar shaped. Cells within the central portion of the enamel organ become separated though they maintain contact by desmosomes and intercellular spaces are filled with significant quantities of glycosaminoglycans. The resultant tissue is known as the stellate reticulum. The section of mesenchyme lying beneath the internal enamel epithelial cells is the dental papilla, while the dental follicle forms the mesenchymal cells surrounding the tooth germ.

At the early bell stage of tooth development, further morphodifferentiation and histodifferentiation of the cells occur. The occlusal pattern of the crown of teeth is mapped out by the configuration of the internal enamel epithelium. The dental lamina breaks down and the enamel organ disconnects from the oral epithelium (Berkovitz et al., 2011).

The enamel organ is characterised by four distinct layers:

The *external enamel epithelium* forms the outer layer of cuboidal cells. Intercellular connections via desmosomes and gap junctions are present and the function of this layer is associated with maintaining the shape of the enamel organ and exchanging substances between it and the external environment. The cervical loop is associated with the growing part of the enamel organ and is located where the external and internal enamel epithelium are continuous.

The *stellate reticulum* layer is characterised by star shaped cells with many branching processes. A high concentration of glycosaminoglycans causes intercellular spaces to become fluid filled due to osmotic effects. Well-developed Golgi complexes and microvilli indicate the cells contribute to secretions of materials present within the extracellular compartments. Cells produce colony-stimulating factor, transforming growth factor beta-1 and parathyroid hormone-related protein which are thought to be associated with the recruitment and activation of osteoclasts within the dental follicle necessary to resorb the adjacent alveolar bone as the developing tooth grows and erupts (Berkovitz et al., 2011).

The *stratum intermedium* layer is similar to the stellate reticulum layer, though their intercellular spaces are smaller and the cells contain significant amounts of alkaline phosphatase. The layer is associated with protein synthesis and the transport of materials to and from the ameloblasts (enamel forming cells in the internal enamel epithelium) (Koyama et al., 2001).

The *internal enamel epithelium* layer is characterised by columnar shaped cells, though they become elongated towards regions where future tooth cusp tips will form. This layer is separated from the peripheral cells of the dental papilla by a basement membrane and cell-free zone (Matthiessen and Rømert, 1980). Down growths of the lingual aspects of the enamel organs indicate the onset of permanent teeth development.

The late bell stage is characterised by the formation of hard tissue. Enamel formation (see section *2.3.1 Amelogenesis*) proceeds dentine formation at the tips of future cusps. Bioactive signals from pre-ameloblasts (enamel forming cells) to

the adjacent mesenchyme dental papilla cells induce morphological changes in dental papilla cells to become columnar and differentiate into odontoblasts (dentine forming cells) (Choung et al., 2013). The presence of dentine then induces ameloblasts to secrete enamel.

2.3.1 Amelogenesis

Amelogenesis is the process of enamel formation. During the crown stage of development, enamel forming cells known as ameloblasts secrete a protein rich matrix during the Secretory stage which is then degraded by proteolytic enzymes and replaced by hydroxyapatite during the Maturation stage.

The internal enamel epithelial cell undergoes several morphological changes during enamel formation. The first stage, the presecretory stage, is characterised by columnar cells which have a reversal of polarity whereby the nucleus moves to the stratum intermedium end of the cell. At the opposite end of the cell, the distal end adjacent to the dental papilla, endoplasmic reticulum and Golgi apparatus organelles form associated with protein synthesis. Such changes form the pre-ameloblast cells. Small amounts of proteins are synthesised that are associated with epithelial/mesenchymal interactions involved in the inducement of mantle dentine secretion by odontoblasts. The basement membrane separating the pre-ameloblasts and dental papilla breaks down, intracellular components such as endoplasmic reticulum and vesicles containing enamel matrix materials increase and are secreted from the distal end into the extracellular space adjacent to the dentine layer. Immediately after the enamel matrix is discharged, calcium hydroxyapatite needle-like crystallites are formed.

Newly secreted immature enamel is composed of approximately 30 % proteins, 20-30 % mineral and 40-50 % water (Berkovitz et al., 2011). Amelogenins form the largest proportion of proteins and are rich in proline and glutamine (Termine et al., 1980; Fincham et al., 1999). They have an internal hydrophobic core, protein-protein domain and a hydrophilic mineral binding domain which permits self-assembly into nanospheres and adhesion onto the c-axis of crystallites. These are thought to act as spacers between growing hydroxyapatite crystallites, determining the dimensions of each crystallite by prohibiting width way growth. As enamel matures, amelogenins are degraded by proteolytic enzymes, matrix metalloproteinase 20 (MMP20), and kallikrein-4 (KLK4) (Bartlett, 2013). In a study on MMP20 and KLK4 proteolysis of amelogenin, researchers observed preferential and selective degradation of amelogenin when adsorbed to HAp than when in solution (Zhu et al., 2014). From the results, Zhu et al. (2014) proposed a new model to describe crystal growth during maturation stage. The model suggests that amelogenin proteins experience morphological changes upon adsorption to HAp crystallites. These changes induce proteolytic degradation by MMP20 and KLK4, which leaves space for the crystallites to grow in both length and width until the crystal surfaces make contact with surrounding amelogenin proteins within the enamel matrix.

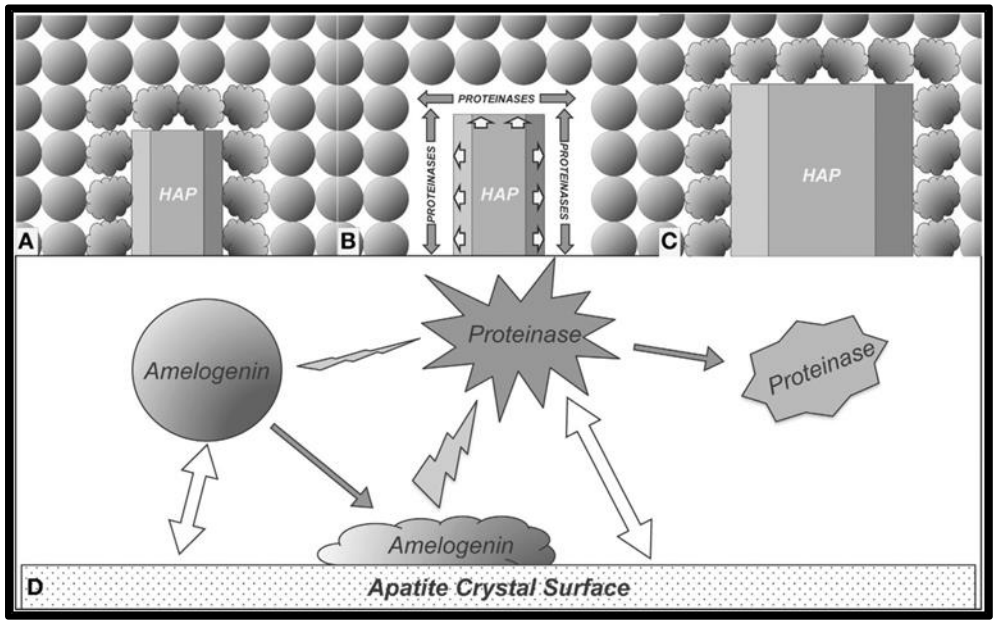

Figure 2.3 Proposed model for enamel crystal growth guided by crystal-amelogenin-proteinase interactions. A) Amelogenin adsorption onto HAp induces morphological changes in the protein. B) Morphological changes induce preferential protein degradation by proteinases. C) HAp grows until crystal contacts surrounding amelogenin molecules within enamel matrix. D) Summary of the proposed model for amelogenin preferential degradation. (Image taken from Zhu et al., 2014)

The importance of amelogenin role in controlling HAp crystallite growth and orientation was further supported during a study where amelogenin-null mice exhibited much thinner enamel layers than mice with normal amelogenin (Gibson et al., 2001).

A study by Fukae et al. (2002) concluded that secretion of EMSP-1 (now known as KLK4) by odontoblasts into enamel at the EDJ facilitates the hardening of enamel and contributed significantly to the functional properties of the EDJ.

Approximately 10 % of the enamel matrix proteins are non-amelogenins. These include the largest protein enamelin. Enamelin is an acidic glycoprotein with a high affinity for binding to HAp and may be associated with nucleation of enamel crystals. Enamelin mutations in humans causes Amelogenesis Imperfecta (Pavlic et al., 2007; Brookes et al., 2011) as in enamelin-knock-out mice (Hu et al., 2008; Smith et al., 2009).

Ameloblastin is expressed by inner enamel epithelial cells and in ameloblasts. Ameloblastin proteins lacking the C-terminus localise at prism boundaries suggesting a role in mineralisation (Smith et al., 2009).

As the ameloblasts migrate outwards, small processes of the odontoblasts may get trapped between them, forming entrapped enamel spindles once mineralisation of the enamel matrix occurs.

At this stage, the distal ends of ameloblasts are flat. Consequently, the first few microns of enamel deposited form crystallites that do not show any sudden changes in orientation i.e. aprismatic enamel.

As ameloblasts move away from the enamel-dentine junction, the distal ends become cone-shaped forming Tomes processes. As crystallites are aligned at right-angles to the ameloblast distal surface, Tomes processes cause a change in the orientation of forming crystallites, forming prismatic enamel, whereby the crystallites at the boundaries of each prism have a sudden change in orientation to form interprismatic enamel. This region of enamel is assumed to be more porous

and most susceptible to demineralisation. Together, the features form a key-hole-like appearance of prismatic enamel.

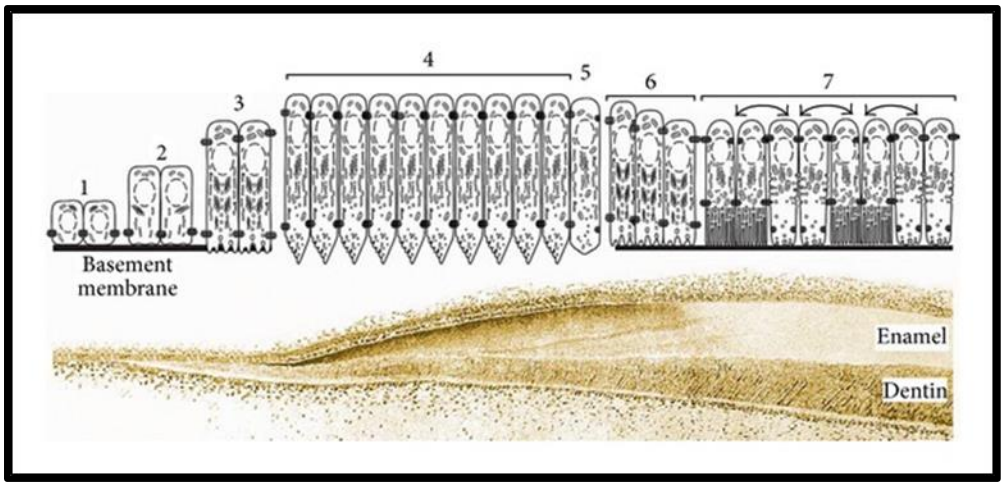

Figure 2.4 Schematic representation of the morphological changes of ameloblasts during the different stages of amelogenesis

The outer region of enamel is characterised by another layer of aprismatic enamel. As at the start of enamel formation at the EDJ, ameloblasts resume a flat shape at the distal secretory ends.

Incremental markings outline periodic changes of crystallites, enamel matrix or enamel prisms. For example, daily cross-striations can be observed approximately 4 µm apart across each prism while enamel striae of Retzius run obliquely to the surface and are produced every 6-10 days outlining the mineralisation front. These striae end as perikymata on the surface of the tooth (Berkovitz et al., 2011).

When enamel has reached its full thickness, ameloblasts morphologically change from secretory cells to maturation cells in the transition stage. Cells become shorter, the number of cells is reduced by as much as 50 % by apoptosis and those

that remain undergo auto-phagocytosis whereby cellular organelles associated with protein synthesis are reduced.

Newly formed enamel consists of approximately 65 % water, 20 % organic material and 15 % calcium hydroxyapatite crystallites by weight (Berkovitz et al., 2011). During maturation stage, hydroxyapatite crystallites increase in width and thickness from 1.5 nm to 25 nm in thickness by overtaking space filled with water and organic matrix as a result of hypermineralisation, dehydration and deproteination.

During maturation stage, ameloblasts undergo alternating morphological changes between smooth and ruffled distal ends termed modulation. These changes may reflect alternating functions of the ameloblast cell from one that is resorptive to another that is secretory. During resorption, ameloblasts remove water and organic matrix to make space for the addition of calcium and phosphate required for mineral growth.

Nucleation of enamel mineral is achieved by epitactic nucleation. This is defined as the growth of one crystalline substance on a different solid surface that has similar lattice spacing, i.e. the organic matrix.

2.3.2 Transport of calcium to the enamel compartment

The size, morphology and integrity of the crystallites formed are determined by the degree of supersaturation of calcium and phosphate in the organic matrix within the growing enamel compartment. Calcium reaches the organic matrix through the enamel organ by intercellular and transcellular pathways, however, exact mechanisms are unclear. Previous studies suggest the enamel epithelia

(ameloblasts) function as barriers to calcium influx to the enamel compartment, indicating calcium transport is highly regulated. For example, ^{45}Ca uptake into developing enamel was substantially lower in the presence of enamel epithelium than in its absence (Bawden et al., 1982; Vicars et al., 1983).

Both intercellular and transcellular calcium transport routes have been indicated from the results of previous studies using ^{45}Ca, though the proportion of each remains unquantified. Evidence suggests intercellular transport of calcium is dependent on the ultrastructure of the junctional complexes at the polar ends of adjacent ameloblasts. These junctional complexes can either be incomplete (leaky) or complete (tight) and calcium transport through them is dependent on the type of complex that is present. Further, the type of junctional complex exhibited may be associated with ameloblast modulation during the maturation stage, with ruffled-end morphology exhibiting tight junctions and therefore restricting calcium transport to transcellular routes and smooth-ended ameloblasts exhibiting incomplete (leaky) junctions and therefore permitting intercellular transport of calcium. However, studies have shown calcium uptake into enamel via intercellular routes occurs in short-time studies (<15 sec after administration) yet is absent in long-time studies (>15 sec after administration) (Hubbard, 2000) indicating that transport is predominantly via the transcellular route and that the type of transport may be kinetically driven. Calcium incorporation into the enamel compartment is minimal when ameloblasts adopt the smooth-ended morphology, indicating that this morphology is incompetent at calcium secretion via a transcellular route,

limiting calcium incorporation into enamel via the leaky junctional complexes (Takano et al., 1982; Takano, 1994).

Further quantitative investigations on the morphological changes ameloblasts undergo during modulation are required to understand their significance in calcium regulation. It may be that the ameloblast modifications are triggered by physiological changes in the confined enamel matrix caused by the infiltration of components from the surrounding interstitial fluid. However, more research is required to substantiate such claims.

Furthermore, ultracentrifugation and microanalysis of immature pig enamel at secretory stage showed higher concentrations of phosphate and lower concentrations of calcium (six- and 10-fold lower for total and free calcium, respectively), magnesium and sodium than in serum, indicating that the enamel compartment was isolated from interstitial fluids. Authors used this as evidence of a transcellular calcium transport mechanism whereby the ameloblasts act as barriers (Aoba and Moreno, 1987).

However, the proportion of intercellular and transcellular routes remains unquantified. Further, caution should be exercised when using the results of calcium tracer studies to make conclusions on calcium transport systems in biological systems as they may lead to over or underestimations.

Calcium regulation is imperative to healthy enamel formation. Further investigations on the functional roles of calcium-binding proteins, plasma membrane Ca-ATPase and calcium store proteins are required to develop our

understanding of the calcium transport mechanisms during amelogenesis. Calcium dyshomeostasis also requires further investigation to understand how ameloblasts manage the heavy calcium burden and to establish whether the large cell deaths during transition and maturation stages are associated with the burden of high calcium concentrations.

Chapter 3 : Enamel demineralisation

3.1 Dissolution mechanisms

Enamel mineral is a calcium deficient form of hydroxyapatite (see section 2.2). In acidic solutions where pH is below a critical value (see section 3.2.1) and the concentration of calcium falls below saturation with respect to enamel; hydrogen ions will dissolve the crystal lattice by reacting with phosphate and hydroxide from within enamel mineral to form HPO_4^{2-} and water, respectively. Consequently, the crystal lattice is disrupted and further ions diffuse out (see section 3.1.3).

Enamel dissolution is a multifaceted process that is influenced by external oral conditions such as pH and temperature as well as genetic factors such as chemical and structural properties of enamel and saliva composition. In addition, proteins also play a major role in the dissolution mechanism of enamel in vivo. For example, statherin binds to hydroxyapatite on the tooth surface and chelates calcium reducing the demineralisation rate by maintaining a supersaturated environment with respect to calcium close to the enamel surface. Statherin also acts as a calcium reservoir that releases calcium during times of undersaturation where enamel is at greater risk of dissolution (Johnsson et al., 1993).

At the nano-crystallite scale, enamel demineralisation produces a series of dissolution pits, which coalesce and spread into larger pits; the initiation of which is thought to commence at areas that are less mineralised, containing impurities such as carbonate which has been observed to increase the demineralisation rate, and contain dislocations (Elliott, 2003).

A characteristic feature of crystals from early carious lesions is the preferential dissolution of a strained central core. It is thought the core, that is parallel with the *c*-axis of the crystal, contains dislocations (Elliot, 2003). The same feature has been observed in carbonated apatite crystals with a carbonate content of more than 1000 ppm. However, carbonated apatite crystals with less carbonate had much lower dissolution rates in the same acids (Arends et al., 1981) indicating that increased carbonate content increases enamel demineralisation rates. However, Wang et al. (2006) observed that demineralisation rates were faster when the direction of acid attack was perpendicular to the core compared to parallel.

Another phenomenon observed at the nano-crystallite scale is the suppression of demineralisation at nano-crystals ≤30nm (Gao et al., 2003; Wang et al., 2006). These nano-crystals exhibited self-preservation regardless of any crystal defects and despite a sustained undersaturation. According to thermodynamic and kinetic rate law principles of mineral dissolution (see Sections *3.1.1 Thermodynamic principle of dissolution* and *3.1.2 Kinetic processes of dissolution*); minerals should maintain a constant dissolution rate when exposed to constant undersaturated conditions, however, the constant composition method used by Wang et al. (2006) indicate that the mechanism of enamel dissolution is far more complex.

Dissolution of enamel is a complex phenomenon that depends upon thermodynamic and kinetic processes. While thermodynamics tells us if a reaction can proceed, kinetics is involved in the step by step mechanism of the reaction and the rate at which it occurs.

3.1.1 Thermodynamic principle of dissolution

Thermodynamics is based on the concept of free energy and tells us if a reaction can occur. It is applicable in metastable and stable equilibrium systems that require a sufficient driving force to favour the transformation of reactants into products (Carrington, 2003).

During material transformations, atomic rearrangements take place. Bonds are broken, new ones are formed and the surrounding atoms are displaced resulting in a momentary increase in local energy characterised by an intermediate (non-equilibrium) state. This state is also known as the transition or activated state. Gibbs free energy (G) is the name given to the free energy in between the two states (Carrington, 2003).

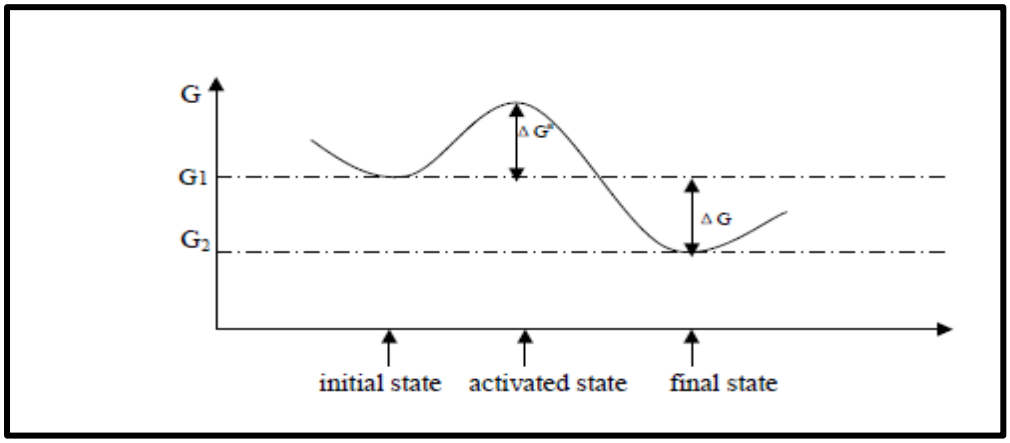

Figure 3.1 The Gibbs free energy diagram showing the free energy minima and maximum (activation state) of a transformation reaction. (Acknowledgement http://www.eng.utah.edu /~lzang/images/lecture-1.pdf)

Figure 3.1 demonstrates that for a reaction to occur the change in Gibbs energy (ΔG) needs to be below zero i.e. G2 – G1 whereby the products are at a lower energy state than the reactants. Also, the increase in energy required to reach the

activated state (ΔG^a) should be small, and the rate should be proportional to the probability to reach activated state.

For $\Delta G < 0$, the products must be at a lower free energy and therefore more stable than the reactants. Free energy refers to the average thermal motion energies of the atoms in the system and is dependent on temperature. The thermal motion of any particular atom varies with time and will occasionally reach the level needed to reach the activated state. If the energy barrier to reach activation state is not reached, the breaking and reforming of bonds results in the formation of metastable phases that will only turn into the most stable state according to the conditions once the barrier is overcome.

Solubility is the propensity for a solute to dissolve in a solvent and arrive at an end point where the potential energy of the system is at its lowest. The solubility of a material is determined by the systems enthalpy (H) defined as the amount of heat energy in the system; entropy (S) defined as the amount of disorder; and temperature (T). For a reaction to be thermodynamically favourable and therefore spontaneous, the change in enthalpy should be negative ($\Delta H < 0$) and the change in entropy should be positive ($\Delta S > 0$).

The entropy of a perfectly crystalline solid at a temperature of absolute zero is zero and is the most stable state it can exist in. When ΔS is negative, and therefore thermodynamically unfavourable, temperature will be the determining factor as to whether the reaction will proceed, as long as the systems ΔH is *sufficiently* lower than the ΔS, so that the total sum of ΔG is negative;

$$-\Delta H \quad - \quad (-\Delta S)T = \ -\Delta G \qquad (1)$$

Where:

ΔH is the change in enthalpy of the system,

ΔS is the change in entropy of the system,

T is the temperature of the system and

ΔG is the change in Gibbs free energy of the system.

As shown in equation 1, depending on the -ΔS value an adequately low temperature will be required for ΔG to be negative and for the overall reaction to be thermodynamically favourable as a relatively higher temperature would result in ΔG being positive therefore making the system thermodynamically unfavourable.

In an excess solid solution system whereby a solid is dissolving in a solvent at a given temperature and pressure equilibrium between the solid and solvent will be achieved. At thermodynamic equilibrium, the total free energy change within a system is equal to zero (Zemanski and Dittman, 1997). In a system where an excess of solid is dissolving in a solvent, this point is known as saturation.

The ΔG in the system goes from:

$\Delta G < 0$

to;

$\Delta G = 0$

Since solubility is assumed to be dependent on temperature, it is important to maintain a constant temperature when conducting solubility experiments that aim to achieve thermodynamic equilibrium i.e. saturation. An endothermic enthalpy of solution implies that with increasing temperature, solubility will increase. Conversely, an exothermic enthalpy of solution implies the opposite. McDowel et al. (1977) investigated the effect of temperature on the solubility of HAp and found a negative temperature coefficient indicating that the solubility product of HAp decreased with increasing temperature. This is an important consideration to make when comparing solubility values of different studies and furthermore suggests the need for standardisation amongst studies measuring solubility.

3.1.2 Kinetic processes of dissolution

Kinetics determines the rate of a reaction or process and is applicable to systems transitioning from non-equilibrium to equilibrium phases or between two equilibrium states. It is involved in the breaking and reformation of bonds and the rearrangement of atoms during the reaction process. Kinetics focuses on the means to overcome energy barriers to finish the transformation reaction from reactants to products at a rate that is proportional to the probability to reach activated state.

Therefore, kinetics can be used to determine the rates of chemical reactions including phase transformation reactions; whereby the atomic arrangement changes but the composition does not.

According to the principles of rate law, the rate order tells us how the concentration of the reactants affects the rate of reaction when temperature remains constant, so that for the reaction:

$$Ca_{10}(PO_4)_6(OH)_2 \rightleftharpoons 10Ca^{2+}\ 6PO_4^{3-} + 2OH^- \quad (2)$$

The rate law is expressed as:

$$R = k[Ca_{10}(PO_4)_6\ (OH)_2\ ]^m \quad (3)$$

Where;

R = rate of reaction

[] = concentration

k = rate constant

^{m}= the rate order, i.e. zeroth, first or second order.

The order of the reaction is the sum of the exponents. For example, when the rate law is as follows:

$$R = k[A][B]^2 \quad (4)$$

Where;

A is a first order and *B* is a second order reaction.

That is, the rate is proportional to the concentration of *A* and the rate is proportional to the concentration of *B* raised by the power of 2.

The order of the reaction i.e. the sum of the exponents will therefore be:

1 + 2 = 3 (5)

To solve the units for *k*:

$$\frac{M}{s} = k(M)^1\,(M)^2 \qquad (6)$$

Therefore;

$$k = M^2 \cdot s \qquad (7)$$

The rate order can only be determined experimentally by finding out how each reactant concentration affects the rate of reaction, respectively.

Dissolution is a kinetically driven process related to the rate at which the end point; that is the most thermodynamically stable end product under the conditions, is reached (Smith, 2015). With regards to the dynamic equilibrium between enamel mineral dissolution and precipitation, this process involves the formation of metastable phases that have higher free energies than the more thermodynamically stable phase hydroxyapatite.

Solubility experiments aim to measure the solubility of solids by dissolving them until saturation is reached and equilibrium is achieved. True thermodynamic solubility values are not associated with any metastable phases that are formed in solution during dissolution, before thermodynamic equilibrium has been reached. Metastable phases that are formed have higher free energies and will undergo a phase transformation into the more stable phase if the activation energy barrier is overcome. However, when the energy barrier is not overcome, any solubility values obtained will be associated with metastable substances and so are kinetic solubility

values and not true thermodynamic solubility values. Caution must therefore be exercised when using solubility experiments to identify the thermodynamic solubility value of a material.

One way to ensure that true thermodynamic equilibrium has been reached is by using analytical techniques such as X-ray diffraction (XRD) to identify if the precipitated product is the same as the initial solid. Another way would be to ensure that the conditions are favourable towards the precipitation of the original solid, for example, by ensuring the calcium and phosphate ratio is maintained at the same stoichiometry as the original solid.

The degree of saturation (DoS) is a scale of 0-1 that represents the amount of ions in solution up to the point of saturation - represented as 1 on the scale. The dissolution rate of enamel can be expressed as a function of the degree of saturation with respect to enamel:

$$R = kA(C_{eq} - C_b)^n \quad (8)$$

Where;

R = rate (g cm^{-2} hr^{-1})

k = rate constant

A = specified surface area

C_{eq} = equilibrium concentration (g cm^{-2})

C_b = concentration (g cm^{-2})

n = variable

From equation 8 (Berner, 1978), it is assumed that the addition and/or presence of ionisable solutes will influence the rate. It is therefore important to ensure ionic concentrations are accounted for and controlled when conducting solubility investigations. Previous studies have highlighted that caution is required to ensure that the monitoring device used to measure dissolution rates is sensitive enough to identify the point at which equilibrium is reached, and must not mistake extremely low rates that are undetectable for the condition of equilibrium (Zhang, et al., 2000).

3.1.3 Dissolution models

Many dissolution models have been formulated based on experimental observations and computer simulations in an attempt to summarise the processes and mechanisms involved in mineral dissolution. However, dissolution models are based on conclusions and assumptions that are formulated from the results of experimental investigations. Therefore, such models are limited to the parameters of each experiment. Also, since dissolution is a complex and multifaceted process; individual models generally only focus on the aspects of dissolution phenomena that the investigative techniques available to them allow. It would therefore be more insightful and informative to study all dissolution models available to gain a more complete and general overview of the enamel dissolution process from all aspects.

3.1.3.1 Diffusion controlled model

This model focuses on the aspect of dissolution involved with the transport of ions to and from the surface and suggests dissolution rate is determined by a driving

force that transports ions across a concentration gradient located at the interface between the surface and undersaturated solution. The interface, known as the Nernst layer, adjacent to the bulk solid is said to be saturated with respect to the bulk solid unlike the kinetic (surface controlled) mechanism which determines the interface to be undersaturated.

3.1.3.2 Kinetic (surface controlled) model

The interface between the bulk solid and undersaturated solution is undersaturated with respect to the bulk solid. The driving force produced as a consequence of ionic chemical potentials across the interface between apatite crystal surfaces and the bulk solution determines demineralisation rate (Dorozhkin, 2012).

3.1.3.3 Mono- and polynuclear models

In the mononuclear model, surface dissolution is described as the detachment of one crystal unit from one centre which then leads to step disintegration of further units. The polynuclear model describes enamel dissolution as a reaction that takes place over multiple centres simultaneously resulting in single crystal steps forming across the surface that then coalesce. This latter model can also take place in multiple steps whereby multiple centres across the surface simultaneously dissolve but in this case result in the dissolution of crystal units within units. Measurements of the radii of structural defects, such as dislocations and inclusions, where the detachment of crystal units are thought to originate from are recorded as being in the range 18-43 Å (Arends and Jongebloed. 1977). Alternatively, crystal unit detachment occurs along the course of a spiral that originates from dislocations with a radius of 8.3-20 Å (Arends and Jongebloed. 1977).

The lateral growth rate of nuclei is assumed to be proportional to the total calcium concentration within a saturated solution and the concentration of calcium ions in a solution. The rate constant is assumed to be related to the frequency of calcium ions entering a kink, and becoming partly dehydrated (Christoffersen et al., 1998). Two studies using atomic force microscopy revealed that the rate determining step was not diffusion controlled but two-dimensional surface nucleation (Onuma et al., 1966; Onuma et al., 1995).

In experiments focused on the growth of crystals; hydroxyapatite seeds were added to a supersaturated solution and changes in ionic concentrations and pH were observed and measured as a function of time. The rate of crystal growth and composition of growing calcium phosphate crystals were determined. The driving force for growth rate was concluded to be related to the degree of supersaturation and growth rate was dependent on the square of the degree of supersaturation, indicating a spiral growth mechanism (Moreno et al., 1977; Moreno et al., 1981; Elliot, 2003). However, such experiments relied on the analysis of small quantities of precipitate grown. Furthermore, the changes that occur within solution, such as the formation of metastable and precursory phases during precipitation, would likely result in any composition analysis being subject to error (Elliot, 2003). Driving forces also change in response to changes within reaction media during growth or dissolution. The constant composition technique overcomes such problems by ensuring the concentration of lattice ions are kept constant by the mechanical addition of Ca^{2+}, phosphate, and OH^- ions triggered by detected changes in ion concentrations within solution from the initial values, by ion

electrodes. The rate of crystal growth can be easily measured from the rate at which the increments are added.

These observations provide a valuable support to the polynuclear model. Furthermore, the polynuclear model was found to be the preferred model dissolution kinetics of fluorapatite followed between the pH range 5.0-7.2, while that of crystal growth followed the polynuclear model within the pH range 5.5-6.5, and the combined mono and polynuclear model at pH 5.0 (Christoffersen et al., 1996; Dorozhkin, 2012). However, publications on the validity of this model at lower pH values are needed to understand dissolution at lower pH values observed in the oral environment after an acidic challenge.

3.1.3.4 Self-inhibition model

A calcium rich layer forms on the surface of apatite during dissolution at pH range 3.7-6.9 using the constant composition technique. Calcium release was observed to be lower than H^+ consumption during the initial stages of dissolution. As dissolution progresses, calcium release increased while H^+ consumption decreased. The overall rate of dissolution decreased as the experiment progressed further until the equivalence level, two H^+ to one calcium ion, was reached (Thomann et al., 1990; Mafe et al., 1992; Schaad et al., 1997).

According to this model, during the initial stages of dissolution, some of the calcium released is adsorbed back onto the surface of apatite resulting in a semi-permeable ionic membrane made up of positively charged calcium ions (Thomann et al., 1993). A Nernst layer is assumed to be adjacent to the calcium rich layer, with both layers affecting the dissolution rate. However, no analysis of the surface composition was

conducted apart from following calcium concentration and pH; therefore counter anions (A^{n-}) supplied by the acid were not accounted for. When anions are not accounted for, the surface layer appears to be calcium rich with respect to the bulk solid, i.e. Ca/P >1.67. However, when counter anions are considered, the ratio becomes Ca/P + A = ~1.67 (Dorozhkin, 2012).

In the absence of countering anions, a double charged layer can form consisting of calcium ions adsorbed onto the surface resulting in a positive charge. A positive charge on the surface of dissolving apatite has been observed in numerous studies; however, it has previously been explained as being due to proton adsorption (Somasundaran, 1968) or a combination of calcium ion and proton adsorption (Bell et al., 1972). However, the self-inhibition model authors did not conduct chemical/composition analysis of the dissolving apatite surface and so their assumption that the positive layer formed is composed of calcium alone is therefore speculative.

3.1.3.5 Congruent/Incongruent dissolution

Congruent dissolution is based on the principle that ions in a solid dissolve simultaneously and the dissolution rate is proportional to their relative molar concentrations. Incongruent dissolution however, states that ions of a solid dissolve non-simultaneously and that dissolution rates vary for each ion; for example, with calcium dissolving faster than orthophosphate (Smith et al., 1974; Brown et al., 1999). Incongruent dissolution is made apparent when the surface layer composition is different to that of the bulk solid or when the relative ionic concentrations in solution vary from the stoichiometry of the solid. However, to

avoid any misleading assumptions; chemical analysis of post demineralisation solutions should be conducted to ensure precipitates have not formed as precipitates that are unaccounted for can lead to lower concentrations of ions being measured in solution. For example, when fluorapatite was dissolved, calcium and fluoride concentrations within the solution were lower than the stoichiometric values with respect to orthophosphate ions indicating incongruent dissolution. However, the lower values were associated with calcium fluoride precipitation (Mistra, 1999).

Studies showing the effect of pH on dissolution mechanisms have shown that in high Ca/P ratio apatites incongruent dissolution is adopted within pH 4.5 < 8.2 conditions. This was explained in terms of re-adsorption of orthophosphate ions on positively charged Ca-deficient hydroxyapatite surfaces. However, quantitative interpretation of adsorption and desorption of ions in high pH conditions such as 8.2 is difficult, especially with regards to calcium ions. In contrast, congruent dissolution of Ca-deficient hydroxyapatite was observed in solutions pH < 4.5.

Transitions between congruent/incongruent dissolution have also been observed in fluorapatite dissolution, where incongruent dissolution transforms into congruent dissolution as the reaction proceeds (Zhu et al., 2009). The initial tendency towards incongruent dissolution was explained as being due to the exchange of mineral bound calcium for H^+ ions in solution (Guidry et al., 2003). Furthermore, the affinity of particular ions for apatites that are present in solution but are not part of the original apatite composition; for example, Na^{2+}, SO_4^{2-} and Cl^-, have been documented and may influence tendencies towards incongruent dissolution under

certain conditions. However, solutions with the same Ca/P ratio as the dissolving solid have been found to follow a congruent dissolution mechanism (Brown et al., 1999).

A drawback associated with the interpretation of data obtained from experiments on the dissolution mechanisms of synthetically prepared fluorapatite and hydroxyapatite, is that the surfaces of such apatites may differ in terms of structural and chemical compositions. Both types of synthetically made apatites have been found to be calcium deficient and non-stoichiometric especially on their surfaces (Bengtsson et al., 2009, Dorozhkin, 2012) resulting in an initial phase of incongruent dissolution which later transforms into congruency.

3.1.3.6 Chemical Model

This model describes dissolution of hydroxyapatite/fluorapatite as a series of chemical reactions consisting of sub unit rather than whole unit detachment that consist of the full 18 ions that makes up a unit cell within the crystal lattice (Dorozhkin, 1997a). This was based on the concept that the complex interconnectivity between unit cells such as the sharing of ions within the crystal lattice structure would likely result in a succession of chemical reactions (see equations 9-12) replacing the pre-existing and commonly used net-reaction (see equation 13).

$$Ca_5(PO_4)_3(F,OH) + H_2O + H^+ \rightarrow Ca_5(PO_4)_3(H_2O)^+ + HF,H_2O \quad (9)$$

$$2Ca_5(PO_4)_3(H_2O)^+ \rightarrow 3Ca_3(PO_4)_2 + Ca^{2+} + 2H_2O \quad (10)$$

$$Ca_3(PO_4)_2 + 2H^+ \rightarrow Ca^{2+} + 2CaHPO_4 \quad (11)$$

$$CaHPO_4 + H^+ \rightarrow Ca^{2+} + H_2PO_4^- \quad (12)$$

Therefore, by default this model assumes that incongruent dissolution is the most likely mechanism of apatite dissolution. However, a limitation of this study was that the formations of the substances described in the equations were not verified by experimental techniques; therefore the model is hypothetical only.

3.1.3.7 Dislocations and Inclusions

Dissolution is thought to commence at sites on the crystal surface that contain dislocations and/or inclusions. The strain energy they cause in crystals give rise to a series of dissolution steps as described in Section *Chapter 328963.1.3.3 Mono- and polynuclear models*. Nucleation of etch pits that form at dislocation outlets continually grow, spreading and coalescing on the crystal surface. The dimensions of etch pits depend on dissolution kinetics and dissolution time, but are generally between 0.1-10 µm in size (Dorozhkin, 2012). Crystals must be sufficiently big to accommodate etch pits; as mentioned above, Gao et al. (2003) observed dissolution is supressed in crystals less than 30 nm. Furthermore, in sufficiently low solutions of undersaturation, the energy barrier increases above that which is achievable for a vacancy to occur on the surface in a time scale that is competitive with other processes. Therefore, the dissolution of apatites is only spontaneous if a critical etch pit size that is associated with a free energy change that surpasses the energy

barrier is achievable. Any size below the critical etch pit size will not produce a sufficient drop in free energy for the process to be spontaneous.

The size, in terms of the height of a step formed on the crystal surface during dissolution has been observed to be similar to the distance between crystal planes. For example, the distance between two (100) surfaces of hydroxyapatite crystal is 0.82nm and the height of a step has been measured to be 0.84nm +/- 0.1nm (Kwon et al., 2009). Also, like the shape of hydroxyapatite and fluorapatite, etch pits are hexagonal.

In conclusion, the nucleation and spreading of etch pits is subject to the conditions being thermodynamically favourable; which ultimately depends on factors such as solution undersaturation and crystal size.

As can be seen from the models described above, enamel dissolution models attempt to break down some of the mechanisms involved during the dissolution process. However, with enamel dissolution being a multifactorial process; it is impossible to provide a general model that incorporates all factors in their entirety and therefore models will always be limited. As stated above, any assumptions made by models are purely based on the findings and observations of the experimental methodology chosen and so are thereby limited by the chosen experimental conditions and type of techniques used to monitor changes during dissolution. At best, dissolution models can be used to explain certain aspects of dissolution phenomena and can be used in conjunction with one another in order to explain the dissolution process in a more encompassing way.

3.1.4 Solubility product of enamel

Caries incidence rates have become a cause for concern within the UK according to the 2016 LGA report (LGA, 2016; Brunton, 2014). Tooth decay is a multifactorial process which is influenced by genetic and environmental factors (Keyes, 1962; Borutta et al., 2010). Such factors include those associated with the host tissue such as the structure and composition of enamel, the pellicle and saliva as well as environmental factors such as diet and socioeconomic status (Hobdell et al., 2003). The kinetics of mineral loss and precipitation is influenced by many factors, including its physical and chemical structure, and the composition and pH, and, also the chemical equilibria between enamel and solution (Dorozhkin, 2012) i.e. the solubility product constant (Ksp).

Thus, the dissolution of bulk enamel is significantly influenced by its Ksp which can be defined as the mathematical product of its dissolved ion concentrations raised to the power of their stoichiometric coefficients. Enamel is a defective calcium deficient form of HAp (Elliott et al., 1994). The Ksp of HAp (Ksp_{HAp}) is defined, from the stoichiometry:

The Ksp of HAp is calculated using the formula:

$$Ca_{10}(PO_4)_6(OH)_2 \rightleftharpoons 10Ca^{2+}6PO_4^{3-} + 2OH^- \quad (13)$$

$$Ksp = \{Ca^{2+}\}^{10}\{PO_4^{3-}\}^6\{OH^-\}^2 \quad (14)$$

where {} denotes ionic activities at equilibrium raised by the power according to the stoichiometry.

Conventional methods of solubility product measurements use chemical equilibrium conditions, and the concentration of solute in the solution at saturation is determined by an analytical procedure. Since solubility is also dependent on temperature, it is important to maintain a constant temperature. However, unlike rate law which must be determined experimentally as discussed in Section *3.1.2 Kinetic processes of dissolution*, the solubility product constant is a mathematical function of the balanced chemical equation and does not depend on experimentation. Though the amount of solid dissolved is the mineral solubility; the Ksp can be calculated from the solubility using equation 14. Both solubility and Ksp are therefore linked and dependent on the pH and temperature of the solvent.

Table 3.1 shows that the published pKsp values (the negative logarithm to the base 10 of the Ksp) for bulk enamel, and those for HAp, fall within the range 110 - 126. This range suggests uncertainties as to whether bulk enamel solubility may be similar to the solubility of HAp and if it is influenced by chemical inclusions. The range of values also suggests incongruent dissolution behaviour of enamel and hydroxyapatite that may be due to their heterogeneous properties through the bulk solid. However, the range also suggests that the pKsp values may be dependent on the choice of experimental protocol, such as the types of materials used (e.g. whether powdered or bulk samples); the methodology; and the analysis/calculations used to calculate the pKsp. That the range in values is due to differences in protocol is also illustrated by the large variations in pKsp values for synthetic HAp.

Table 3.1 Published $pKsp_{enamel/HAp}$ values with summaries of methodologies.

Ksp	Reference	Substrate and method
106-116	Patel and Brown (1975)	Human powdered enamel. pH range 4.5-7.6. Measured the amounts dissolved to calculate Ksp.
110 *(Apparent* solubility product 116)	Zhang et al., (2000)	Contact Microradiography assessed the demineralisation of sections of enamel in lactic acid solutions ranging pH 5 – 5.07 over a range of DS_{en} values (0.28-0.79) that were based on a $pKsp_{enamel}$ of 110. Suggest that enamel may have an *apparent* solubility product of 116 based on experimental findings.
116	Shellis et al., (1993)	Enamel powder equilibrated with 4 or 17 mM of H_3PO_4 at 37°C. Amounts dissolved were measured and used to calculate the ion activity product at equilibrium = Ksp.
117	Dawes (2003)	HAp Ksp cited in special feature article
118	McDowell et al., (1977)	4g synthetic hydroxyapatite. Ion concentrations at equilibrium then measured. Ksp determined as a function of temperature.
Enamel: 117.6 HAp: 121.82 (Pooled from pH 4.5-5.5)	Shellis and Wilson (2004)	Powdered synthetic HAp. Premolar enamel powder. 5mg equilibrated with acetic buffers at pH 4.5, 5.0 (0.15 M) 5.5 (0.2 M) in a range of degrees of saturation (range of pI_{HA}) at 37°C. Mass fraction dissolved plotted against pI_{HA} to give distribution curves at each pH. No statistical difference in pH differences.
126	Pan and Darvell (2007)	Solid HAP titrated with KCl solutions at pH 3.2, 3.6 and 4.1 at 37°C. Dissolution monitored using a semiconductor-diode laser scattering system that peaked each time solid was added and disappeared when all solid dissolved. Same solution was adjusted to a decreasing pH using 1M HCl.

Dissolution is a kinetically driven process related to the rate at which the end point is reached. For the solubility product of bulk enamel ($pKsp_{Benamel}$) to be accurately calculated from solubility measurements, all phases and possible ion-pairs that are

present during dissolution need to be accounted for as a lack of information on the resulting equilibria results in imperfect calculations (Pan and Darvell, 2009a). Chemical speciation of a solution is the chemical form and concentrations of each species present and can be derived using the thermodynamic principals of mass balance (Quinn and Taylor, 1992). Speciation software is used to calculate the chemical speciation of complex systems. Ion speciation programs rely on databases that report up to date experimental results for speciation constants as well as the methods and conditions of the experiments reported.

When using dissolution studies to determine the solubility product of bulk enamel, its physical and chemical heterogeneities need to be taken into consideration (Zhang et al., 2000; Bechtle et al., 2012). For example, demineralisation rates of prismatic, interprismatic and aprismatic enamel are not the same due to differences between, the organisation of crystals, the presence of more soluble material, and the porosity (Boyde, 1967; Shellis and Dibdin, 2000; Shellis. 1996). On a chemical compositional level, enamel is a substituted calcium hydroxyapatite. Its composition varies with ions such as F^-, CO_3^{2-} and Mg^{2+} replacing OH^-, PO_4^{3-} and Ca^{2+} within the stoichiometry altering the solubility of enamel (Aoba, 1997; West and Joiner, 2014; Liu et al., 2016). Thus, variations in enamel solubility may be related to variations within the structural and chemical composition of enamel.

The affinities of ions found in solution for calcium have been investigated. Citrate ions from citric acid solution at the solid-solution interface replaced orthophosphate on the surface of synthetic hydroxyapatite caused by a higher

affinity of citrate ions for calcium sites and formed an acid-calcium complex. These complexes can either remain adsorbed on the surface or can detach causing decalcification (Yoshida et al., 2002). Similar experiments with other acids such as acetic and lactic acid would shed light on the decalcification mechanism of hydroxyapatite and fluorapatite in a range of solutions with different pH and undersaturation levels.

Solubility values that are associated with metastable substances are kinetic solubility values and not true thermodynamic solubility values. At thermodynamic equilibrium, the total free energy within the system is equal to zero (DeVoe, 2016). In a system where an excess of solid is dissolving in a solvent, this point is known as saturation. Thermodynamic solubility values are not associated with any metastable phases that are formed in solution during dissolution before thermodynamic equilibrium has been reached. Metastable phases that are formed have higher free energies than the thermodynamically more stable phase that will have the lowest free energy at a specific temperature and pressure. Metastable phases that are formed prior to true thermodynamic equilibrium between the original solid solution will undergo a phase transformation into the more stable phase if the activation energy barrier is overcome.

Therefore, if we are to assume that enamel mineral is hydroxyapatite, and that hydroxyapatite is the most stable phase under the conditions, then we would expect all metaphases to transform into hydroxyapatite before thermodynamic equilibrium is reached. Therefore, the kinetics of enamel demineralisation would be

controlled in part by a hydroxyaptite-like phase from which the apparent-$pKsp_{Benamel}$ can be determined using speciation software.

In the absence of nucleation by the most stable phase, the next most stable phase will form, for example, Pan and Darvell (2009b) observed nucleation of the more soluble dicalcium phosphate dihydrate instead of hydroxyapatite on octacalcium phosphate when excess solid octacalcium phosphate was added to a solution with a low pH. This is consistent with an Ostwald succession.

For similar reasons discussed above, previous studies that have attempted to derive the solubility product of enamel, have highlighted that caution must be exercised when relying on kinetic studies to derive solubility products (Zhang et al., 2000). Furthermore, caution must also be extended to ensuring that the monitoring device used to record dissolution rates is sensitive enough to identify the point at which equilibrium is reached and must not mistake extremely low rates that are undetectable, for the condition of equilibrium. Therefore, techniques such as X-ray techniques that can monitor changes within the solution and/or solid have an advantage over other techniques such as light scattering.

It is important to acknowledge that any conclusions made based on experimental data are limited to the experimental conditions only. For example, decreasing pH is related to increased dissolution (Gao et al., 2001) but also impacts on the solubility product. However, published data on the effect of pH on the solubility product of enamel is contradictory, e.g. Shellis and Wilson (2004) found no statistical

difference in the solubility product of powdered enamel at different pH values between 4.5 and 5.5 whereas the earlier studies of Patel and Brown (1975) reported lower solubility product values of 106-116 over a pH range of 4.5-7.6. However, both experiments were conducted using powdered enamel as the substrate, and therefore similar results would be expected.

However, further similar kinetic studies will be needed to measure enamel solubility at a range of pH conditions, and at different temperatures in order to replicate the changing conditions of the oral environment and to identify if such variables affect the $pKsp_{Benamel}$. Such measurements will also confirm or otherwise the marked change in slope of the solubility isotherm for HAp at around pH 3.9 as reported by Pan and Darvell (2007).

3.2 Types of enamel loss

3.2.1 Dental caries

A multifactorial process involving the simultaneous interplay of diet, plaque, time and the host; with the latter including a plethora of genetically related factors from saliva quantity and quality to enamel composition and structure (Cummins, 2013).

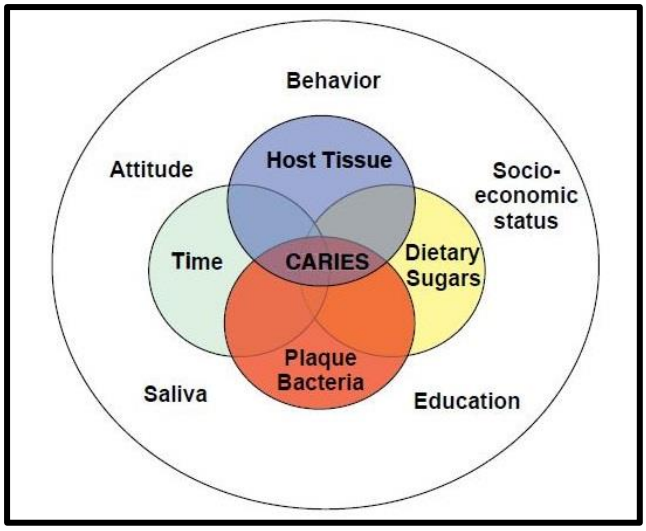

Figure 3.2 Venn diagram of the range of factors influencing the commencement and progression of caries. (Image from Cummins, 2013)

Plaque bacteria such as *Streptococcus mutans* metabolise dietary carbohydrates within plaque to generate organic acids such as lactic, propionic and acetic acids, reducing the pH. If pH falls below a critical value determined by the calcium and phosphate concentrations in solution, the solution will become undersaturated with respect to enamel and it will demineralise. The critical pH value is generally accepted as being 5.5 but due to substantial individual variations such as the composition of the solution surrounding enamel, this value can vary from person to person (Dawes, 2003).

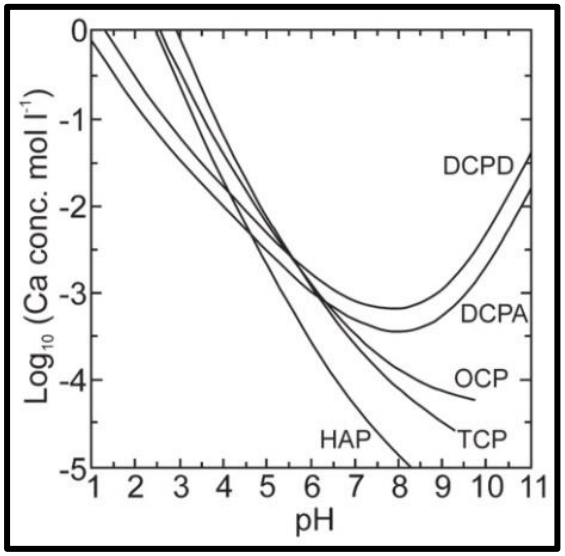

Figure 3.3 The solubility isotherm describes the relationship between calcium concentration, pH and calcium orthophosphate solubility (Image from Elliott, 2003).

The solid lines in **Figure 3.3** show the solubility isotherms for a range of octacalcium phosphates. The solid lines depict the locus of pH and calcium concentrations at which each mineral starts to dissolve. Any point above a line represents a solution that is supersaturated with respect to the mineral at a specific pH; a point below a line represents a calcium concentration and pH value at which the mineral would dissolve. As can be seen from the phase diagram, any point below a pH of approximately 5.5 at a calcium concentration of 3 mM (normal oral calcium concentrations) would result in hydroxyapatite dissolution (Anderson et al., 2001). However, the solubility isotherm of enamel may differ due to impurities particularly carbonate within enamel in addition to the reasons discussed above.

Approximately 90 % of caries incidences occur in pits and fissures of teeth. The initial characteristic feature of dental caries is sub-surface demineralisation where enamel loss occurs below the tooth surface. At this initial stage, a white spot lesion

on the surface develops and appears whiter than unaffected areas due to an increase in porosity of an intact surface layer approximately 0.03 mm in thickness (Dawes, 2003). Further progression of caries leads to the intact surface layer breaking down to form a cavity. This is due to a reduction in support for the enamel prisms above the caries cavity. The insufficiently supported area therefore becomes weaker and is subjected to otherwise bearable compressive and sheer loading forces leading to possible fracture of the intact surface layer. Ultimately, without intervention, caries can eventually lead to the destruction of the whole tooth.

If caries is successfully arrested and if the affected enamel surface has not reached cavitation stage and still remains a white spot lesion, enamel can be remineralised using topical treatments alongside patient oriented treatment plans that identify aetiological factors and therefore effectively optimise oral health and hygiene. However, if white spot lesions are exposed to dietary chromogens, brown spot lesions can form. It is important to ensure caries treatment is successful before attempting to remineralise or fill the affected area using fillings, as this can lead to secondary caries which can be more destructive.

Contemporary management of caries embraces the minimum intervention dentistry approach which aims to remove minimal dental tissue when tackling a carious lesion, unlike historical treatments which removed all the effected and surrounding tissue, whilst not compromising on the outcome.

3.2.2 Histological features of a carious lesion

The histological features of caries change according to the stage of caries progression and are therefore an indication of how far caries has progressed. The

initial development of an early stage caries lesion results in a white chalky appearance on the surface of the tooth – a white spot lesion. This area appears white because of micro-pores forming on the surface due to bacterial fermentation of carbohydrates producing lactic acid. The acid travels through these pores into the bulk of enamel resulting in an underlying cavity that shows up as a dark lesion below the surface of the enamel as shown in **Figure 3.4**.

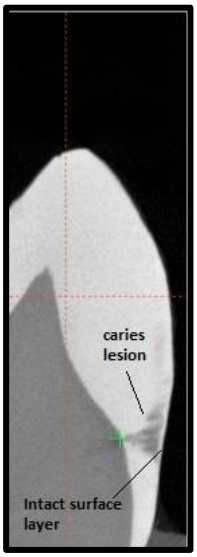

Figure 3.4 X-ray microtomographic image of an upper 1st molar showing a natural caries lesion with the characteristic intact surface layer and typical cornical shaped lesion below the surface.

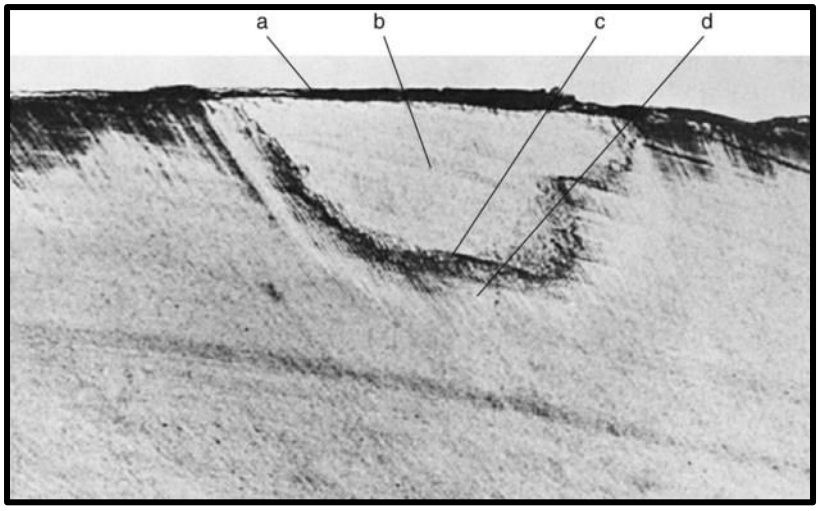

Figure 3.5 Cross-section of a caries lesion using polarised light microscopy and quinoline. Labels a-d show the four main characteristic zones; surface zone (a), body of lesion (b) dark zone (c) and translucent zone (d). (Image from Silverston et al., 1981)

In a study on the mineral content through a caries lesion using XMT, Cochrane et al., (2012) demonstrated that the mineral content of enamel through an early caries white spot lesion changes non-linearly from the surface to the EDJ.

As can be seen in **Figure 3.6**, mineral content increases from A-B confirming an intact surface layer before entering the body of the lesion shown by a decrease in mineral content from B-D. A rise in mineral content from D-F signifies the end of the lesion and start of unaffected inner enamel. If caries is left to progress further, it can infect the dentine layer beneath the enamel crown and this can lead to dentine hypersensitivity. Further progression toward the pulp can eventually lead to the destruction of the whole tooth. Polarised light microscopical examination using quinolin shows four main characteristics of a carious lesion as shown in **Figure 3.5**.

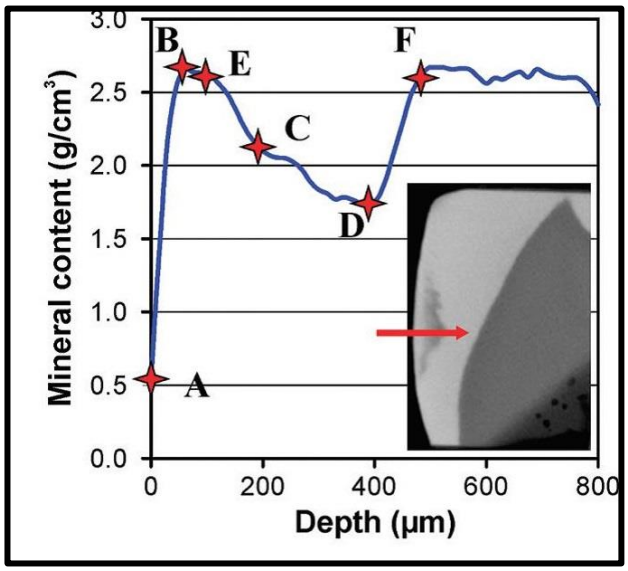

Figure 3.6 Mineral content (g/cm^{-3}) through an enamel white spot lesion going from outer to inner enamel towards the EDJ (from letters A-F). (From Cochrane et al., 2012)

The surface zone of a caries lesion is an intact enamel layer present during the initial stages of caries. The production of organic acid by plaque bacteria forms pores within the surface which can lead to infiltration of bacteria deeper into enamel (Selwitz et al., 2007).

Calcium and phosphate ions released from the demineralisation of deeper layers in addition to the ions provided by saliva can remineralise this layer. With the incorporation of fluoride ions from topical products such as toothpastes and gels, the surface layer can become more mineralised with a greater resistance to subsequent acid attacks than unaffected normal enamel. However, this layer can eventually breaks down due to the stresses and strains caused by masticatory processes coupled with a lack of support from the demineralised enamel layers beneath it if caries is not arrested.

The body of the lesion is the site where most demineralisation takes place, bacteria may be present here. The central region of the lesion body has a pore volume of

25% while its periphery has a pore volume of approximately 5%. The dark zone is the advancing front of the lesion and has a pore volume of 2-4%. Here, a lack of quinoline uptake due to small pore size and low pore volume results in a dark band when imaging with polarised light. The zone shows positive birefringence when the section is placed in quinoline and viewed by polarised light. The positive birefringence is related to small pores which are inaccessible to quinoline or media of large molecular sizes. The spaces are filled with air or vapour which is of low refractive index. This results in positive birefringence which reverses the negative birefringence of enamel. A study on the relationship between DE structure and caries progression showed the dark zone was absent in some of the deciduous enamel samples investigated (Mortimer, 1970). The absence of the zone was attributed to instances when acid attack was rapid in areas that were poorly formed. This indicated that DE caries attacks are more rapid due to poorly formed enamel or a lower mineral content compared to PE. However, a previous report showed that the same phenomenon can also occur in PE and is not exclusive to DE (Crabb 1966). The inner most zone; the translucent zone, appears as a structureless area that is unrecognisable clinically and radiographically. Submicroscopic pores at enamel rod boundaries and striae of Retzius in the translucent zone approximately total 1% in volume (Heymann et al., 2014).

When enamel is subjected to an acid attack; two forms of micromorphologic patters have been observed. Type 1 pattern is characterised by the preferential demineralisation of prism cores as shown in **Figure 3.7a**, whereas the type 2

pattern is characterised by preferential demineralisation along the interprismatic regions as shown in **Figure 3.7b**.

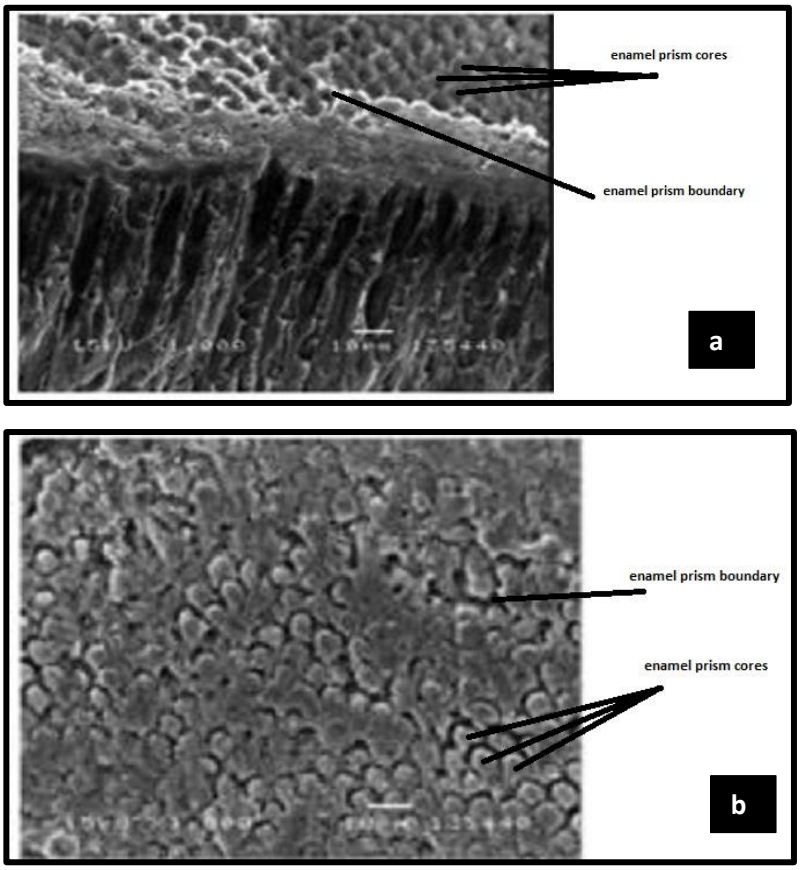

Figure 3.7 a and b SEM images of artificial caries lesions after samples were soaked in 50 mM lactic acid at pH 4.4 for 4 days. Preferential demineralisation of enamel along the prism cores (a) and prism boundaries (b) were observed. The increase in porosity can expose deeper regions within enamel to bacterial invasion leading to the characteristic zones of a caries lesion (Images from Ngoc et al., 2016).

Whilst topographical microscopic images such as those taken by SEM of carious lesions have improved our understanding of the caries process in terms of the effects of an acidic attack on histological features on the surface of enamel, further insight of features throughout the bulk of a caries lesion can be obtained through three dimensional imaging techniques such as X-ray microtomography and laser

scanning confocal microscopy, particularly when studying early caries lesions at the white spot stage where subsurface demineralisation takes place. However, the resolution of such images do not compare with SEM images which can achieve a resolution down to the nanometre scale enabling images of individual crystallites that make up the prismatic, interprismatic and aprismatic features of enamel to be observed in more detail. Using a combination of complimentary imaging techniques would therefore provide greater insight of the histological features of a carious lesion and lead to a greater understanding of the caries process.

3.2.3 Causes of caries

Caries is a disease caused by the fermentation of carbohydrates by acidogenic plaque bacteria resulting in the production of organic acids such as lactic, acetic, formic and propionic acids leading to dissolution of enamel and dentine (Featherstone, 2008). Caries is a dynamic and complex process and the rate of progress is dependent upon many factors including microbiology, tooth ultrastructure, tooth mineral composition, saliva, diffusion processes, kinetics of demineralisation, pH and remineralisation.

The oral cavity is host to a plethora of microorganisms that reside within a biofilm which covers the surfaces of the hard and soft tissues. The commencement of an oral disease such as caries is triggered by a change in the oral environment that favours the proliferation of some species over others. For example, the regular consumption of sugary foods favours acidogenic and aciduric species such as mutans streptococci (MS) and lactobacilli over others. This proliferation tips the delicate and harmonious balance that exists between species and between the

demineralisation characteristics of species and remineralisation properties of saliva within a healthy oral state (Takahashi, 2011).

As stated above, caries is a dynamic process, the progression of which is determined by many factors. Consequently, individual differences between factors including saliva composition and amount, mineral structure, microflora and mineral composition all determine the likelihood of an individual experiencing caries and also the rate of caries progression.

Vertical transmission of oral microflora from caregivers to infants is a key event in the early acquisition of MS. Good parental oral hygiene is therefore an important preventative measure in reducing the risk of the development of early childhood caries in children. The microflora populates the soft tissue in the infant's oral cavity later covering the teeth as a biofilm after their eruption. Heavy inoculation with MS can lead to caries and cause pain and discomfort. This can lead to additional health risks such as malnutrition (Acs et al., 1992) and iron deficiency if the child refuses to eat due to pain associated with early childhood caries (Clarke et al., 2006).

Early childhood caries can also be caused by inappropriate feeding methods such as bottle feeding milk and fruit juices. Sugary drinks collect near tooth surfaces surrounding the teat for prolonged periods of time, especially at night, providing acidogenic bacteria with carbohydrates needed to produce organic acids that lead to enamel demineralisation, particularly buccally, of the maxillary primary incisors and first primary molars in a way that reflects the pattern of eruption (Kawashita, 2011).

Studies have shown that caries incidence correlates negatively with socioeconomic status negatively; with greater incidences found amongst individuals from poorer backgrounds. Education is also associated with caries incidence and a lack of access to educational resources on hygiene and healthy lifestyles has been found to increase the risk of developing caries (Kawashita, 2011).

Rampant caries most commonly occurs in individuals who have a reduced level of protection from caries within the oral environment. Xerostomia is a condition whereby an individual suffers from an inability to produce saliva. This condition can be due to genetic factors or can be drug induced. Lacking the protective qualities of saliva such as its antibacterial, antifungal and calcium and phosphate content properties exposes the individual to rampant and reoccurring infections.

3.2.4 Caries incidence rates amongst children and adults

Incidence rates amongst children and adults are generally reported in national surveys conducted by health authorities and independent researchers in collaboration with clinical examiners. The DMFT and dmft (decay, missing, filled teeth) system is a universal scoring system that is used to measure the prevalence of tooth decay in permanent and deciduous teeth, respectively, and to identify trends in caries prevalence over time. Populations are commonly grouped by age and/or by region and percentages of caries incidence amongst groups are recorded and often compared.

Studies have observed there to be significant differences in caries incidence rates amongst children between countries. For example, in 1999, the caries incidence rate amongst children between the ages of 2-5 years in the USA was 27% this is in stark contrast to the caries incidence rate amongst children of the same age in the Philippines at 59% and 94% for 2 and 5 year olds (Kawashita et al., 2011; Cariño et al., 2003).

Reports on caries incidence have indicated that there is a general decrease in prevalence amongst western children. However, between 1988 – 1994 and 1999 – 2004 there was an increase in caries prevalence from 24.2% to 27.9% in the USA (Kawashita et al., 2011). This may be due to the increase in sugary drinks and foodstuffs consumed in the USA during this time period. In a survey on dietary changes between 1965 and 1996 amongst Americans, a decline in milk consumption was replaced with an increase in soft drink consumption (Cavadini et al., 2000). Authors expressed concern, particularly amongst adolescents, as the decrease in overall dairy consumption in addition to a decline in vegetable intake correlated with mineral deficiencies, in particular calcium and phosphorous deficiencies, exposing adolescents to a greater risk of developing caries and osteoporosis (Cavadini et al., 2000). Nonetheless, most surveys report a decrease in caries incidence rates amongst both children and adults in the western world. For example, the proportion of caries free children in England has been recorded as; 69.1% in 2008 and 72.1% in 2012 to 75.2% in 2015, an increase in caries free children by 8.8% since 2008 (Patel, 2012). In Norway, the percentage of caries free children was recorded as 80.1%. The DMFT score has also fallen from 1.1 in 2008

and 0.9 in 2012 to 0.8 in 2015, a decrease in severity of 27.3% since 2008 (PHE, 2015).

Comparing data from different reports is difficult as the boundaries different reporters use to define the level of caries severity differ. For example, while some may use a grading system of 1-5 to define the severity of a caries lesion within a tooth; such as in Skeie et al. (2005) study, others may only use the DMFT grading score to measure the level of severity, while others may only choose to record caries lesions that have reached cavitation stage thereby ignoring white spot lesions completely; as in Cariño et al. (2003) study as well as in the oral health survey report on dental decay incidence amongst five-year old children in 2015 carried out and reported by Public Health England (PHE, 2015).

Caution must be exercised by reporters when deciding on the criteria used to identify a carious lesion as it can lead to underestimations with regards to the prevalence of caries incidence. Differences between the methodological approaches used in such surveys also puts limitations on the comparisons one can make between reports. To obtain a clear and precise overview of caries prevalence, consistency between methodologies of surveys conducted is required. This would allow for direct comparisons between regions, ages, countries and socioeconomic status from different surveys. Such inconsistencies in the criteria systems used to detect carious lesions has been addressed by the International Caries Detection and Assessment System (ICDAS) which was developed by an international team of caries researchers to integrate carious lesion detection criteria systems into one standard system (Gugnani et al., 2011).

3.2.5 Erosion

Erosion is the term used to describe the non-carious pathological loss of tooth tissue by a chemical process involving acids. Research conducted on dental erosion has increased significantly over the last 40 years with an increase from 5 studies per year in the 1970's to over 50 a year in 2006 (Lussi, 2006). This increase in research reflects the dietary changes that have taken place over the last few decades. Decreases in the consumption of nutritionally beneficial food has been followed by an increase in processed, acidic, sugary foods which has correlated with an increase in mineral deficiencies, especially amongst adolescents (Lussi, 2006). Concerns have been raised with regards to the increased risks associated with calcium and phosphate deficiencies, such as the increased risk of developing chronic illnesses such as osteoporosis and caries. Such concerns have contributed to the surge in research focused on erosion and caries.

3.2.6 Histological features of erosion

The pattern of erosive tooth wear differs according to the aetiology. Erosion that is due to an increase in the consumption of acidic foodstuffs and beverages such as citric acid from fruit juices, results in dental tissue loss from the palatal and labial sides of teeth. Initially, the affected areas appear roughened like etched enamel but prolonged periods of erosion lead to smooth and polished surfaces.

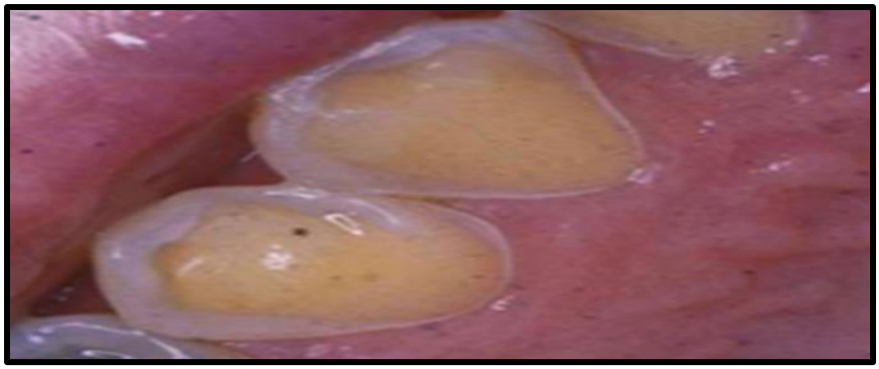

Figure 3.8 Severe dental erosion showing bulk enamel mineral loss and the exposed underlying dentine layer (Ganss et al., 2014).

Over time, initial surface mineral loss turns into bulk mineral loss resulting in the microhardness level of enamel decreasing which ultimately increases susceptibility to physical wear (Ganss et al., 2014).

Removal of enamel during dental work is not a form of erosion as erosion can be defined as the gradual loss of dental whereas loss through dental treatment is instant, requiring only a few minutes.

3.2.7 Causes of erosion

Extrinsic causes of erosion are mainly associated with the consumption of acidic drinks from containers such as cans and bottles that direct the beverage directly onto the labial and palatal surfaces of mainly the maxillary teeth. Shallow lesions form and in the case of habitual consumption lesions can occur on other parts of the tooth. Other extrinsic factors associated with tooth erosion is chlorination from chlorinated swimming pools where the chlorine reacts with water to form hydrochloric acid - increasing the risk to regular swimmers such as athletes, and industrial chemical fumes in factories – increasing the risk to factory workers.

Medication can also lead to dental erosion, for example the oral administration of medicaments including iron tonics (James and Parfitt, 1953) and acid to dissolve renal calculi.

Intrinsic causes of dental erosion include the exposure of teeth to stomach acid. This is usually caused by the reflux, regurgitation and vomiting of gastric acids caused by either psychosomatic or somatic causes, for example; anorexia and bulimia and alcoholism, pregnancy and gastrointestinal disorders respectively (Imfeld, 1996). The nature of intrinsic erosion caused by endogenous acid results in a characteristic tissue loss of the palatal surfaces of upper anterior teeth and premolars showing characteristic shallow lesions with some areas showing significant enamel loss and exposure of dentine (**Figure 3.8**).

Idiopathic erosion is dental tissue loss as the result of unknown origins. Whilst the characteristic features of erosion are present on dental surfaces, the aetiology is unknown. However, observations from a study on the salivary flow rates of patients suffering from idiopathic erosion have shown that patients had lower unstimulated salivary flow rates than controls (Woltgens, et al., 1985) indicating that erosion is associated with salivary buffer capacity, and by the pellicle formed by salivary mucins.

Abrasion describes the wearing away of dental tissue through mechanical processes involving foreign objects or substances such as tooth brushing. The pattern of wear depends on the type of the aetiology and can be either diffuse or localised.

Attrition is the removal of dental tissue through tooth to tooth contact such as through grinding of teeth resulting in dental loss primarily along the occlusal and incisal surfaces of teeth. Proximal surfaces are also affected during mastication.

Abfraction results in wedge shaped defects at the cementoenamel junction. Masticatory or parafunctional forces from hyper- or the malocclusion are believed to cause tooth flexure exposing effected teeth to strong tensile compressive and shearing stress provoking fractures in enamel at the cementoenamel junction.

3.2.8 The role of the pellicle and saliva

There are many components of the oral environment that are associated with maintaining the overall health of the oral cavity, examples include; ecosystems of microbes, multitudes of proteins and saliva. These three main components interact to form a biofilm that covers teeth known as the pellicle (Gibbons et al., 1985).

The pellicle is a complex and multi-layered film that gradually builds up during periods in between brushing. It has a multi-functional role that includes; protecting the enamel from the external environment, providing a selective permeable barrier, regulates mineralisation and demineralisation (Moreno et al., 1977) and modulates the microbial flora on the enamel surface (Gibbons et al., 1985, Al-Hashimi and Levine, 1989).

Some of the techniques used to study the pellicle include amino acid analysis, immunologic techniques and gel electrophoresis which have identified the pellicle as being predominantly composed of selectively absorbed salivary proteins and non-salivary proteins (Al-Hashimi and Levine, 1989). However, the amount of

pellicle that can be obtained from an individual is extremely small - in the order of a few micrograms, limiting any direct biochemical characterisation of *in vivo* pellicle proteins (Lendenmann et al., 2000). However, attempts have been made; for example, a study on the chemical analysis of the acquired pellicle formed in two hours on cleaned human teeth was conducted by Sönju and Rölla (1973). In their investigation protein adsorption on the enamel surface increased within the first 1.5 hours after cleaning with pumice, and there were no significant differences between the proteins adsorbed on the upper molars, upper incisors and lower anteriors indicating that region was not a factor. They also observed a high amount of acidic amino acids lending support to the claim that selective adsorption of acidic proteins on enamel surfaces takes place. The amount of pellicle obtained from the same surface area at 30-minute time intervals varied. This was explained as being due to the changes in both the flow rate and protein content of saliva over time. However, a previous study by Pruitt et al., (1969) showed that increased phosphate concentration was associated with the desorption of salivary proteins from hydroxyapatite indicating that changing phosphate levels in saliva may be associated with pellicle formation within the oral cavity.

Sampling methods used to collect pellicle samples for analysis vary amongst researchers leading to some inconsistencies in data published. For example, the insolubility of the pellicle in dilute hydrochloric acid has led some researchers to opt for a collection method whereby enamel is partially demineralised to obtain the pellicle; however, this can lead to the loss of pellicle components which may result in an underestimation of pellicle components. Other methods include isolating

specific areas of cleaned teeth followed by drying of a newly formed pellicle formed over a specific time period; usually 2 hours, before scraping the tooth surface and collecting samples in glass wool (Sönju and Rölla, 1973; Al-Hashimi and Levine, 1989). Another method collects the dried pellicle using PVDF membranes soaked in 0.5 M sodium bicarbonate buffer pH = 9 as swabs, this is then followed by vortexing and sonification to extract the pellicle (Yao et al., 2003).

An additional complication associated with pellicle sampling methods that involve the removal of the pellicle from tooth surfaces is that it will always distort the hierarchical structure the pellicle forms on enamel surfaces *in vivo.* Recent studies have shown that the hierarchy of pellicle components is essential to maintaining the delicate balance between health and disease initiation.

The pellicles intricately composed structure has been made evident through studies on salivary proteins and early pellicle formation. Studies have shown that in 2-hour *in vivo* enamel pellicle, specific salivary molecules were found to comprise the early enamel pellicle, these included; sIgA, glycosylated species of α-amylase, non-phosphorylated species of cysteine containing phosphoproteins and high molecular weight salivary mucin (Al-Hashimi and Levine, 1989). Such observations demonstrate that only selected members of salivary protein families constitute the early enamel pellicle. In addition to the specific adsorption of proteins onto enamel, proteins may also undergo alterations such as proteolytic degradation once bound onto the enamel surface.

Proteins in dental plaque serve as an ecological determinant of the composition of the microbial community; they support adhesion, growth and are a major source of

nutrition. The degradation of proteins is in itself complex and in some cases, requires the cooperation and coordination of many different species of oral bacteria. For example, mucin MUC5B is a complex oligomeric glycoprotein with a heterogeneous molecular mass (14 - 40 x 10^6 Da), many oligosaccharides and different compositions and charges; its degradation is sequential and involves the removal of its oligosaccharide and polypeptide backbone by interspecies cooperation. In a study on the degradation of MUC5B; Wickström et al. (2009) showed that incubating MUC5B with individual bacterial strains that were known to be involved in the degradation process failed to degrade MUC5B on their own, whereas when a consortium of bacterial strains was used degradation was successful. This indicates that the coordination of enzymes from different bacterial species is a requirement for the degradation of salivary proteins that make up the pellicle.

In addition to bacterial interactions, evidence from studies suggests proteins interact to provide additional functional benefits. For example, α-amylase is a calcium binding protein with antibacterial properties and forms ionic complexes with salivary cystatin SA-I which is a thiol protease inhibitor with antiviral properties (Korant et al., 1985). It is suggested that the complex may modulate the microbial colonisation on the tooth surface. In a further study on cystatin SA-I, researchers showed a higher expression of a truncated version of cystatin SA-I (14 kDa) in pre-treatment saliva than post treatment saliva samples from patients newly diagnosed with stage 1 oral squamous cell carcinoma indicating that cystatin SA-I may

potentially be used as a salivary biomarker for oral squamous cell carcinoma (Shintani et al., 2010).

The complex nature of the pellicle as described above highlights the need to characterise and analyse the components of mature rather than early formed pellicle that may only be a few layers thick and/or may not have formed all the necessary interactions such as cross-links required to provide the full functional properties of a mature pellicle. While the analysis of a 2 hour pellicle, such as used in the studies described above, provides valuable information on the initial composition, it is more advantageous to analyse the composition and structure of mature pellicles in order to obtain a complete understanding of the dynamics and interactions between all components and layers formed. For example, studies on the protective function of the pellicle on enamel against demineralisation have shown that it is only effective at reducing demineralisation after a minimum of 18 hours *in vivo* and a minimum of 4 days *in vitro* (Lendenmann et al., 2000). Furthermore, the time difference between the *in vivo* and *in vitro* results lends support to findings that the oral environment functions more effectively when its constituents can interact.

Saliva is composed of antifungal and antimicrobial agents, proteins, immunoglobulins, enzymes, mucins, nitrogenous products such as urea and ammonia, water and electrolytes including sodium, potassium, bicarbonates, calcium, phosphate and magnesium. All the components of saliva interact in related function. Whole saliva is therefore regarded as greater than the sum of its parts. For example, to maintain the pH and buffering capacity of saliva, bicarbonates,

phosphates and urea interact; to cleanse and aggregate microbes', macromolecules and mucins interact; to modulate demineralisation and remineralisation, calcium, phosphate and proteins such as statherin interact; and to maintain and provide antibacterial and antifungal properties; immunoglobulins, proteins and enzymes interact.

In a study on salivary MUC5B, Raynal et al. (2002) showed that the gel-forming properties of saliva were dependent on interactions between MUC5B and other salivary components, and not just on MUC5B alone. Authors suggested cross-links between salivary components and MUC5B may contribute to the gel-like property of saliva.

The pH of saliva ranges from 6.5-7 and is secreted from the major and minor salivary glands and from gingival crevicular fluid which contains oral bacteria and food debris. Major salivary glands include the parotid glands located opposite to the maxilliary first molars. The submandibular and sublingual glands are located on the floor of the mouth. In the lower lip, tongue, palate, cheeks and pharynx are minor glands.

Table 3.2 Percentage contribution towards daily unstimulated salivary flow from main salivary glands (Daily unstimulated salivary flow percentage result taken from Humphrey and Williamson, 2001).

Salivary gland	Daily unstimulated salivary flow contribution
Parotid	20%
Submandibular	65%
Sublingual	7-8%
Other minor glands	<10%

The downregulation of mineral precipitation is an important property of saliva. Saliva is supersaturated with respect to enamel mineral; therefore, a lack of mineral inhibition can lead to the spontaneous formation of excessive mineral deposition known as calculus.

In addition to providing the pellicle with components, saliva also regulates the demineralisation and remineralisation of enamel. For example, inhibiting salivary macromolecules such as acidic proline-rich proteins (PRPs) and statherin have been shown to reduce the crystal growth rate of hydroxyapatite seeds in supersaturated solutions with respect to hydroxyapatite (Moreno et al., 1979). The reduction in growth rate was found to be directly proportional to the extent of proline-rich protein and statherin absorption on to hydroxyapatite seeds.

Statherin and PRPs are present within both parotid and submandibular saliva, and adsorb onto hydroxyapatite at the interface between the tooth surface and saliva. The adsorption of these macromolecules is believed to be dependent on the chemical and structural features of each macromolecule and is selective and

localised to sites where crystal growth initiates. These surfaces are thought to be more reactive.

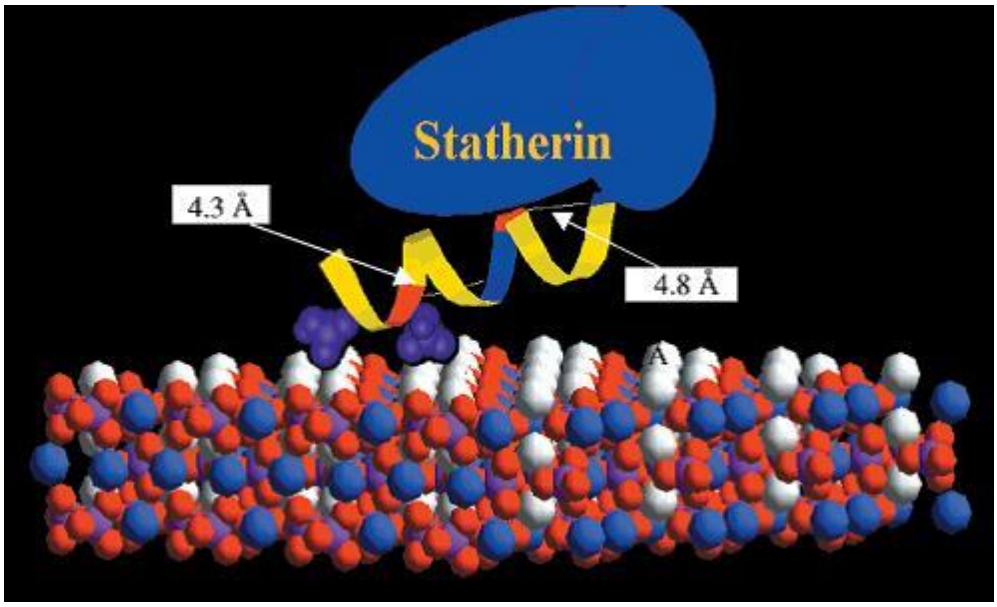

Figure 3.9 Schematic model showing statherin interacting with the 001 face of HAP, with calcium ions in white and phosphoserines in purple (Long et al., 2001).

In a study on the effect of PRPs and statherin on the crystal growth rates of hydroxyapatite, Moreno et al. (1981) showed that the bulkier PRPs were more effective at crystal growth inhibition than the less bulky statherin molecule, in terms of the relative proportions of macromolecules adsorbed. Although a greater proportion of statherin was shown to have been adsorbed onto hydroxyapatite, on a mol-per-mol basis, for the adsorbed macromolecule, PRPs inhibited crystal growth more effectively. This suggests that the mechanism for crystal growth inhibition by these molecules is to physically block crystal growth sites thereby inhibiting calcium and phosphate adsorption.

The results of the study also suggest that adsorption of these molecules onto hydroxyapatite is dependent on their molecular structures. For example, adsorption activity appeared to be associated with the length of a negatively charged terminal on both PRP and statherin molecules. While PRPs possess a negatively charged, phosphoserine-containing, 30-residue amino-terminal segment; statherin contains a 5-residue amino terminal that is negatively charged (Moreno et al., 1981).

In a study where the flow rate, pH, buffering capacity, total antioxidant capacity and total calcium and protein of saliva in caries-free and caries-active children was determined, results showed that there was no significant difference in the flow rate, pH, buffering capacity and calcium concentration between caries active children and caries-free children. However, there was a correlation between salivary secretion rate and caries activity, but only a weak correlation between pH and buffering capacity with caries activity (Preethi et al., 2010). Previously, another similar study showed that while calcium and phosphorus concentrations were higher in caries free children plaque samples compared to caries-active plaque samples, the difference was insignificant in terms of calcium saliva concentrations. However, the Ca/P ratio was shown to be considerably higher in caries–free samples than caries-active samples indicating that the ratio is an important factor that appears to be associated with caries (Shaw et al., 1983). Other studies have shown an association between phosphorus levels and caries incidence that indicates an inverse relationship between phosphorus and dental caries incidence (Shannon et al., 1962, Shannon and Feller, 1979). Ashley et al., (1991) showed that calcium and inorganic phosphate concentrations in childrens plaque samples were

lower than in adults at 7.16 μg/mg and 12.21 μg/mg of calcium, respectively and 5.14 μg/mg and 8.16 μg/mg phosphorus, respectively. Childrens stimulated saliva was also shown to contain less calcium than adults measured at 5.09 mg/100ml and 5.93 mg/100ml, respectively, and also for unstimulated saliva measured at 5.76 mg/100ml and 6.33 mg/100ml, respectively. The study also identified a direct relationship between salivary and plaque concentrations of calcium and inorganic phosphorus. The authors suggest mineral concentrations of saliva influence those in plaque during acidic challenges. During sugar intake, phosphorus levels may fall as flow rate increases and saliva becomes undersaturated with respect to calcium and phosphate due to the fall in pH inducing a rise in mineral concentration within plaque fluid resulting in calcium and phosphate outward diffusion. High calcium and phosphate concentrations in stimulated saliva may slow down the outward movement whilst low mineral concentrations in stimulated saliva may encourage outward diffusion.

Whilst the characterisation of individual salivary components is essential to our understanding of each molecules characteristics and functional properties within saliva, caution must be exercised when using such results to explain mechanisms within the oral environment. As discussed above with regards to the pellicle, our understanding of salivary functions and mechanisms would benefit from more studies on the interactions between salivary constituents in addition to those on individual components.

Chapter 4 : Comparisons between deciduous and permanent enamel

Mammals have a diphyodont dentition, a type of dentition that is characterised by two successive sets of teeth; the deciduous teeth succeeded by the permanent teeth. Although publications on DE go as far back as the 1960's, there are relatively few studies compared to the number of studies that have exclusively focused on PE, and fewer even more so with regards to studies on comparisons between the two enamel types. Further, the results of previous research often conflict due to differences in methodologies and techniques used.

The lack of research on DE may be a consequence of the notion that because deciduous teeth fall out any research on them would be time wasted. However, recent reports by Public Health England (2015) and some media coverage has highlighted a trend over the last few years that shows an increasing number of children admitted into dental hospitals for GA extractions, with PHE stating that this has become a strain on the NHS and thus is a cause for concern.

Previous studies have shown faster demineralisation rates in DE compared to PE and have attributed the difference in rates to many factors such as DE having; a higher carbonate content (Sønju Clasen and Ruyter, 1997), a lower mineral content (Mortimer, 1970), the presence of a neonatal line that is less mineralised and being approximately half the thickness of PE (Mortimer, 1970).

Many reviews and previous literature on DE such as; Bhatt and Nelson, (1989); Lippert et al., (2004) and Neel et al., (2016) agree that the lack of knowledge on

deciduous teeth requires further research. Furthermore, research focused on the demineralisation/remineralisation characteristics and mechanisms requires the use of quantitative techniques with high resolution capabilities to ensure information on physico-chemical processes is accurate. Information derived from such experiments can be used to help educate clinicians and patients, screen for anti-caries agents and promote behaviour change.

4.1 Structural differences

4.1.1 Dimensions

The mean growth of the deciduous crown is from 6 to 14 months, whereas in permanent teeth the mean crown growth is from 3 to 4 years. Consequently, the mean thickness of DE is 1.14 mm compared to PE at 2.58 mm (Oliveira et al., 2010).

Anterior deciduous crowns are wider mesiodistally relative to their crown lengths than are permanent crowns. The buccal cervical ridges are more prominent, especially on the maxillary and mandibular first molars whereas the buccal and lingual surfaces are flatter above the cervical curvatures than in permanent molars. This narrows the occlusal surfaces.

In a study comparing the microstructural and mineral compositional differences in DE and PE, Oliveira et al. (2010) measured prism head diameters in DE and PE. Results from the study showed DE and PE to be similar with mean prism head diameters of 3.47 µm and 4.34 µm, respectively ($p>0.05$). The mean number of prisms per square millimetre was also measured at the outer surface and at the EDJ. Results showed that while both DE and PE exhibited a decrease in the number

of rods per square millimetre from the outer surface to the EDJ, DE had more rods in each region with; 14.1 rods per square mm at the surface compared to 13.6 in PE and 15.2 rods per square mm near the EDJ in DE compared to 14.0 rods per square mm in PE. However, prism head diameters may be dependent on the tooth type, for example, Fosse (1968) and Mortimer (1970) measured higher prism diameters in deciduous and permanent canines (4-7 µm and 6 µm, respectively). Further, there are discrepancies in the data regarding prism densities on the outer and inner surfaces of enamel. For example, Fosse (1964) calculated a mean number of 21,904 prisms per mm^2 on the outer surface and 47,089 on the inner surface. The major discrepancies in data of both investigations highlight the extent to which the choice in technique and methodology influences data.

4.1.2 Surface features and incremental markings

Enamel grows incrementally according to periods of slow and fast growth during development. Incremental markings represent regular secretions occurring throughout the growth period unlike those that are accentuated lines associated with disturbances during tooth formation, such as Owen's lines and irregular striae of Retzius (Dean, 2000). Using polarised light microscopy and SEM, ultradian markings (daily markings) that include cross-striations (alternating daily varicosities and constrictions along prisms) and long period lines such as striae of Retzius have been viewed (**Figure 4.1**). Long period lines are spaced 6-10 days apart in human adult enamel (Dean, 2000).

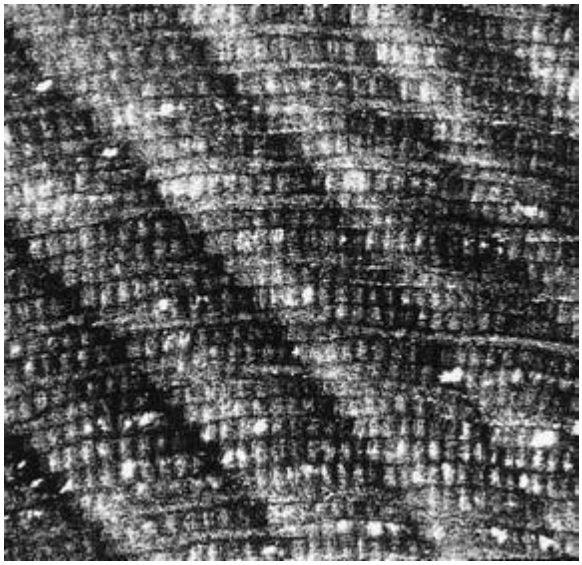

Figure 4.1 Laser confocal photomicrograph showing daily cross-striations between striae of Retzius in enamel. (Image taken from Dean 2000).

Cross-striations are associated with daily enamel matrix deposition rates of ameloblasts. Shellis (1984a) calculated the changes in the enamel extension rate in humans using daily cross-striations and observed a reduction in enamel extension from 20 microns per day at the cuspal region to 4 microns per day at the cervical region of human permanent teeth.

In a study on the appositional life span of ameloblasts in DE and PE, Massler and Schour (1946) used the growth potential of ameloblasts; stated to be a product of the rate of secretion and time during which the cell was active (its functional life span) to compare DE and PE ameloblast activity. Results showed that for a deciduous second molar and permanent first molar the average length of an enamel rod was 1100 µm and 1600 µm, respectively; the average daily rate of apposition was 5.5 µm per day and 4.5 µm per day, respectively; and the average life span of an ameloblast was 200 days and 355 days, respectively. Average daily

rate of apposition was greater in all deciduous teeth compared to permanent teeth studied, indicating that enamel apposition is faster in DE than in PE. However, Mahoney (2011) recorded much slower daily secretion rates in deciduous first molars as 3.37 µm for inner enamel, 3.87 µm for middle and 4.76 µm for outer enamel. Results also showed the neonatal line formed during the stress of birth formed over a 3-8 day period with width measurements within the range 10-25 µm. Cross striations were absent adjacent to the neonatal line in postnatal enamel but were present in prenatal enamel adjacent to the neonatal line (**Figure 4.2**).

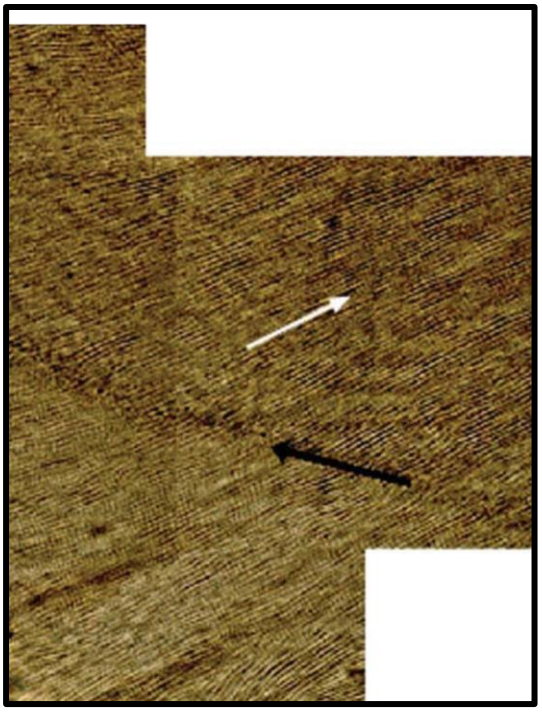

Figure 4.2 Incremental marking in a deciduous second molar showing the neonatal line (black arrow direction) and enamel prism direction (white arrow). (Image taken from Mahoney, 2011)

4.2 Compositional differences

4.2.1 Enamel composition and mineralisation level

According to Mortimer (1970), the lower level of mineralisation and relative thinness of DE are the main differences between DE and PE. In the study, which used contact microradiography and monochromatic energy to measure mineral content, the DE mean mineral percentage was recorded to be 80.6 % mineralised compared to PE at 89.7 %, however, maximum mineralisation values of DE and PE show a much smaller difference between the two enamel types at 90 % and 92 %, respectively (Mortimer, 1970). It is worth noting that the study by Mortimer (1970) did not include PE and so comparisons between DE and PE were made using the mineralisation measurements of PE from the Angmar et al. (1963) previous study.

In a study on the influence of chemical composition on caries progression in DE and PE, Sønju Clasen and Ruyter (1997) investigated the influence of carbonate content and carbonate position within the hydroxyapatite structure on caries progression in human permanent and DE. Using FTIR spectrometry, a quantitative determination of carbonate in the hydroxide (type A) and phosphate (type B) positions were made. Calibration curves using synthesised hydroxyapatite permitted determination of the quantities of each type within DE and PE. Results showed that DE contained significantly more type A carbonate (0.25 wt%) than PE (0.22 wt%) and that the sum of carbonate (type A and type B) was also significantly higher in DE compared to permanent (2.23 wt% and 2.15 wt%, respectively). Authors concluded carbonate may be one of several factors contributing to faster caries progression in deciduous teeth. However, the results from studies in the literature

that have compared the carbonate content in DE and PE often conflict. For example, Naujoks et al. (1967) investigated the carbonate content within different regions of DE and PE (occlusal, middle and cervical) by measuring the amount of carbon dioxide released from enamel powder once dissolved in 0.5 N sulphuric acid. Results showed there were no significant differences between the regions within each enamel type and further no significant differences between each enamel type when p=0.05. The study also aimed to identify whether a relationship exited between the characteristic 'circular caries' often identified on cervical regions of DE and chemical composition. No differences in the calcium, sodium and carbonate content between DE and PE were measured. However, results did show differences in the phosphate and nitrogen contents of DE and PE, with a relatively low percentage of phosphate in the cervical region of deciduous teeth compared with permanent teeth (p<0.02). The higher Ca/P ratio confirmed results from a previous study that showed the ratio in DE to be 2.06 (Bird et al., 1940). Since calcium and carbonate content was shown to be similar to PE, authors suggested calcium must be bound in forms other than $CaCO_3$. Based on the higher nitrogen (N_2) content the study concluded that calcium may be bound to proteins within the cervical region and suggested circular caries in DE may be associated with a low P/N_2 ratio.

DE appears to be optically more opaque which may represent greater porosity and therefore a lower level of mineralisation (Bosch et al., 1980). Studies using the floatation microdensitometry method have shown that DE is less dense and less variable than other enamel types (Weatherell et al., 1967), however, fluctuations in

density within PE have also been observed with pockets of less dense mineral in various regions throughout PE being recorded. This highlights the heterogeneity within both enamel types and further serves to emphasise the importance of taking enamel region into consideration when conducting investigations on enamel mineralisation levels. It may be that differences observed between DE and PE mineralisation levels in previous studies are due to different investigations taking enamel samples from different regions on the enamel crown.

In another study on the mineralisation differences between DE and PE, Wilson and Beynon (1989) used contact microradiography to compare DE and PE. Results showed that while there were some significant differences between individual values at certain regions extending from the EDJ towards outer enamel, there were also many measurements that showed no significant differences. For example, at the occlusal region near outer enamel PE had a mineralisation level of 88.6 % v/v whereas in DE the value was 84.8 % v/v showing a significant difference ($p < 0.001$). However, DE showed a significantly higher ($p < 0.001$) level of mineralisation near the EDJ at the cervical region than PE, 81.2 % v/v and 77.8 % v/v, respectively. Further, many individual values at regions between the occlusal and cervical, and EDJ and outer enamel showed no significant difference, for example; 83.2 % v/v and 82.7 % v/v for PE and DE respectively.

In conclusion, the differences between DE and PE in terms of their respective compositions and mineralisation levels required further investigation as results from previous studies often conflict. The inconsistencies observed highlights the need to conduct experiments that are inclusive of both enamel types and further

that the areas for analysis are considered in terms of the location on the crown. A further consideration to make is to ensure both enamel types are unaffected by carious lesions before any analysis is undergone. In doing so, both enamel types can be exposed to identical experimental conditions and measured with the same quantitative technique. This would eliminate the possibility of artefacts and problems associated with extrapolating data. Previous reports that extrapolate data of one enamel type to explain data of another enamel type is not conducive for providing information on the similarities and differences of DE and PE and often results in over/underestimations, as demonstrated and discussed in this section.

4.3 Demineralisation rates of deciduous and permanent enamel recorded in literature

In 1981, Featherstone and Mellberg compared the progress of artificial caries lesions in DE and PE blocks using Rhodamine B dye imbibition whereby the depth of dye after artificial caries lesions in both enamel types at different time points was compared using spectrofluorometry. Results showed that DE caries progress was 1.5 times faster than in PE and that dye uptake, measured by extracting the imbibed dye in ethanol, was 8.2 µg cm^{-2} (± 3.3 µg cm^{-2}) and 5.7 µg cm^{-2} (± 1.9 µg cm^{-2}) for DE and PE respectively. However, authors did not state whether these differences were statistically significant and further, when the standard deviations given in parenthesis are considered, it may be that variations between individual values may have been insignificant. In addition, the authors did not mention details

on the locations analysed such as whether the natural surfaces of enamel were used for analysis or cross-sections. This is an important aspect to consider when investigations are comparative in nature as previous studies; such as those mentioned in Section 4.2 Compositional differences have shown mineralisation levels depend on the region of enamel and mineralisation influences caries progression. The method used to measure the depth of rhodamine B in each enamel type also has obvious limitations as it depends on an assumption that all the dye will be extracted from the pores within each sample when samples are immersed in ethanol. This may lead to underestimations if 100% of the dye does not escape.

Using the constant composition technique whereby a mechanical automated mechanism was used to ensure the dissolution media undersaturation level remained constant during enamel dissolution; Wang et al., (2006) measured and compared the demineralisation rates of DE and PE. Results showed that during the initial linear stage of dissolution, DE and PE dissolution rates were $1.5 \pm 0.5 \times 10^{-10}$ mol mm^{-2} min^{-1} and $2.6 \pm 0.5 \times 10^{-11}$ mol mm^{-2} min^{-1}, respectively. Results also showed both DE and PE stopped demineralising after a certain time even though the dissolution media was assumed to be undersaturated with respect to HAp. After SEM analysis of solutions, authors concluded that both enamel types exhibited nanocrystals approximately 30 nm in size that were kinetically protected against further dissolution. However, the degree of saturation relative to HAp used in the study was based upon a solubility product of 5.52×10^{-118}. The halt in demineralisation may have been due to the solubility product being too low which

would have assumed enamel to be more soluble than it actually is. It may be that enamel solubility is actually much lower than previously assumed.

In another study on the influence of enamel type, temperature and exposure time on enamel erosion, Amaechi et al., (1999) used transverse microradiography to measure mineral loss and lesion depth when samples were exposed to orange juice. Both lesion parameters were shown to be significantly lower with decreased temperature. Lesion parameters significantly increased with increasing exposure time to orange juice and both parameters were significantly greater in DE than in PE. Erosion progress was shown to be 1.5 times faster in DE than PE supporting Featherstone and Mellberg's (1981) results. However, results of the study contradict those of Maupome et al., (1999) which show there were no significant differences between DE and PE microhardness tests after treatment with fresh cola. DE and PE showed sharp decreases in Vickers Units from baseline (344.2 and 350.8, respectively) to day 8 of treatment (155.2 and 149.8, respectively). However, results showed that saliva did significantly influence Vickers hardness values by reducing the decrease after exposure to cola.

The results of Maupome et al (1999) study suggests is that greater demineralisation incidence in children's enamel may be due to differences in salivary compositions and flow rates between children and adults rather than differences between enamel types. For example, Watanabe and Dawes (1990) showed that the flow rate of unstimulated whole saliva in children was significantly slower at 0.22 mL/min, than in adults. The volume of saliva in the mouth before swallowing (VMAX = 0.50 mL) and after swallowing (RESID = 0.38 mL) was also shown to be significantly

lower. However, the average thickness of the salivary film in the mouth was very similar to adults at 0.06 - 0.09 mm.

Further, Issa et al., (2003) showed no significant differences were measured with transmission microradiography between DE and PE when exposed to lactic acid gel. In terms of mineral loss and lesion depth, DE was lower on both parameters at 913.2 vol.% μm and 36.1 μm, respectively compared to PE which showed a mineral loss of 1108.8 vol.% μm and lesion depth of 38.8 μm. Further, the mineral content in the surface layer of the lesion formed in DE was significantly higher than in PE in the absence of fluoride, however in the presence of fluoride, though both enamel types showed significant reductions in mineral loss and lesion depth, PE showed a higher mineral content in the surface layer of the lesion formed.

As highlighted above, the uncertainties in the literature that compares DE and PE may be due to differences in the methodologies adopted. Quantitative techniques that are accurate e.g. those that use monochromatic energies or use a focal plane in imaging techniques, and have high resolutions are beneficial to our understanding. Enamel types should also be exposed to identical conditions. These precautions are necessary for limiting artefacts and ensuring comparisons are accurate and reliable.

SECTION 2: CHARACTERISTICS OF X-RAYS FOR DENTAL HARD TISSUE RESEARCH

Chapter 5 : The electromagnetic spectrum

The electromagnetic spectrum can be defined as the range of wavelengths over which electromagnetic radiation extends. The wavelengths of the different types of electromagnetic radiation are important characteristics to know as they determine their uses in technology.

Radio waves have the longest waves at 10^{5}-10^{-3} metres and are useful in transmitting information over long distances. Infrared (IR) waves are at 10^{-3}-10^{-6} metres and can be used for short range communication. Devices such as television remote controls and mobile phones use IR technology. The middle region of the spectrum is occupied by visible light and ultraviolet waves with wavelengths of 4-7 x 10^{-7} and 10^{-7}-10^{-9} metres respectively, whereas X-rays and Gamma rays occupy the opposite end of the spectrum known as the narrow band; with wavelengths at 10^{-9}-10^{-11} metres and 10^{-11}- 10^{-14} metres, respectively (Oxford Dictionary of Science, 2010).

The very short wavelengths of X-rays and gamma rays give them the ability to penetrate material down to the atomic level which makes them useful for medical and scientific investigations. While X-rays are ideal in providing information about atomic and molecular structures of living organisms, gamma rays are mainly used to sterilise medical equipment and kill cancer cells during radiotherapy.

Electromagnetic radiation results from the acceleration of electric charge and the electric and magnetic fields associated with it. These electric and magnetic fields can be described as oscillating waves that propagate through space perpendicular

to one another and also to the direction of propagation at the speed of light (2.9979 x 10^8 metres per second) when in a vacuum.

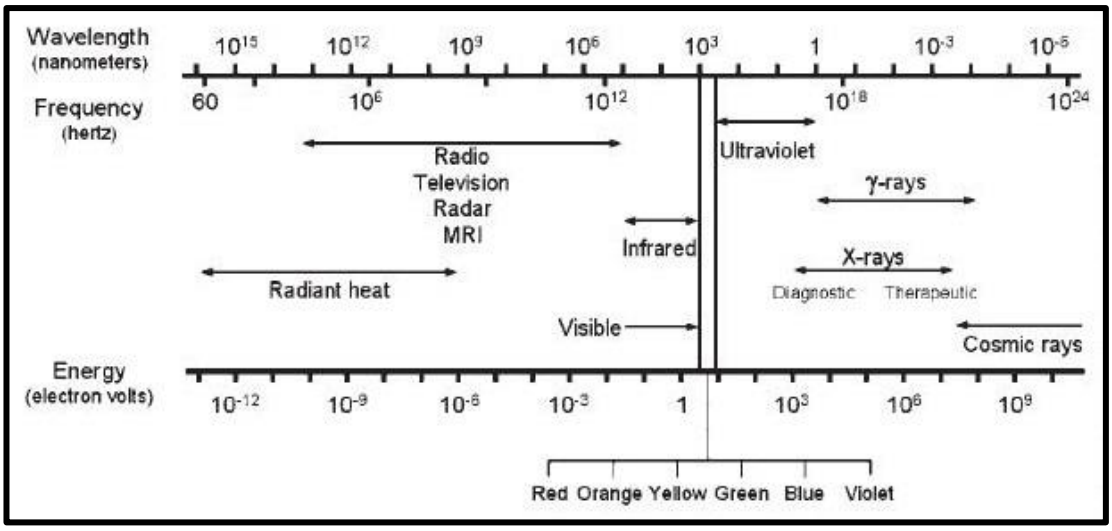

Figure 5.1 The Electromagnetic spectrum as a function of wavelength, frequency and energy. (Image taken from Seibert, 2004)

The idea that radiation travels through space in the form of waves; known as Classical Wave Theory, was accepted up until the end of the 19th century. Thomas Youngs monochromatic light experiment observed that when monochromatic light is passed through a pair of slits, alternating light and dark bands are observed on a screen which are thought to represent the crests and troughs of the waves from the beams of light emerging from each slit. The theory suggests that the light bands represent when the crests or troughs from each beam reach the screen at the same time, the dark bands represent a crest and a trough from each beam reaching the screen simultaneously, thereby cancelling each other out.

Classical wave theory relies on two assumptions:

- Intensity of a wave is the energy incident per unit area per unit time.
- Energy carried by an electromagnetic wave is proportional to the square of the amplitude of the wave.

While classical theory explained interference and diffraction phenomena of light, it failed to explain the absorption and emission of light with regards to the photoelectric effect whereby observations suggest;

- the existence of a threshold frequency – according to classical theory, the energy of a wave is proportional to its squared amplitude, therefore if sufficient intensity is used electrons would gain enough energy to break free regardless of the frequency.

- the immediate emission of photoelectrons – classical theory predicts electrons require time to absorb sufficient energy to break free, therefore a delay in electron ejection would be observed if a low energy source is used to supply energy to the electrons, this does not happen with photoelectrons (Agostini et al., 1988).

- the independence of photoelectron kinetic energy on intensity but its dependence on frequency – classical theory suggests the kinetic energy of an electron is dependent on intensity of the incident wave not on the frequency while the photoelectric effect suggests the opposite is true.

Radiation is emitted in discrete units called quanta rather than continuously like a wave and the energy of a quantum is related to the frequency (v) as follows:

$$E = h\nu \qquad (15)$$

Where E is the energy, h is Planck's constant 6.62607 x 10^{-34} j/s and v is the frequency.

The formula agrees with observations over the entire electromagnetic spectrum wavelength range.

Additionally, light is composed of photon particles which can be absorbed by electrons either whole or not at all, explaining the immediate emission of photoelectrons when a light source hits the surface of a metal. The energy of a photon is given by Plank's equation. For a given metal, there is a threshold frequency (v_0) below which no electrons will be emitted. The energy required to release an electron is known as the work function (W), any energy above which, will be converted to the kinetic energy of the released electron.

Therefore, if;

$$v_0 = W$$

then no electrons will be emitted as there would be no energy left for kinetic energy.

The relationship of energy for an emitted electron is therefore:

$$E = h\nu = W + m_e u^2/2 \quad (16)$$

Where m_e is the mass of the electron and u is its velocity[1].

The Heisenberg Uncertainty Principle is a qualitative argument that explains the inability to simultaneously identify the position of a subatomic particle and its momentum. It purports that if an electron is bound close to the nucleus it must have a small electrostatic energy and so the uncertainty in its position would also be small. However, if the electron is to have small kinetic energy, its momentum and therefore the uncertainty in its momentum would also be small. According to the principle, if the uncertainty in the momentum is small, the uncertainty in its position must be large as both cannot be determined simultaneously (Busch et al., 2007).

An atom size scale is dependent on the minimum possible energy state the atom can achieve and that the uncertainty of the simultaneous determination of both position and momentum of a particle must be greater than Planck's constant. Overall, the size scale of an atom is determined by a compromise between the kinetic and electrostatic energies of the atom so that the average distance between an electron and the nucleus is the distance that achieves the minimum total energy of the atom. Atomic size determines the type of X-rays a metal atom produces, in terms of the X-ray energy produced when bombarded with electrons from a negative cathode. Atomic size is therefore a crucial factor involved in X-ray quantitative techniques such as XMT and SMR as they rely on an understanding of how particular X-ray energies travel through specific materials.

The production of X-rays and how atomic number determines the X-ray energy will be discussed in more detail in the following sections.

5.1 X-ray production

X-ray photons are produced by bombarding a metal target (a positive anode) with electrons from a negative cathode within an X-ray tube (Mould, 1995) (see section 5.2.1 for more on X-ray tubes). The incident electrons interact with the orbital electrons of the target atom resulting in the production of either heat or characteristic X-rays. An Auger electron can also be produced from the transfer of energy to an electron which is then emitted. Removal of inner shell electrons, e.g. from either; K-, L-, M- and O-shells, requires a specified minimum amount of energy known as the 'critical excitation' energy to create a vacancy in an inner shell. X-rays are produced when electrons from the outer shells replace the removed electron, and this de-excites the ionised atom (**Figure 5.2**).

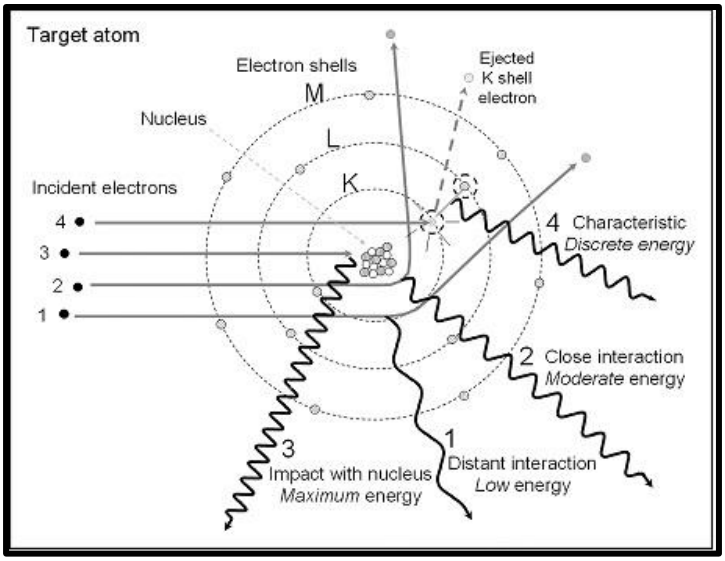

Figure 5.2 X-ray production corresponding to different regions of a target atom when bombarded with incident electrons (1-4). Characteristic X-rays are

produced when an inner shell vacancy, created by knocking off an electron from an inner shell is filled by an electron from an outer shell (4). (Image taken from Seibert, 2004)

5.1.1 Characteristic X-rays

Characteristic line spectrums are produced when an outer shell electron fills the initial vacancy in an inner shell which de-excites the ion, thus leaving a final vacancy in that shell (**Figure 5.3**). The energy of the line is equal to the difference in binding energies of the shells with the initial and final vacancies[2]. Depending on the atomic number of the target atom, the X-ray spectra can include lines from the K, L, M and O series, corresponding to the shells (**Figure 5.3**). The probability that a vacancy in a shell will results in the production of X-rays is the fluorescent yield of that shell, defined as the number of characteristic X-rays per primary vacancy emitted from the shell (Byrne and Howarth, 1969).

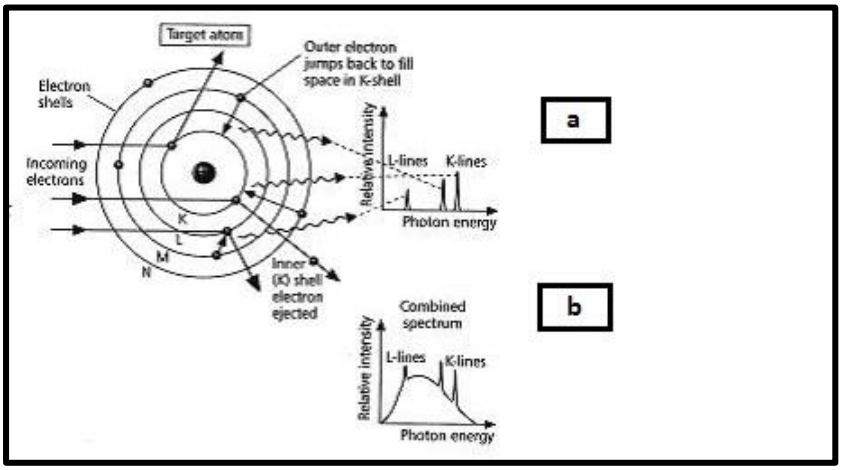

Figure 5.3 Characteristic X-ray production from L- and K-shells and the corresponding line spectrum produced (a). Combined Bremsstrahlung and discrete (characteristic) energy, respectively (b) (Image taken from Pope, 1998).

Bremsstrahlung radiation is produced when incident electrons are decelerated when they come into close proximity of the target atom nucleus, due to attractive forces with the positive protons within the nucleus. The electrons change course dependent on the size of the target atom and its nucleus. The corresponding kinetic energy lost from the incident electrons due to the extent of their deceleration is converted to bremsstrahlung radiation. Electrons that come in close proximity to the nucleus can lose all their energy, producing maximum energy output. The probability of this occurring is very low as this is extremely rare. The energy output produced by a decelerated electron decreases with increasing distance from the nucleus and the probability of decelerated electrons incidences also increases with distance. As a result, a linear spectrum showing an increasing number of X-rays (intensity) as output energy decreases is produced (**Figure 5.4**).

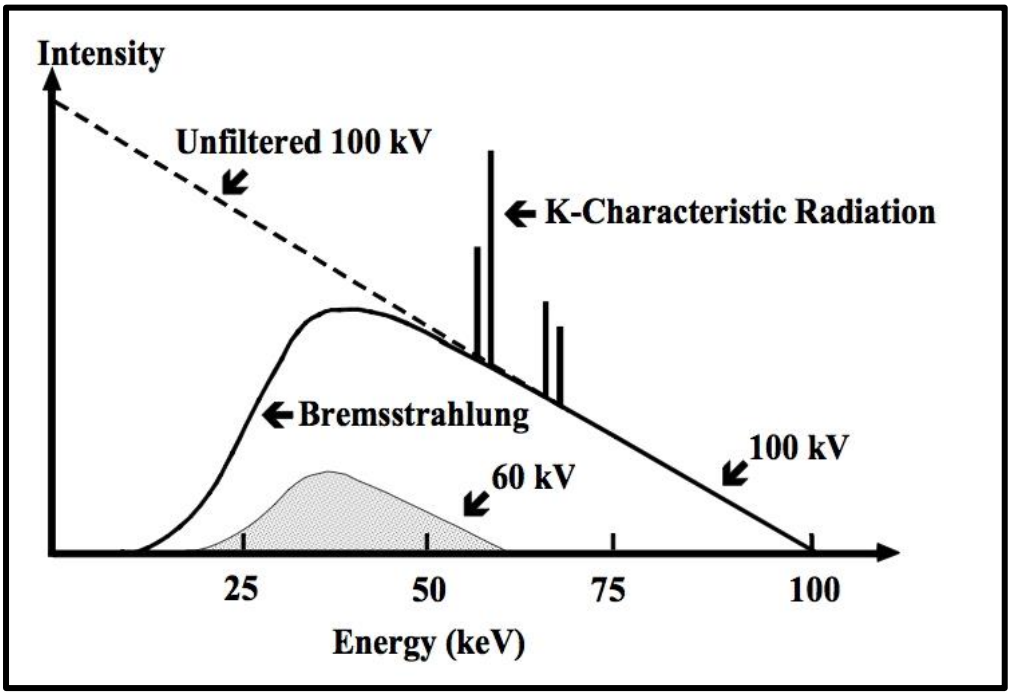

Figure 5.4 Unfiltered Bremsstrahlung radiation (dotted lines) and filtered Bremsstrahlung radiation (continuous line) at 100kV. Intensity reduces as

lower energy X-rays are attenuated and are therefore undetected. Intensity increases with increased voltage (60kV and 100kV).

However, when X-rays travel through a medium they are filtered (attenuated) with lower energy X-rays increasingly attenuated (see section 5.2.3 for more on X-ray attenuation). The resultant spectrum therefore shows low intensities of high energy X-rays followed by an increase in intensity at medium energy X-rays, followed by a further decrease in intensity at lower energy X-rays due to an increase in attenuation (**Figure 5.4** (continuous line)).

The individual sub-shells of a shell, other than the K-shell, have characteristic fluorescent yields and Auger yields, and the flux of X-rays depends on the initial distribution of vacancies among the sub shells. However, details concerning the de-excitation of the L-shell and higher shells is limited as the situation is complicated by the presence of sub-shells, e.g. initial vacancies may be transferred from one sub shell to another in what is known as Coster-Kronig transitions (Bambynek et al., 1972) resulting in there being little theoretical work on yields and contradictory experimental results (Byrne and Howarth, 1969). In comparison, research focused on the K-shell fluorescent yield has been more extensive as it only holds 2 electrons and so only 2 yields are concerned. As a result, K X-rays are the most useful for diagnostic imaging (Seibert, 2004).

5.1.2 X-ray tube

Approximately 1% of the energy in an electron beam is converted to photons when electrons bombard a metal target to generate X-rays. The rest is converted to heat.

The anode (metal target) is therefore rotated 360° so that a fresh surface, rather than the same surface, is continually exposed to the large amount of heat generated by the electron beam bombarding it.

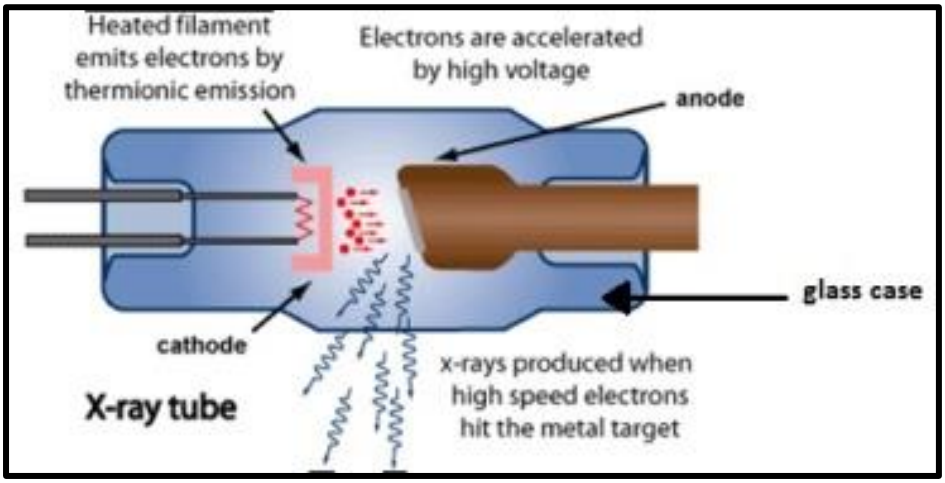

Figure 5.5 schematic diagram of a typical X-ray tube showing the emission of electrons from a heated cathode bombarding the target (anode) and producing X-rays.

5.2 X-ray interactions with matter

As demonstrated by the Bremsstrahlung spectrum in **Figure 5.4**, X-rays are attenuated when they interact with matter, with an increase in attenuation as X-ray energy decreases - as shown by the decrease in X-ray intensity as energy decreases. This is distinct from unfiltered X-rays, such as those travelling in a vacuum, where intensity increases with decreasing X-ray energy.

The interaction of X-rays with matter depends on the amount of energy the incident photon possesses relative to the sub-atomic particle it hits.

5.2.1 Rayleigh scattering

Elastic collisions are defined as collisions where no kinetic energy is lost and conservation of momentum is observed, meaning that the linear momentum of particles within a system where no external forces are applied is constant in direction and magnitude irrespective if reactions occur in parts of the system. Being a parametric process, this type of collision results in the incident photon retaining its energy after collision with an electron strongly bound to the inner orbital (Williams, 2009).

X-rays with low energies at approximately 10keV interact with matter through coherent scattering also known as Rayleigh or Thomson scattering which is elastic (Daniel et al., 2013). This is because electrons are temporarily exited by the incident beam, but not enough to be knocked out of their shells'; they then relax and release electromagnetic energy. The sum of the released energy exits as a scattered photon that equates to the incident beam photon energy (Cooke, 2009).

5.2.2 Compton scattering

Compton scattering is inelastic scattering whereby there is partial transfer of energy from an incident photon to an electron. An X-ray photon of lower energy and therefore greater wavelength than the incident photon is scattered at an angle that is different from the incident photon due to interaction with an electron. The dislodged high-speed electron is called a Compton scattered electron or recoil electron (Blumenthal and Gould, 1970).

In Compton scattering, the incident photon energy is far greater than the work function of the attenuating material, electrons are therefore considered as “free electrons” with which incident photons collide transferring some of their energy to the electron and causing it to recoil.

There is an inverse relationship between the scattered photon and ejected electron energy, i.e. if the electron recoils with a large kinetic energy then the X-ray will have an associated low amount of energy, given that the total amount of energy within the system must remain constant (Cooke, 2009).

The angle that the recoiled electron is emitted depends on the energy transferred from the incident photon. If maximum energy is transferred, the electron will follow the same course as the incident photon and the photon will change direction by 180°. If the amount of energy is minimal, the electron will recoil at an angle of 90° to the incident photon with minimal deflection of the photon. Most electrons recoil at angles within these two extremes (Cooke, 2009).

With the understanding that low energy X-rays attenuate more than high energy X-rays when travelling through a medium, as shown by the Bremsstrahlung spectrum, it therefore follows that the amount of scattered radiation due to low energy X-rays, i.e. when electrons recoil with low kinetic energy, will be greater than the amount of scatter radiation from high energy X-rays, i.e. when electrons recoil with high kinetic energy due to a larger transfer of energy from the high energy X-ray upon collision.

Whilst Compton scattering is independent of atomic number – the interaction process only involves free electrons, it is dependent on the physical density and the electron density of the material. Also, the mass attenuation coefficient (MAC) for Compton scatter decreases with increasing beam energy e.g. MAC is inversely proportional to keV as shown in **Figure 5.6** below.

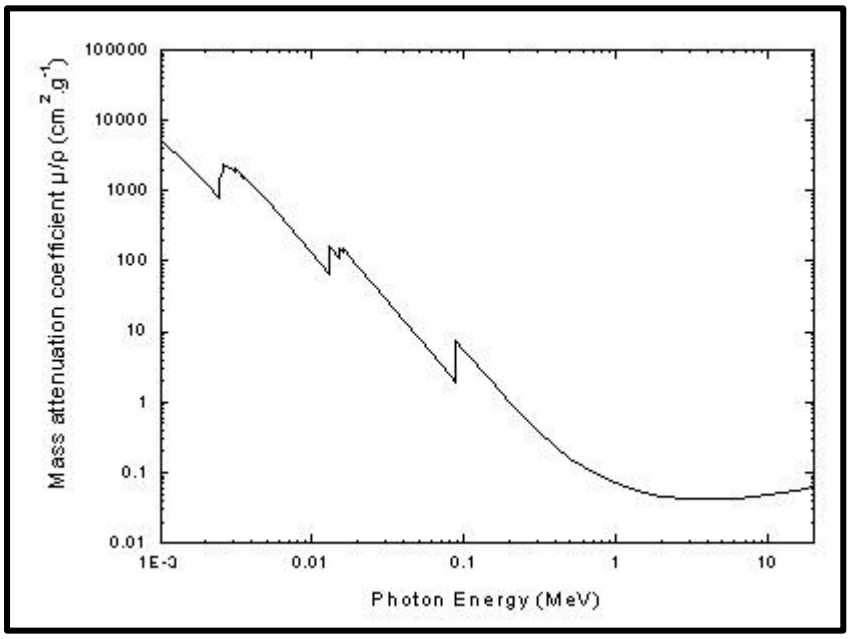

Figure 5.6 Mass attenuation coefficient (cm^2 g^{-1}) of a material is inversely proportional to the photon beam energy $(MeV)^3$.

At energies of 100keV the absorption of radiation is mainly due to Compton scattering (Daniel et al., 2013).

5.2.3 Photoelectric effect

An inner shell electron with a slightly lower binding energy than the incident photon is dislodged (Pratt et al., 1973). An outer shell electron fills the vacancy. A

characteristic X-ray is emitted that is equal to the energy difference between the two electron shells. When the work function is much lower than the incident X-ray photon energy, the electron will exit at a high angle to the photon whereas when the work function is similar to the photon energy is will exit close to parallel with the photon (Daniel et al., 2013). Photoelectric absorption is the dominant process for incident X-ray energies up to 500KeV (Daniel et al., 2013) (see section 5.1.1 for more on characteristic X-rays).

5.2.4 Pair production

Pair production occurs when the incident photon energy is greater than 1.02MeV. Upon interaction with the electric field of the nucleus; the photon energy is converted into electron (e-) and positron particles (e+). The newly formed electron eventually reduces a nearby atom requiring an electron, while the positron destructively interacts with another nearby electron resulting in their rest masses converting into two photons with equal energy distribution of 0.511 MeV each, each moving in the opposite direction (Daniel, 2013).

5.2.5 Photodisintegration

When an incoming photon is captured by the nucleus and all the energy of the X-ray is absorbed, a particle from the nucleus is ejected. For such an interaction to occur; the incident X-ray photon should have energy greater than 10MeV. In excessively high energy beam interactions with a nucleus, the nucleus becomes so unstable that particles such as protons, neutrons, deuteron and even an alpha particle can be emitted. Due to the very high energies of x-rays needed for this type of interaction it is sometimes not used in radiography.

5.2.6 X-ray attenuation of hydroxyapatite

The way in which X-rays interact and are attenuated by HAP, is widely studied and understood and has consequently led to the development of many X-ray techniques used in dental research such as; scanning microradiography, X-ray diffraction and X-ray microtomography (Ishikawa et al., 1993; Elliott et al., 1997; Peters et al., 2000; Anderson et al., 2004). Using HAp as a standard to compare with enamel - considered to be an impure form of HAp, is a direct way to measure the mineral content of enamel with respect to HAp.

The linear attenuation coefficient (LAC) of a material refers to the degree to which a material of known thickness interferes with the path of an incident X-ray beam of known energy and nature. This value accounts for the number of atoms in a cubic cm volume of material and the probability of a photon from an incident beam being scattered or absorbed from the nucleus or electron of the attenuating material. It is expressed in units of cm^{-1}.

When scattered, the photon will either retain all or lose some of its energy to the atom and continue on at a different direction. When X-rays are absorbed, their energy is transferred to the atom.

The LAC is specific to the material and so can be used to identify unknown materials and to also quantify the amount of a specific material in a sample. Therefore, attenuation of X-rays is dependent on the energy of the incident beam, the density and nature of the target material and the atomic number of the material.

In materials that have a homogeneous composition and where monochromatic X-rays are used, an exponential relationship between the incident (I_0) and transmitted beam (I) energies is observed. This is expressed by the Beer-Lambert Law whereby:

$$I = I_0 e^{-\mu x} \quad (17)$$

Where; e is a proportionality constant that reflects the total probability of a photon being scattered or absorbed, x is the thickness of the sample material and μ is the LAC[4].

At a given incident beam energy, the LAC of a material can change with varying degrees of density. A lower LAC for a given material indicates it has a low density, e.g. LAC through water vapour would be lower than LAC through ice as the probability of a photon hitting a water particle is less likely in vapour. Therefore, the mass attenuation coefficient (MAC), μ_p, is used to normalise the LAC by the density and describes the attenuation per unit density of material (Jonson, 1993), so that;

$$\mu_p = \mu/p \quad (18)$$

Where; p is the density and μ is the LAC (Hubbell, 1982).

MAC values are typically expressed in units of cm^2g^{-1} and values for various characteristic wavelengths are reported in the International Tables for Crystallography (Creagh and Hubbell, 1992).

For substances containing more than one element, the MAC is important as it takes into consideration the weighted average of the MACs for each element (Hubbell, 1982). Therefore, for HAp the MAC would be calculated as follows:

$$\mu_p = w_1 (\mu/p)_{ca} + w_2 (\mu/p)_p + w_3 (\mu/p)_o + w_4 (\mu/p)_H \quad (19)$$

Where w is the weight of the corresponding element and μ/p is the MAC for each corresponding element. The MAC for HAp is 4.69 g/cm^2 calculated for AgKα radiation at 22.1 KeV.

5.2.7 Energy bands

Electrons occupy distinct shells that are divided into energy levels (sub shells) orbiting the nucleus within the atom.

A solid is made up of many atoms; therefore, energy levels overlap to accommodate the electrons of neighbouring atoms and results in denser energy levels. Eventually distinct energy levels become very close to the point where adjacent discrete energy levels form energy ranges or bands as the molecular orbitals become increasingly larger as atoms continue to join together to form the solid. Discrete energy levels now form a continuous distribution of energy within a band due to the Pauli Exclusion Principle which states that electrons cannot exist in identical energy states (Massimi, 2005).

At absolute zero, electrons pack into the lowest available energy states. Band gaps occur between the boundaries of two energy bands that the electrons can occupy as they have finite widths, the borders between energy bands and band gaps are known as Fermi levels (**Figure 5.7**). Band gaps are leftover energy ranges where no electrons can occupy due to a lack of energy.

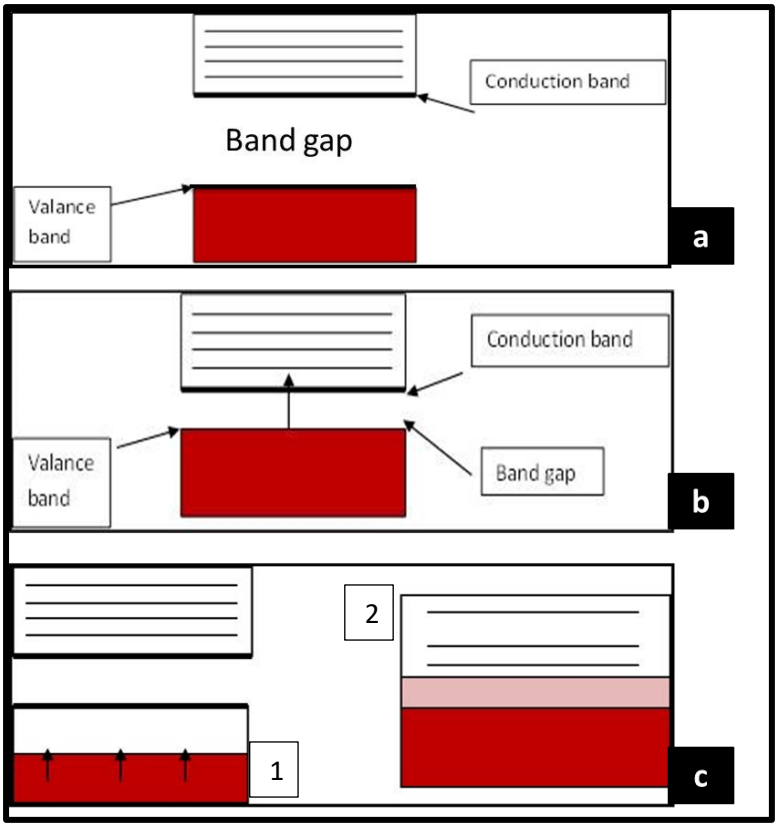

Figure 5.7a-c Band gaps and energy levels of an insulator, semi-conductor and conductor, respectively. Electrons cannot jump across the band gap when an electric field is applied to an insulator as the band gap is too large (a). Electrons in a semi-conductor can jump across the band gap if energy is applied (b). In a conductor (c), electrons can either occupy higher energy levels within the same energy band (1) or the valence and conductor bands will overlap resulting in there being no band gap (2).

In semiconductors, such as germanium and silicon, there is a distinct band gap above and below the Fermi level (**Figure 5.7b**). The band below the Fermi level is the valance band and the band above the Fermi level is the conduction band. The valance band is the highest range of electron energies where electrons are present at absolute zero temperature and the conduction band is the lowest range of vacant electron states where no electrons are present at absolute zero temperature.

When an electric field is applied, the ability to excite electrons in the valance band to the extent that they cross the band gap into the conduction band is a reflection of how conductive the material is.

Electron movement depends on the Fermi level of a body; i.e. the thermodynamic work required to add an electron to it. The Fermi level can be described as the thermodynamic equilibrium level at which there would be a 50% probability of an energy level being occupied by an electron (**Figure 5.8**).

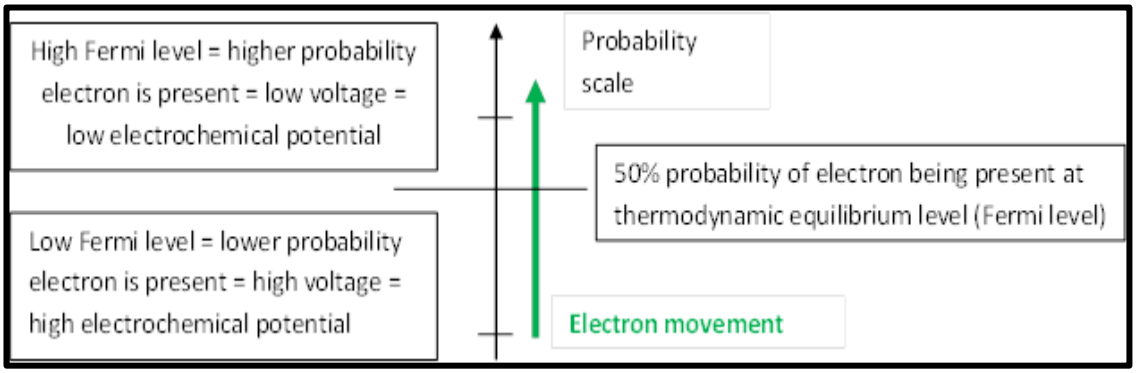

Figure 5.8 Illustration describing Fermi level and the implications on electron movement.

Electrons will move from a low Fermi level (high voltage) to a higher Fermi level (low voltage level) from a high electrochemical potential to a lower electrochemical potential.

5.3 Advantages of using X-rays for dental research

The main advantage of using X-rays for dental research is that the resolution achieved is far greater than that achievable for techniques using light. For example, in a study on deriving the solubility product of enamel from demineralisation rates,

Zhang et al., (2000) discuss the importance of using accurate and high resolution monitoring techniques when attempting to derive solubility constants from kinetic data since it is difficult to distinguish between very low rates of demineralisation and no demineralisation, i.e. to identify equilibrium between demineralisation and remineralisation.

Techniques such as X-ray microtomography, scanning microradiography and scanning electron microscopy provide information at the micron and sub-micron length scale allowing researchers direct access to microstructures and processes that otherwise could not have been viewed using light microscopy.

As our understanding of X-ray characteristics and X-ray interactions with different types of matter develops, and as databases providing information on X-ray attenuation coefficients of different materials expand; techniques such as scanning microradiography and X-ray microtomography are continually being improved. For example, the use of monochromatic X-ray radiation rather than polychromatic X-rays in XMT imaging minimises artefacts associated with beam-hardening of polychromatic radiation whereby lower energy X-rays -“soft X-rays” are absorbed preferentially leaving only higher energy photons or “hard X-rays” (hence the term “beam-hardening”) resulting in artefacts appearing as dark bands or cupping effects (Davis et al., 2008).

SECTION 3: QUANTITATIVE TECHNIQUES

Chapter 6 Quantitative techniques used to study enamel

Understanding biophysical phenomena requires the use of quantitative data that can be interpreted through the use of statistical analysis. Biological phenomena such as biomineralisation and pathogenic mechanisms like caries are complex and are influenced by multifactorial processes. Quantitative research techniques such as X-ray and light scattering devices that quantify photons attenuated or scattered by a material are therefore required to conduct comparative research in a highly controlled setting. For example, samples can be exposed to different conditions under controlled settings in order to compare the effectiveness of each condition; samples can be investigated before and after treatments. As data collected is quantitative, statistical analysis such as t-tests can be conducted to identify whether differences between conditions are significant or insignificant.

6.1 X-ray microtomography (XMT)

The discovery of X-rays revolutionised diagnostic medicine by introducing a non-invasive technique for seeing inside the body. The attenuation coefficient of a specimen determines the two-dimensional (2D) image produced, more specifically; each point on the image created is a summation of all the attenuation coefficients of the features throughout the depth of the specimen through which the X-ray beam passes.

The main limitation of two-dimensional X-ray images is the loss of information throughout the depth of a specimen as three-dimensional data is compressed into a two-dimensional plane. Features such as tumours can be missed because of greater attenuating overlapping tissues. Moreover, different features with similar attenuation coefficients cannot be distinguished from one another leading to further underestimations and inaccuracies. The size of a feature relative to the surrounding mass is also a limiting factor with decreasing size requiring a greater difference in X-ray absorption between the surrounding mass and the feature in order for it to be identified (Davis and Wong, 1996).

Such limitations associated with two-dimensional X-ray imaging do not apply to computed tomography (CT) as three-dimensional images are produced. XMT improves upon this to produce images with a resolution of micrometres. Linear attenuation coefficients are accurately measured at different angles of the specimen to capture features present throughout the depth of a specimen. Morphology can therefore be mapped precisely.

Tomography digitally cuts open a specimen using X-rays ("tomos" is Greek for "slice"), by directing X-rays through a slice plane at different angles and measuring their decrease in intensity. The distribution of X-ray attenuation is then reconstructed mathematically. Slices are stacked up to form the 3D image of the specimen.

In addition to imaging, XMT is also used for quantitative analysis of mineralised tissues, as long as there is a *priori* knowledge of composition. The relationship between the mass absorption coefficient of a known substance and its LAC can be

used to measure the mineral densities of hard tissues, as described in section *5.2.6 X-ray attenuation of hydroxyapatite*. An accurate measurement of the mineral densities of hard biological tissues, such as bones and teeth, in relation to their morphology is essential to the development of our understanding of biomineralisation mechanisms, processes and also of pathological pathways. For example, low mineral density is associated with greater demineralisation rates in teeth (Wilson and Beynon, 1989) which are heterogeneous in terms of mineral density (Djomehri et al., 2015), therefore the risks associated with caries will be greater where mineral density is known to be low; such as at the cervical margins and within fissures. Quantification of the local mineral content and mineral gradients within enamel will therefore facilitate the development of more effective prevention strategies against caries.

One of the main advantages XMT has over light microscopy in studying histomorphometry of hard tissues is the ability to use unaltered whole specimens, with the only requirement being that they should be small enough to fit into the scanning volume. This makes XMT ideal for studying whole tooth specimens. Conventional light microscopy requires sectioning of calcified tissues which are ground down to a thickness of 80-100 µm sections so that transmitted light can penetrate the sample under observation. Producing thin sections of hard tissues such as enamel is challenging due to the brittle nature of such tissues fracture is common. However, lateral spatial resolution of approximately 0.3 µm can be achieved (Engelke et al., 1993) although light microscopy is limited to only

producing images for histological and morphological purposes and unlike XMT cannot accurately and quantitatively assess the degree of mineralisation.

The following sections will provide background information on XMT in terms of how it works with a description of the X-ray generation technique and imaging processing used. Previous studies on enamel using XMT will also be described and discussed to evaluate XMT as an effective quantitative measurement technique in dental research. Section 4, Chapter 7 of this report will then give an account of how the XMT system at Queen Mary University of London was used to quantify and compare the mineral concentrations and mineral gradients of DE and PE in this study.

6.1.1 XMT apparatus and function

Unlike X-ray transmission computed (axial) tomography (CT or CAT) scanners where a ring of detectors are mounted around a central specimen (**Figure 6.1**), the MuCAT 2 XMT scanner at QMUL comprises of a turntable which holds the specimen and rotates it about an axis perpendicular to a cone shaped X-ray beam that is detected by a single detector positioned opposite to the X-ray source (**Figure 6.2**).

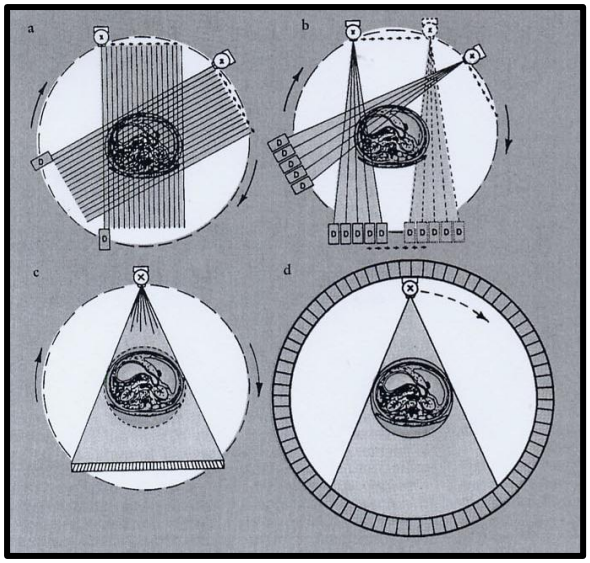

Figure 6.1 Evolution of geometries of X-ray CT scanners (a) First generation scanner - a pencil X-ray beam is translated and rotated to cover the object being imaged. (b) Second generation scanner - a diverging fan beam and detector array are translated and rotated. (c) Third generation scanner - a fan beam source and detectors rotate together. (d) Fourth generation detector - a rotating fan beam source and a stationary ring of detectors (image taken from Hendee, 1995).

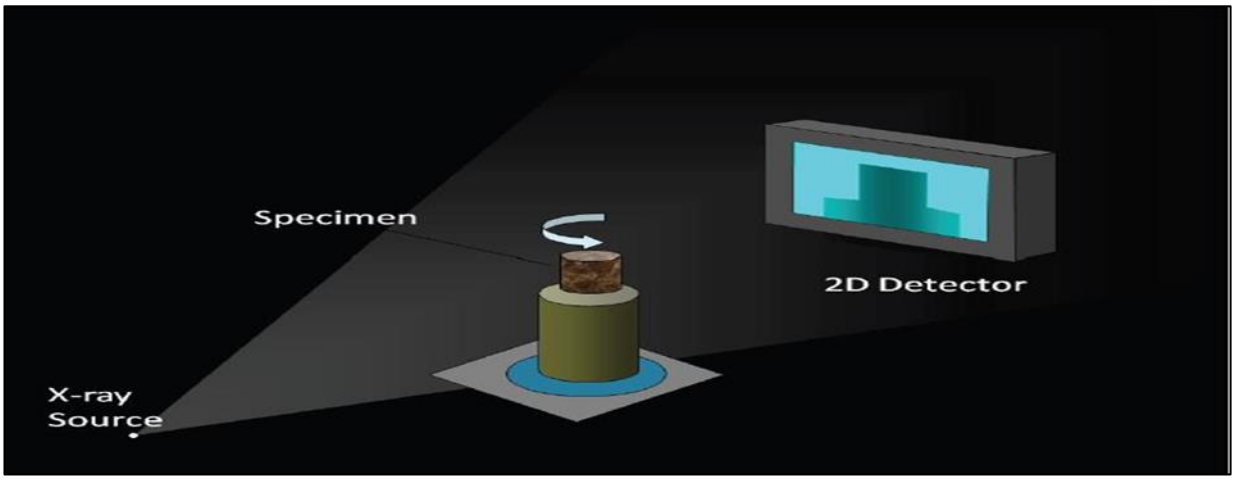

Figure 6.2 Image showing the layout of the XMT MuCAT 2 scanner used at QMUL (image taken from Evershed et al., 2012).

The camera (Spectral Instruments, Tucson, Arizona) is a 800S series charged coupled detector (CCD) system with a 16 megapixel Fairchild CCD485 sensor

attached via a fibre-optic faceplate to an approximately 100µm thick columnated Caesium Iodide scintillator (Applied Scintillation Technologies, Harlow, Essex, UK) - needed to convert the X-rays into visible light that the camera can detect. A cooling system is also needed to ensure the CCD remains at -30^{o}C. This is achieved by using the fibre-optic piece which acts as a thermal insulator to the CCD as well as stops X-rays from reaching and disrupting the CCD (Davis *et al.*, 2013). However, although exposure levels required for XMT can cause damage to the CCD device, studies suggest that damage is minimal at energies below 60keV (Allinson, 1994).

Increased exposure time is a method used to compensate for the reduction in signal to noise ratio due to the lower flux of X-rays in conventional microfocus X-ray sources than in full-sized medical CT scanners. Time –delay integration (TDI) is a technique developed to overcome systematic errors such as ring artefacts resulting from inhomogeneities in detector responsiveness due to increased exposure time (Davis et al., 2013).

Flat panel detectors have the advantage of being able to produce a higher geometric magnification factor than CCD detectors as the flat panel detector and X-ray source can be placed further apart because they are bigger, thus a thicker scintillator can be used to obtain the same resolution. Determining the thickness of the scintillator is a compromise between making it thin enough to reduce light scatter and giving good resolution but thick enough to absorb a good proportion of X-ray photons. Nonetheless, CCDs have a higher dynamic range; good linearity and TDI mode can only operate using CCDs.

6.1.2 XMT X-ray generation

A 225 kV microfocus X-ray generator with 5µm focal spot size from X-tek (Nikon Metrology, Tring, Hertfordshire, UK) is used. A cylindrical tungsten target is used to produce a polychromatic cone shape X-ray beam.

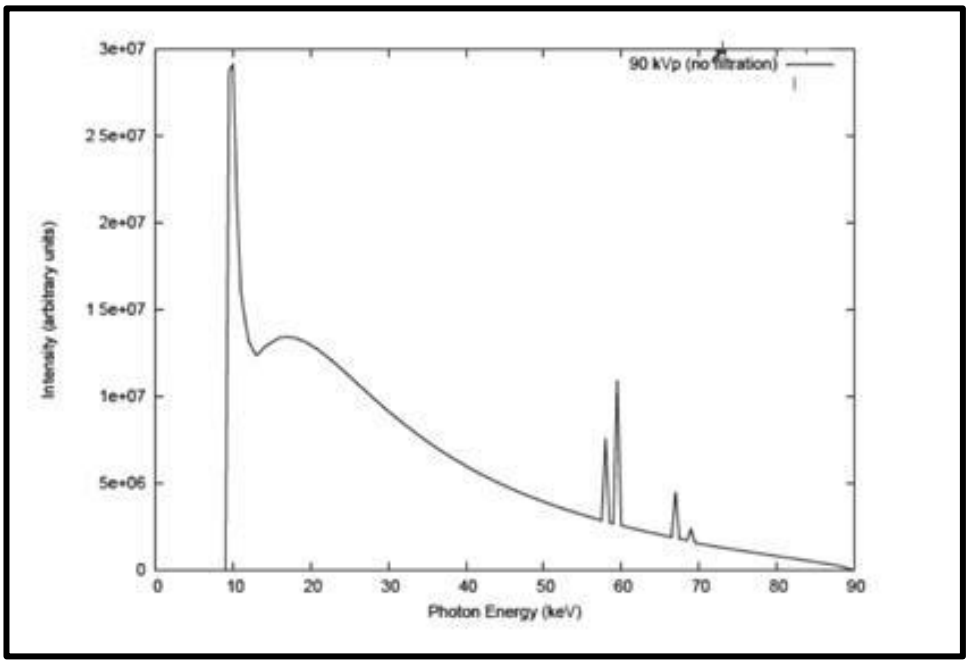

Figure 6.3 Unfiltered tungsten X -ray emission spectrum at a peak potential of 90 kV. (Image taken from Poludniowski et al., 2009)

An energy selective photon counting system records photons in a narrow energy window that is centred on a characteristic peak in the X-ray spectrum to reduce artefacts associated with polychromatic radiation.

6.1.3 3D Imaging processing

Dark and light projections with the shutter closed and open (but without the specimen) are taken before scanning to correct for leakage and scatter from the apparatus. The CCD485 chip has a pixel size of 15µm, binned at 2 x 2 and a further 2

x 2 after TDI readout, giving a recorded pixel size of 60µm. This is a close match for the scintillator thickness (100µm).

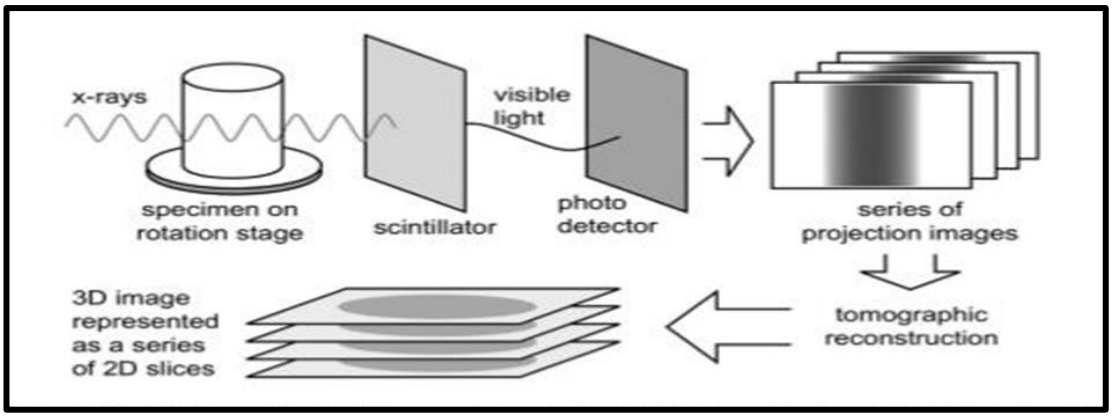

Figure 6.4 A schematic diagram showing the scanning and reconstruction process to create a 3D image (Landis and Keane, 2010).

In TDI mode, the camera and aperture are moved through the beam in synchrony with the clocking of the CCD and with the CCD's serial register perpendicular to the motion. Thereby, each pixel in a row on the image is composed of the charges stored by each of the CCD elements (in a column). This eliminates the occurrence of ring artefacts due to variations in detector element sensitivities (**Figure 6.5** and **Figure 6.6**). The exposure time is the time taken for the CCD to move by its own width. This can vary as the recorded image can have a width of up to 2700 pixels and is 1000 pixels high (Davis et al., 2013).

For further increases in dynamic range, frame averaging is performed whereby a number of individual exposures are averaged to simulate long exposures.

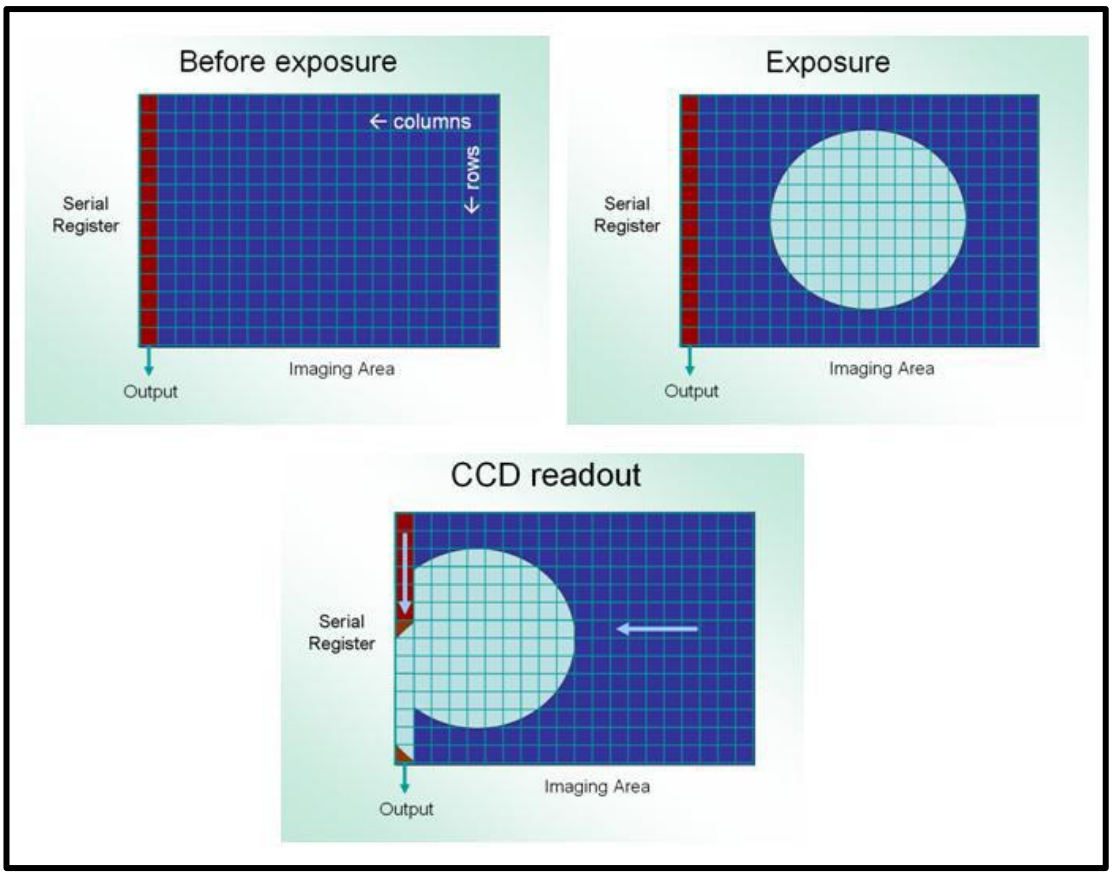

Figure 6.5 CCD reads out the data obtained from a circle being imaged. The camera and aperture are moved through the beam in synchrony with the clocking of the CCD and with the CCD's serial register perpendicular to the motion.

To increase special resolution by a factor of 2 while maintaining the signal to noise ratio, exposure will need to be increased by a factor of 16 with a 10,000-fold increase required for a 10-fold improvement in resolution. This is because noise is inversely proportional to the product of the pixel step size and the square of the number of photons detected. To reduce the pixel by half, beam width needs to be halved, therefore exposure time would need to increase by a factor of two if pixel width is halved and again by another factor of two if pixel depth is halved.

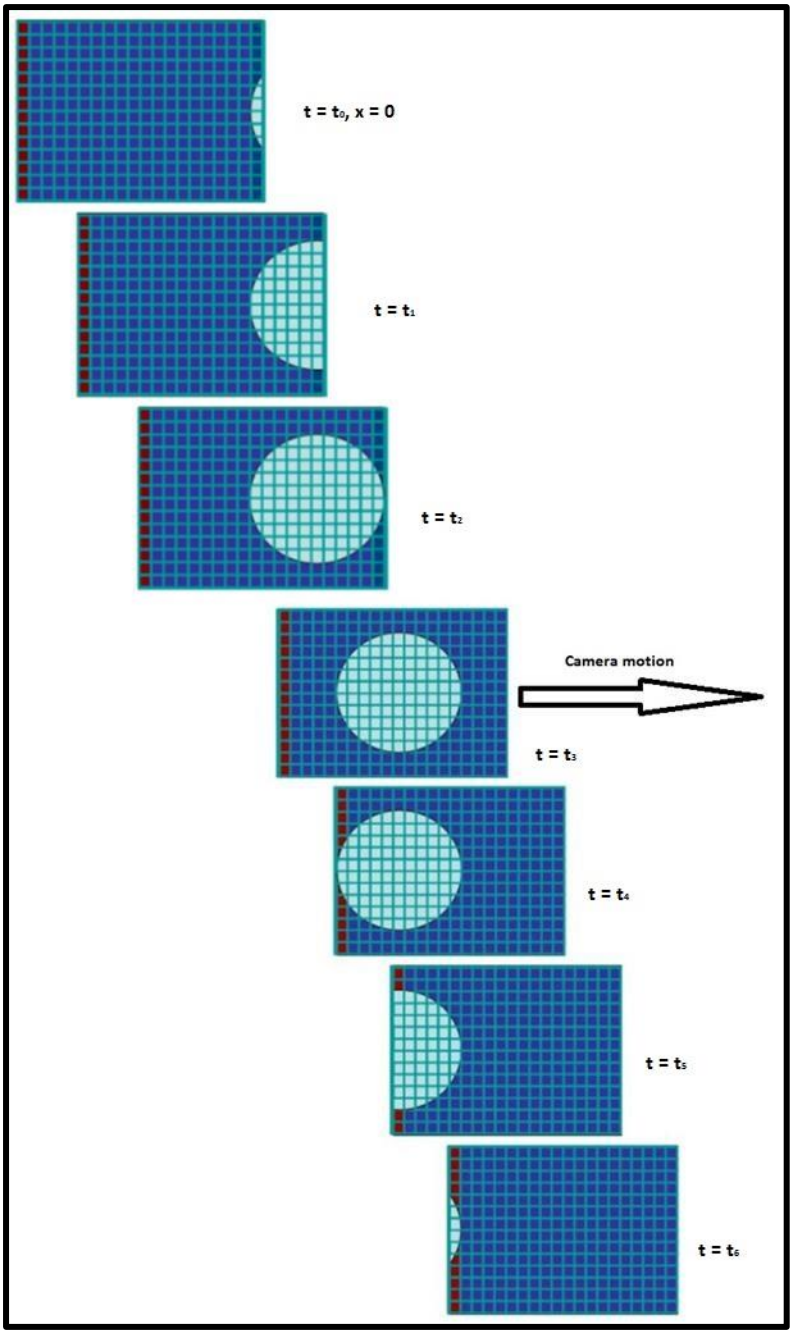

Figure 6.6 Time sequence showing TDI CCD read out of the captured image. The camera and aperture move through the X-ray beam capturing and reading out data simultaneously.

6.1.3.1 Beam hardening and Calibration

When a polychromatic beam travels through a sample, low energy photons are attenuated preferentially causing beam hardening. Images appear to show greater

attenuation at the periphery of objects (appearing brighter) than nearer the centre, this is known as cupping or dishing artefacts. In addition, the amount of beam hardening for a given level of attenuation varies according to the composition of the attenuating material. Any correction curves employed must therefore be adjusted for both operating voltages and specimen material type. To account for such variables, linearisation curves are derived from experimental attenuation data. To correct for beam hardening of hard tissues such as enamel and hydroxyapatite, aluminium has been used as a filter to the X-ray beam and also to calibrate the polychromatic beam to monochromatic energy. Aluminium is used as a calibrator for hydroxyapatite as it has similar X-ray attenuation versus energy characteristics to hydroxyapatite due to both having similar atomic numbers. Also, hydroxyapatite attenuation does not exceed or approach the maximum attenuation for aluminium, thus reducing further errors associated with the extrapolation of data as with polynomials (Davis et al., 2008).

An aluminium step wedge composed of 0.5 mm thick individual aluminium sheets is then used for calibration (**Figure 6.7**). Each step increases in thickness by the incremental addition of 2 sheets on either side of the central sheet. Each step can be scanned individually to avoid scatter from thinner steps.

Figure 6.7 Aluminium step wedge for X-ray attenuation measurement used for calibration and beam hardening correction. Each step is scanned one step at a time to reduce scatter from other steps (Image taken from Evershed et al., 2012).

At first, the beam is pre-hardened (filtered) using a combination of a 1.2 mm aluminium and 50 µm copper filter. This removes soft X-rays thereby reducing the overall width of the spectrum and therefore reducing the differences between the beam hardening of aluminium and hydroxyapatite. However, filtering the beam reduces the signal to noise ratio by reducing X-ray flux which requires longer exposure times to compensate for the reduction.

Linearisation transforms the measured attenuation to the value that would be anticipated for monochromatic radiation at a pre-determined energy. Linearisation depends on both the X-ray spectrum in terms of accelerating potential; target material; take-off angle; filtering and scintillation material and thickness, and on the

composition of the specimen, hence the linearisation curve is derived from experimental attenuation data using the aluminium step wedge.

Table 6.1 Variations in linear attenuation coefficient of enamel and dentine with decreasing energy (keV) (Image adapted from Dowker et al., 1997).

Energy (keV)	*Linear attenuation coefficient (cm^{-1})*	
	Enamel	*Dentin*
400	0.29	0.21
300	0.32	0.24
200	0.39	0.28
100	0.59	0.41
75	0.82	0.54
50	1.67	1.01
40	2.78	1.63
30	5.88	3.34
25	9.74	5.47
20	18.40	10.26

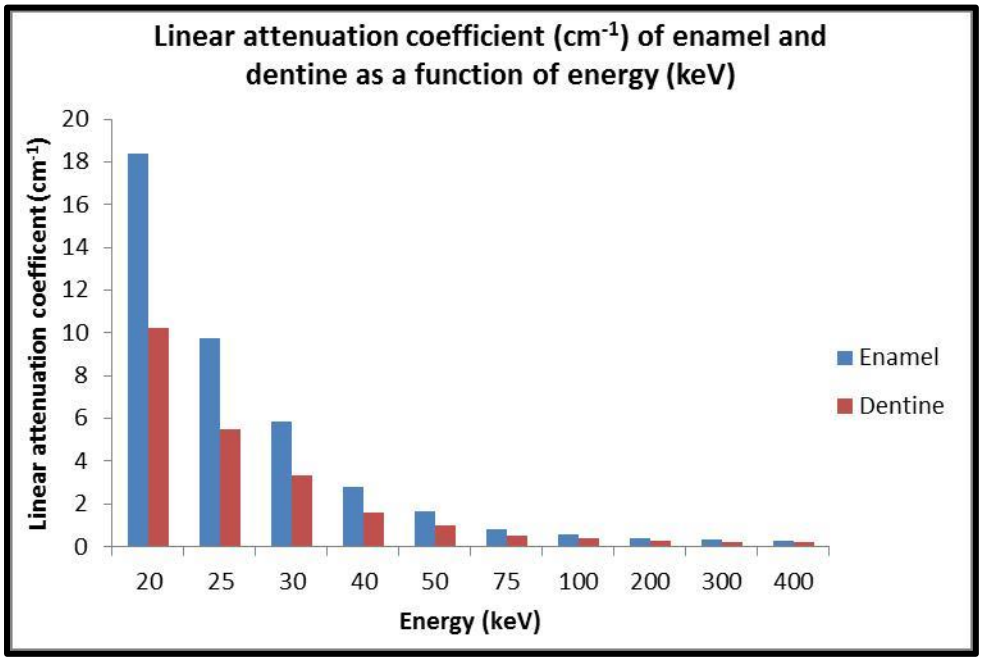

Figure 6.8 Plotted data from **Table 6.1** showing LAC of enamel and dentine as a function of increasing energy

Attenuation measurements are made from average grey levels within each step as it increases in thickness between 1 and 50 layers of aluminium. Then a polynomial is fitted to derive the linearisation curve. When operated at an X-ray acceleration voltage of 90 kV, the XMT system at QMUL gives a similar value of attenuation using polychromatic radiation (approximately 50%) for a 6 mm thickness of aluminium as would a monochromatic source at energy of 40 keV with the same thickness (Davis et al., 2013). The LAC of the sample in the final reconstruction are therefore calibrated to the measured aluminium LAC at 40 keV as if monochromatic energy were used; so that each CCD column (corresponding to image rows) is fitted using a 5^{th} order polynomial curve, to the calculated attenuation for aluminium at 40 keV.

Recently, an improved calibration system has been employed which offers an increased range of attenuations available. A carousel comprising an odd number of metal sheets of known composition are illuminated individually by the cone-shaped X-ray beam (**Figure 6.9**).

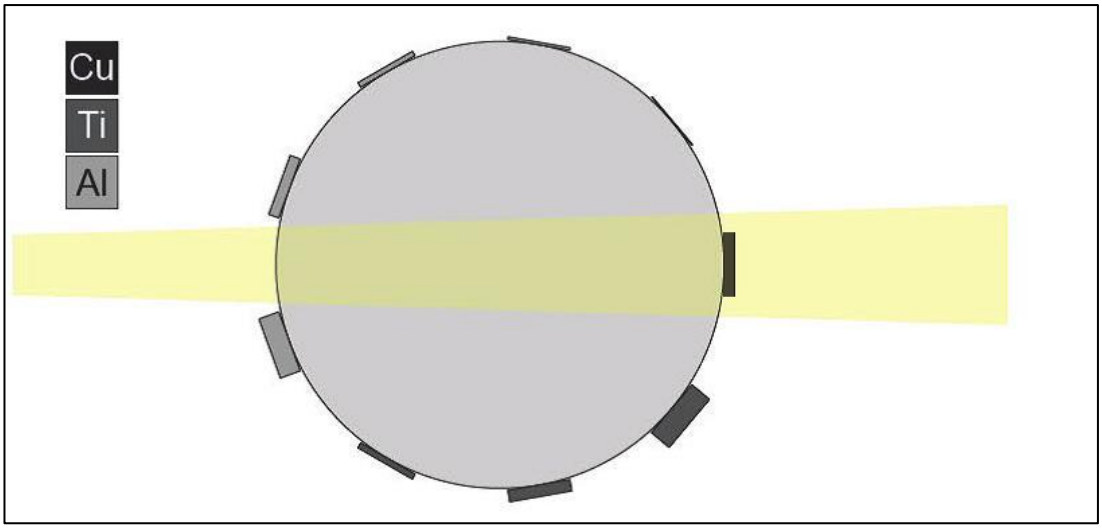

Figure 6.9 Schematic of the beam hardening carousel showing the illumination of copper by the X-ray beam. (Image taken from Evershed et al., 2012).

Once the attenuations of all the metals have been collected, a similar correction as used by the aluminium step wedge method can be made for an arbitrary specimen like hydroxyapatite, whereby the correction should equate the measured attenuations of the carousel metals to those that would be produced by a median monochromatic energy. The energy selected will produces 50 % photon attenuation in the same thickness of aluminium as would be required to produce 50 % attenuation of a polychromatic beam at the voltage used.

6.1.4 XMT studies on enamel

Mineral concentration calculations of hydroxyapatite using LAC measurements from XMT have been shown to be accurate, with absolute accuracy of the LAC of better than 1% when compared with measurements of density using mass and volume calculations of hydroxyapatite. In a study on the efficacy of caries excavation determined using XMT, before and after excavation scans were taken of

an upper left third molar with a caries lesion. By subtracting post-excavation scans from pre-excavation scans using in-house alignment software (Davis et al., 2013), the mineral content distribution by means of measuring the LAC within healthy tissue, tissue near the excavation boundary and within the removed infected tissue were compared. A grey-level of up to 255 was used, where black represented 0 and white 3.4 cm^{-1} linear attenuation coefficient. Results showed that the LAC of healthy dentine was 1.5 cm^{-1}, 1.2 cm^{-1} near the pulp, 1.4 cm^{-1} at the deepest part of the removed material, and 1.2 cm^{-1} approximately 0.4 mm away from the excavation boundary. Studies comparing data between different excavation techniques are important as they highlight the risks associated with compromising pulp vitality during such dental procedures. Different methods can be compared to determine those that are ideal for minimal invasive dentistry (Ahmed et al., 2012).

In a similar study, XMT was used to measure the progression of crater growth during sequential application of Er: YAG laser to human enamel and dentine (Mercer et al., 2003). Laser crater depth and volume was plotted as a function of applied energy. Results showed that there was a linear relationship between crater depth and applied energy and between crater volume and applied energy. The advantage of using XMT for studies that quantify the efficiency of dental techniques is that values can be obtained from a series of measurements on the same sample over time, as it is a non-destructive technique.

Contrast adjustments of XMT images permits identification of subtle differences in mineral concentration within teeth so that histological features due to external trauma or pathology such as calculus can be observed (**Figure 6.10**). For example,

adjustments in XMT image contrast can highlight areas of hypermineralisation such as calculus and the presence of dead-tracts which can be traced in 3-dimensions. This permitted changes in the pulp, such as pulp recession and the formation of pulp stones to be related to external trauma and pathology.

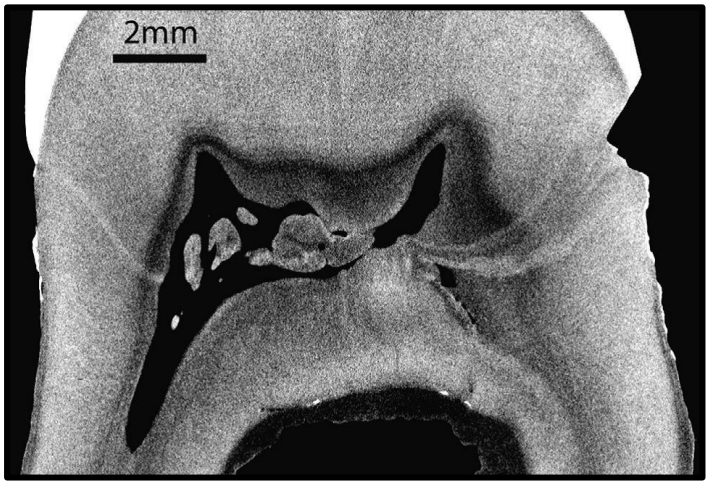

Figure 6.10 Single slice from a reconstructed high contrast XMT image through a tooth showing dead tracts extending from a groove at the enamel-cementum junction towards the pulp, where secondary dentine deposition can be seen. (Image taken from Davis et al., 2013).

XMT can also be used to determine the efficacy of dental restorative materials. A molar treated using the atraumatic restorative treatment method with strontium based glass-ionomer cement (GIC) was scanned with XMT. The tooth was scanned immediately after treatment and again a week after treatment. Results showed an increase in radio-opacity with a mean increase in LAC of 0.04 cm^{-1} in the tissue surrounding the GIC a week after treatment, corresponding to a strontium concentration of 4 mg cm^{-3}. A corresponding decrease in radio-opacity was observed in the GIC adjacent to the tissue indicating strontium leached out from the GIC (Davis et al., 2013).

Such studies showcase XMT ability to detect slight changes in LAC because of ion infiltration into dental hard tissues from dental materials. Three-dimensional imaging also permits time dependent studies to be performed. For example, samples can be rescanned to determine the efficacy of treatment such as the transfer of ions from a GIC over time, as the sample can be scanned whole rather than sectioned, in which case only one time point can observed.

6.2 Scanning microradiography (SMR)

SMR is an X-ray absorption technique that enables the monitoring of mineral loss in thin sections of enamel samples during remin/demineralisation studies (Anderson et al., 1998).

Developed to overcome some of the limitations of conventional (contact) microradiography which required samples to be in contact with a photographic film SMR can measure mineral changes in real time as solutions can be circulated through SMR cells within which samples are mounted (**Figure 6.13**).

To determine mineral content from an X-ray experiment the attenuation based on either the thickness or the mass per unit area can be used and expressed as either a quantity of mineral per unit volume or per unit mass, respectively. As thickness can be determined accurately, attenuation measurements for a given thickness - whereby the expression for the mineral content is expressed per unit volume rather than mass per unit area, is generally used in radiographic studies (Elliott et al., 1997).

The amount of attenuation of monochromatic X-rays by a homogenous material is obtained by measuring the incident (I_0) and transmitted (I) beam intensities, and has an exponential relationship between the two variables. Beer-Lambert Law expresses this relationship:

$$I = I_0\, e^{-\mu x} \qquad (20)$$

Where;

x is the thickness of the medium

μ is the linear attenuation coefficient (LAC).

The LAC describes the probability of attenuation of a photon of a given energy per unit thickness of a material and is expressed in units of cm^{-1}(see Section 5.2.6 X-ray attenuation of hydroxyapatite).

6.2.1 Uses of SMR

SMR is used to determine the projected mineral mass (this is proportional to the mineral concentration when sections are uniform in thickness) of samples such as enamel, dentine and bone. Samples can be continuously exposed to test solutions such as demineralisation/remineralisation solutions and continuously monitored in real-time providing real-time changes in mineral mass over time. In such studies mineral mass profiles at different time points after treatment can be plotted as a function of distance from the mineral surface. This provides valuable information on the characteristics of mineral loss/gain. For example, in a study on the demineralisation of enamel and hydroxyapatite at increasing ionic strengths, results showed that when ionic strength was increased by the addition of inert ions into

the demineralising solutions, the rate of mineral loss increased and the characteristic surface layer that forms on enamel and hydroxyapatite samples during demineralisation was significantly reduced, providing evidence in support of the hypothesis that subsurface demineralisation in enamel and hydroxyapatite may result from coupled diffusion between inward transport of acid and the outward transport of mineral ions (Anderson et al., 2004).

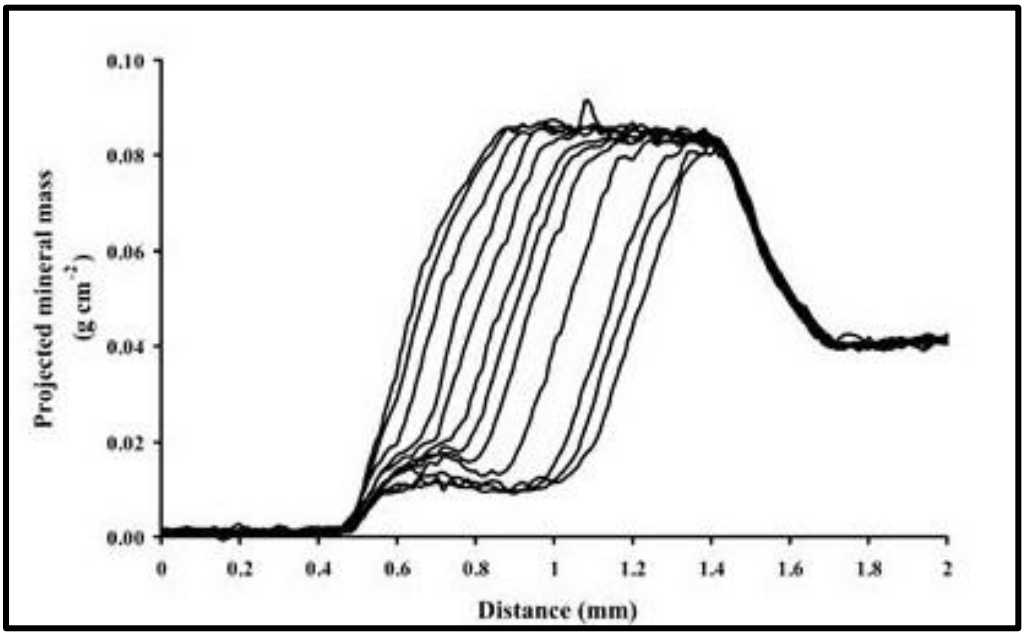

Figure 6.11 Mineral concentration profiles taken at 13 h intervals during demineralisation of enamel, in buffer at pH = 4.0 with 0.51 mol l^{-1} KCl (image taken from Anderson et al., 2004).

In a similar study on subsurface demineralisation, Anderson et al., (1992) investigated the influence of enamel heterogeneity on subsurface formation. Results showed that both enamel and synthetic hydroxyapatite samples exhibited similar subsurface formations indicating that such features in enamel such as

gradients in solubility, rate of dissolution and chemical composition were not essential features for subsurface lesions.

Fluoride content on the surface of enamel was attributed to an increase in enamel resistance to demineralisation, compared to hydroxyapatite samples, when exposed to acid from two directions. The SMR study quantified the reduction in mineral loss due to an increase in fluoride content under the conditions used, an example of how SMR can be used to quantitatively assess the influence of apatite compositions on demineralisation rates of dental hard tissues.

SMR was also used to assess the influence of the degree of saturation with respect to hydroxyapatite (DS_{HAP}) on demineralisation rates and subsurface formation. Results showed that pH did not influence the rate as much as the DS_{HAP} but that demineralisation was linear with time (Gao et al., 2001). The authors discussed the early lesion formation process of enamel suggesting a two-stage process of a pre-quasi-equilibrium followed by a quasi-equilibrium stage. The authors also suggested that during initial stages, surface enamel dissolves and the solution within its pores consequently change to maintain the composition of the surface zone (pre-quasi-equilibrium stage). Any demineralisation after this stage only takes place in the subsurface zone. Ions diffuse out through enamel and in doing so, preserve the composition of the solution in the surface zone and consequently preserve the surface zone itself.

Contrary to the findings on pH from the Gao et al., (2001) study and from Margolis and Moreno (1985) study whereby both studies indicated that the driving force for the formation of a caries lesion is better described in terms of the degree of

saturation with respect to hydroxyapatite, Theuns et al., (1983) carried out microradiograph studies on a range of pH values 4.0 – 6.0 and concluded that pH was the predominant factor that influences demineralisation rate in artificial carious lesions. However, differences between pH 4.0 and 4.5 were indistinguishable. Also, values were grouped into pH ranges so that pH 4.0 - 4.5 were compared with pH 5.0 - 6.0 rather than each pH value being compared individually, and so whilst the study showed that large changes in pH influence demineralisation, small differences may not.

As can be seen, SMR is a quantitative technique that can be utilised to investigate a variety of factors involved in the demineralisation/remineralisation of enamel. It has superseded conventional contact microradiography and techniques based on light scattering with regards to accuracy, resolution and repeatability. The real-time technique permits continuous measurements which in turn provide valuable information on the demineralisation characteristics of dental hard tissues.

6.2.2 SMR X-ray generation

A microfocus X-ray generator (BRUKER AXS B. V., The Netherlands) comprising a PANalytical® X-ray tube with a silver target is used to produce a characteristic Kα peak at 22.1 keV (see Section *5.1.1 Characteristic X-rays*). A 15 µm diameter beam is produced using a 15 µm aperture made of 90 % gold and 10 % platinum.

6.2.3 X-ray High Purity Germanium detection system.

The X-ray detection system used for the SMR system at QMUL uses a high purity germanium (HPGe) semiconductor detector (Ametek, PA, USA) to detect photons.

The high atomic number of germanium (Z = 32) ensures that most of the incident beam energy is lost and that the intrinsic peak efficiency for germanium is high; that is that the ratio of the number of pulses recorded in the detector to the number of radiation quanta on it is high. Semiconductors such as HPGe and lithium drifted silicon detectors, produce pulses that are proportional to the absorbed X-ray energy.

As described in section *5.2.7 Energy bands*, semiconductor detectors have a relatively small band gap compared to insulators. When an electron acquires enough energy to jump the band gap from the valence band into the conduction band, the electron hole (vacancy) formed can be filled with another electron from a higher valence shell. These electron-hole pairs are the basic information carriers in solid state detectors (Neamen, 2012).

Germanium detectors are semiconductor diodes which have a P-I-N structure. The intrinsic region (I) is sensitive to ionising radiation. Upon photon interaction with the intrinsic region the charge carriers (electrons-hole pairs) produced are swept to the P and N electrodes by the electric field. This charge is in proportion to the energy of the incident photon and is converted to a voltage pulse by an integral charge sensitive preamplifier.

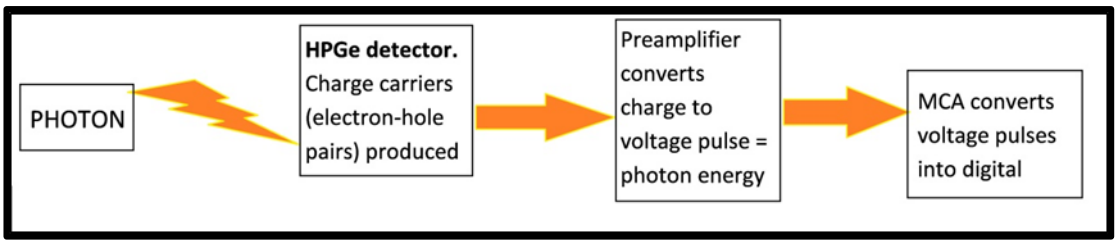

Figure 6.12 A flow diagram depicting the sequential turn of events induced by the impact of photon energy on a germanium detector used in SMR.

6.2.4 Multi-Channel Analyser (MCA)

The voltage pulses produced by the preamplifier are converted by a multi-channel analyser (MCA) into digital pulses (**Figure 6.12**) these are part of a digital spectrometer, DSPEC PLUS™ (Digital Gamma-Ray Spectrometer, ORTEC®, Ametec, PA, USA). The MCA consists of a multi-channel buffer (MCB) which contains an analogue-digital converter (ADC). This converts inputted analogue data into digitised incoming pulse heights and displays this memory as a histogram. The software program MAESTRO is needed to run the process.

Pulses are sorted according to their amplitude into channels corresponding to specific narrow amplitude ranges which determine the digital resolution and are chosen according to detector type and energy range. A pulse-height spectrum is formed with the Y-axis as the number of counts and X-axis as pulse height. The digital spectrometer allows spectrum capture which permits electronic monochromatisation.

Signal processing takes time, the term “dead time” is considered the time taken to process the signal while “live time” is the time available to receive a signal. Dead time can be determined by the MCA system in order to ensure data is correct. The

sum of all counts from all the channels is equal to the total number of pulses produced by the detector over the duration of the measurement period. At high count rates, corrections must be made to account for dead time or any pile ups whereby two closely spaced pulses may appear as one pulse.

To ensure that the signal to noise ratio (SNR) is maintained high, germanium detectors are encased inside a vacuum that provides thermal contact with a storage dewar filled with liquid nitrogen. This maintains a constant low temperature (-196°C) and is required to combat the increases in temperature associated with the production of thermally generated charge carriers in semiconductors. These thermally generated charge carriers are produced as a consequence of the small band gaps in semiconductors; these increase noise and therefore reduce resolution.

6.2.5 X-Y scanning stage

Sections are encased within environmental cells through which test media can be circulated. Cells are mounted on an X Y stage where they can be “stepped” at step sizes dictated by the investigator across a 15 µm X-ray beam. Section points are scanned for a duration also dictated by the investigator e.g. 60 s, and the transmitted intensity is measured.

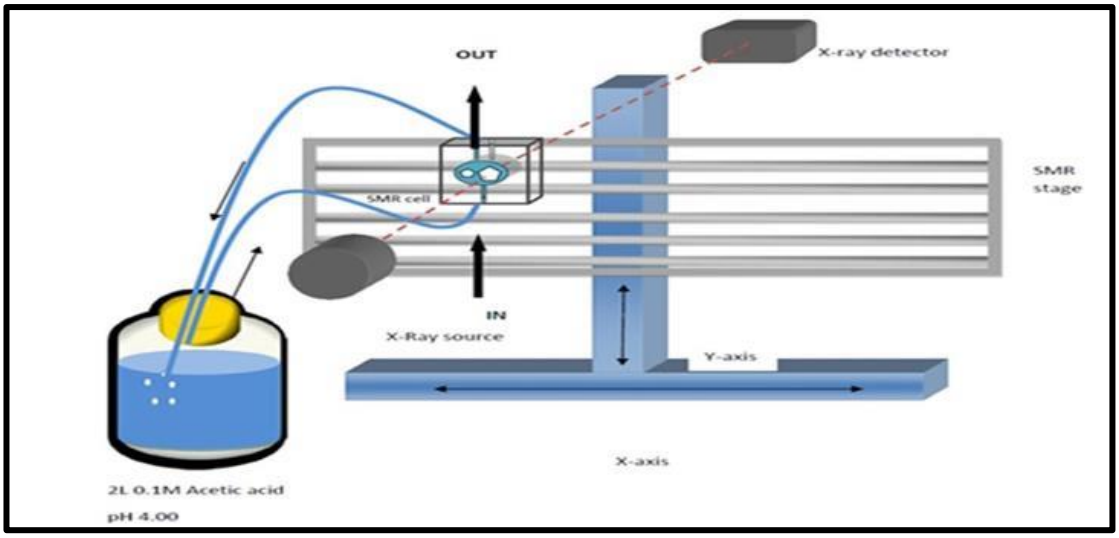

Figure 6.13 Schematic diagram of SMR experimental set up.

6.2.6 Advantages of using SMR

Conventional contact microradiography (CMR) requires specimen contact with a photographic emulsion, which is then irradiated with X-rays to produce images (**Figure 6.14**). Contact microradiography does not permit real-time measurements unlike scanning microradiography which in addition also permits multiple (up to 10) sections to be analysed independently of one another in one setting; thereby allowing the exposure of many samples to different test media such as different pH conditions, degrees of saturation and chemical composition (**Figure 6.13**).

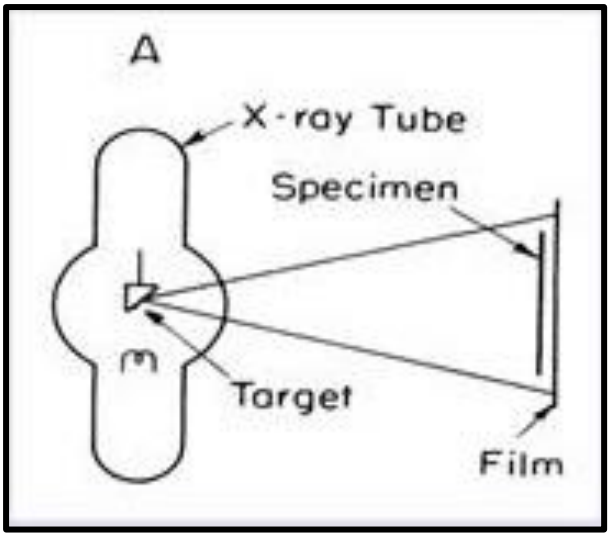

Figure 6.14 Schematic diagram of contact microradiography (image taken from Cosslett, 1957)

In comparing photon counters such as used in SMR with photographic emulsions such as used in CMR, the former technique is superior in terms of having an increased dynamic range, accuracy and greater sensitivity. While CMR can record information at resolutions better than 0.5 µm, its main disadvantage is a reduced SNR compared with SMR. Energy dispersive photon counting systems used in SMR have low noise levels, typically less than 1 photon s^{-1} in the absence of X-rays. Determinations of intensity are therefore almost entirely due to photon statistics, whose standard deviation can be measured as they follow a Poisson distribution. Standard deviation can be reduced by increasing exposure time. However, increased exposure time will increase dead-time and so corrections must be made at higher count rates in order to avoid errors in determining the correct I_0 value needed to calculate absolute measurements of mineral concentration (Elliott et al., 1997).

To minimise artefacts associated with the use of polychromatic radiation, the pulse height analyser used in SMR can be set to focus on an energy band centred on a particular peak such as Mo Kα or Ag Kα peaks at a particular energy thereby emulating monochromatic energy.

Optimum resolution and accuracy can be achieved through a delicate balance between exposure time and maintaining detector responsiveness, as over-exposure can lead to increased dead-time and errors if appropriate corrections cannot be made. Therefore, accurate measurements during real-time recordings of changes in mineral mass can be achieved thereby providing valuable information about the solubility of biological hard tissues such as enamel as well as the remineralising potential of therapeutic agents such as fluoride and zinc (Mohammed, 2014).

6.4 Confocal laser scanning microscopy (CLSM)

Tomographic three-dimensional images are generated by scanning a specimen at different depths with a monochromatic laser light source. It is a non-destructive technique that sections thick samples without the need for physical sectioning.

Fluorescence is when a sample is illuminated and it absorbs light of one wavelength and emits it as another. The emitted light is then collected by a camera or detector which then produces an image based on the incoming signal intensity.

Unlike other optical light techniques that flood the entire sample with light, such as in Epifluorescence, in CLSM the sample, living or inanimate, is illuminated by a laser that is focused on a small spot at a chosen focal plane (laser spot is 100 nm) with planes above and below receiving a significantly lower intensity of light thereby

appearing blurred due to weaker signals from the out of focus planes. Any out-of-focus light that is reflected by the sample is rejected by a pin hole located in front of a detector that receives the in-focus incoming signal (Kus, 2015). In this way, CLSM produces highly defined and clear images unlike other light techniques that produce whole field-of-view images using a camera which can lead to degradation of the image.

6.4.1 CLSM apparatus and function

The CLSM (Olympus LX81 with Fluoview FV1000 scanner software, version 4.1) apparatus compartments as shown in **Figure 6.15** are:

- A laser. Laser lines can be chosen from a spectrum via a selection devise to match with chosen fluorophores used in an experiment.
- A beam splitter which separates the excitation from the emitted light in the fluorescent beam path.
- A stage to place samples.
- A scanner unit based on two or more mirrors that guide the focussed laser beam across the specimen pixel by pixel.
- An oil immersion objective lens that determines the resolution.
- A Z-control which focuses on any plane within the sample and can be moved in the axial direction in steps greater than 10 nm.
- An adjustable pinhole which excludes out-of-focus light and thus permits optical sectioning. It defines the optical thickness of the slice and depends on the objective lens.
- A detector or Photomultiplier (PMT).

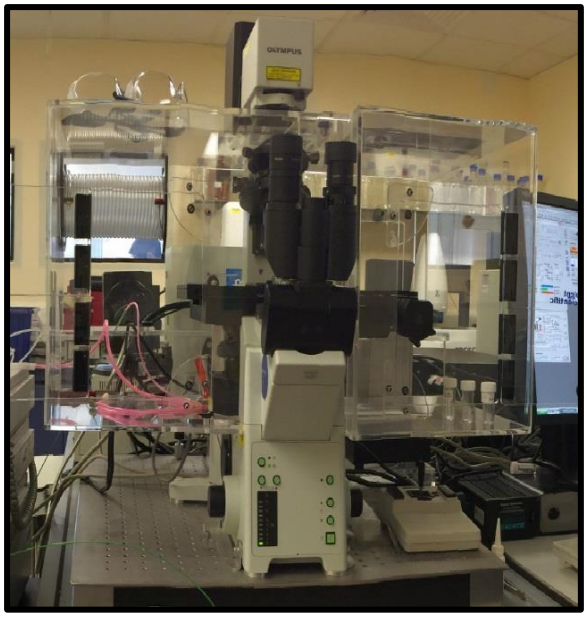

Figure 6.15 CLSM apparatus set up at GlaxoSmithKline, Weybridge.

The laser beam (100 nm in diameter) is first filtered by density filters which adjust the intensity of the beam. The beam then hits a set of internal motorised scanning mirrors that tilt the laser beam in X Y directions, collectively in a raster fashion (rectangular grids of pixels). The beam is brought to the back focal plane of the objective lens which focuses the beam onto the sample at a specified focal plane.

In fluorescent mode, part of the reflected light beam will reflect into the objective lens along the same path as the incident laser beam. The light is then passed through a dichroic mirror which reflects the fluorescent beam (containing the image information) away from the laser and towards the detector, and emission filters are used to separate the reflected fluorescent light from the reflected laser light. The dichroic mirror works by having different reflectivities for each wavelength of incoming light[5]. In non-fluorescent mode, the light reflected from

the sample to be examined will pass through a polariser that will only permit light with a different polarisation angle from the initial laser light to pass.

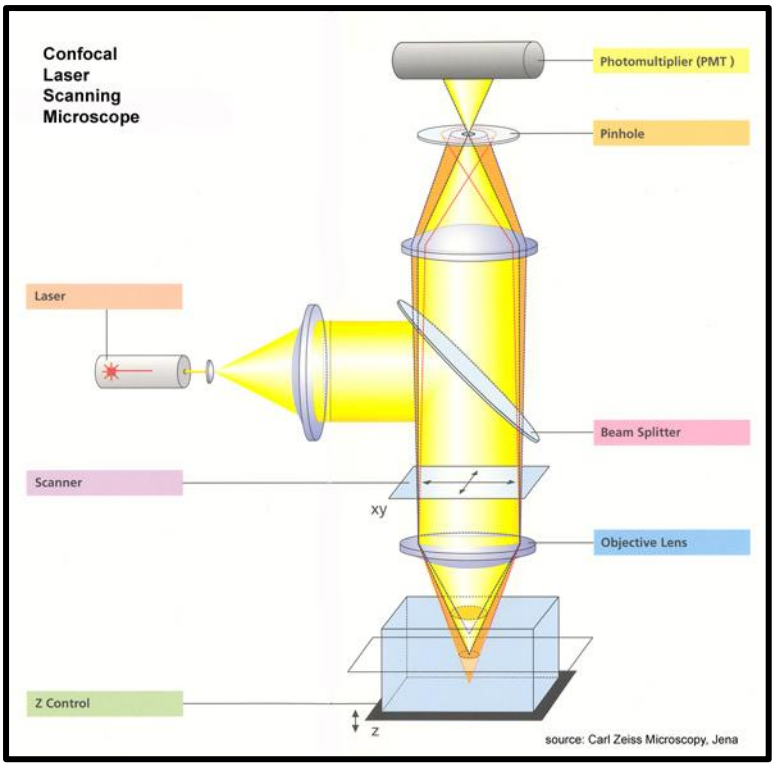

Figure 6.16 schematic diagram showing the internal components of a CLSM system[6].

The permitted light that is reflected from the sample is collected by a photomultiplier tube (PMT) detector. The PMT collect photons and amplifies their signal. The output from the PMT is an electrical signal with amplitude that is directly proportional to the initial light signal. The analogue signal is converts a digital signal by an analogue to digital converter. As the laser moves across the sample, the collection of light at each pixel is sent to the detector which creates the image pixel by pixel. Optical-sectioning can be achieved by the analysis of different focal planes within the sample. Digitisation permits image display on a computer monitor

permitting three-dimensional image reconstruction using computer software[6]. In this way, high resolution three-dimensional images of live and inanimate samples can be reconstructed. Also, dynamic changes within samples such as cells can be observed by continuous scanning on the same focal plane.

6.4.2 CLSM uses

In fluorescent mode, CLSM settings can be adjusted to detect reflected light at wavelengths corresponding to wavelengths emitted by specific fluorescent dyes. Such dyes bind to specific molecules and so this setting of CLSM permits the utilisation of fluorescent dyes to identify specific internal features within samples. For example, CLSM has been used to study the composition of dental plaque (Zhou and Li, 2015). Through in situ studies CLSM can be used to obtain images of biofilm components in their natural hydration state (Hao, et al., 2013). Through continuous scanning and using specific fluorochromes to dye specific components interactions between proteins and viable and dead microflora can be observed in situ providing valuable information on the formation stages and dynamic physiological processes of biofilms. For example, in a study that investigated biofilm formation by wild type, flagella mutants and type IV pili mutants of *Pseudomonas aeruginosa,* green fluorescent protein (GFP), which exhibits bright green fluorescence when exposed to light in the blue to ultraviolet range, was used to tag the three types of *P. aeruginosa* (Klausen et al., 2003). Results showed that the three types of *P. aeruginosa* formed different biofilm structures. Further, when flagella and type IV mutants were tagged with yellow fluorescent protein (Yfp) and cyan fluorescent protein (Cfp) tags, time-lapse CLSM in multicolour imaging mode showed that initial

microcolony formation occurred by clonal growth followed by the wild-type spreading over the substratum by means of twitching motility. Results also showed that wild-type *P. aeruginosa* biofilms had dynamic compositions with extensive motility, competition and selection the biofilm development. When compared with SEM, CLSM requires less sample preparation before scanning. For example, during sample preparation for analysis with SEM, structural damage can be accumulated during steps such as dehydration, fixing, embedding and dyeing, whereas CLSM sample preparation only requires the use of fluorescent dyes if the fluorescent mode is adopted.

CLSM can provide qualitative and quantitative measurements of the structural changes and physiological processes within living cells over time when used as a real-time technique. Measurements of the area of a sample can be obtained through quantitative analysis of the fluorescent intensity of components within specified areas. In this way, the determination of cellular components, composition and distribution can be made.

Quantum dots (QDs) are semiconductor particles a few nanometres in size that emit light at specific frequencies when excited by light or electricity. QDs have been used as fluorochromes and their use has been shown to simplify CLSM multicolour detection. For example, the nucleosomes in the nuclei of six groups of human epithelial cells were labelled separately with six colours of QD Streptavidin conjugates with corresponding emission maximums at 525, 565, 585, 605, 655 and 705 nm. A 488 nm laser line from an argon laser CLSM system was used to excite the labelled cells. The fluorescent signals from each colour of the conjugates were

collected by the multicolour detection capacity of the CLSM, indicating that all cells were successfully excited using a single laser line of 488 nm. Authors concluded that the use of QDs simplify CLSM systems and makes them more affordable for multicolour detection (Wu and Bruchez, 2004). Multicolour detection by CLSM permits observations of multiple QDs within cells at the same time; therefore increased understanding of the networks of signalling pathways within cells is achievable through their use as fluorochromes in CLSM.

6.4.3 CLSM in dental research

CLSM can also be used to compare different experimental techniques. For example, Yamada et al., (2003) study compared the surface roughness of cavities formed on enamel and dentine by three different types of lasers; Nd:YAG, Er:YAG and CO_2 lasers in order to evaluate the irradiation effect of each laser on enamel and dentine surfaces by combining morphological observations with quantitative surface roughness analysis. Results showed that Nd:YAG had a flake-like surface, Er:YAG an imbricate pattern and cracks within dentine where observed when irradiated with CO_2 laser. The study also compared SEM images with CLSM images and found that whilst SEM produced images with better resolution, CLSM three-dimensional images permitted observations and quantitative measurements of cavity depths.

In another study on dental enamel, CLSM and rhodamine B fluorescent dye were used to assess the remineralising potential of several agents (Gonzalez-Cabezas et al., 1998). Rhodamine B is used in biology as a staining fluorescent dye and is tuneable around 610 nm when used as a laser dye. It has a molar mass of 479.02

and solubility in water of approximately 15 g/L. In the study, enamel sections were demineralised for 96 hours, and then half of each specimen was coated with acid-resistant nail varnish. Samples were then treated for 20 days to a cyclic remineralisation regimen which consisted of a 4 hour acidic daily challenge, a 1 min remineralising treatment of either 0, 250 or 1,100 ppm F dentifrice slurries (1:2 dentrifice:water) and 20 hours of pooled human saliva at room temperature. After the remineralisation regimen samples were stained with 0.1 mM rhodamine B for 1 hour. CLSM images showed significantly greater remineralisation in the fluoride treated samples compared to samples treated with the non-fluoride dentifrice and baseline samples (samples only exposed to demineralisation). This was indicated by a lower intensity of fluorescence detected from rhodamine B in the remineralised samples than in samples that were not exposed to fluoride or dentifrices and is thought to be due to a decrease in Rhodamine B dye penetration through the enamel voids (Fontana et al., 1996). CLSM data was also compared with microradiographic data obtained from the same experiment and authors concluded that there were no significant differences between the data obtained from both techniques and that there was a significantly high Pearson correlation coefficient between the results obtained from the two techniques.

However, as with all light techniques, photobleaching is a limitation and a balance between exposure time and the effect of photobleaching (Maggiano et al., 2006); especially of live samples because of phototoxic effects, should be considered. Another consideration to make when using CLSM is the signal to noise ratio as an increase in signal leads to an inevitable increase in noise. Therefore, a balance

between increasing gain and laser settings to increase the signal received should be balanced with the consequence of increased noise and photobleaching.

Another consideration to account for when choosing CLSM over other light techniques such as Epifluorescence scanners is speed. While CLSM can produce higher resolution images, these are produced at the expense of speed. As pixel grid increases in size, pixel size decreases and images are produced at a higher resolution, however, an increased pixel grid takes longer to scan than a smaller pixel grid with greater pixel sizes.

SECTION 4: EXPERIMENTAL WORK

Chapter 7 Measurement of the mineral concentration of deciduous and permanent enamel by x-ray microtomography

Clinical observations indicate that there are significantly more instances of demineralisation in children than in adult enamel and that the number of hospital admissions is not only on the increase, but that tooth decay is the principal reason for children's hospital admissions (LGA, 2016).

The rise in hospital admissions reported by the LGA requires the attention of investigative research to identify the major factors involved in DE demineralisation and to understand why hospital dental admission rates are significantly higher amongst children than for adults. An increased consumption of sugary and acidic foodstuff amongst children and teens has been highlighted as one of the main causes for this rise making the necessity for such research is even more important in order to contribute towards the development of more effective anti-caries agents.

The upcoming sugar tax implementation on food and beverages that will take place in April 2018 clearly demonstrates the U.K. Government's acknowledgment of the need to implement a plan of action when dealing with diseases associated with sugar consumption.

However, tooth decay is a multifactorial process which is influenced by genetic and environmental factors (Keyes, 1962, Brambilla et al., 1999). Such factors include those associated with the host's tissue such as the structure and composition of enamel, the pellicle and saliva, and environmental factors such as socioeconomic status and diet.

The influence that each factor independently has on enamel dissolution is important in the development of our understanding enamel demineralisation. Being able to quantify the impact that each factor has on enamel demineralisation would enable us to gain a clearer and more comprehensive understanding of the processes involved in enamel demineralisation and would therefore ultimately lead to the development of more effective caries and erosion prevention strategies.

It is therefore important to design research experiments that focus on quantifying the effect that each factor has on the demineralisation of teeth. Therefore, in this study, an *in vitro* experimental design was chosen using the MuCAT 2 XMT scanner at QMUL to quantitatively measure the mineral concentrations and mineral distributions of DE and PE in order to assess whether DE and PE were significantly different. It was assumed that a significantly lower mineral concentration in DE would contribute to greater demineralisation rates and a higher risk of developing caries in DE than in PE. All other factors such as the pellicle and saliva were excluded to make direct comparisons between DE and PE mineral contents and mineral profiles.

The XMT results were then compared with SMR results obtained from a demineralisation experiment to identify a relationship between mineral

concentration of enamel and demineralisation rate (see Chapter 10 for a discussion on the results obtained from both techniques).

7.1 XMT materials and methodology

Twenty-nine pairs of anonymous human deciduous and permanent whole enamel crowns that were either exfoliated or extracted for orthodontic purposes were scanned with the MuCAT 2 XMT scanner at QMUL to determine and compare the mean mineral concentrations in both enamel types (XMT settings are described in section 7.1.2). After XMT image reconstruction (refer to section 6.1.3), scans of each whole enamel crown provided approximately 909 XMT image slides depending on the size of the specimen. These slides could be viewed in the XY, XZ or YZ aspect using Tomview and Image J computer analysis software. Tomview is a digital imaging program developed by Professor Graham R. Davis at QMUL.

Using Image J software version 1.8.0 three XMT slides in the XY aspect that were located approximately half way through each of the enamel crowns were analysed for mineral distribution and mean mineral concentration. This was achieved using line scans with a resolution of 15 µm that provided greyscale values going from the EDJ towards the buccal surface at the occlusal third of the enamel crowns as shown in . To calculate the mineral concentrations from the greyscale values provided by the line scans, the LAC was first calculated from the corresponding greyscale values at each point along a line scan by dividing the greyscale number by the scale setting used, here the scale was set at 75. Mineral concentration values could then be calculated from the LAC values using equation 21. Depending on the enamel thickness each line scan provided approximately 135 greyscale values.

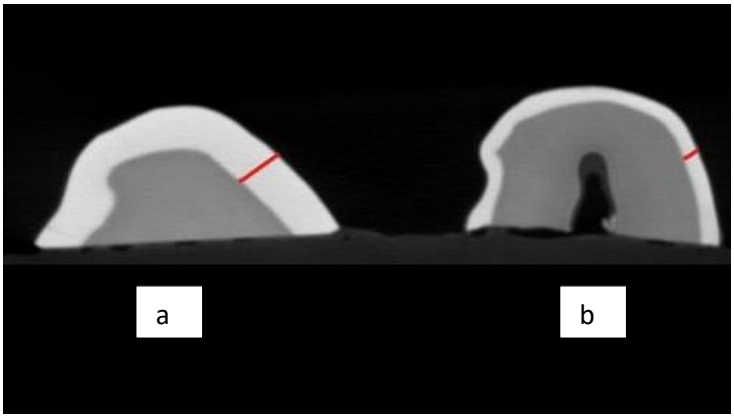

Figure 7.1 Typical XMT image of a permanent (a) and deciduous (b) tooth section. Red lines show the regions analysed for mineral concentration using Image J.

The mineral concentration was calculated by multiplying the LAC by the density profile of 100 % HAp divided by the LAC of 100 % HAp as shown in equation 21:

$$mineral\ concentration\ (g\ cm^{-3}) = LAC\ x\ \frac{DP\ 100\%\ HAp}{LAC\ 100\%\ HAp} \quad (21)$$

Where;

LAC = Linear attenuation coefficient

DP = Density profile

The mean mineral concentration of DE and PE was calculated from the line scans obtained from all 29 enamel samples from each group.

7.1.1 Preparation of human dental enamel sections

Twenty-nine crowns of deciduous and permanent teeth were stored in 0.05 % thymol solution which was changed every 3 months. Roots were cut off using a diamond saw (Microslice 2, Malvern Instruments, UK) and the crowns were then

placed in 20 ml plastic vials (Sigma-Aldrich V6755) and scanned with XMT using the setting described below.

7.1.2 XMT settings

Scanning time for an adult premolar was just over 13.5 hours to produce approximately 909 projections at a resolution of 15 µm. A voltage of 90 kV and a current of 8.1 µA were calibrated with a virtual hydroxyapatite step wedge and carousel (as described in section 6.1.3) to 40 KeV equivalent monochromatic energy.

7.2 XMT results

Analysis of approximately 1200 points from XMT line scans of twenty-nine DE and PE samples showed gradients in mineral concentration from outer enamel towards the EDJ (**Figure 7.2** and **Figure 7.3**). The range in mineral concentration in DE was 1.61 g cm^{-3} – 3.03 g cm^{-3} and the range in PE was 1.94 g cm^{-3} – 3.19 g cm^{-3}. However, no significant difference (t-test value 0.09 ($p = 0.05$)) in the mineral concentrations of both enamel types were observed, although DE showed a greater mean mineral concentration than PE (**Figure 7.4**).

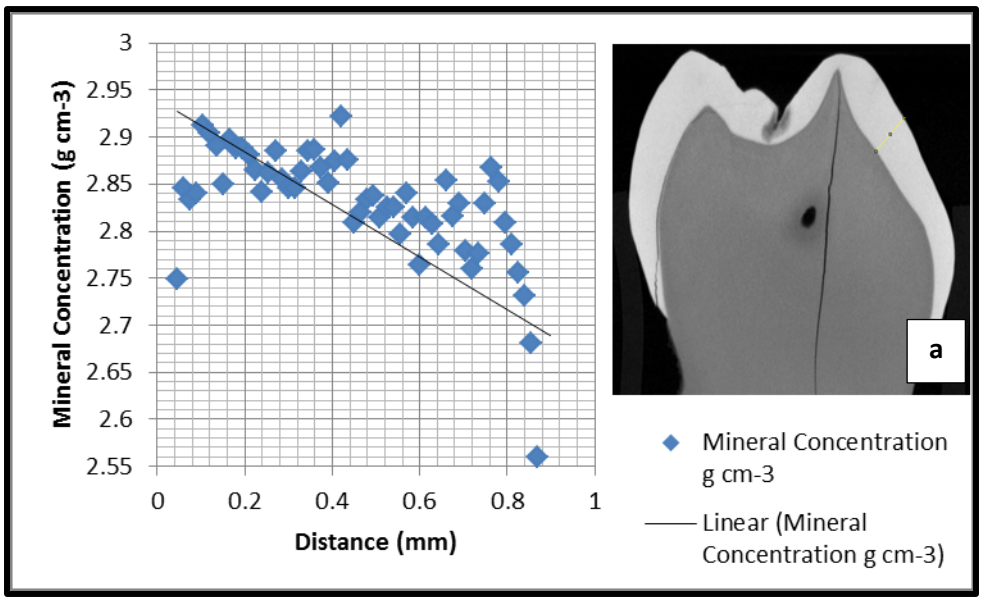

Figure 7.2 Typical mineral concentration line profile plot of a human DE molar. A decrease in mineral concentration is observed from outer enamel towards the EDJ. Inserted XMT image of the deciduous tooth (a) with the line scan location (yellow line) from which mineral concentration data was calculated.

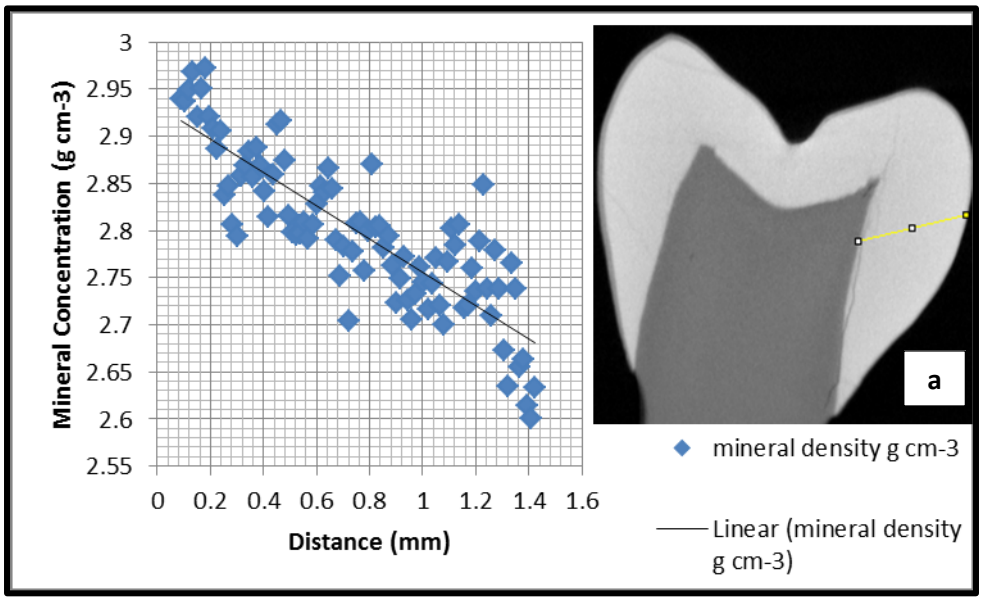

Figure 7.3 Typical mineral concentration line profile plot of a human permanent premolar showing a decrease in mineral concentration from outer enamel towards the EDJ. Inserted XMT image (a) shows the line scan (yellow line) region from which the mineral concentration data was obtained.

Figure 7.4 and

Table 7.1 shows DE mean mineral concentration was 2.49 g cm^{-3} and PE mean mineral concentration was 2.48 g cm^{-3}.

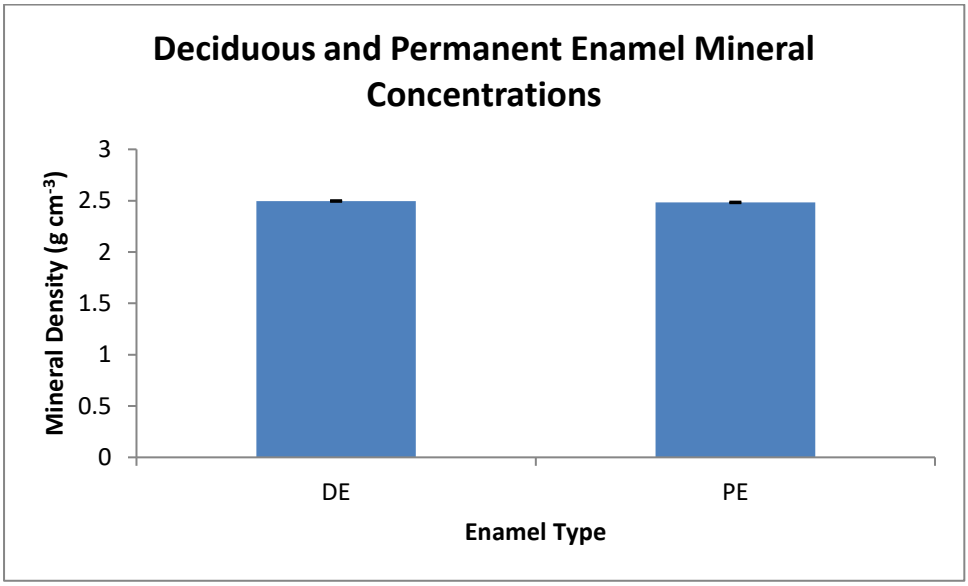

Figure 7.4 Mean mineral concentrations for DE and PE scanned by XMT.

Table 7.1 Mean mineral concentration for DE and PE with standard errors given (n = 29).

Enamel type	Mineral concentration (g cm-3)	SE (g cm-3)
Deciduous	2.49	0.0076
Permanent	2.48	0.0074

7.3 XMT discussion

According to these results the greater demineralisation rates and higher caries incidence rates observed in DE may not be due to a greater porosity in DE as there

is not a significant difference between the mineral densities of both enamel types according to t-test analysis ($p=0.05$), contrary to previous reports (Wang et al., 2006). The low standard errors calculated from the standard deviations of the data confirm that the results are reliable and accurate. An alternative explanation of the greater rates observed include lower protective qualities in children's saliva such as lower calcium and phosphate levels and lower protein content such as statherin and histatin, than in adult saliva.

The protective functions of calcium and phosphate in saliva has been extensively studied and research has shown that mechanisms involving proteins significantly influence demineralisation/remineralisation pathways. A lower calcium concentration is associated with a lower thermodynamic driving force for enamel mineral precipitation at normal oral pH and consequently a higher thermodynamic driving force for enamel mineral dissolution at low pH. This, paired with the fact there is a greater intake of sugary snacks amongst children and teenagers over the last 50 years, only reinforces the alternate suggestion given above.

For example, Anderson et al., (2001) used atomic adsorption spectroscopy to measure total calcium concentrations in children and adult unstimulated and stimulated saliva samples. The study showed a lower calcium concentration in children saliva samples than adult saliva but no significant difference in phosphate concentration (Anderson et al., 2001) for both unstimulated and stimulated samples. Authors concluded that based on thermodynamic considerations alone, children were exposed to an increased risk of demineralisation compared with

adults and that consequently, the critical pH would be higher in children than in adults.

With regards to salivary proteins, studies have also shown significant differences between the protein content in children saliva than in adults, showing higher concentrations of α-amylase, type II regulatory subunit of protein kinase A, high-molecular weight proteins (>90kDa) and low molecular weight proteins (<30kDa) (Sivakumar et al., 2009).

While absolute accuracy of LAC has been shown to be better than 1%, studies have shown that LAC measurements consistently show an over-estimation of 0.7% (Davis et al., 2013) compared to density measurements measured by mass and volume (measured by XMT). This may be due to slight overestimations of volume in volume measurements due to partial volume effects, i.e. loss of data because of limited resolution, resulting in an under-estimation of the density. Additionally, since volume measurements using tomography is greatly dependent on voxel size, porosity is a problem especially with regards to volume measurements in tooth tissues. Calibration based on attenuation measurements and adjusted to specimen composition is therefore essential to ensure good quantification of LAC at an equivalent monochromatic energy in reconstructed images. Since LAC values in tooth tissues and hydroxyapatite are primarily determined by calcium, slight variations in mineral composition will not impact greatly on mineral concentration measurements which can be determined if the chemical composition is known (Davis et al., 2013).

7.4 XMT conclusion

XMT measurements of the mineral concentrations from 29 pairs of DE and PE samples showed gradients in mineral profiles from outer enamel towards the EDJ in both enamel types.

Contrary to previous claims that associate faster demineralisation rates in DE to lower mineral concentrations, no significant difference was observed between the mean mineral concentrations of DE and PE obtained from over 1200 points in each enamel type. Though the lowest mineral concentration value measured was in DE and the highest value measured was in PE, this did not contribute to significant differences in the mean mineral concentrations of each enamel type.

Chapter 8 Measurements of the apparent solubility product of bulk human deciduous and permanent enamel using scanning microradiography

As discussed in section 3.1.4 Solubility product of enamel, the kinetics of mineral loss and precipitation is influenced by factors such as surface structure, pH, composition and the chemical equilibria between enamel and solution (Dorozhkin, 2012) which together dictate the solubility product constant, Ksp, as defined in equation 14.

The range of solubility products as shown in **Table 3.1** suggests many uncertainties including whether the pKsp values may be dependent on the choice of experimental protocol (please refer to Section 3.1.4 Solubility product of enamel). In addition, these uncertainties are further confounded with regards to understanding DE demineralisation characteristics; while there is a plethora of data from experiments aimed at understanding the solubility of human PE, there is much less information available on DE solubility. These uncertainties highlight the need for research on permanent and DE that employ quantitative techniques and methodologies that are reliable, accurate, sensitive and that can be validated. This is particularly important for experiments that aim to identify the solubility product value of enamel as the value wholly relies on the techniques sensitivity in identifying the state of equilibrium between solid and solution, and not miss-identifying extremely low demineralisation rates that are undetectable by the technique, for equilibrium.

In this study, an SMR real-time methodology was used to measure the rate of bulk deciduous and permanent human enamel mineral loss in demineralising solutions that contained increasing concentrations of calcium and phosphate. The calcium concentration at which the rate ceased (i.e. equilibrium) was then compared with calculated results of the degree of saturation (values ranged from 0-1, where 0 is equivalent to a saturated solution in this study) at a range of pKsp values of hydroxyapatite. These values were calculated using an ionic speciation program (Chemist) based on the conditions used in the SMR experiment and accounted for the different species that would be present in the dissolution media under the conditions used (**Figure 8.5**) shows an example of a typical Chemist plot using a pKsp of 118.

In this way, the corresponding pKsp values of deciduous and permanent human enamel could be identified as the calculated pKsp that had a degree of saturation of 0 (i.e. saturated solution) at a calcium concentration equal to the calcium concentration required to cease demineralisation in the SMR experiment for DE and PE.

No chemical analyses of solutions were required as changes on the bulk surfaces of the enamel samples in response to increasing degrees of saturation in the solutions were monitored. In this way, equilibrium between solid and solution could be detected when demineralisation ceased and could be validated if further additions

of calcium and phosphate increments to the demineralising solution showed an increase in projected mineral mass, i.e. remineralisation was observed.

In this study, a novel kinetic method was used to measure the *apparent*-pKsp$_{BEnamel}$ under conditions relevant to caries, in conjunction with a speciation program so that the *apparent*-pKsp$_{BEnamel}$ value could be calculated at conditions of pH = 4.0 and 25◦C. The rate of demineralisation of natural unaltered surfaces of human permanent and DE blocks was measured using SMR to determine the effective solubility in an inorganic caries-like demineralising solution with a decreasing degree of undersaturation with respect to HAp.

8.1 SMR materials

SMR is an X-ray absorption technique that enables the monitoring of mineral loss (and eventually gain once equilibrium is surpassed) in thin sections of enamel samples during demin/remineralisation studies (Anderson et al., 1998). Developed to overcome some of the limitations of conventional (contact) microradiography which required samples to be in contact with a photographic film, SMR can measure mineral changes in real time as solutions can be circulated through SMR cells, within which samples are mounted, at a controlled rate simulating salivary flow.

In this study, the integrated mode of SMR (**Figure 6.13**) was used whereby the direction of acid attack was parallel to a 15 µm diameter X-ray beam so that

changes in the projected mineral mass from the surface could be measured as mineral was lost from the surface and receded to the enamel dentine junction (Anderson et al., 1998). The X-ray set was operated at a maximum voltage of 41 kV and a current of 0.7 mA. The transmitted X-ray intensity for energies selected at 22.1 keV at each point was measured and the mass of absorbing mineral determined. Since demineralisation is nearly linear with time under constant chemical conditions (Wang et al., 2006; Elliott et al., 1994); the rate of projected mineral mass loss of the same enamel sample at decreasing degrees of undersaturation with respect to HAp could be measured.

8.1.1 Preparation of human dental enamel blocks

Eleven pairs of different DE and PE blocks were prepared from 11 deciduous and 11 permanent teeth extracted for orthodontic purposes, with the roots removed and discarded and stored in 0.05 % thymol solution which was changed every 3 months at room temperature were analysed. Ethical approval was granted by Queen Mary Research Ethics Committee (QMREC 2011/99).

Teeth were cut parallel to the buccal tooth face into 2 mm thick enamel blocks with the natural buccal surfaces intact using a diamond cutting saw (Microslice 2, Malvern Instruments, UK). The enamel blocks were mounted in SMR cells with the natural surfaces exposed (**Figure 8.1**). Each was scanned with X-ray Microtomography (XMT) to identify caries free (unaffected) areas suitable for analysis with SMR. The SMR cells were then mounted on the XY stage of the SMR apparatus. The samples were initially immersed in deionised water circulated using

a peristaltic pump as previously described in Mishra et al. (2008) for 48 h to ensure the samples were fully hydrated prior to the commencement of the dissolution experiment. The temperature was maintained at 25 +/- 1 °C throughout the experiment.

8.1.2 Demineralising solution

2.0 L of pH = 4.0 acetic acid 0.1 M (Anderson et al., 2004) was prepared using 12 g of pure acetic acid (≥ 99.5 %, FG, Sigma-Aldrich), diluted with deionised water and adjusted to a pH of 4.0 with a 1.0 M stock solution of KOH (≥ 85 %, ACS reagent, Sigma-Aldrich) using a pH meter (Orion-pH/ISE meter Model 710).

8.1.3 Preparation of calcium and phosphate increments

0.66 g increments of $CaCl_2$ (anhydrous, powder, 99.99%, Sigma-Aldrich) and 0.822 g increments of K_2HPO_4 (ReagentPlus®, ≥99.0 %, Sigma-Aldrich), were weighed so that any additions of each increment into the 2.0 L of acetic acid solution would give an increment in concentration of 3.0 mM calcium and 1.8 mM phosphate (Ca/P 1.67).

8.1.4 SMR environmental cell

Pairs of DE and PE blocks were placed within SMR cells with their natural buccal surfaces exposed. The SMR cells ensure that each enamel sample within each cell was exposed to identical conditions (**Figure 8.1**). This ensured that reliable comparisons could be made between the two enamel types without the problems associated with comparing data from two different experiments.

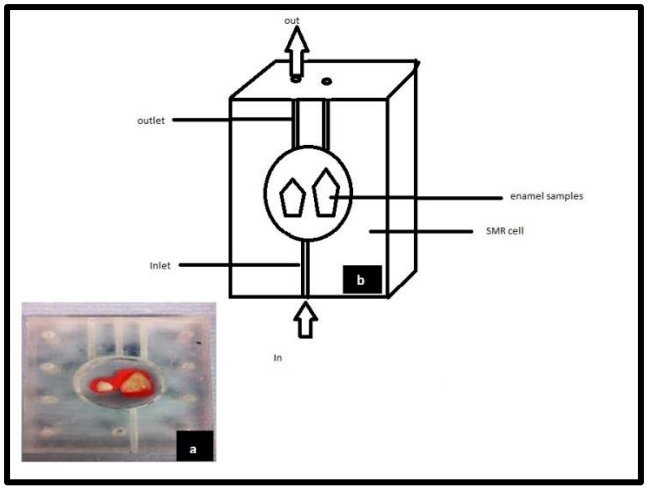

Figure 8.1 A photo (a) and schematic diagram (b) of human DE and PE blocks in an SMR cell with Figure b showing the flow of acid into and out of the cell.

8.1.5 Experimental set up

DE and PE blocks in SMR cells were mounted onto the SMR X Y stage and scanned using AgKα radiation at 22.1 KeV (see **Figure 6.13**).

Acetic acid was pumped through the cells using a peristaltic pump (Watson Merlow 205U) so that the direction of acid attack was parallel to the X-ray beam and so that the mineral mass changes at 5 points, 1 mm apart on each enamel block could be monitored.

8.1.6 SMR system responsiveness

Before the commencement of the demineralisation experiment, SMR system responsiveness was tested by monitoring the systems response to a sudden change in solution from that of 0.1 M acetic acid pH 4.0 demineralising an enamel block to water and then back to acetic acid. The system responded immediately each time the solution was switched (**Figure 8.2**).

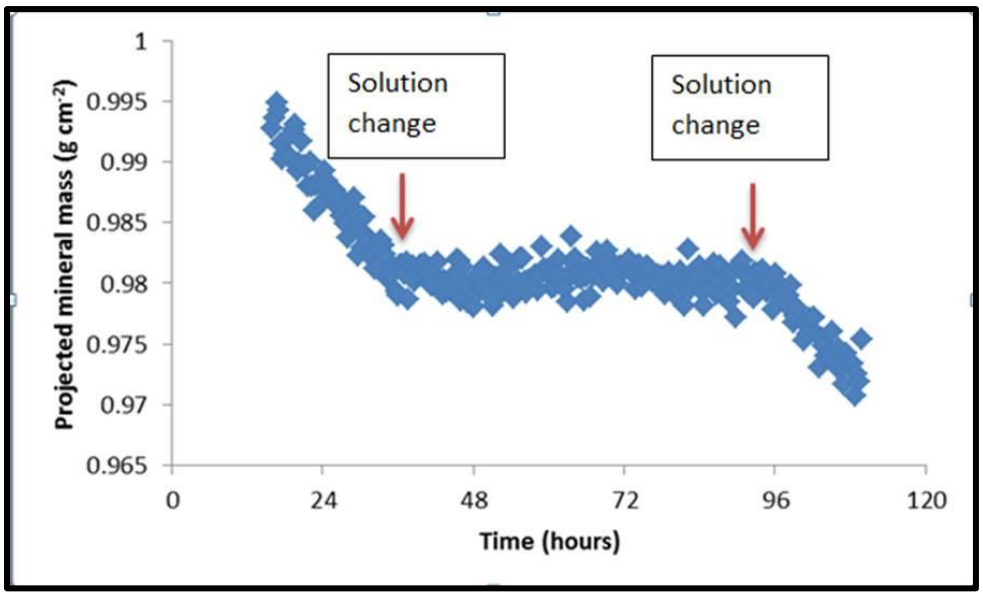

Figure 8.2 Projected mineral mass plot of SMR system responsiveness to changes in solution from enamel being demineralised in 0.1 M acetic acid pH 4.0 to water and back to acetic acid. Red arrows depict times of solution change over from acetic acid to water (first red arrow) then from water to acetic acid (second red line).

8.1.7 Mineral mass measurements

The mineral mass of enamel was calculated using the mass absorption coefficient (μ_m) of pure hydroxyapatite for AgKα radiation at 22.1 keV (4.69 cm^2 g^{-1}). The integrated mineral mass per unit area (m) at each data point is:

$$m = \frac{1}{\mu_m} \ln \frac{No}{N} \quad (22)$$

Where;

μ_m is mass attenuation coefficient of HAp for AgKα radiation at 22.1 keV.

N_0 is number of incident photons

N is number of transmitted photons

The error in the mass of HAp per unit area attributable to photon statistics is calculated by:

$$\delta m = \frac{1}{\mu_m}\left(\frac{1}{\sqrt{N}}\right) \quad (23)$$

Where,

δm = error in mass

μ_m = Mass attenuation coefficient of HAp

N = number of transmitted photons

For enamel samples with a count time of 60 seconds, typical transmitted X-ray photons for AgKα radiation at 22.1 KeV is typically 50000, the error in the mass of hydroxyapatite per unit area attributable to photon statistics would therefore be approximately ±0.5% (using a MAC of 4.69 $cm^2\ g^{-1}$).

8.1.8 Area scans and point selection

Before the dissolution experiment, SMR area scans were carried out in order to locate the samples on the XY stage and to select the coordinates of approximately 5 points suitable for measuring mineral mass changes that were caries free as identified using XMT.

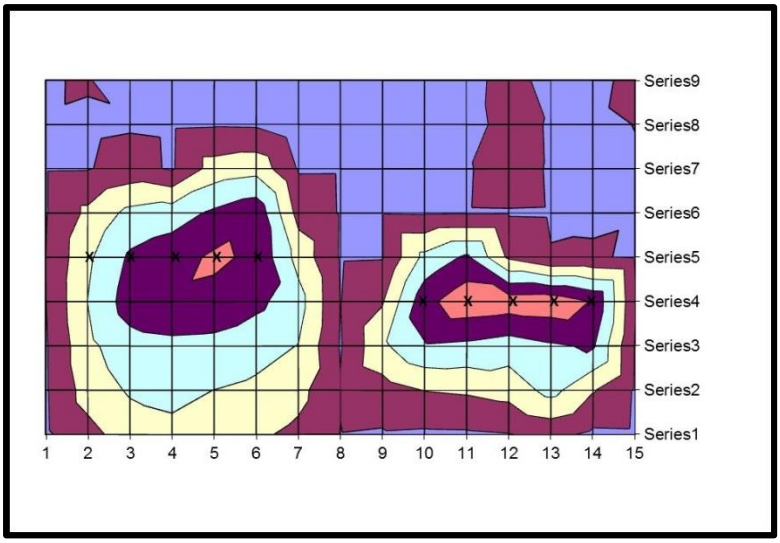

Figure 8.3 Typical SMR area scan of a permanent and DE sample. On average 5 co-ordinate points 1 mm apart (shown as 'x') were identified for SMR analysis.

Points for SMR analysis ran horizontally across the buccal enamel surface from distal to mesial sides and were 1 mm apart (**Figure 8.3**).

8.1.9 Standardisation procedure

The transmitted photon counts from the samples were standardised against measurements taken from a synthetic HAp compressed disc (standard material) located in an SMR cell adjacent to the SMR cells containing the enamel samples. The HAp disc has a homogenous composition that was not subjected to any treatment. Standardisation was used to compensate for any fluctuations in the generation of X-rays or any instability of the photon counting system.

The standard was scanned before and after each enamel section for a count time of 30 seconds to ensure a large number of data points were obtained for good statistical accuracy.

8.2 SMR methodology

8.2.1 Calcium and phosphate increment additions

The concentration of calcium and phosphate in the demineralising solution was increased incrementally by 3.0 mM calcium and 1.8 mM phosphate, respectively (Ca/P 1.67) every 48 hours. Steps were taken to ensure pH was unchanged. The rate of demineralisation of the enamel samples was measured at each increase in calcium/phosphate concentration increment using SMR.

8.2.2 Using linear regression to determine demineralisation rate

Mean demineralisation rates were calculated using linear regression from the projected mineral mass curves obtained from SMR analysis of selected points on the enamel surface (**Figure 8.4**).

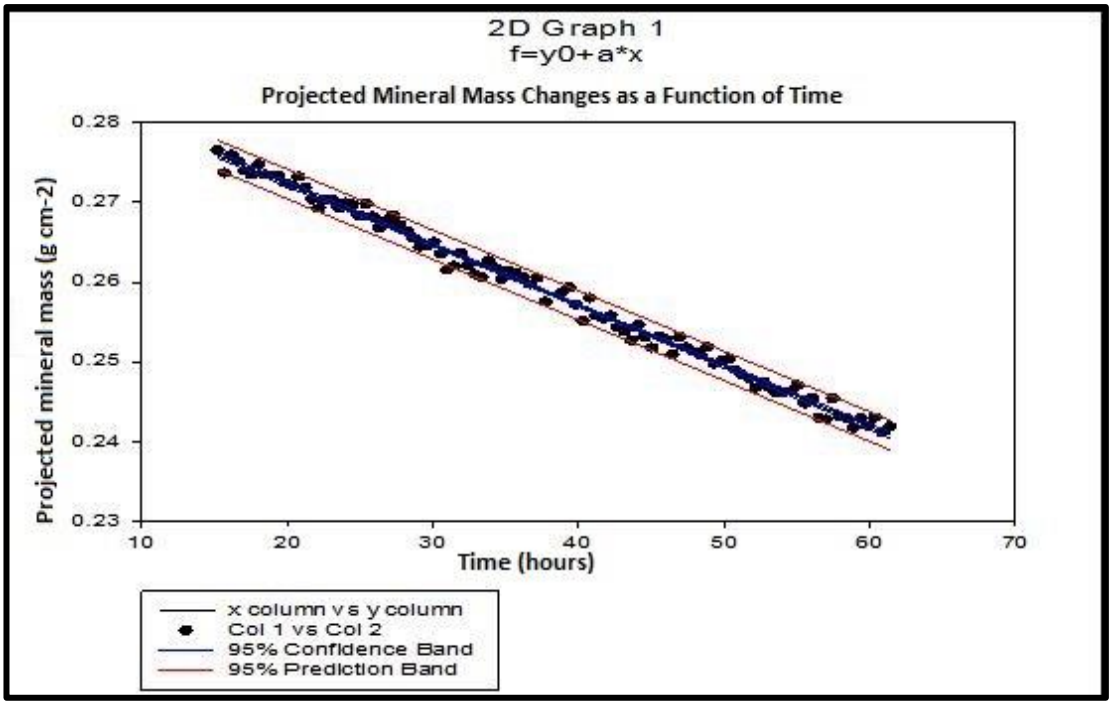

Figure 8.4 Typical SMR showing the linear changes in projected mineral mass of enamel with time and the 95% confidence intervals (p = *<0.0001*) in 0.1 M acetic acid solution at pH = 4.0.

The rate of mineral loss was determined from the gradient in units of grams per unit exposed area per hour. The typical time between successive data points on the same sample was about 10 min.

8.3 SMR results

8.3.1 Calculation of degree of saturation of demineralising solutions used

An ionic speciation program, Chemist (MicroMath, Missouri, USA) was used to calculate the degree of saturation with respect to hydroxyapatite (DS_{HAp}) for acetic acid at pH = 4.0 in a range of solutions with increasing calcium concentrations identical to those used in the SMR measurements. This calculation was repeated for

a range of pKsp values from 116 to 126, and the degree of saturation as a function of calcium concentration was then plotted for each pKsp value. Non-linear plots for all pKsp values were observed as shown in **Figure 8.5**.

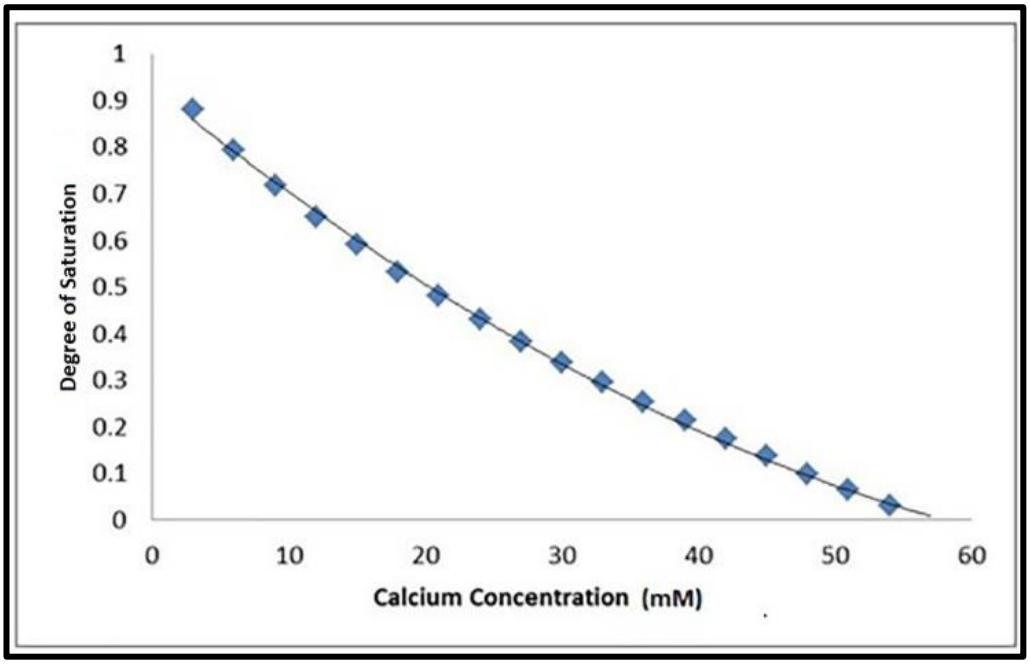

Figure 8.5 A typical Chemist plot for a pKsp of 118 showing thermodynamic equilibrium is reached at 57 mM of calcium at the x-intercept, under pH = 4.0 at 25 °C conditions. The degree of saturation with respect to HAp was calculated based on the conditions and calcium and phosphate concentrations used in the SMR experiment.

The calcium concentration at equilibrium (in this study when the saturation was 0) was determined from each plot by identifying the x-intercept of the regression curve; these were then plotted for each pKsp value (**Figure 8.6**).

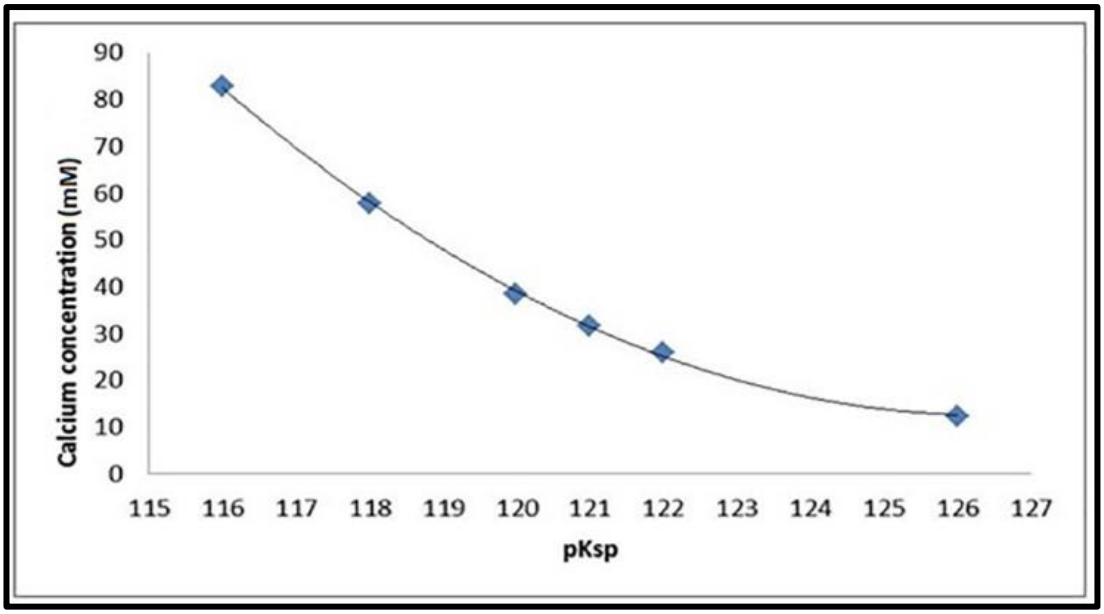

Figure 8.6 Calcium and phosphate concentration (mM) in equilibrium with HAp as a function of published pKsp values for HAp, assuming pH = 4.0, 0.1 M acetic acid and 25 °C, as calculated by Chemist.

8.3.2 Deciduous and permanent enamel demineralisation rate as a function of increasing calcium concentration

The SMR results showed that the demineralisation rates of DE and PE are similar (**Figure 8.7** and **Table 8.1**) and that differences in the rates were insignificant (student t-test value = 0.53, *p=0.05*).

Table 8.1 Mean DE and PE demineralisation rates as measured by SMR. T-test analysis showed differences were not significant (*p>0.05*)

Mean DE demineralisation rate (g cm^{-2})	Mean PE demineralisation rate (g cm^{-2})
6.74E-04	6.11E-04

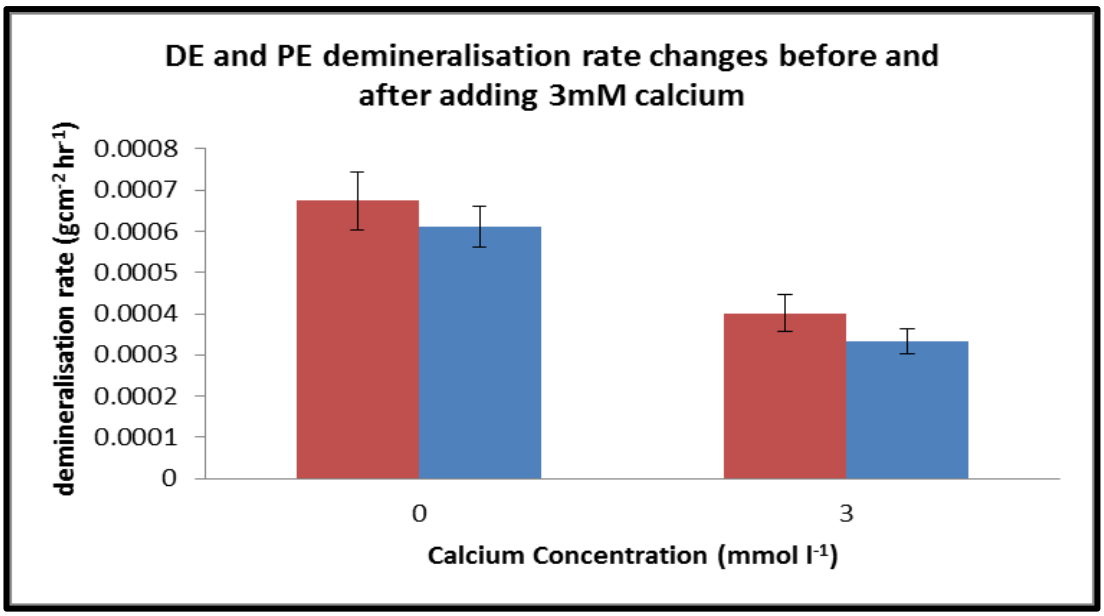

Figure 8.7 Demineralisation rates of DE (red) and PE (blue) at baseline (pH = 4.0, 0.1 M acetic acid) and after adding 3 mM calcium concentration to the acid.

From the SMR data, the calcium concentration required to halt demineralisation for permanent and DE was approximately 32 and 32.5 mM, respectively (**Figure 8.8** and **Figure 8.9**). These calcium values (required for saturation under the conditions used) were then used to determine the corresponding pKsp value from the Chemist plots.

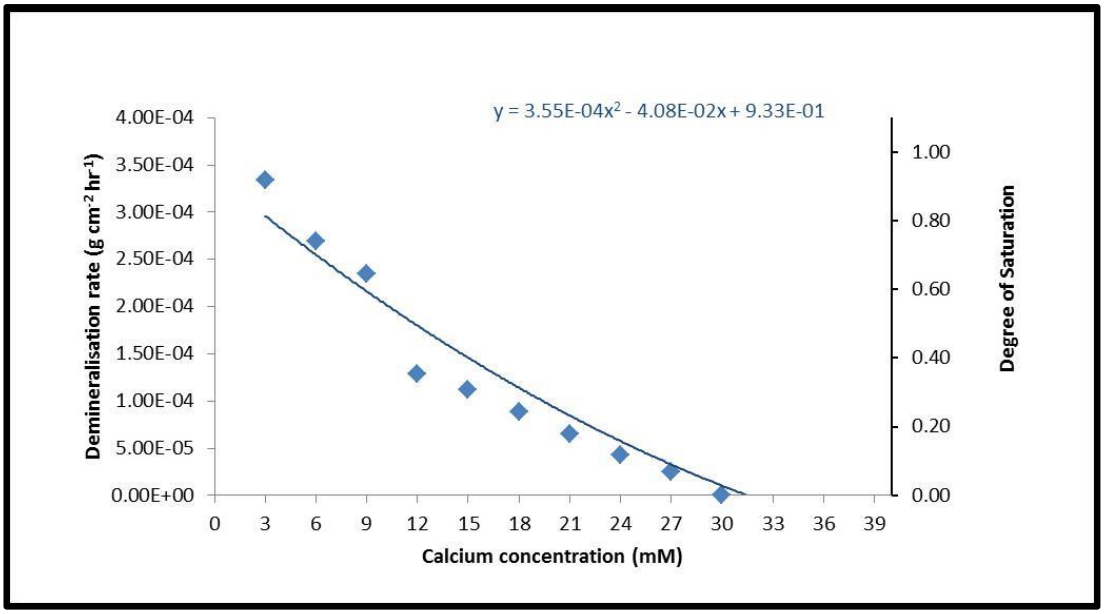

Figure 8.8 PE demineralisation rate as a function of increasing calcium concentration at pH = 4.0 and 25 °C based on results from the SMR experiment fitted to a pKsp trend line of 121 (solid line) to show similarities in trend. Rate is zero at a calcium concentration of approximately 30 mM.

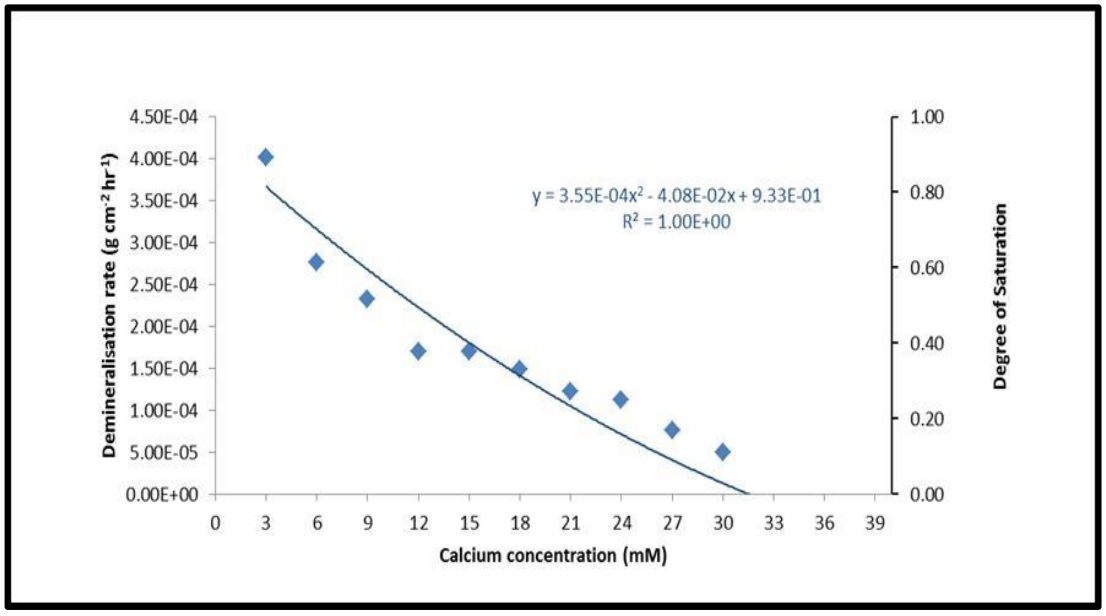

Figure 8.9 DE demineralisation rate as a function of increasing calcium concentration at pH = 4.0 and 25 °C based on results from the SMR experiment fitted with a pKsp trend line of 121 (solid line) to show similarities in the trend. Rate is zero at a calcium concentration of approximately 32 mM calculated using MATLAB from the x-intercept of the curve.

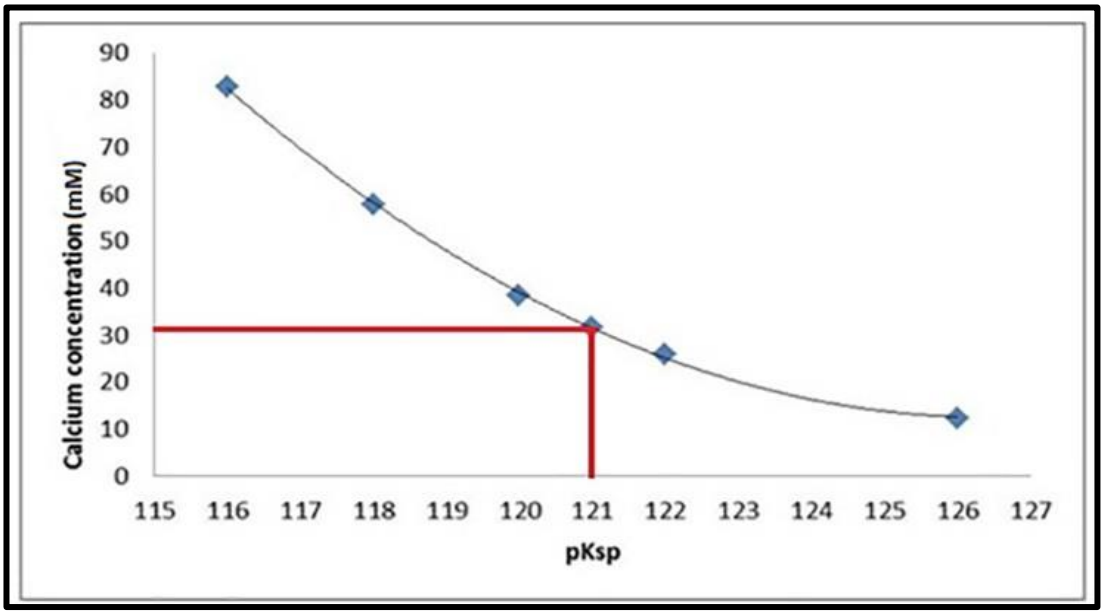

Figure 8.10 At a pKsp of 121, a calcium concentration of approximately 31 mM is required for saturation of a solution with respect to HAp at pH = 4.0.

Table 8.2 Calculated pKsp values and the corresponding calcium concentrations required to reach saturation with respect to hydroxyapatite, in 0.1 M acetic acid, pH=4.0 at 25°C.

pKsp	Minimum calcium concentration (mM) to reach saturation with respect to HAp
116	82.8
118	57.8
120	38.5
121	31.4
122	25.9
126	12.4

Deciduous and permanent human bulk enamel demineralisation rates halt at approximately 32.5 and 30 mM calcium concentrations, respectively. According to

the speciation program Chemist, this corresponds to a pKsp of 121 for both enamel types.

Further, when enamel demineralisation trend was compared to the linear regression curves of pKsp values 120, 121 and 122, the trend for 121 was much closer, as shown in **Figure 8.11** and **Figure 8.12**.

The trends in data for PE and DE are both similar to the trend in data shown for the degree of saturation at pKsp 121, indicating that the trend in demineralisation rate of bulk human DE and PE closely match the trend observed for the degree of saturation as a function of increasing calcium concentration for a pKsp of 121.

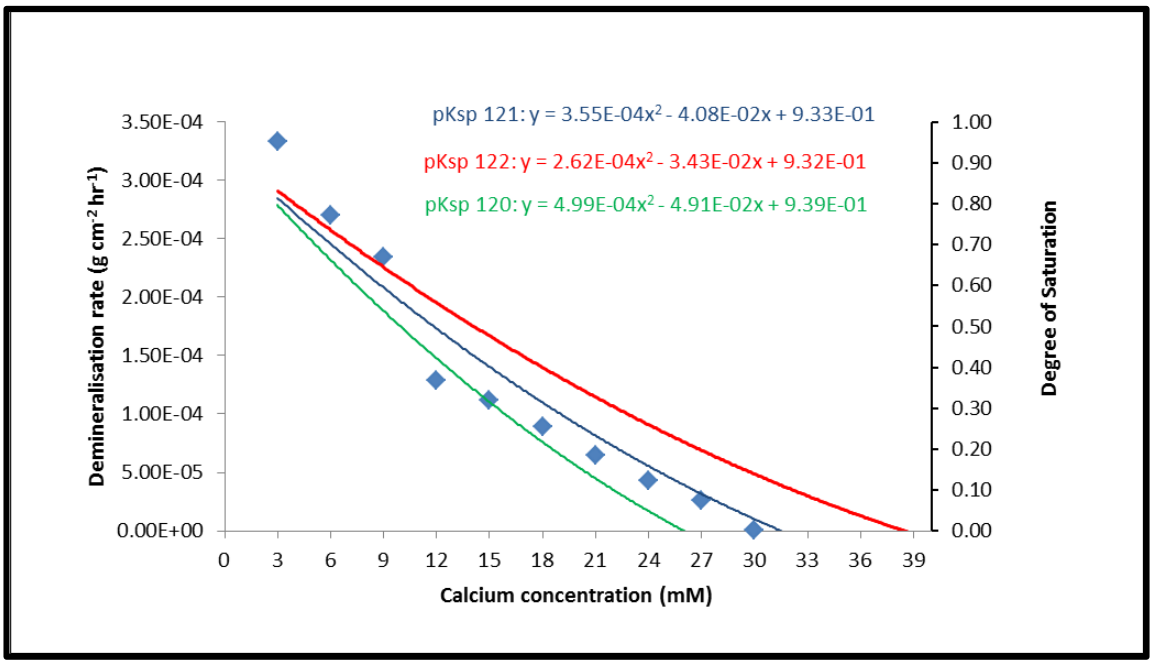

Figure 8.11 PE demineralisation rate trend (blue diamonds) compared with the calculated (speciation program) degree of saturation trend at a pKsp 121 for HAp (blue solid line) as a function of increasing calcium concentration in acetic acid pH = 4.0 at 25°C. When degree of saturation = 0 = equilibrium between HAp and solution has been achieved.

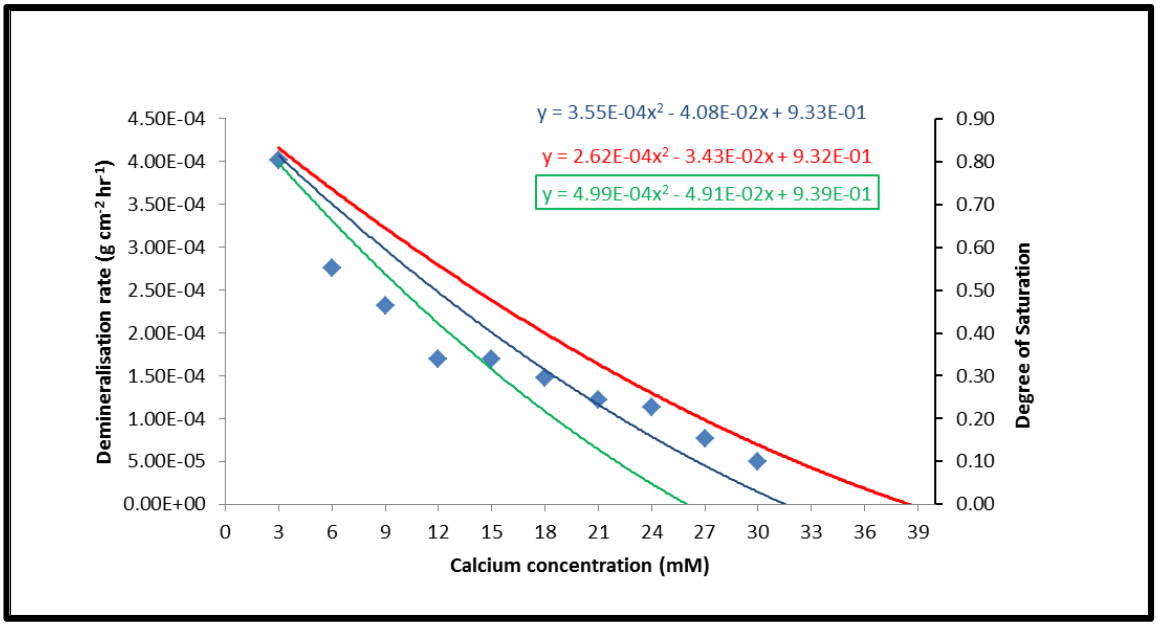

Figure 8.12 DE demineralisation rate trend (blue diamonds) compared with the degree of saturation trend at HAp pKsp values; 121 (blue solid line); 120 (red solid line) and 122 (green solid line) as a function of increasing calcium concentration in acetic acid pH = 4.0 at 25°C.

As shown in **Figure 8.12**, the calcium concentration required to achieve equilibrium under the conditions used at a pKsp of 120 and 122 are far from that recorded from the SMR kinetic data, whereas a pKsp of 121 is significantly closer at approximately 32 mM.

The pKsp value of 121 was further justified as the closest fit for enamel using the sum of least squares calculation.

Table 8.3 Least squares method for pKsp values 121, 120 and 122 fitted to DE SMR data. A pKsp value of 121 fits the enamel data the best with a value of 0.056 compared to 0.205 and 0.065 for 120 and 122, respectively.

pKsp	121	120	122
Least squares	0.056	0.205	0.065

Table 8.4 Least squares method for pKsp values 121, 120 and 122 fitted to PE SMR data. A pKsp value of 121 fits the enamel data best with the value of 0.08 compared to 0.17 and 0.15 for pKsp values 120 and 122, respectively.

pKsp	121	120	122
Least squares	0.08	0.17	0.15

To ensure the SMR technique correctly identified equilibrium between the solution and enamel at 30 mM, a further increment addition of calcium and phosphate was added. An increase in mineral mass would validate the SMR reading. **Figure 8.13** shows the increase in mineral mass observed after the additional increment of calcium and phosphate was added.

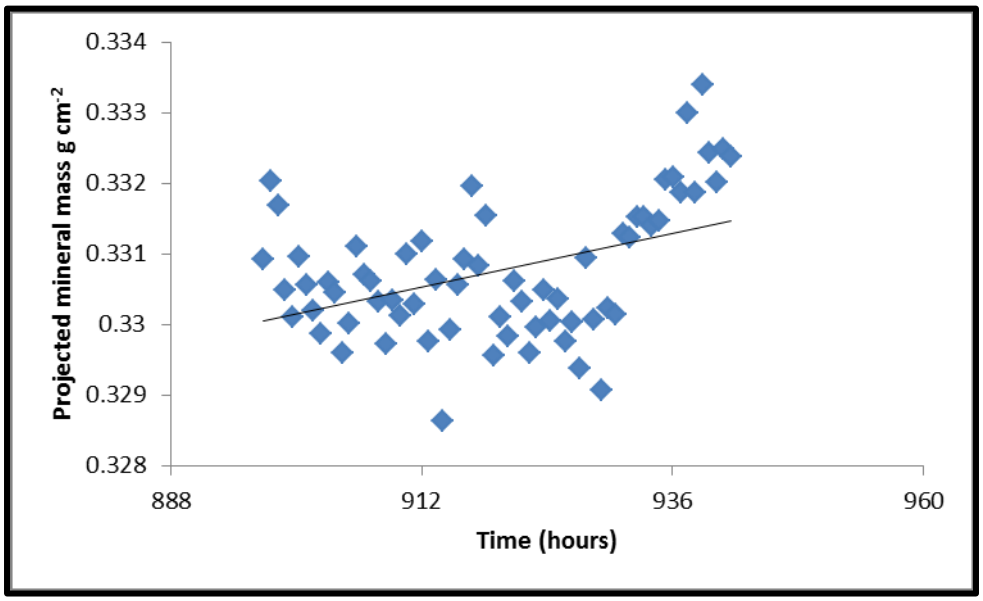

Figure 8.13 SMR readings of projected mineral mass changes in enamel after a total of 33 mM of calcium was added to the demineralising solution. An increase in mineral mass validated the SMR detection of equilibrium.

8.4 SMR discussion

The SMR experiments showed that DE and PE have similar demineralisation rates (6.11×10^{-4} and 6.7×10^{-4} g cm^{-2}, respectively), similar demineralisation trends as a function of increasing calcium concentration and similar trends to the trend in data observed for the calculated degree of saturation for a pKsp 121 as a function of increasing calcium concentration. The results suggest there were no significant differences between DE and PE under the conditions used.

The apparent-$pKsp_{BEnamel}$ value of 121 measured in this study is higher than many previously reported values (see **Table 3.1**), and higher than many values reported for pure HAp. As mentioned above, the methodology may influence the values reported for enamel and hydroxyapatite (Dorozhkin, 2012, Liu et al., 2013).

The relevance of the proposed methodology is that it provides a means of measuring real-time dissolution of enamel under caries simulating conditions that are highly controlled and precise using a photon counting system with minimum error (see Section 8.1.7 Mineral mass measurements). The real-time technique overcomes problems associated with measuring at intervals whereby a loss of information could lead to underestimations based on the data obtained (Anderson et al., 1998). It also eliminates the possibility of producing artifacts associated with sample distortion due to physically moving the sample between treatment environments e.g. demineralising media, and recording devise e.g. contact microradiograph as SMR permits constant monitoring of the sample during the treatment period.

The SMR data showed that the bulk human permanent and DE demineralisation at pH = 4.0 was reduced to zero at a calcium concentration of 30 mM and 32.5 mM, respectively. Correlation with the speciation software pKsp plots shows these correspond to a pKsp value of 121. **Figure 8.11** and **Figure 8.12** show consistencies between the SMR kinetic data trends and speciation software data trends indicates that the method was appropriate.

Figure 8.8 and **Figure 8.9** show that the decrease in demineralisation rate was non-linear (rather than linear as would be expected from simple first-order dissolution kinetics) similar to that obtained from speciation calculations for all pKsp values (**Figure 8.5**). This is consistent with what would be predicted for the calcium phosphate ternary system (Leaist et al., 1990).

As discussed earlier it is important to account for all possible phase transformations, and equilibria, as a lack of information on the resulting equilibria results in imperfect calculations (Pan and Darvell, 2007). Ion speciation programs rely on databases that report experimental results for speciation constants as well as the methods and conditions of the experiments reported. The similarities observed in the data from the SMR method and the speciation software confirms the methodology. The small standard errors also indicate that there was little variation in the demineralisation rates between samples.

The similarities observed between DE and PE in the SMR experiment contradict what has been reported in previous publications and what has been observed in the clinic as highlighted by the LGA report mentioned in Chapter 7. The similarities between the two enamel types as shown in the SMR results here suggest that factors other than the structural and chemical composition of DE and PE may contribute to the greater caries incidences and faster demineralisation rates reported for DE (Petersson et al., 1981 and Sønju Clasen 1997). For example, lower protective qualities of childrens saliva, such as a lower calcium and phosphate content and protein composition may result in an increased caries risk for children and may be the reason why such high incidences are reported in the clinic.

To relate the findings to a clinical situation, the speciation software was used to model the equilibrium conditions as a function of pH for the pKsp values under the conditions used in the experiment.

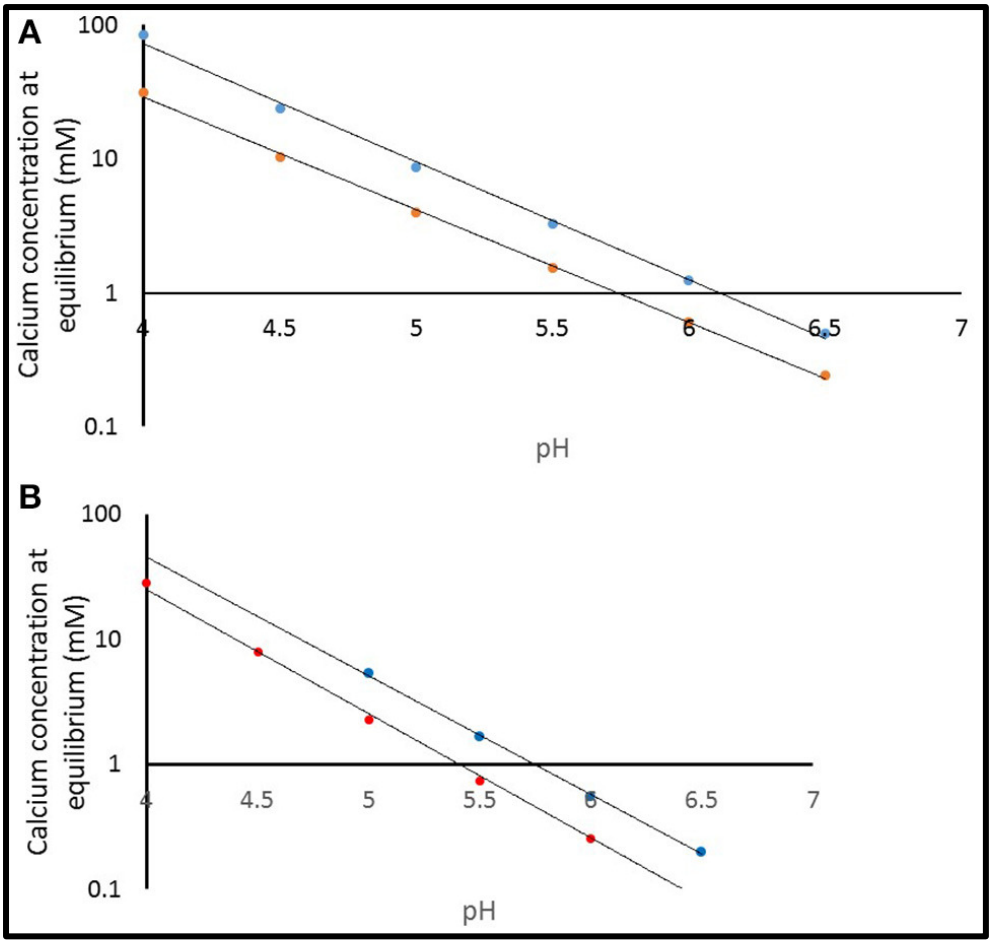

Figure 8.14 A/B (A) Calculated calcium concentration required for equilibrium at pKsp values of 116 (blue) and 121 (red) for a demineralisation solution of 0.1 M acetic acid. (B) Calculated calcium concentration required for equilibrium at pKsp values of 116 (blue) and 121 (red) with only that acid or base required for pH condition.

Figure 8.14A shows the calcium concentration required for equilibrium under the conditions used, including acid concentration and temperature (plotted on a log scale) for a pKsp value of 116 (blue), and for a pKsp of 121 (red). This shows that at pH = 4.0, the calcium concentration required for equilibrium for a pKsp =116 would be 85 mM, whereas for pKsp = 121 this would only be 31 mM. However, let us consider a calcium concentration of 1 mM, cited as the value of free calcium concentration in saliva (Lagerlof, 1983). Then, from **Figure 8.14A**, this would suggest that saturation would occur only at pH above 6.0. This is often called the

"critical pH" (Dawes, 2003). However, using a value of pKsp = 121, then this would suggest a much lower "critical pH" (at a calcium concentration of 1 mM). Of course, these calculations were performed with an acid concentration of 0.1 M, which is high for oral conditions. **Figure 8.14B** is a repeat of this calculation, but with no fixed acetic concentration (and is therefore not necessarily repeatable in a laboratory) but represents the opposite extreme with a zero acetic acid concentration. This reduces the critical pH value, assuming a free calcium ion concentration of 1.0 mM (Lagerlof, 1983). The oral environment acid concentration is likely to be somewhere between these extremes, but this calculation confirms that a pKsp value of 116 is too low, and that it is likely to be nearer to 121, otherwise there would be insufficient calcium in the oral environment to prevent enamel being undersaturated. It is also likely that other factors including salivary proteins (Kosoric et al., 2010) also play a role in the protective function of enamel and will modify the apparent solubility product.

Whilst these results provide an insight into the dynamics of enamel dissolution under pH = 4.0 conditions at 25◦C, the result is for bulk enamel only, and based on an *in vitro* design, and so it is important to acknowledge that any conclusions made are limited to these conditions only. For instance, further similar SMR studies are required to determine the effect of pH. An increase in dissolution rate is observed when pH is reduced (Gao et al., 2001). Furthermore, published data on the effect of pH on the solubility product of enamel is contradictory, e.g., Shellis and Wilson (2004) found no statistical difference in the solubility product of powdered enamel at different pH values between 4.5 and 5.5 whereas the earlier studies of Patel and

Brown (1975) reported lower solubility product values of 106–116 over a pH range of 4.5–7.6. The inconsistency in results is in spite of both experiments using powdered enamel as the substrate which again highlights the advantage of using bulk enamel as the substrate rather than powdered. Such measurements will also confirm or otherwise the marked change in slope of the solubility isotherm for HAp at around pH 3.9 as reported by Pan and Darvell (2009a, b).

Also, further similar SMR studies are required to study the influence of different ionic substitutions on both enamel and HAp powder, including carbonate, Mg^{2+}, F^{-}, etc. as they would provide significant further information on the chemistry of the demineralisation processes in DE and PE and would confirm or otherwise suppositions that a higher carbonate content in DE contributes to faster demineralisation rates and a greater risk of caries than PE (Goldberg, 2017). On a chemical compositional level, enamel is a substituted calcium hydroxyapatite (Neel et al., 2016). Its composition varies with ions such as F^{-}, CO_2^{-3} and Mg^{2+} replacing OH^{-}, PO_4^{3-} and Ca^{2+} within the stoichiometry allegedly altering the solubility of enamel (Aoba, 1997; Elliott, 2003; West and Joiner, 2014; Liu et al., 2016). Thus, the site of source material may be a critical factor. Also, similar studies are required too for a comparison of bulk enamel values with values obtained for powdered hydroxyapatite, similar to the studies reported in **Table 3.1**.

Further, the physical and chemical heterogeneities within enamel should not be ignored (Zhang et al., 2000; Bechtle et al., 2012). For example, demineralisation rates of prismatic, interprismatic and aprismatic enamel are not the same due to

differences between the organisation of crystals, the presence of more soluble material, and the porosity (Boyde, 1965; Shellis, 1996; Shellis and Dibdin, 2000). In DE, the neonatal line exhibits a disrupted crystal structure due to the onset of birth and experiments have shown differences in the demineralisation rates between the neonatal line and regular enamel. For example, in a study on the demineralisation rates of pre-natal, post-natal and neonatal line enamel Mishra et al., (2009) showed that while rates were similar in pre- and postnatal, rates at the neonatal line were slower suggesting a protective function against caries progression in DE. Similarly, the aprismatic region observed in permanent and deciduous outer enamel has been associated with having a protective function and contributing to reduced demineralisation rates (Kuhar et al., 1997, Oliveira et al., 2010). This layer has been shown to exhibit a more organised crystal structure where crystals are aligned parallel to each other in a tightly packed fashion. DE has been shown to have a wider aprismatic region than PE; this may therefore act as an additional protective outer layer that may be required to compensate for a lack of protection elsewhere in a child's oral environment, such as lower calcium and phosphate levels or lower protein content in childrens saliva.

Further solubility measurements are therefore needed to investigate the influence of the structural or chemical heterogeneities of enamel on the demineralisation rate. As the enamel is etched away and moves toward the enamel dentine junction there are changes in demineralisation rate resulting from gradients in ionic substitutions within enamel structure (Anderson and Elliott, 2000). In addition,

within enamel, the processes of demineralisation and remineralisation may not be co-localised, with ions diffusing in different directions (Anderson and Elliott, 1992).

8.5 SMR conclusion

It is important to measure the solubility of enamel under caries like conditions using a precise measuring system in order to accurately derive the solubility product. This information is relevant to the development of our understanding of caries and erosion and to develop preventative measures such as to screen anticaries agents.

In conclusion, the SMR method described here provides greater insight into bulk human enamel dissolution by measuring the effect of calcium concentration on the dissolution kinetics of deciduous and permanent bulk enamel demineralisation under standardised caries-like conditions. The measured $pKsp_{BEnamel}$ value of ~121 for both enamel types is similar to that reported by Shellis and Wilson (2004) for pure HAp and is in agreement with recent suggestions that $pKsp_{BEnamel}$ is higher than that reported previously in literature, and may be much closer to the value for pure HAp suggesting enamel is much less soluble than previously thought.

The similarities observed in the SMR solubility experiment suggest that DE and PE demineralise in a similar way in terms of rate and trend and therefore clinical observations that indicate a greater caries risk in children is likely due to differences in the oral environments between adults and children even more so than differences in structure and composition between each enamel type. However, further similar kinetic studies will be needed to measure enamel solubility at a

range of pH conditions, temperatures, and, for example, the influence of salivary proteins, in order to replicate the changing conditions of children and adult oral environments.

Chapter 9 Confocal laser scanning microscopy (CLSM) experiment

Confocal laser scanning microscopy (Olympus LX81 with Fluoview FV1000 scanner software version 4.1), was used to image outer, inner and EDJ of DE and PE. The aim of this study was to identify differences in the structural features of DE and PE in terms of their prismatic, interprismatic and aprismatic features (see Section 6.4 Confocal Laser Scanning Microscopy (CLSM) for an introduction on the technique).

Faster demineralisation rates in DE have been attributed to larger interprismatic widths than in PE, as these regions in enamel possess a greater degree of porosity than in prismatic enamel due to the changes in orientation of the enamel crystallites at the prism junctions. Therefore, measurements were taken of prism head diameters, interprismatic thicknesses and aprismatic widths, using the computer program Image J in both enamel types to identify differences between the two enamel types.

The dissolution characteristics of enamel have also been attributed to enamel heterogeneity. Therefore, measurements of features at the outer, inner and near the EDJ of enamel in both groups were recorded to identify and compare changes in features from the enamel surface towards the EDJ.

9.1 CLSM materials and methodology

9.1.1 Preparation of human enamel sections

Ten pairs of human deciduous and permanent teeth extracted for orthodontic purposes and stored in deionised water were sectioned parallel to the buccal tooth surface to produce 2 mm thin cross-sections. Sections were then immersed in 10 ml 0.1 mM Rhodamine B dye (0.044g of fluorescence grade Rhodamine B, sourced from Sigma-Aldridge was dissolved in 1 litre of deionised water to make a 0.1 mM stock solution) for 5 days (**Figure 9.1**).

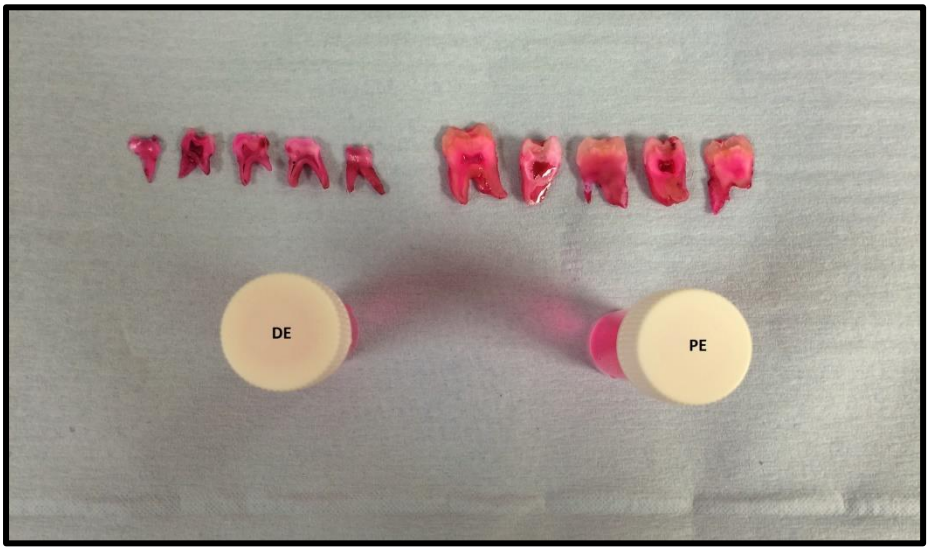

Figure 9.1 Human deciduous and permanent tooth sections soaked in 100 ml 0.1mM Rhodamine B dye.

To obtain a smooth surface for CLSM analysis and to ensure high resolution images, a series of Silica Carbide grinding papers (sourced from Buehler, UK) were used to

wet grind the enamel sections in the following grinding sequence: p1200 > p2500 > p4000, resulting in a final polished surface of 1 µm.

9.1.2 CLSM settings

The confocal laser scanning microscope (Olympus LX81 with Fluoview FV1000 scanner software version 4.1) fluorescent mode was used and the 543 nm green excitation laser and dichroic mirror 405 / 473 / 543 / 635 were selected to detect reflected light at wavelengths corresponding to Rhodamine B emitted wavelengths. The monochromatic setting was set to 560 – 610 nm wavelengths. Laser intensity was set at 50%, scanning speed was set at 10 µs/pixel.

Sections were placed on microscope slides and coated with 1 drop of Zeiss Immersol 518 N immersion oil (Fisher Scientific, UK). Images showing depths of up to 30 µm into enamel samples for both deciduous and permanent enamel sections were achieved.

CLSM images were obtained from; outer, inner and EDJ enamel of DE and PE sections. Images were analysed using Image J to quantitatively compare prism structures in both enamel types.

9.2 CLSM results

Rhodamine B penetrated both DE and PE up to depths of 60 µm, primarily along the interprismatic regions where porosity is greater (**Figure 9.2 a-c** and **Figure 9.3 d-f**, respectively).

Comparisons between DE and PE revealed significant differences between; outer, inner and EDJ prism widths (**Table 9.1**). Images showing depths of up to 60 µm into enamel samples for both deciduous and permanent enamel sections were achieved.

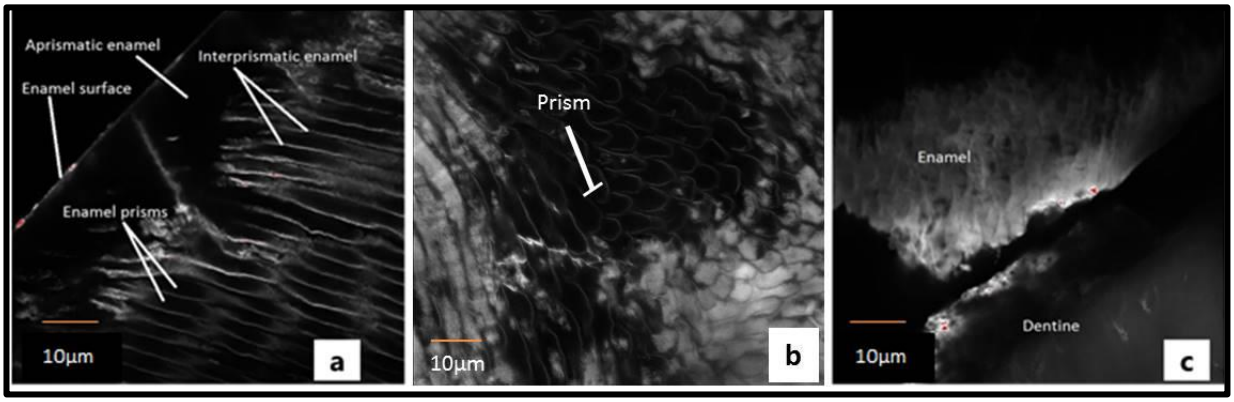

Figure 9.2 Typical CLSM images of Rhodamine B dye penetration of DE (a-c) showing outer, inner and EDJ regions, respectively.

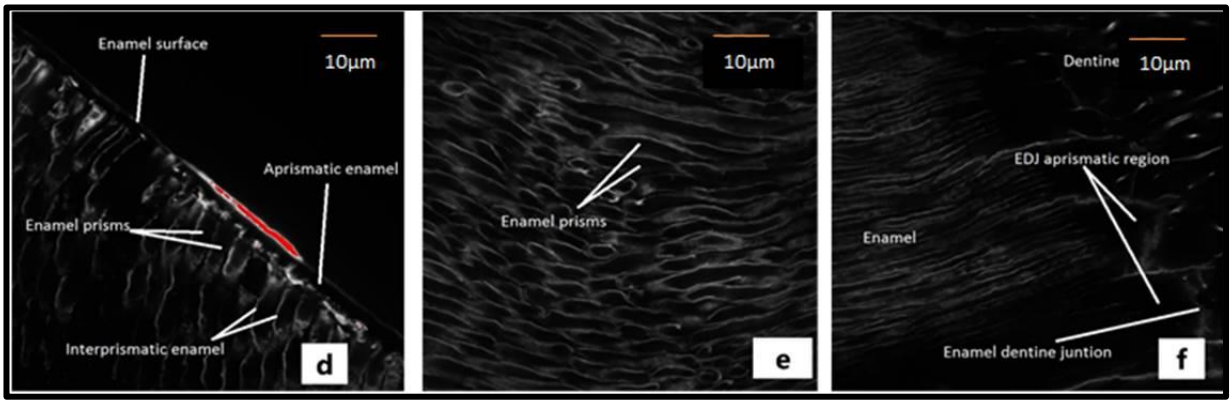

Figure 9.3 Typical CLSM images of permanent (d-f) enamel showing outer, inner and EDJ regions, respectively.

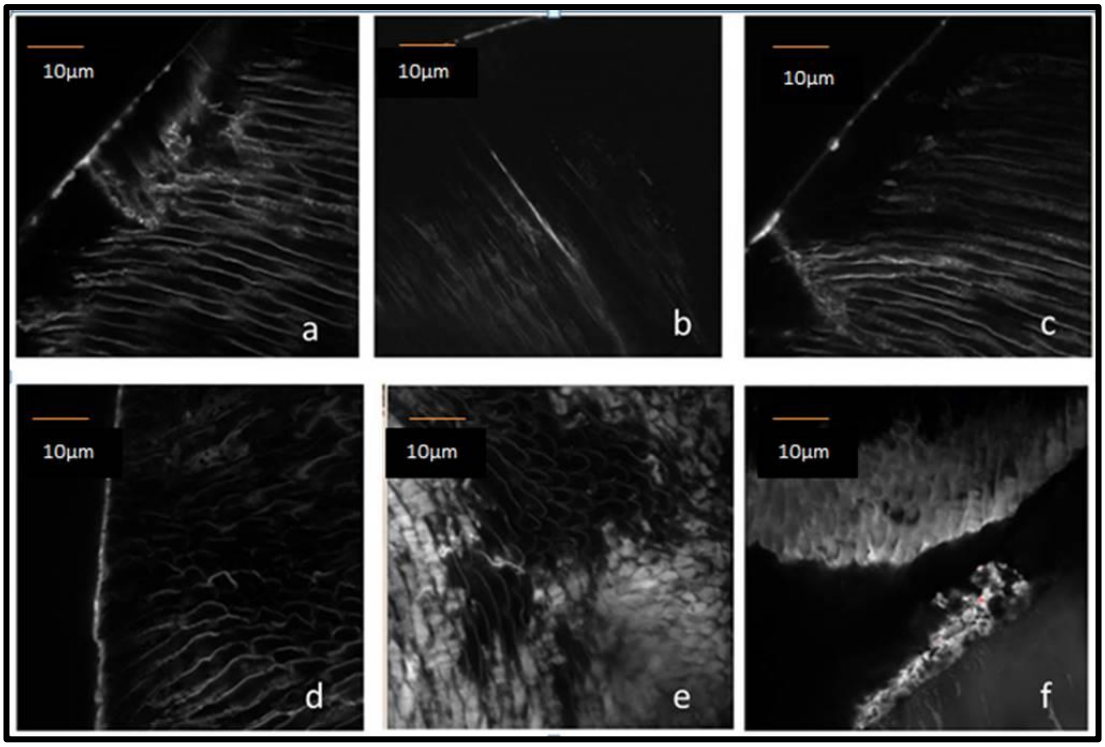

Figure 9.4 Typical CLSM images showing the aprismatic region in DE (a-d), Prismatic enamel in the middle of DE (e) and prismatic enamel near the EDJ, also showing dentine tubules in DE (f)

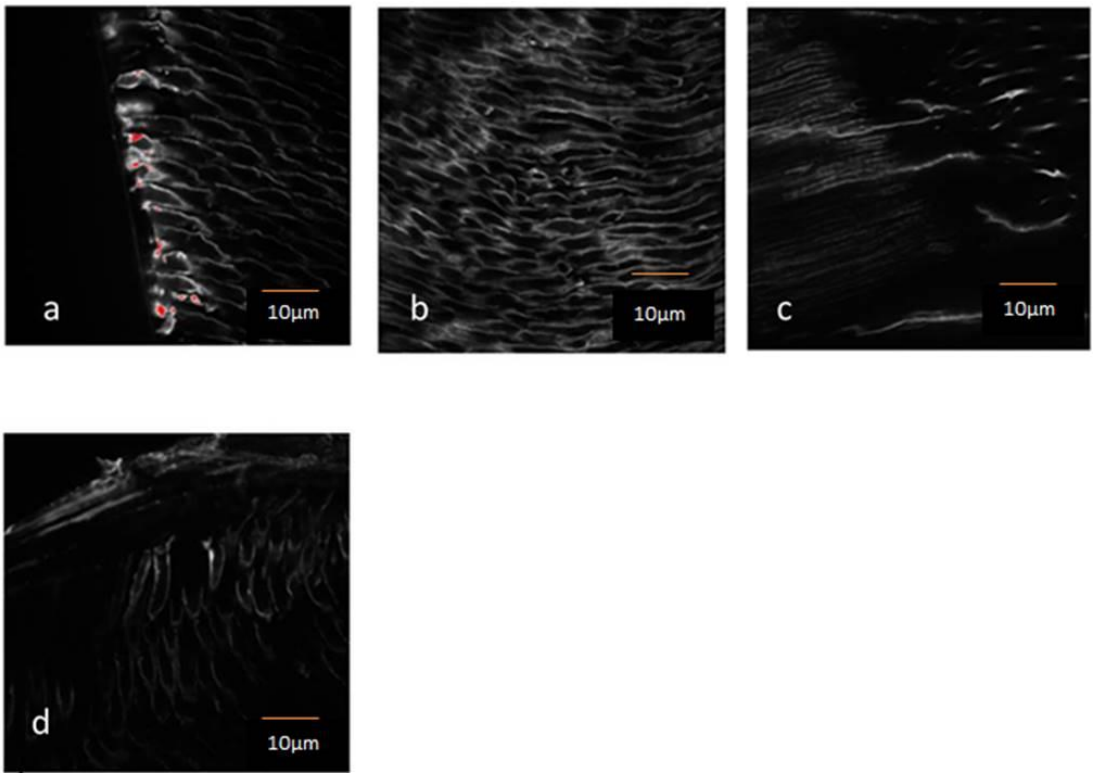

Figure 9.5 Typical CLSM images of PE showing outer (a and d), middle (b) and prisms near the EDJ with dentine tubules (c)

Rhodamine B penetrated both enamel cross-sections up to a depth of 60 µm through pores between crystals and prisms, i.e. through the interprismatic regions where crystal organisation is not as tightly packed as crystals bundled within prisms due to changes in crystal orientation. This permitted observation of different features within enamel and therefore allowed for quantitative assessment and comparisons of such features between DE and PE using Image J software. Image J analysis revealed significant differences between; outer, inner and EDJ prism widths (**Table 9.1**).

Table 9.1 DE and PE mean prism widths from outer, inner and EDJ enamel and aprismatic and interprismatic widths (standard errors are in parenthesis). Number of samples = 10.

Enamel region	DE (µm)	PE(µm)
Outer	5.51 (± 0.13)	6.3 (± 0.2)
Inner	5.5 (± 0.18)	4.8 (± 0.17)
EDJ	5.26 (± 0.1)	2.78 (± 0.15)
Aprismatic thickness	23.6 (± 1.0)	5.3 (± 0.16)
Interprismatic thickness	0.48 (± 0.02)	0.47 (± 0.02)

The most noticeable difference was observed in the aprismatic regions of DE and PE. **Figure 9.2a** and **Figure 9.3d** show typical widths of the aprismatic region in DE and PE, respectively. As shown in **Table 9.1**, the mean aprismatic width of DE was significantly greater than the mean aprismatic width in PE with the region in DE being 77.4 % wider. Rhodamine B dye was unable to penetrate the aprismatic region of both enamel types indicating a tightly packed crystallite structure as shown in **Figure 9.4**a-d and **Figure 9.5**a and d, where Rhodamine B is shown to accumulate (red and white regions) on the natural surface of both enamel cross-

sections as it was unable to enter enamel through the outer natural surface or through the aprismatic region below the surface.

As shown in **Table 9.1**, prism widths remained relatively constant from outer enamel towards the EDJ in DE but varied significantly in PE. For example, outer, inner and EDJ prism widths in DE were 5.51-, 5.5- and 5.26 µm, respectively whereas in PE prism widths reduced from 6.3- to 4.8- to 2.78 µm at the outer, inner and EDJ regions.

However, contrary to previous reports that attribute wider interprismatic regions in DE to their supposedly faster demineralisation rates, no significant differences between DE and PE mean interprismatic widths was observed (0.48 µm and 0.47 µm, respectively).

9.3 CLSM discussion

When used in fluorescent mode and adjusted to Rhodamine B settings CLSM provided high resolution images of DE and PE cross-sections at a depth of up to 60 µm. Analysis of the images produced with Image J software permitted accurate quantitative assessment of the features throughout for both enamel types which consequently permitted accurate quantitative comparisons of features between both enamel types to be made.

Rhodamine B dye successfully infiltrated DE and PE primarily through interprismatic regions where intercrystallite spaces are larger than pores present within prisms and between crystallites at the aprismatic regions. This allowed for good observational assessment of the features within both enamel types as shown in

Figure 9.2 and **Figure 9.3**. However, although Rhodamine B dye permits visualisation of internal structures and processes of enamel using CLSM; it is carcinogenic, decomposes in chlorinated water and must be refrigerated as its stability is temperature dependent.

Gonzalez-Cabezas et al., (1998) successfully used CLSM and Rhodamine B dye to evaluate the remineralisation efficacy of a fluoridated dentifrice. After treatment with a fluoridated dentifrice, remineralised enamel was indicated by a decrease in intensity of Rhodamine B fluorescence detected by CLSM compared to enamel samples at baseline. This was thought to be due to an increase in mineral content that prohibited the infiltration of Rhodamine B dye into the remineralised areas. To validate the technique, the CLSM data was compared with microradiographic data obtained from the same experiment. The authors concluded that there was a significantly high Pearson correlation coefficient between the results and that no significant differences between the data obtained from both techniques were identified.

The results of this study provide valuable insight of the structural features within DE and PE. **Figure 9.2** and **Figure 9.3** clearly show differences and similarities between DE and PE microstructural features. Image analysis of internal features using Image J was quick and easy yet provided valuable quantitative measurements of prismatic, interprismatic and aprismatic dimensions and orientations which allowed for accurate comparisons to be made within and between each enamel type. From the comparisons made between DE and PE, two main differences stood out; the aprismatic region in DE was 77.4 % wider than in PE and unlike the

reduction in prism head diameters from outer towards the EDJ in PE, DE prism head diameters were consistent throughout all enamel regions (**Table 9.1**). The consistency observed in the prism head widths within DE may be due to the faster enamel matrix deposition rate and faster mineralisation time observed in DE during amelogenesis compared to PE (Lunt and Law, 1974; Moorrees et al., 1963 and Shellis, 1984b). The smaller prism widths near the EDJ in PE observed in this study are consistent with previous reports that have shown PE to have a larger prism density nearer the EDJ than in middle or outer enamel. Boyde (1969) attributed the increase in prism head diameters from EDJ to outer enamel within PE to a decrease in ameloblast numbers during secretory stage. The death of ameloblasts (approximately 50 %) is thought to result in an increase of enamel matrix deposited per remaining ameloblast to cover the increasing surface area. Therefore, the shorter secretory stage in DE may results in few ameloblast deaths as the time is shorter. Prism widths would therefore remain consistent throughout DE as observed in this study. However, further studies on ameloblast number changes throughout amelogenesis in DE are required to substantiate this reasoning.

Preferential acid propagation via the interprismatic regions rather than via prismatic regions has been observed in previous studies (**Figure 3.7b**). Therefore, smaller prism widths resulting in an increased prism density may provide a greater level of protection from acid propagation towards the less mineralised and more porous adjacent dentine layer which would in turn protect access of harmful substances such as bacteria and acid towards the pulp.

Although the DE samples in this study do not exhibit the same increase in prism density near the EDJ as does PE, the significantly greater aprismatic region in DE as shown in **Figure 9.2a** and **Table 9.1** may also have a protective function. For example, the inability of Rhodamine B dye to penetrate this region indicates that the crystallites here are tightly packed and prohibit the entry of substances. This is consistent with previous reports that have shown the aprismatic region to consist of crystallites that are organised parallel to each other in a tightly packed fashion and that the organisation is greater within DE than within PE (Fava et al., 1997). Also, as DE is significantly thinner than PE, the thicker aprismatic region may provide greater protection to compensate. Further, longer acid etching times for dental material applications on DE is also attributed to their larger aprismatic regions suggesting that the layer has a protective function.

However, additional studies are required to explore the possible protective function of aprismatic enamel, for example by comparing the demineralisation rates of aprismatic enamel with prismatic enamel using SMR to identify if there are differences in the rates.

Previous reports that have shown faster demineralisation rates in DE attribute the faster rates to wider interprismatic regions in DE than in PE (Shellis, 1984b). Contrary to these previous reports, the results of this study show that there are no significant differences between the mean interprismatic widths of DE and PE (0.48 µm (SE = ± 0.02 µm) and 0.47 µm (SE = ± 0.02 µm), respectively) as shown in **Table 9.1**. The small standard errors indicate small variations between samples used, implying the results are reliable and the technique accurate. These results suggest

that the faster demineralisation rates and higher incidences of caries amongst children are due to other factors such as a lower level of protection of saliva, against caries and erosion.

Typical scan times using CLSM were approximately 8 minutes to produce image slices up to a depth of 60 μm within each sample. As discussed in Section 6.4.1 CLSM apparatus and function, focusing the microscope on a focal plane permits the use of monochromatic light to produce clear images without blurring effects caused by out of focus reflected light reaching the detector. This is imperative for visualisation of microstructural features within enamel and especially when making quantitative measurements of internal features as out of focus images may result in overestimations of their dimensions.

As mentioned above, Rhodamine B dye could infiltrate both enamel types via the interprismatic regions due to larger spaces within these regions. However, as can be seen from **Figure 9.2** and **Figure 9.3**, features within the prisms and in the aprismatic region could not be visualised. It is assumed that the crystals within these regions are tightly packed, as shown from scanning electron microscope images (**Figure 3.7**) which prohibits the infiltration of Rhodamine B dye. Therefore, whilst the crystals within these regions cannot be visualised, when CLSM is used in fluorescent mode the use of Rhodamine B dye can still offer information about the crystal organisation within these areas, i.e. no infiltration implies tightly packed crystals that suggests enamel protection from acid infiltration.

Further CLSM studies are required to provide information on the structural features of carious lesions within DE and PE. The larger aprismatic region in DE may result in

different histological characteristics of a carious lesion than the typical 'V' shape that characterises a carious lesion in PE, although further investigations are required to confirm this (Ripa et al., 1966 and Ripa 1966). Whilst SEM images would provide higher resolution images of surface topology, CLSM and Rhodamine B fluorescent dye would permit observation in 3D and would highlight, through fluorescence imaging, the pathways that acid infiltration would preferentially take through enamel. For example, CLSM and rhodamine B dye images taken before, and after, acid treatment at increasing time intervals would provide valuable information of the progression of a carious lesion in both DE and PE. However, Rhodamine B dye cannot be removed once used in sections and therefore fresh enamel sections would be required for imaging after each acid treatment.

9.4 CLSM conclusion

To conclude, CLSM used in fluorescent mode in combination with Rhodamine B dye yielded high resolution images that highlighted microstructural features within both DE and PE that permitted quantitative measurements to be taken of enamel features using Image J software. Significant differences between prism head diameters and their respective sizes throughout each enamel type were observed and showed a more consistent prism diameter width value throughout DE compared to PE. This may be due to the faster enamel matric deposition rates and mineralisation rates during amelogenesis of DE. Also, the larger aprismatic region in DE is also provides a protective layer to compensate for DE. This is evidenced by the lack of Rhodamine B dye observed by CLSM in this layer which suggests a tightly

packed organisation of enamel crystals in DE with minimum pores and may therefore act as a barrier to external harmful substances.

It has been suggested enamel dissolution begins at the interprismatic regions due to a greater porosity, this has been attributed to higher caries incidences in children (Shellis, 1984b; Sabel et al., 2012). However, here the results show that there was no significant difference between the interprismatic widths within both enamel types, suggesting that the faster rates and higher incidences reported may be due to other factors, for examples, lower calcium and phosphate concentrations within children's saliva.

Similar CLSM studies are required to gain a greater understanding of the carious process within DE. For example, the mechanism used by Rhodamine B dye to infiltrate enamel is similar to acid in terms of the pathways they take. Further studies would provide valuable information of the caries process during lesion progression through the different layers of enamel. This information could be used to create caries and erosion models that are based on a better understanding of the physical mechanism of acid propagation through the different features within DE and PE.

SECTION 5: OVERALL FINDINGS

Chapter 10 Overall discussion

Uncertainties remain concerning the extent of the differences and similarities between DE and PE in terms of their respective physical microstructural features, the functions of these structural features, their chemical compositions and how these structural and chemical features influence dissolution behaviours. The uncertainties are in part due to the various methodologies previous reports have adopted to compare the two enamel types. For example, extrapolating data from experiments on PE to explain dissolution behaviour in DE or comparing results obtained from two different experiments on DE and PE where each is subjected to different methodologies and techniques have often been used. In addition, the use of accurate imaging techniques with high resolution capabilities is important when comparing dimensions of internal enamel features, to reduce the chances of overestimations, as discussed in Sections 6.1 X-ray microtomography (XMT) and 6.4 Confocal laser scanning microscopy (CLSM). Both XMT and CLSM techniques use filtering devices of polychromatic energies to ensure only monochromatic radiation is detected by the detector so that undesirable artefacts, such as dishing and blurring effects are reduced in the final image. SMR also simulates computerised monochromatic energy by fitting data obtained from polychromatic energy to monochromatic energy over a selected narrow energy range using polynomial fitting. In this way, projected mineral masses can be calculated using the MAC value for HAp at the same energy (see Section 5.2.6 X-ray attenuation of hydroxyapatite for more on calculating mineral masses using MAC values).

Also, to minimise inaccurate comparisons, techniques that are non-destructive and those that can monitor dissolution trends and rates in real-time are required. In this study, the quantitative measurements of the structural features within DE and PE and their respective demineralisation rates using XMT, CLSM and SMR has permitted accurate comparisons of DE and PE that are reliable, accurate and repeatable.

The results of the imaging techniques used in this study *i.e.* XMT and CLSM have shown both enamel types are heterogeneous in terms of their respective mineral distribution and structural arrangement of enamel. For example, both enamel types exhibited a linear decrease in mineral concentration from outer enamel towards the EDJ and exhibit prismatic, aprismatic and interprismatic enamel regions that are similar in terms of their locations but are different in terms of their relative sizes. For example, as shown in **Table 9.1**, while DE prism head diameters are consistent throughout enamel, PE prism heads increase in size from the EDJ to outer enamel. As discussed in Section 9.3 CLSM discussion, the differences observed may be due to the different enamel matrix deposition and enamel mineralisation rates during the secretory and maturation phases of amelogenesis, or, may be associated with possible changes in the secretory face of the Tomes processes in PE during enamel matrix deposition. Boyde (1965) characterised the relationship between enamel prism orientation and Tomes processes by suggesting that prisms represent the fossilised path traced by Tomes processes during enamel secretion, indicating prismatic features are dictated by Tomes processes. Fosse (1964) attributes the increase in prism diameter size from the EDJ to the enamel surface in PE to the

increase in surface area of the enamel surface of a tooth relative to its EDJ during enamel deposition, and to the fact that ameloblast numbers do not increase accordingly once enamel secretion begins. To the contrary, ameloblast numbers decrease throughout the course of amelogenesis by the death of a certain portion (approximately 50 %) (Hubbard, 2000), consequently this requires an increase in the surface area covered by the remaining ameloblasts (Boyde, 1969). It is this increase in enamel matrix secretion by the remaining ameloblasts that is thought to result in the increase in prism head widths from the EDJ to the outer surface.

If the increase in prism diameter from the EDJ towards outer enamel is due to an increase in enamel matrix secretion by the remaining ameloblasts as an attempt to compensate for a reduction in ameloblast numbers over time, then it would follow ameloblast numbers in DE would remain relatively constant as the secretory stage in DE is much shorter and therefore there would be less cell deaths. The secretion of enamel matrix and therefore enamel prism diameters throughout DE would therefore also remain constant, as observed in this study. Further, the increase in surface area of the surface of DE with respect to the EDJ (a consequence of the growing enamel crown), is not as substantial in DE as it is in PE, because DE is thinner. Therefore, the need to secrete larger amounts of enamel matrix by the ameloblasts in DE to compensate for the increase in surface area of enamel relative to the EDJ would not be as great as it would be in thicker PE. Therefore, DE prism diameters would remain constant. However, further studies on the relationship between ameloblast numbers and enamel matrix deposition rates and volumes in

DE and PE throughout the secretory stage are required to confirm or otherwise such explanations for the differences in prism widths observed in DE and PE.

Similarities in the demineralisation rates of DE and PE measured by the SMR solubility experiment in this study ($p>0.05$) did not reflect the differences observed in the prism diameters of DE and PE as measured by CLSM ($p<0.05$). This suggests prism diameter does not influence demineralisation rates as rates in DE and PE were similar, though prism diameters were not.

However, interprismatic width measurements from this study contradict previous studies that have reported greater widths in DE, and have attributed this feature to greater demineralisation rates in DE. On the contrary, the results in this study show that enamel type has similar interprismatic widths ($p>0.05$) and no difference in demineralisation rates ($p>0.05$). Combined, the SMR and CLSM results from this study therefore support claims that there is a relationship between interprismatic widths and demineralisation rates and that there is a positive correlation between interprismatic widths and demineralisation rates (Oliveira et al., 2010), but contradict claims that suggest the interprismatic widths of DE and PE are different (Shellis, 1984b).

CLSM images of the outer region of enamel in both DE and PE show a distinct dark region. This indicates this area prohibited the infiltration of Rhodamine B dye and suggests interprismatic and thus prismatic enamel are absent in this region - as Rhodamine B was able to infiltrate via the pores in interprismatic enamel, yet was not able to in this outer region. When this information is combined with the XMT data which showed that the outer portion of enamel contained the highest mineral

concentration, the results from both studies indicate that this region is an aprismatic region, supporting the results of some previous studies and contradicting other studies that suggest the region does not exist in DE and PE (Fava et al., 1997). Further, a tightly packed crystallite organisation can be assumed based on the CLSM data, as no dye was able to penetrate.

The results in this study show that the mean aprismatic width in DE was approximately 77 % wider than observed in PE samples. The significant difference observed may be due to premature disappearance of the Tomes processes during the beginning stages of outer enamel formation in DE compared to PE, which would thus lead to the formation of a larger aprismatic region in DE. However, further studies on the morphological changes of ameloblasts within DE and PE at each stage of amelogenesis are required to gain a greater understanding of why such structural differences in DE and PE are present.

As discussed in Section 8.4 and Chapter 3, the methodologies and techniques used to measure demineralisation and remineralisation kinetics are important aspects of investigations that aim to determine rates in order to and obtain solubility product values of enamel or HAp. In this study, to ensure rates were accurately measured by SMR, measurements of demineralisation rates during increased calcium and phosphate concentrations, *i.e.* solutions with an increasing degree of saturation with respect to HAp, were compared with theoretical values of the degree of saturation for a range of pKsp values that were calculated using a speciation program (Chemist). The similarities between the SMR data and speciation program results validated the methodology and technique used. Similarities were observed

in terms of the trend in data - with both being non-linear and in terms of the amount of calcium and phosphate required to reach saturation (halt dissolution) with respect to HAp.

As the determination of the solubility product value of a mineral depends on the resolution capability of the technique employed to identify equilibrium between dissolving mineral and solution, *i.e.* when demineralisation rate is equal to zero, further calcium was added after the SMR data showed demineralisation rate was zero. An increase in projected mineral mass measured by SMR showed that the SMR system had correctly identified saturation of the solution. Further, before commencement of the demineralisation experiments, SMR sensitivity to changes in the chemical environment was assessed by measuring a dissolving mineral in acid and then switching the acid for water. The SMR measurements instantly changed from that of showing a loss of mineral to showing no loss which validated the resolution capability of the SMR (**Figure 8.2**).

The techniques used in this study were complementary by providing distinct quantitative and qualitative measurements which considered together have provided an overview of the physico-chemical characteristics of DE and PE. XMT image analysis of DE and PE using Image J showed that contrary to previous assumptions, DE and PE are similar in terms of their respective mineral concentrations. **Figure 7.4** and

Table 7.1 shows DE mean mineral concentration was 2.49 g cm^{-3} and PE mean mineral concentration was 2.48 g cm^{-3}. These results suggest the demineralisation rates of each enamel type would be similar. This was confirmed when SMR

measurements of demineralisation rates in DE and PE showed insignificant differences (**Figure 8.7**). CLSM image analysis of DE and PE further supported SMR and XMT data by showing that each enamel type had similar interprismatic widths (**Figure 9.2b** and **Figure 9.3b**). As discussed, interprismatic regions of enamel are thought to influence demineralisation rates as these regions contain the greatest intercrystallite spaces within enamel and show preferential demineralisation.

Considering in total, the results from all the experiments conducted suggest that demineralisation rate differences between DE and PE as observed in previous experiments and in the clinical studies, and reports may be due to external factors such as differences within the external oral environment of children and adults such as saliva free calcium concentrations and salivary protein concentrations (Ashley et al., 1991; Sivakumar et al., 2009) rather than differences concerning their enamel structure or composition.

For example, as discussed in Section 3.2.8 The role of the pellicle and saliva, the saliva and pellicle play significant roles in regulating the demineralisation and remineralisation of enamel. The pellicle is a complex and multi-layered film that has a multi-functional role that includes the protection of enamel from external environmental hazards; acting as a selective permeable barrier; regulating mineralisation and demineralisation (Moreno et al., 1977) and modulating microbial flora on the enamel surface (Gibbons et al., 1985, Levine et al., 1985). In light of the results of this study which suggest external factors are associated with the greater caries incidences amongst children recorded, further studies on the pellicle and saliva composition and flow rates in children are required to gain a

greater understanding of the roles these external factors have on DE demineralisation and caries risk.

For example, inhibiting salivary macromolecules such as acidic proline-rich proteins (PRPs) and statherin have been shown to reduce the crystal growth rate of hydroxyapatite seeds in supersaturated solutions with respect to hydroxyapatite as reported in Moreno et al., (1977) study. The reduction in growth rate was measured to be directly proportional to the extent of proline-rich protein and statherin absorption on to hydroxyapatite seeds. Additionally, statherin has also been shown to act as a calcium chelator (Johnsson et al., 1993). In undersaturated solutions with respect to HAp, the gathered calcium is released by statherin to induce an increase the degree of saturation in the localised area adjacent to the tooth surface. Therefore, further studies on PRPs and statherin concentrations within children's saliva and their adsorption characteristics on DE would highlight any association these molecules have with the demineralisation rates of DE compared to PE.

In addition, results from a study on oral proteins by Korant et al., (1985) suggested proteins interact to provide functional benefits for the oral environment. For example, α-amylase is a calcium binding protein with antibacterial properties that forms ionic complexes with salivary cystatin SA-I which is a thiol protease inhibitor with antiviral properties. It is suggested that this protein complex may modulate the microbial colonisation on the tooth surface. Regulation of the microbial colonisation on the tooth surface is fundamental to protection against caries onset. As with the onset of most oral diseases, there is a disruption in the ecosystem of

the oral microflora induced by a change in environmental conditions that leads to the proliferation of one microbial species over another. Proteins with antimicrobial and antifungal properties help to regulate the microflora and maintain balance. The higher caries incidence rates observed amongst children may therefore be associated with a reduction in the protective qualities of such modulating proteins and salivary components. Further studies on the antimicrobial properties of children's salivary and pellicle components are required to confirm or otherwise an association between caries incidence rates and pellicle and salivary components.

Further, studies on the protective function of the pellicle against enamel demineralisation have shown mature pellicles are more effective at reducing demineralisation both *in vivo* and *in vitro* than immature pellicles (Lendenmann et al., 2000). This lends support to theories that suggest greater interactions between oral components result in greater protection against disease onset. This infers that the oral environment functions more effectively when its constituents can interact. With respect to children, it may be that due to differences in diet and/or metabolism, a child's pellicle in comparison to an adult's pellicle may be much less complex and may not reach the same level of maturity as an adult's pellicle over the same time period and will therefore offer a weaker level of protection. However, further studies on the pellicle formation process and interactions of pellicle components in children are required to gain a greater understanding of the relationships between pellicle composition and protection level against demineralisation and caries.

As shown by the SMR results in this study (Section 8.3 SMR results), DE and PE responded to changes in calcium and phosphate in a similar way with both demineralisation rate trends exhibiting a non-linear decrease as a function of increasing calcium and phosphate concentration. This was similar to the theoretical trend of degree of saturation (proportional to chemical driving force) calculated by the speciation program (**Figure 8.5**). This is consistent with what would be predicted for the calcium phosphate ternary system (Leaist et al., 1990). As discussed earlier, it is important to account for all possible phase transformations (Pan and Darvell, 2007).

Greater caries incidences and faster demineralisation rates amongst children as observed in the clinic suggests that there may be differences in the calcium and phosphate concentrations within the oral environments of children and adults *in vivo.* This has been made evident in previous reports that have shown children saliva contains less calcium than adult saliva (Ashley et al., 1991). Further, calcium and phosphate concentrations and a higher Ca/P ratio have been shown to be considerably higher in caries-free children plaque than caries-active plaque samples (Shaw et al., 1983) and higher in adults plaque than in childrens plaque (Ashley et al., 1991). In other studies on phosphorus levels, an inverse relationship between phosphorus and caries incidence was found (Shannon et al., 1962, Shannon and Feller, 1979). Further studies comparing the free calcium and phosphate concentrations and ratios in children and adult pellicles and saliva are required to identify the importance of such elements on demineralisation rates.

10.1 Clinical implications

Overall, the results of this study suggest that although there are anatomical differences within DE and PE, as show from the CLSM section of this report, these differences do not contribute significantly to a change in demineralisation rates between the two enamel types nor their demineralisation trends.

From a clinical aspect, the CLSM results support current clinical procedure of longer etching times in children than in adults with regards to preparation for dental adhesives during dental procedures, even though DE is much thinner. The aprismatic region observed was significantly greater in DE than in PE and showed no infiltration of rhodamine B dye. This was indicative of a tightly packed surface layer that may function to protect DE from acid infiltration.

The higher rates in caries incidences amongst children as reported by clinical observations may be due to differences in the external factors of the oral environments in children and adults rather than structural or chemical differences within their enamel. This is further validated by the SMR study which was designed such that both enamel types were investigated under identical conditions. The results from the SMR study ultimately showed that in terms of both rates and trends, both enamel types were similar.

These results suggest that the risk of caries onset and progression in children may be higher than in adults because of differences in their respective oral protein and salivary compositions rather than structural or compositional differences within each enamel type. However, this is not to say that structural differences do not

contribute to greater demineralisation rates or a higher caries risk. For example, greater interprismatic regions within any enamel type would contribute to greater demineralisation rates in the same way that a greater aprismatic region would provide a greater level of protection against acid propagation. However, based on the results of this report, the structural differences between DE and PE did not result in greater demineralisations rates in either, suggesting other factors are involved in the greater demineralisation rates and greater caries incident rates observed in children.

As shown in **Figure 8.14**, when pH is considered under the conditions of the SMR experiment used in this study and at a pKsp value of 121 and 116, a calcium concentration of 85 mM would be required to halt demineralisation in pH 4.0 conditions at a pKsp of 116. However, at a pKsp of 121, the amount of calcium required reduces to 31 mM. Further, when the standard value for oral calcium concentration is considered, *i.e.* 1 mM, at a pKsp of 116 the pH at which demineralisation would halt under such conditions *i.e.* the "critical pH", would be above 6.0, whereas at a pKsp of 121, the critical pH at a calcium concentration of 1 mM would be approximately 5.75. This is true for an acetic acid concentration of 0.1 M, which is high for oral conditions. The actual critical pH would be lower under oral conditions. However, the results confirm that a pKsp of 116 is too low for oral calcium concentrations of 1 mM, and that it is likely to be nearer 121. Furthermore, when children's salivary calcium content is considered, previous reports have suggested concentrations may be even lower than the 1 mM measured in adults and have been measured at 9.9 mg/L (0.247 mM) (Moreira et al., 2009), this would

increase the critical pH even further. A pKsp of 121 is therefore more practical under oral conditions.

Chapter 11 Overall conclusion

The results from the XMT, CLSM and SMR investigations have together provided a balanced and precise depiction of the similarities and differences between DE and PE in terms of their microstructural features. The study has also identified relationships between the microstructural features within DE and PE with their respective.

The CLSM imaging technique showed that there are microstructural differences between DE and PE in terms of prism head diameters and aprismatic regions, however, when these results are considered alongside the SMR results, the differences in microstructural features do not influence the demineralisation rates or characteristics of each enamel type, as both rates were similar. However, the results from both studies suggest that interprismatic regions within enamel may influence demineralisation rates, as both enamel types exhibited similar interprismatic widths and both showed similar demineralisation rates, indicating that there is a positive correlation between interprismatic region and demineralisation rate.

Further, the XMT study showed insignificant differences between the mineral concentrations within DE and PE, contrary to previous studies. However, the XMT result complemented the SMR results, indicating that there is an association between mineral concentration and demineralisation rate in DE and PE, and that this is also likely to be a position correlation.

The methodologies of each experimental set up permitted simultaneously observations of both enamel types which limited the drawbacks associated with extrapolating data from different experiments.

As highlighted by Government and clinical reports, the increase in dental hospital admissions and higher caries incidence rates amongst children compared to adults has become a cause for concern and merits the attention of further scientific research in order to understand the reasons behind these differences.

The results of this study has provided evidence that indicates the higher caries incidence rates amongst children compared to adults is associated with differences between the external oral environments of children and adults rather than differences between the internal enamel features of each enamel type as differences measured between the demineralisation rates of each enamel type were insignificant according to the SMR study. Therefore, future studies that use quantitative techniques to compare the factors associated with the external oral environments of children and adults will provide information that will contribute to our understanding of the differences in rates observed in the clinic.

To conclude, the combination of quantitative techniques used have successfully achieved the aim of this study which was to "compare the microstructural features within DE and PE and relate the microstructural features within both enamel types to their respective demineralisation characteristics". The quantitative measurements made highlighted the associations between microstructural features and demineralisation characteristics of each enamel type. Based on the resolution

capacities, use of monochromatic energy and the methodological set up; the results of this study are considered to be reliable and accurate.

Chapter 12 Future studies

Further investigations on the oral environments of children, for example measuring calcium concentrations in saliva and the pellicle, the effect of diet on salivary and pellicle compositions and the associations these environmental factors have with the demineralisation characteristics of DE are required to understand the higher caries incidence rates amongst children than in adults. It is possible that the calcium and phosphate concentrations within saliva influence the outward diffusion of these ions from plaque (Ashley et al., 1991). Therefore, lower calcium and phosphorus concentrations in saliva may lead to higher caries incidences than in adults. In addition, Ashley and Wilson (1978) showed a direct relationship between the inorganic phosphorus concentrations of plaque and phosphorus concentrations in stimulated mixed saliva in children and in stimulated parotid saliva in young adults. However, future studies should ensure fairness in their methodologies when comparing saliva and plaque compositions, and element concentrations between adults and children as saliva and plaque samples from each group will vary according to many factors including the time of day, the area of the mouth (Dawes and Jenkins, 1962) and diet (Wilson and Ashely, 1990). Individual variations in these factors may obscure any relationship between plaque and saliva compositions and demineralisation rates. Further, studies on the pellicle maturation levels that are achieved in adults and children would provide valuable information regarding the influence that pellicle maturity has on enamel protection from demineralisation and caries incidence. As discussed in Section 3.2.8 The role of the pellicle and saliva,

previous studies have shown that functional characteristics of the pellicle depend on the level of maturity it reaches.

Overall, further similar studies that compare DE and PE under identical conditions are required in order to avoid the drawbacks associated with extrapolating data from previous experiments. Furthermore, the techniques that are used to measure differences in DE and PE should be quantitative and should use monochromatic energy in order to avoid artefacts that may lead to under/overestimations and conflicting results, as demonstrated in previous reports.

References

Acs, G., Lodolini, G., Kaminsky, S. and Cisneros, G. J. (1992) Effect of nursing caries on body weight in a pediatric population. *Pediatr. Dent.* 14 5: 302-305.

Agostini, P. and Petite, G. (1988) Photoelectric effect under strong irradiation. *Contemp. Phys.* 29: 57-77

Ahmed, M., Davis, G. R. and Wong, F. S. (2012) X-Ray microtomography study to validate the efficacies of caries removal in primary molars by hand excavation and chemo-mechanical technique. *Caries Res.* 46: 561–7.

Ashley, F. P., Coward, P. Y., Jalil, R. A. and Wilson, R. F. (1991) Relationship between calcium and inorganic phosphorus concentrations of both resting and stimulated saliva and dental plaque in children and young adults. *Arch. Oral Biol.* 36 6: 431-434

Ashley, F. P. and Wilson, R. F. (1978) The relationship between calcium and phosphorus concentrations of human saliva and dental plaque. *Arch. Oral Biol.* 23: 69-73

Al-Hashimi, I. and Levine, M. J. (1989) Characterisation of in vivo salivary derived enamel pellicle. *Arch. Oral. Biol.* 34: 289-295

Allinson, N. M. (1994) Development of non-intensified charge-couple device area X-ray detectors. *J. Synchrotron Rad.* 1: 54–62

Amaechi, B. T., Higham, S. M. and Edgar, W. M. (1999) Factors influencing the development of dental erosion *in vitro*: enamel type, temperature and exposure time. *J. Oral Rehabil.* 26: 624-630

Anderson, P., Bollet-Quivogne, F. R. G., Dowker, S. E. P. and Elliott, J. C. (2004) Demineralisation in enamel and hydroxyapatite aggregates at increasing ionic strengths. *Arch. Oral. Biol.* 49: 199-207

Anderson, P. and Elliott, J. C. (1992) Subsurface demineralisation in dental enamel and other permeable solids during acid dissolution. *J. Dent. Res.* 71 8: 1473-1481

Anderson, P., and Elliott, J. C. (2000). Rates of mineral loss in human enamel during in vitro demineralization perpendicular and parallel to the natural surface. *Caries Res.* 34: 33–40. Doi: 10.1159/000016567

Anderson, P., Hector, M. P. and Rampersad, M. A. (2001) Critical pH in resting and stimulated whole saliva in groups of children and adults. *Int. J. Paediatr. Dent.* 11: 266-273

Anderson, P., Levinkind, M. and Elliott, J. C. (1998). Scanning microradiographic studies of rates of in vitro demineralisation in human and bovine dental enamel, *Arch. Oral Biol.* 43: 649-656.

Angmar, B., Carlstrom, D. and Glas, J. E. (1963) Studies of the ultrastructure of dental enamel. IV. The mineralization of normal human enamel. *J. Ulrastruct. Res.* 8: 12-23

Aoba, T. (1997). The effect of fluoride on apatite structure and growth. *Crit. Rev. Oral Biol. Med.* 8: 136–153. doi: 10.1177/10454411970080020301

Aoba, T. and Moreno, E. C. (1987) The enamel fluid in the early secretory stage of porcine amelogenesis: chemical composition and saturation with respect to enamel. *Calcif. Tissue Int.* 41: 86-94.

Arends, J. and Jongebloed W. L. (1977) Dislocations and dissolution in apatites: theoretical considerations. *Caries Res.* 11: 186-188

Arends, J. and Jongebloed W. L. (1981) Apatite single crystals. Formation, dissolution and influence of CO32- ions. *Rec. Trav. Chim. Pays-Bas*. 100: 3-9

Bambynek, W., Crasemann, B., Fink, R. W., Freund, H. U., Mark, H., Swift, C. D., Price, R. E. and Rao, P. V. (1972) X-ray fluorescence yields, auger, and Coster-Kronig transition probabilities. *Rev. Mod. Phys.* 44 4: 716 - 808

Bartlett, J. D. (2013) Dental Enamel Development: Proteinases and their enamel matrix substrates. Hindawi Publishing Corporation, *ISRN Dentistry* Volume 2013: 1-24

Bawden, J. W., Crenshaw, M. A., Takano, Y. and Hammarstrom, L. (1982) Ion transport through the enamel organ. An update. *J. Dent. Res*. 61: 1552-1554.

Bell, L. C., Posner, A. M. and Quirk, J. P. (1972) Surface charge characteristics of hydroxyapatite and fluorapatite. *Nature*. 239: 515-517

Bengtsson, Å., Shchukarev, A., Persson, P. and SjÖberg, S. (2009) A solubility and surface complexation study of non-stoichiometric hydroxyapatite. *Geochim. Cosmochim. Acta.* 73: 257-267

Berkovitz, B. K. B., Moxham, B. J., Linden, R. W. A. and Sloan, A. J. (2011) *Master dentistry: oral biology.* London, Churchill Livingstone Elsevier. 113-121.

Berner, R. A. (1978). Rate control of mineral dissolution under earth surface conditions. *Am. J. Sci.* 278: 1235–1252. doi: 10.2475/ajs.278.9.1235

Bechtle, S., Ozcoban, H., Lilleodden, E. T., Huber, N., Schreyer, A., Swain, M. V., et al. (2012). Hierarchical flexural strength of enamel: transition from brittle to damage-tolerant behaviour. *J. R. Soc. Interface* 9: 1265–1274. doi: 10.1098/rsif.2011.0498

Bhat, M. and Nelson, K. B. (1989) Developmental Enamel Defects in Primary Teeth in Children with Cerebral Palsy, Mental Retardation, or Hearing Defects: A Review. *Adv. Dent. Res.* 3 2: 132-142.

Bird, M. J., French, E. L., Woodside, M. R., Morrison, M. I. and Hodge, H. C. (1940) Chemical analysis of DE and dentine. *J. Dent. Res.* 19: 413-423. doi: 10.1177/00220345400190040801

Blumenthal, G. R. and Gould, R. J. (1970) Bremsstrahlung, synchrotron radiation, and Compton scattering of high-energy electrons traversing dilute gases. *Rev. Mod. Phys*. 42: 237-270

Borutta, A., Wagner, M., and Kneist, S. (2010). Early childhood caries: a multifactorial disease. *OHDMBSC.* 9: 32–38.

Bosch, J. J. ten, Borsboom, P. C. F. and Cate, J. J. ten (1980) A non-destructive method for monitoring de- and remineralisation of enamel. *Caries Res.* 14: 90-95

Boyde, A. (1965) Structure of developing mammalian dental enamel. In: ed. *M. V. Stack and R. W. Fearnhead: Tooth enamel.* London, John Wright & Son Ltd. 163-167.

Boyde, A. (1967). The development of enamel structure. *Proc. R. Soc. Med.* 60: 923–928.

Boyde, A. (1969) Correlation of ameloblast size with enamel prism pattern: use of scanning electron microscope to make surface area measurements. *Z. Zellforsch.* 93: 583—593

Brambilla, E., Twetman, S., Felloni, A., Cagetti, M. G., Canegallo, L., Garcia-Godoy, F. and Strohmenger, L. (1999) Salivary mutans streptococci and lactobacilli in 9- and 13-year-old Italian schoolchildren and the relation to oral health. *Clin. Oral Invest.* 3: 7-10

Brookes, S. J., Kingswell, N. J., Barron, M. J., Dixon, M. J. and Kirkham, J. (2011) Is the 32-kDa fragment the functional enamelin unit in all species? *Eur. J. Oral Sci.* 119 Suppl. 1: 345–350 doi: 10.1111/j.1600-0722.2011.00869.x

Brown, P. W. and Martin, R. I. (1999) An analysis of hydroxyapatite surface layer formation. *J. Phys. Chem. B.* 103: 1671-1675

Brunton, P. (2014). Summary of: continuing development of an oral health score for clinical audit. *Br. Dent. J.* 216: 526–527. doi: 10.1038/sj.bdj.2014.380

Busch, P., Heinonen, T. and Lahti, P. (2007) Heisenberg's uncertainty principle. *Phys. Rep.* 452: 155 – 176

Byrne, J. and Howarth, N. The K-shell fluorescence yield and atomic shell structure effects. (1969) *J. Phys. B: Atom. Molec. Phys.* 3: 280-292

Cariño, K. M, G., Shinada, K. and Kawagunchi, Y. (2003) Early childhood caries in northern Philippines. *Community Dent. Oral Epodemiol*. 31: 81-89

Carrington, G. (2003) *Basic Thermodynamics*. Oxford. *Oxford University Press*

Cavadini, C., Siega-Riz, A. M. and Popkin, B. M. (2000) US adolescent food intake trends from 1965 to 1996. *Arch. Dis. Child.* 83: 18-24.

Choung, H. W., Lee, J. H., Lee, D. S., Choung, P. H., Park, J. C. (2013) The role of preameloblast-conditioned medium in dental pulp regeneration. *J. Mol. Histol.* 44 6: 715-721

Christoffersen, J., Dohrup, J. and Christoffersen, M. R. (1996) The importance of formation of hydroxyl ions by dissociation of trapped water molecules for growth of calcium hydroxyapatite crystals. *J. Cryst. Growth.* 186: 275-282

Christoffersen, M. R., Dohrup, J. and Christoffersen, J. (1998) Kinetics of growth and dissolution of calcium hydroxyapatite in suspensions with variable calcium to phosphate ratio. *J. Cryst. Growth.* 186: 283-290

Clarke, M., Locker, D., Berall, G., Pencharz, Kenny, P. D. J. and Judd, P. (2006). Malnourishment in a population of young children with severe early childhood caries. *Pediatr. Dent*. 28 3: 254-259.

Cochrane, N. J., Anderson, P., Davis, G. R., Adams, G. G., Stacey, M. A. and Reynolds, E. C. (2012) An X-ray Microtomographic Study of Natural White-spot Enamel Lesions. *J. Dent. Res.* 91**:** 185-191.

Cooke, K. (2009) X-ray interactions with matter In *Cherry, P. and Duxbury, M. A. Practical Radiotherapy Physics and Equipment*. Oxford, Blackwell Publishing Ltd. 4: 36-48

Cosslett, V.E. (1957) The scope of the proceedings. Cambridge, *Cambridge Proceedings*. 3-16.

Crabb, H. S. M. and Mortimer, K. V. (1966) Dental caries and enamel structure. *Nature*, London. 209: 611-612

Creagh, D. C. and Hubbell, J. H. (1992). X-Ray Absorption (or Attenuation) Coefficients, Sec. 4.2.4. In: *Wilson, A. J. C. (ed.) International Tables for Crystallography*. Kluwer Academic Publishers, Dordrecht.

Cummins, D. (2013) The development and validation of a new technology, based upon 1.5% arginine, an insoluble calcium compound and fluoride, for everyday use in the prevention and treatment of dental caries. *J. Dent*. 41 2: S1–S11.

Cuy, J. L., Mann, A. B., Livi, K. J., Teaford, M. F. and Weihs, T. P. (2002) Nanoindentation mapping of the mechanical properties of human molar tooth enamel. *Arch. Oral Biol.* 47: 281-291

Daniel, O., Ogbanje, G. and Jonah, S. A. (2013) X-rays and scattering from filters used in diagnostic radiology. *IJSRP.* 3: 1-11

Davis, G. R., Jain, N. and Elliott, J. (2008) A modelling approach to beam hardening correction. *Proc. of SPIE.* 7078: 1-10. doi: 10.1117/12.794808

Davis, G. R., Evershed A. N. and Mills, D. (2013) Quantitative high contrast X-ray microtomography for dental research. *J. Dent.* 41 5: 475-482. doi: 10.1016/j.jdent.2013.01.010.

Davis, G. R. and Wong, F. S. L. (1996) X-ray microtomography of bones and teeth. *Physiol. Meas.* 17: 121-146

Dawes, C. (2003) What Is the Critical pH and Why Does a Tooth Dissolve in Acid? *J. Can. Dent. Assoc.* 69 11:722–4

Dawes, C. and Jenkins, G. N. (1962) Some inorganic constituents of dental plaque and their relationship to early calculus formation and caries. *Arch. Oral Biol.* 7: 161-172.

Dean, M. C. (2000) Incremental markings in enamel and dentine: what they can tell us about the way teeth grow. In Teaford, M., Meredith Smith, M. and Ferguson, M. (Eds.). (2000). Development, Function and Evolution of Teeth. Cambridge, Cambridge University Press. 9: 119-130 doi:10.1017/CBO9780511542626

DeStafano, F., Anda, R. F., Kahn, H. S., Williamson, D. F., and Russell, C. M. (1993) Dental disease and risk of coronary heart disease and mortality. *B. M. J.* 306: 688-691

DeVoe, H. (2016). *Thermodynamics and Chemistry, 2nd Edn Version 8*. Maryland, MD; Pearson Education, Inc.

Djomehri, S. I., Candell, S., Case, T., Browning, A., Marshall, G. W. and Yun, W. et al. (2015) Mineral Density Volume Gradients in Normal and Diseased Human Tissues. *PLoS ONE* 10 4: 1-24 doi:10.1371/journal.pone.0121611

Dorozhkin, S. V. (2012) Dissolution mechanism of calcium apatites in acids: A review of literature. *World. J. Methodol.* 2(1): 1-17. doi:10.5662/wjm.v2.i1.1

Dorozhkin, S. V. (1997a) Acidic dissolution mechanism of natural fluorapatite. II. Nanolevel of investigations. *J. Cryst. Growth.* 182: 133-140

Dorozhkin, S. V. (1997b) Surface reactions of apatite dissolution. *J. Colloid. Interface Sci.* 191: 489-497

Dowker, S. E. P., David, G. R. and Elliott, J. C. (1997) X-ray microtomography non-destructive three-dimensional imaging for in vitro endodontic studies. *Oral Surg. Oral Med. Oral Pathol. Oral Radiol. Endod.* 83: 510-516

Dowker, S. E. P., Elliott, J. C., Davis, G. R., and Wassif, H. S. (2003) Longitudinal Study of the Three-Dimensional Development of Subsurface Enamel Lesions during in vitro Demineralisation. *Caries Res*. 37: 237–245. doi.org/10.1159/000070865

Elliott, J. C. (2003) Structure and Chemistry of the Apatites and Other Calcium Orthophosphates. In *Studies in Inorganic Chemistry 18.* Elsevier. 4: 259-295

Elliott, J. C., Anderson, P., Gao, X. J., Wong, F. S. L., Davis, G. R., and Dowker, S. E. P. (1994). Application of scanning microradiography and X Ray microtomography to studies of bones and teeth. *J. X-ray Sci. Technol.* 4: 102–111.

Elliott, J. C., Holcomb, D. W. and Young, R. W. (1985) infrared determination of degree of saturation of hydroxyl by carbonate ions in human dental enamel. *Calcif. Tissue Int.* 37: 372-375

Elliott, J. C., Wong, F. S. L., Anderson, P., Davis, G. R. and Dowker, S. E. P. (1997) Determination of mineral concentration in dental enamel from X-ray attenuation measurements. *Connect. Tissue Res.* 38: 61-72

Engelke, K., Graeff, W., Meiss, L., Hahn, M. and Delling, G. (1993) High spatial resolution imaging of bone mineral using computed microtomography. Comparison with microradiography and undecalcified histologic sections. *Invest. Radiol.* 28: 341–9

Evershed, A. N. Z., Mills. D. and Davis, G. R. (2012) Multi-species Beam Hardening Calibration Device for X-Ray Microtomography, Developments in X-Ray Tomography VIII, SPIE 8506. doi: 10.1117/12.928933

Fava, M., Watanabe, I., Moraes, F. F. and Costa, L. R. R. S. (1997) Prismless enamel in human non- erupted deciduous molar teeth: A scanning electron microscopic study. *Rev. Odontol. Univ. Sao. Paulo.* 11: 239–243.

Featherstone, J. D. B. (2008) Dental caries: a dynamic disease process. Symposium report. *Aust. Dent. J.* 53: 286–291 doi: 10.1111/j.1834-7819.2008.00064.x

Featherstone, J. D. B. and Mellberg, J. R. (1981) Relative rates of progress of artificial carious lesions in bovine, ovine and human enamel. *Caries Res.* 15: 109-114

Ferguson, D. B. (1999) Oral bioscience. Edinburgh, Churchill Livingstone. 197-208

Fincham, A. G., Moradian-Oldak, J. and Simmer, J. P. (1999). The structural biology of the developing dental enamel matrix. *J. Struct. Biol.* 126: 270–299. doi: 10.1006/jsbi.1999.4130

Fontana, M., Li, M., Dunipace, A. J., Noblitt, T. W., Fischer, G., Katz, B. P. and Stookey, G. K. (1996) Measurement of enamel demineralisation using microradiography and confocal microscopy. *Caries Res.* 30: 317–325

Fosse, G. (1964) The number of prism bases on the inner and outer surface of the enamel mantle of human teeth. *J. Dent. Res.* 43: 57–63.

Fosse, G. (1968). A quantitative analysis of the numerical density and the distributional pattern of prisms and ameloblasts in dental enamel and tooth germs. III. The calculation of prism diameters and numbers of prisms per unit area in dental enamel. *Acta. Odontol. Scand.* 26: 315–336.

Fukae, M., Tanabe, T., Nagano, T., Ando, H., Yamakoshi, Y., Yamada, M., Simmer, J. P. and Oida, S. (2002) Odontoblasts enhance the maturation of enamel crystals by secreting EMSP1 at the enamel-dentine junction. *J. Dent. Res*. 81 10:668- 672

Ganss, C. and Lussi, A. Schlueter N. The Histopathology of Dental Erosion: The Histological Features and Physical Properties of Eroded Dental Hard Tissues. (2014) In *Lussi, A. Ganss, C. (Ed) Erosive Tooth Wear. Monogr Oral Sci. Basel, Karger*. 25: 99-107

Gao, H., Ji, B., Ingomar, L. J., Arz, E. and Fratzl, P. (2003) Materials become insensitive to flaws at nanoscale: lessons from nature. *Proc. Natl. Acad. Sci. U.S.A*. 100: 5597-5600

Gao, X. J., Fan, Y., Kent, R. L. Jr., Van Houte, J., and Margolis, H. C. (2001). Association of caries activity with the composition of dental plaque fluid. *J. Dent. Res*. 80: 1834–1839. doi: 10.1177/00220345010800091201

Gibbons, R. J., Etherden, I., Moreno, E.C. (1985) Contribution of stereochemical interactions in the adhesion of Streptococcus sanguis C5 to experimental pellicles*. J. Dent. Res.* 64 2: 96–101.

Gibson, C. W., Yuan, Z. A., Hall, B., Longenecker, G., Chen, E. and Thyagarajan, T. et al. (2001) Amelogenin-deficient mice display an amelogenesis imperfecta phenotype. *J. Biol. Chem*. 276: 31871–31875. doi: 10.1074/jbc.M104624200

Goldberg, M. (2017) Deciduous Tooth and Dental Caries. *Ann. Pediatr. Child Health.* 5 1: 1120.

Gonzalez-Cabezas, C., Fontana, M., Dunipace, A. J., Li, Y., Fischer, G.M. and Proskin, H.M. (1998) Measurement of enamel remineralization using microradiography and confocal microscopy. A correlational study. *Caries res.* 32 5: 385–392. doi: cre32385 [pii].

Gugnani, N., Pandit, K., Srivastava, N., Gupta, M. and Sharma, M. (2011) International Caries Detection and Assessment System (ICDAS): A New Concept. *Int. J. Clin. Pediatr. Dent*. 4 2: 93–100.

Guidry, M. W. and Mackenzie, F. T. (2003) Experimental study of igneous and sedimentary apatite dissolution: control of pH, distance from equilibrium, and temperature on dissolution rates. *Geochim Cosmochim Acta.* 67: 2949-2963

Hao, L., Li, J., Kappler, A. and Obst, M. (2013) Mapping of heavy metal ion sorption to cell-extracellular polymeric substance-mineral aggregates by using metal-selective fluorescent probes and confocal laser scanning microscopy. *AEM.* 79 21: 6524-6534.

Hendee, W. R. (1995). X-Rays in Medicine. *Phys. Today.* 48 11: 51-56.

Heymann, H. O., Swift, E. J. and Ritter, A. V. (2014) Sturdevant's Art & Science of Operative Dentistry – E-book, 6th Ed. Elsevier. 2: 54-59

Hobdell, M. H., Oliveira, E. R., Bautista, R.,Myburgh, N. G., Lalloo, R., Narendran, S., et al. (2003). Oral diseases and socio-economic status (SES). *Br. Dent. J.* 194: 91–96. doi: 10.1038/sj.bdj.4809882

Hu, J. C., Hu, Y., Smith, C. E., McKee, M. D., Wright, J. T., Yamakoshi, Y., Papagerakis, P., Hunter, G. K., Feng, J. Q., Yamakoshi, F. and Simmer, J. P. (2008) Enamel defects and ameloblast-specific expression in Enam knock-out/lacz knock-in mice. *J. Biol. Chem.* 283 16: 10858-71.

Hubbard, M. J. (2000) Calcium transport across the dental enamel epithelium. *Crit. Rev. Oral Biol. Med.* 11 4: 437-466

Hubbell, J. H. (1982) Photon mass attenuation and energy-absorption coefficients from 1keV to 20MeV. *Int. J. Appl. Radiat. Isot.* 33: 1269-1290

Humphrey, S. P. and Williamson, R. T. (2001) A review of saliva: normal composition, flow, and function. *J. Prosthet. Dent.* 85 2: 162-9.

Imfeld, T. (1996) Dental erosion. Definition, classification and links. *Eur. J. Oral. Sci.* 104: 151-155

Ishikawa, K., Ducheyne, P. and Radin, S. (1993) Determination of the Ca/P patio in calcium-deficient hydroxyapatite using X-ray diffraction analysis. *J. Mater. Sci. Mater. Med.* 4: 165-168

Issa, A. I., Preston, K. P., Preston, A. J., Toumba, K. J. and Duggal, M.S. (2003) A study investigating the formation of artificial sub-surface enamel caries-like lesions in deciduous and permanent teeth in the presence and absence of fluoride. *Arch. Oral Biol*. 48: 567—571

James, P. C. M and Parfitt, G. J. (1953) Local effects of certain medicaments on the teeth. *Br. Med. Jr.* 2: 1252-1253

Jonson, R. (1993) Mass attenuation coefficients, quanitites and units for use in bone mineral determinations. *Osteoporosis Int.* 3: 103-106

Johnsson, M., Levine, M. J. and Nancollas, G. H. (1993) Hydroxyapatite binding domains in salivary proteins. *Crit. Rev. Oral Biol. Med.* 4 3/4: 371-378

Kawashita, Y., Kitamura, M. and Saito, T. (2011) Early Childhood Caries. *I. J. D.* 2011: 1-7

Keyes, P. H. (1962). Recent advances in dental caries research. *Int. Dent. J.* 12: 443–464.

Klausen, M., Heydorn, A., Ragas, P., Lambertsen, L., Aaes-Jorgensen, A., Molin, S. and Tolker-Nielsen, T. (2003) Biofilm formation by Pseudomonas aeruginosa wild type, flagella and type IV pili mutants, Molecular Microbiology, 48 6: 1511–1524. doi: 10.1046/j.1365-2958.2003.03525.x.

Korant, B. D., Brzin, J. and Turk, V. (1985) Cystatin, a protein inhibitor of cysteine proteases alters viral protein cleavages in infected human cells. *Biochem. Biophys. Res. Commun.* 127: 1072-1076

Kosoric, J., Hector, M. P., and Anderson, P. (2010). The influence of proteins on demineralization kinetics of hydroxyapatite aggregates. *J. Biomed. Mater. Res. A.* 94: 972–977. doi: 10.1002/jbm.a.32759

Koyama, E., Wu, C., Shimo, T., Iwamoto, M., Ohmori, T., Kurisu, K., Ookura, T., Bashir, M. M., Abrams, W. R., et al. (2001). Development of stratum intermedium and its role as a Sonic hedgehog-signalling structure during odontogenesis. *Dev. Dyn.* 222: 178–191

Kuhar, M., Cevc, P., Schara, M. and Funduk, N. (1997) Enhanced permeability of acid-etched or ground dental enamel. *J. Prosthet. Dent.* 77 6: 578-582

Kus, J. (2015) Application of confocal laser-scanning microscopy (CLSM) to autofluorescent organic and mineral matter in peat, coals and siliciclastic sedimentary rocks — A qualitative approach. *Int. J. Coal Geol.* 137: 1–18

Kwon, K. Y., Wang, E., Chang, N. and Lee, S. W. (2009) Characterisation of the dominant molecular step orientations on hydroxyapatite (100) surfaces. *Lanhmuir.* 25: 7205-7208

Lagerlof, F. (1983). Effects of flow-rate and pH on calcium-phosphate saturation in human-parotid saliva. *Caries Res.* 17, 403–411. doi: 10.1159/000260694

Leaist, D. G., Anderson, P., and Elliott, J. C. (1990) Diffusion coefficients for the ternary system Ca(OH)2-H3P04-Water. *J. Chem. Soc. Faraday Trans.* 86, 3093–3095. doi: 10.1039/FT9908603093

Lendenmann, U., Grogan, J. and Oppenheim, F. G. (2000) Saliva and dental pellicle – A review. *Adv. Dent. Res.* 14: 22-28

Levine, M. J., Tabak, L. A., Reddy, M. S and Mandel, I. D. (1985) Molecular Basis of Oral Microbial Adhesion. *Ed. Mergenhagen, S. E. and Rosan, B*. ASM Washington. D.C. 125-130

Lippert, F., Parker, D. M. and Jandt, K. D. (2004) Susceptibility of deciduous and permanent enamel to dietary acid-induced erosion studied with atomic force microscopy nanoindentation. *E. J. S.* 112 1: 61-66.

Liu, Q., Huang, S., Matinlinna, P. J., Chen, Z. and Pan, H. (2013). Insight into biological apatite: physiological properties and preparation approaches. *Biol. Med. Res. Int.* 2013, 1–13. doi: 10.1155/2013/929748

Liu, Q., Chen, Z., Pan, H., Darvell, B. W. and Matinlinna, J. P. (2016) Effect of magnesium on the solubility of hydroxyapatite. *Eur. J. Inorg. Chem.* 2016, 5623–5629. doi: 10.1002/ejic.201601056

Local Authority Association: Public Health England report (2015). Oral health survey of five-year-old children 2015: A report on the prevalence and severity of dental decay. 1-41

Local Government Authority Report (2016). Tackling Poor Oral Health in Children, Local Governments Public Health Role. London, UK: Public Health England.

Long, R. J., Shaw, J. W., Stayton, P. S. and Drobny, G. P. (2001) Structure and dynamics of hydrated statherin on hydroxyapatite as determined by solid-state NMR. Amer. Chem. Soc. 40 51: 15451-15455

Lu, X., Zhang, H., Guo, Y., Wang, Y., Ge, X., Leng, Y. and Watari, F. (2011) Hexagonal hydroxyapatite formation on TiO_2 nanotubes under urea modulation. *Cryst. Eng. Comm.* 13: 3741-3749 doi: 10.1039/C0CE00971G

Lunt, R. C. and Law, D. B. (1974) A review of the chronology of calcification of deciduous teeth. *J. Am. Dent. Ass.* 89: 599-606
Lussi, A. (2006) Erosive tooth wear – A multifactorial condition of growing concern and increasing knowledge. In *Lussi. A (ed) Dental Erosion*. Monogr. Oral Sci. Basel, Karger. 20: 1-8

Mafe, S., Manzanares, J. A., Reiss, H., Thomann, J. M. and Gramain, P. (1992) Model for the dissolution of calcium hydroxyapatite powder. *J. Phys. Chem.* 96: 861-866

Maggiano, C., Dupras, T., Schultz, M. and Biggerstaff, J. (2006) Spectral and photobleaching analysis using confocal laser scanning microscopy: a comparison of modern and archaeological bone fluorescence. *Mol. Cell. Probes*, 20: 3–4: 154–162. doi: 10.1016/j.mcp.2005.11.009

Mahoney, P. (2011) Human deciduous mandibular molar incremental enamel development. *Am. J. Phys. Anthropol*. 144: 204-214. doi:10.1002/ajpa.21386

Margolis, H. C., and Moreno, E. C. (1985). Kinetic and thermodynamic aspects of enamel demineralisation. *Caries Res.* 19: 22–35. doi: 10.1159/000260826

Massimi, M. (2005) Pauli's exclusion principle: the origin and validation of a scientific principle. Cambridge University Press. 1: 8

Massler, M. and Schour, I. (1946). The appositional life span of the enamel and dentin-forming cells: I. Human deciduous teeth and first permanent molars. *J. D. R.* 25: 145-150.

Matthiessen, M. E. and Rømert, P. (1980) Ultrastructure of the human enamel organ. II. Internal enamel epithelium, preameloblasts, and secretory ameloblasts. *Cell Tissue Res*. 205 3: 371-82

Maupoméa, G., Aguilar-Avilab, M., Medrano-Ugalde, H. A. and Borges-Yáñez, A. (1999) In vitro quantitative microhardness assessment of enamel with early salivary pellicles after exposure to an eroding cola drink. *Caries Res.* 33: 140–147

McDowel, H., Gregory, T.M., and Brown,W. E. (1977) Solubility of Ca5(P04)3OH in the system Ca(OH)2- H3P04- H20 at 5, 15, 25, and 37◦C. *J. Res. Natl. Bur. Stand. A Phys. Chem*. 81A, 273–281. doi: 10.6028/jres.081A.017

Mercer, C. E., Anderson, P. and Davis, G. R. (2003) Sequential 3D X-ray microtomographic measurement of enamel and dentine ablation by an Er:YAG laser. *Br. Dent. J.* 194 2: 99-104

Mishra, S., Thomas, H. F., Fearne, J. M., Boyde, A., and Anderson, P. (2009). Comparison of demineralisation rates in pre- and postnatal enamel and at the neonatal line. *Arch. Oral Biol.* 54: 101–106. doi: 10.1016/j.archoralbio.2008.09.013

Mistra, D. N. (1999) Interaction of citric or hydrochloric acid with calcium fluorapatite: precipitation of calcium fluoride. *J. Coll. Interf. Sci.*220: 387-391

Mohammed, N. R. (2014) Effects of zinc and fluoride on *in vitro* enamel demineralisation conditions relevant to dental caries. PhD thesis. Institute of dentistry, QMUL, London, UK

Moorrees, C. F. A., Fanning, E. A. and Hunt E. E. (1963) Formation and resorption of three deciduous teeth in children. *Am. J. phys. Anthrop.* 21: 205-213

Moreira, A. R., Passos, I. A., Sampaio, F. C., Soares, M. S. M. and Oliveira, R. J. (2009) Flow rate, pH and calcium concentration of saliva of children and adolescents with type 1 diabetes mellitus. *Braz. J. Med. Biol. Res*. 42: 707-711.

Moreno, E. C. and Varughese, K. (1981) Crystal growth of calcium apatites from dilute solutions. *J. Cryst. Growth.* 53: 20-30.

Moreno, E. C., Varughese, K. and Hay, D. I. (1979) Effect of human salivary proteins on the precipitation kinetics of calcium phosphate. Calcif. Tissue Int. 28 1: 7-16.

Moreno, E. C., Zahradnik, R. T., Glazman, A. and Hwu, R. (1977) Precipitation of hydroxyapatite from dilute solutions upon seeding. *Calcif. Tissue Res.* 24: 47-57.

Mortimer, K. V. (1970). The relationship of DE structure of dental disease. *Caries Res.* 4: 206–223.

Mould, R. F. (1995) The early history of X-ray diagnosis with emphasis on the contributions of physics 1895-1915. *Phys. Med. Biol.* 40: 1741-87.

Naujoks, R., Schade, H. and Zelinka, F. (1967) Chemical composition of different areas of the enamel of deciduous and permanent teeth (the content of Ca, P, CO_2, Na and N_2) *Caries Res.* 1: 137-143.

Neamen, D. A. (2012) Semiconductor physics and devices: basic principles, New York, McGraw-Hill.

Neel, E. A. A., Aljabo, A., Strange, A., Ibrahim, S., Coathup, M., Young, A. M., et al. (2016). Demineralisation–remineralization dynamics in teeth and bone. *Int. J. Nanomedicine* 11: 4743–4763. doi: 10.2147/IJN.S107624.

Oliviera, M., Torres, C. P., Gomes-Silva, J. M., Chinelatti, M. A., Menzes, F. Palma-Dibb, R. G. and Borsatto, M. C. (2010) Microstructure and mineral composition of dental enamel of permanent and deciduous teeth. *Microsc. Res. Tech*. 73: 572–577.

Onuma, K., Ito, A., Tateishi, T. and Kameyama, T. (1995) Growth kinetics of hydroxyapatite crystal revealed by atomic force microscopy. *J. Cryst. Growth.* 154: 118-125.

Onuma, K., Ito, A. and Tateishi, T. (1996) Investigation of a growth unit of hydroxyapatite crystal from measurements of step kinetics. *J. Cryst. Growth.* 167: 773-776

Oxford Dictionary of Science (2010), Oxford, Oxford University Press, 105.

Pan, H. B. and Darvell, B. W. (2009a) Calcium phosphate solubility; the need for re-evaluation. *Cryst. Growth Des.* 639–645. doi: 10.1021/cg801118v Q20

Pan, H. B. and Darvell, B. W. (2009b). Solid titration of octacalcium phosphate. *Caries Res*. 43: 322–330. doi: 10.1159/000226231

Pan, H. B., and Darvell, B.W. (2007) Solubility of hydroxyapatite by solid titration at pH 3–4. *Arch. Oral Biol.* 52, 618–624. doi: 10.1016/j.archoralbio.2006.12.007

Patel, P. R., and Brown, W. P. (1975). Thermodynamic solubility product of human tooth enamel, powdered sample. J. Dent. Res. 54, 728–736. doi: 10.1177/00220345750540040601

Patel, R. (2012) The state of oral health in Europe: Report commissioned by the platform for better oral health in Europe. Better oral health European platform. 1-68

Pavlic, A., Petelin, M. and Battelino, T. (2007) Phenotype and enamel ultrastructure characteristics in patients with ENAM gene mutations g.13185-13186insAG and 8344delG. *Arch Oral Biol.* 52 3: 209-17.

Peters, F., Schwarz, K. and Epple, M. (2000) The structure of bone studied with synchrotron X-ray diffraction, X-ray absorption spectroscopy and thermal analysis. *Thermochim. Acta*. 361: 131-138

Petersson, L. G. and Derand, T. (1981) Development of artificial carious lesions in enamel after F-varnish (Duraphat) and F-Fe-A1-solution treatment. *Swed. Dent. J.* 5: 219—223.

Poludniowski, G., Landry, G., DeBlois, F., Evans, P. M. and Verhaegen, F. (2009) SpekCalc: a program to calculate photon spectra from tungsten anode x-ray tubes, *Phys. Med. Biol*. 54: 433–438

Pope, J. (1998). Diagnostic X-rays. In: *Medical Physics: Imaging.* Heinemann Educational Publishers. 28-47.

Public Health England (2015) Tackling poor oral health in children local government's public health role.

Pratt, R. H., Ron, A. and Tseng, H. K. (1973) Atomic photoelectric effect above 10keV. *Rev. Mod. Phys.* 45: 273-325

Preethi, B. P., Reshma, D. and Anand, P. (2010) Evaluation of flow rate, pH, buffering capacity, calcium, total proteins and total antioxidant capacity levels of saliva in caries free and caries active children: an in vivo study. *Ind. J. Clin. Biochem.* 25(4): 425-428

Pruitt, K. M., Caldwell, R. C., Jamieson, A. D. and Taylor, R. E. (1969) The interaction of salivary proteins with tooth surface. *J. Dent. Res.* 48: 818-823

Quinn, G. W., and Taylor, D. M. (1992). NSPEC: a chemical speciation program for personal computers. *Analyst* 117, 689–691. doi: 10.1039/an9921700689

Raynal, B. D. E., Hardingham, T. E., Thornton, D. J. and Sheehan, J. K. (2002) Concentrated solutions of salivary MUC5B mucin do not replicate the gel-forming properties of saliva. *Biochem. J.* 362: 289-296

Ripa, L. W., Gwinnett, A. J. and Buonocore, M. G. (1966) The 'prismless' outer layer of deciduous and permanent enamel. *Arch. Oral Biol.* 11: 41-48

Ripa, L. W. (1966) The histology of the early carious lesion in primary teeth with special references to a 'prismless' outer layer of primary enamel. *J. Dent. Res.* 45: 5-11

Robinson, C., Weatherell, J. A. and Hallsworth, A. S. (1971) Variation in composition of dental enamel within thin ground tooth sections. *Caries Res.* 5: 44-57

Sabel, N., Robertson, A., Nietzsche, S. and Nor´en, J. G. (2012) Demineralization of Enamel in Primary Second Molars Related to Properties of the Enamel. *Sci. World J.* Volume 2012. Article ID 587254. 1-8. doi:10.1100/2012/587254

Schaad, P., Poumier, F., Voegel, J. C. and Gramain, P. (1997) Analysis of calcium hydroxyaptites dissolution in non-stoichiometric solutions. *Colloids Surf. A.* 121: 217-228

Seibert, J. A. (2004). X-Ray imaging physics for nuclear medicine technologists. Part 1: Basic principles of X-ray production. *J. Nucl. Med. Technol.* 32 3: 139-147

Selwitz, R. H., Ismail A. I. and Pitts N. B. (2007) Dental caries. *Lancet.* 369: 51–59

Shannon, I. L. and Feller, R. P. (1979) Parotid saliva flow rate, calcium, phosphorus, and magnesium concentrations in relation to dental caries experience in children. *Pediatr dent.* 1: 16-20

Shannon, I. L., Isbell, G. M. ,Gibson, W. A. and O'Leary, T. J. (1962) Inorganic phosphate concentration in body fluids as related to dental caries status. *J. Dent. Res.* 41: 1373-1377

Shaw, L., Murray, J. J., Burchell, C. K. and Best, J. S. (1983) Calcium and phosphorus content of plaque and saliva in relation to dental caries. Caries. Res. 17: 543-548

Shellis, R. P. (1984a) Variations in growth of the enamel crown in human teeth and a possible relationship between growth and enamel structure. *Arch. Oral Biol.* 29: 697-707.

Shellis, R. P. (1984b) Relationship between human enamel structure and the formation of caries-like lesions in vitro. *Arch. Oral Biol.* 29: 975-981

Shellis, R. P. (1996). A scanning electron microscopic study of solubility variations in human enamel and dentine. *Arch. Oral Biol*. 41, 473–484. doi: 10.1016/0003-9969(96)00140-9

Shellis, R. P., Wahab, F. K. and Heywood, B. R. (1993) The hydroxyapatite ion activity product in acid solutions equilibrated with human enamel. *Caries Res.* 27 5: 365-372

Shellis, R., and Dibdin, G. (2000). “Enamel microporosity and its functional implications,” in *Development, Function and Evolution of Teeth*, eds M. Teaford, M. Meredith Smith, and M. Ferguson (Cambridge: Cambridge University Press), 242–251. doi: 10.1017/CBO9780511542626.017

Shellis, R. P. and Wilson, R. M. (2004) Apparent solubility distribution of hydroxyapatite and enamel apatite. *J. Colloid Interface Sci*. 278: 325-332

Shintani, S., Hamakawa, H., Ueyama, Y., Hatori, M. and Toyoshima, T. (2010) Identification of a truncated cystatin SA-I as a saliva biomarker for oral squamous cell carcinoma using the SELDI ProteinChip platform. *Int. J. Oral Maxillofac. Surg.* 39: 68-74

Silverstone, L. M., Johnson, N. W., Hardie, J. M. and Williams, R. A. D. (1981) Enamel caries. In: *Dental caries: Aetiology, pathology and prevention*. London: MacMillan. 133:161

Simmons, L. M., Al-Jawad, M., Kilcoyne, S. H. and Wood, D. J. (2011) Distribution of enamel crystallite orientation through an entire tooth crown studied using synchrotron X-ray diffraction. *Eur J Oral Sci*. 119 (Suppl. 1): 19–24 doi: 10.1111/j.1600-0722.2011.00909.x

Sivakumar, T., Hand, A. R. and Mednieks, M. (2009) Secretory proteins in the saliva of children. *J. Oral Sci.* (51)4: 573-580

Skeie, M. S., Espelid, I., Skaare, A. B. and Gimmestad, A. (2005) Caries patterns in an urban preschool population in Norway. *EJPD.* 1: 16-22

Smets, B. M. J. (1987) Phosphors based on rare-earth, a new era in fluorescent lighting. *Mater. Chem. Phys.* 16 3-4: 283-299

Smith, B. T. (2015). *Remington Education: Physical Pharmacy, 1st Edn*. London, UK: Pharmaceutical Press.

Smith, A. N., Posner, A. M. and Quirk, J. P. (1974) Incongruent dissolution and surface complexes of hydroxyapatite. *J. Coll. Interf. Sci.* 48: 442-449

Smith, C. E., Wazen, R., Hu, Y., Zalzal, S. F., Nanci, A., Simmer, J. P. and Hu, J. C. C. (2009) Consequences for enamel development and mineralization resulting from loss of function of ameloblastin or enamelin. *Eur. J. Oral Sci*. 117 5: 485–497. doi:10.1111/j.1600-0722.2009.00666.x.

Somasundaran, P. (1968) Zeta potential of apatite in aqueous solutions and its change during equilibration. *J. Coll. Interf. Sci.* 27: 659-666

Sønju Clasen, A. B., Øgaard, B., Duschner, H., Ruben, J., Arends, J. and Sønju, T. (1997) Caries development in fluoridated and non-fluoridated deciduous and

permanent enamel in situ examined by microradiography and confocal laser scanning microscopy. *Adv. Dent. Res.* 11 4: 442—447.

Sønju Clasen, A. B. and Ruyter, I. E. (1997) Quantitative determination of type A and type B carbonate in human deciduous and permanent enamel by means of fourier transform infrared spectrometry. *Adv. Dent. Res.* 11 4: 523-527

Sönju, T. and Rölla, G. (1973) Chemical analysis of the acquired pellicle formed in two hours on cleaned human teeth *in vivo. Caries Res.* 7: 30-38

Takahashi N. and Nyvad, B. (2011) The role of bacteria in the caries process: ecological perspectives. *J. Dent. Res.* 90 3: 294-303.

Takano Y (1994). Histochemical aspects of calcium regulation by the enamel forming cells during matrix formation and maturation. *Acta. Anat. Nippon.* 69: 106-122.

Takano, Y., Crenshaw, M. A. and Reith, E. J. (1982). Correlation of ^{45}Ca incorporation with ameloblast morphology in the rat incisor. *Calcif. Tissue. Int.* 34: 211-213.

Termine, J. D., Eanes, E. D. and Conn, K. M. (1980). Phosphoprotein modulation of apatite crystallization. *Calcif. Tissue Int.* 31: 247–251. doi: 10.1007/BF02407188

Theuns, H. M., Van Dijk, J. W. E., Jongebloed, W. L. and Groeneveld, A. (1983) The mineral content of human enamel studied by polarizing microscopy, Microradiography and Scanning Electron Microscopy. *Arch. Oral. Biol.* 28(9): 797-803

Thomann, J. M., Voegel, J. C. and Gramain, P. (1990) Kinetics of dissolution of calcium hydroxyapatite powder. III: pH and sample conditioning effects. *Calcif. Tissue Int.* 46: 121-129

Thomann, J. M., Voegel, J. C. and Gramain, P. (1993) Quantitative model for the dissolution of calcium hydroxyapatite with a perm-selective ionic interface. *J. Coll. Interf. Sci.* 157: 369-374

Vicars, T. M., Stanfield, C.N., Crenshaw, M.A. and Bawden, I. W. (1983). The effects of ATP depletion and ionophore A23187 on calcium transport in the secretory rat enamel organ. *Arch. Oral. Biol*. 28: 513-516.

Wang, L. J., Tang, R., Bonstein, T., Bush, P. and Nancollas, G. H. (2006) Enamel demineralisation in primary and permanent teeth*. J. Dent. Res.* 85 4: 359 – 363.

Watanabe, S. and Dawes, C. (1990) Salivary Flow Rates and Salivary Film Thickness in Five-year-old Children. *J. Dent. Res.* 69 5: 1150 – 1153. doi.org/10.1177/00220345900690050601.

Watika, M., Tsuchiya, H., Gunji, T. and Kobayashi, S. (1981) Three-dimensional structure of Tomes' processes and enamel prism formation in the kitten. *Arch. Histol. Jap.* 44 3: 285-297

Weatherell, J. A., Weidmann, S. M. and Hamm S. M. (1967) Density patterns in enamel. *Caries Res.* 1: 42-51.

West, N., and Joiner, A. (2014). Enamel mineral loss. *J. Dent.* 42: 2–11. doi: 10.1016/S0300-5712(14)50002-4

Wickström, C., Herzberg, M. C., Beighton, D. and Svensäter, G. (2009) Proteolytic degradation of human salivary MUC5B by dental biofilms. *Microbiology* 155: 2866-2872

Williams, D. and Carter, B. (2009) Transmission Electron Microscopy. Springer US. 4: 23-38. doi: 10.1007/978-0-387-76501-3

Wilson, R. F. and Ashley, F. P. (1990) Relationships between the biochemical composition of both free smooth surface and approximal plaque and salivary composition and a 24-hour retrospective dietary history of sugar intake in adolescents. *Caries Res.* 24, 203-210.

Wilson, P. R. and Beynon, A. D. (1989) Mineralization differences between human deciduous and permanent enamel measured by quantitative microradiography. *Arch. Oral. Biol.* 34: 85-88

Woltgens, J. H. M., Vingerling, P., De Blieck-Hogervorst, J. M. A. and Bervoets, D. J. (1985) Enamel erosion and saliva. *Clin. Prev. Dent.* 7: 8-10

Wong, F. S. L., Anderson, P., Fan, H. and Davis, G. R. (2004) X-ray microtomographic study of mineral concentration distribution on DE. *Arch. Oral. Biol.* 49: 937-944

Wu, X. and Bruchez, M. P. (2004) Labelling cellular targets with semiconductor quantum dot conjugates. *Methods Cell Biol.* 75: 171-183

Yamada, M. K., Uo, M., Ohkawa, S. and Watari, F. (2003) CLSM and SEM quantitative analysis of surface topography of human teeth irradiated by Nd:YAG, Er:YAG and CO2 lasers. *Int. Congr. Ser.* 1248 (C): 135–137. doi: 10.1016/S0531-5131(02)01295-5.

Yao, Y., Berg, E.A., Costello, C.E., Troxler, R.F., Oppenheim, F.G. (2003) Identification of protein components in human acquired enamel pellicle and whole saliva using novel proteomics approaches*. J. Biol. Chem.* 278: 5300–5308.

Yoshida, M., Yoshida, Y., Inoue, S., Lambrechts, P., Vanherle, G., Nomura, Y., Okazaki, M., Shintani, H. and Van Meerbeek, B. (2002) Adhesion / decalcification mechanisms of acid interactions with human hard tissues. *J. Biomed. Mater. Res.* 59: 56-62

Zemanski, M. and Dittman, R. (1997) *Heat and thermodynamics: an intermediate textbook*. London: McGraw-Hill

Zhang, Y. P., Kent, R. L. and Margolis, H. C. (2000) Enamel demineralisation under driving forces found in dental plaque fluid. *Eur. J. Oral. Sci.* 108: 207-213

Zhou, X. and Li, Y. (2015) Techniques for oral biology. In *Zhou and Li Eds Atlas of Oral Microbiology: From healthy microflora to disease*. London, Academic Press 15 – 40. ISBN: 978-0-12-802234-4

Zhu, Y., Zhang, X., Chen, Y., Xie, Q., Lan, J., Qian, M. and He, N. (2009) A comparative study on the dissolution and solubility of hydroxyapatite and fluorapatite at 25°C and 35°C. *Chemical Geology.* 268: 89-96

Zhu, L., Liu, H., Witkowska, H. E., Huang, Y., Tanimoto, K., and Li, W. (2014) Preferential and selective degradation and removal of Amelogenin adsorbed on hydroxyapatites by MMP20 and KLK4 *invitro. Front. Physiol.* 5 268. *doi: 10.3389/fphys. 2014.00268*

Websites

1. https://www.britannica.com/science/quantum-mechanics-physics
   (accessed 09/08/2017)

2. http://www.kayelaby.npl.co.uk/atomic_and_nuclear_physics/4_2/4_2_1.html
   (accessed 10/08/2017)

3. https://www.nucleonica.com/Application/Help/Helpfiles/Appendix3.htm
   (accessed 17/08/2017)

4. https://www.nde-ed.org/EducationResources/CommunityCollege/Radiography/Physics/attenuationCoef.htm
   (accessed 17/08/2017)

5. https://www.rp-photonics.com/dichroic_mirrors.html
   (accessed 08/09/2017)

6. http://bitesizebio.com/19958/what-is-confocal-laser-scanning-microscopy/
   (accessed 08/09/2017)

Appendix

Appendix A

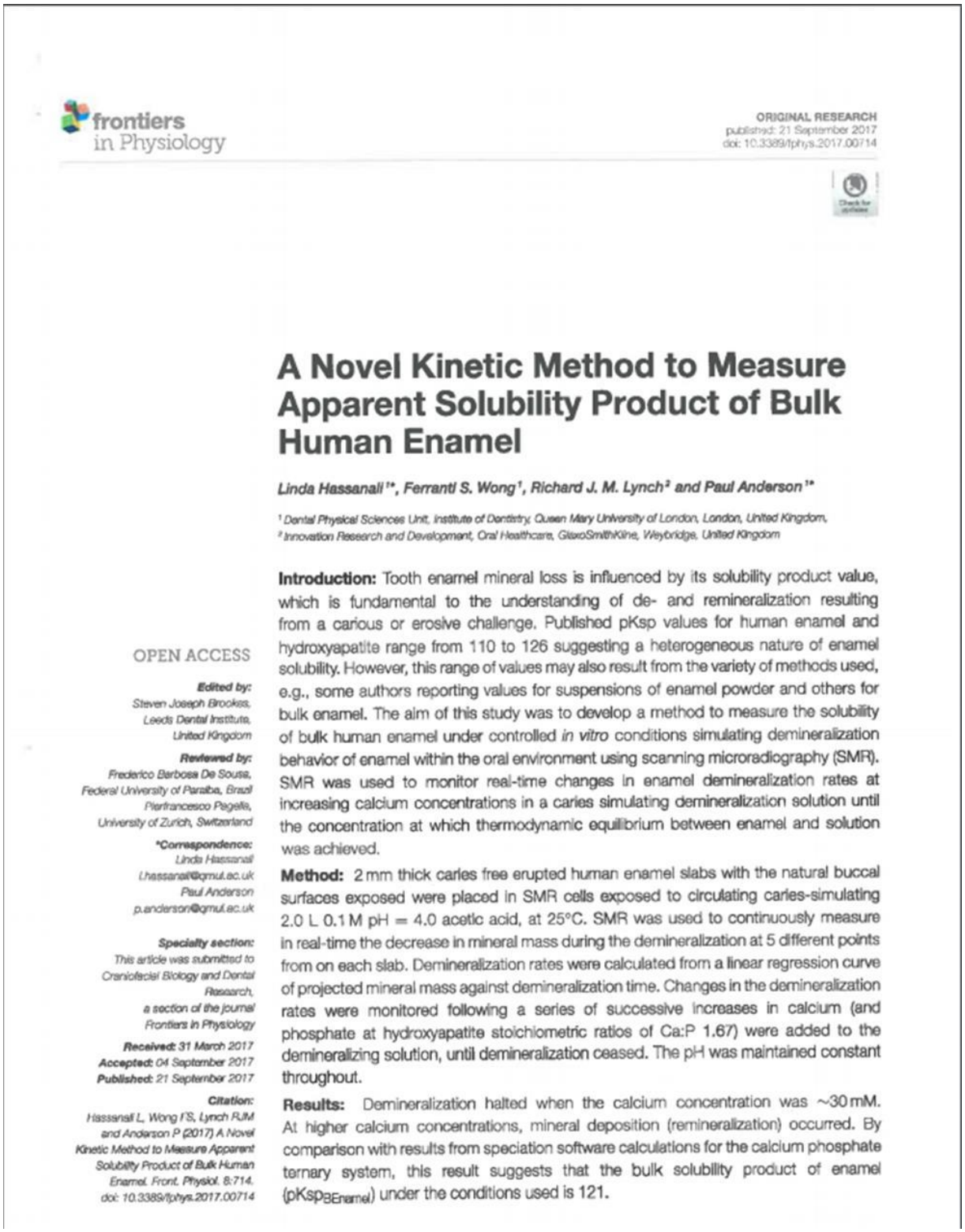

frontiers in Physiology

ORIGINAL RESEARCH
published: 21 September 2017
doi: 10.3389/fphys.2017.00714

A Novel Kinetic Method to Measure Apparent Solubility Product of Bulk Human Enamel

Linda Hassanali[1], Ferranti S. Wong[1], Richard J. M. Lynch[2] and Paul Anderson[1]**

[1] Dental Physical Sciences Unit, Institute of Dentistry, Queen Mary University of London, London, United Kingdom,
[2] Innovation Research and Development, Oral Healthcare, GlaxoSmithKline, Weybridge, United Kingdom

Introduction: Tooth enamel mineral loss is influenced by its solubility product value, which is fundamental to the understanding of de- and remineralization resulting from a carious or erosive challenge. Published pKsp values for human enamel and hydroxyapatite range from 110 to 126 suggesting a heterogeneous nature of enamel solubility. However, this range of values may also result from the variety of methods used, e.g., some authors reporting values for suspensions of enamel powder and others for bulk enamel. The aim of this study was to develop a method to measure the solubility of bulk human enamel under controlled *in vitro* conditions simulating demineralization behavior of enamel within the oral environment using scanning microradiography (SMR). SMR was used to monitor real-time changes in enamel demineralization rates at increasing calcium concentrations in a caries simulating demineralization solution until the concentration at which thermodynamic equilibrium between enamel and solution was achieved.

Method: 2 mm thick caries free erupted human enamel slabs with the natural buccal surfaces exposed were placed in SMR cells exposed to circulating caries-simulating 2.0 L 0.1 M pH = 4.0 acetic acid, at 25°C. SMR was used to continuously measure in real-time the decrease in mineral mass during the demineralization at 5 different points from on each slab. Demineralization rates were calculated from a linear regression curve of projected mineral mass against demineralization time. Changes in the demineralization rates were monitored following a series of successive increases in calcium (and phosphate at hydroxyapatite stoichiometric ratios of Ca:P 1.67) were added to the demineralizing solution, until demineralization ceased. The pH was maintained constant throughout.

Results: Demineralization halted when the calcium concentration was ~30 mM. At higher calcium concentrations, mineral deposition (remineralization) occurred. By comparison with results from speciation software calculations for the calcium phosphate ternary system, this result suggests that the bulk solubility product of enamel ($pKsp_{BEnamel}$) under the conditions used is 121.

OPEN ACCESS

Edited by:
Steven Joseph Brookes, Leeds Dental Institute, United Kingdom

Reviewed by:
Frederico Barbosa De Sousa, Federal University of Paraíba, Brazil
Pierfrancesco Pagella, University of Zurich, Switzerland

***Correspondence:**
Linda Hassanali
l.hassanali@qmul.ac.uk
Paul Anderson
p.anderson@qmul.ac.uk

Specialty section:
This article was submitted to Craniofacial Biology and Dental Research, a section of the journal Frontiers in Physiology

Received: 31 March 2017
Accepted: 04 September 2017
Published: 21 September 2017

Citation:
Hassanali L, Wong FS, Lynch RJM and Anderson P (2017) A Novel Kinetic Method to Measure Apparent Solubility Product of Bulk Human Enamel. Front. Physiol. 8:714. doi: 10.3389/fphys.2017.00714

Discussion: The apparent $pKsp_{BEnamel}$ under these conditions was higher than many previous reported values, and much closer to those previously reported for HAp. However, this is a bulk value, and does not reflect that enamel is a heterogeneous material, nor the influence of ionic inclusions.

Keywords: enamel, demineralization, solubility, calcium, phosphate, scanning microradiography, solubility product

INTRODUCTION

Tooth decay is a multifactorial process which is influenced by genetic and environmental factors (Keyes, 1962; Borutta et al., 2010). For example, caries related illnesses have become a cause for concern within the UK according to a recent LGA 2013 report (Brunton, 2014; Local Government Authority Report, 2016). Such factors include those associated with the host tissue such as the structure and composition of enamel (Robinson et al., 1995), the pellicle and saliva (Leung and Darvell, 1991) as well as environmental factors such as diet and socioeconomic status (Lalloo and Myburgh, 1999; Hobdell et al., 2003). The kinetics of mineral loss and precipitation is influenced by many factors (Gibbs, 1873; Arends, 1981; DeVoe, 2016), including its physical (Nancollas, 2005) and chemical structure, and the composition and pH, and, also the chemical equilibria between enamel and solution (Dorozhkin, 2012), i.e., the solubility product constant (Ksp). Thus, the dissolution of bulk enamel is significantly influenced by its solubility product (which is defined as the mathematical product of its ion activities raised to the power of their stoichiometric coefficients). Enamel is a calcium deficient form of HAp (Elliott et al., 1994). The Ksp of HAp (Ksp_{HAp}) is defined, from the stoichiometry:

$$Ca_{10}(PO_4)_6OH_2 \leftrightarrows 10Ca^{2+} + 6PO_4^{3-} + 2OH^- \quad (1)$$

and therefore:

$$Ksp_{HAP} = \{Ca^{2+}\}^{10}\{PO_4^{3-}\}^{6}\{OH^-\}^{2} \quad (2)$$

where $\{\}$ denotes ionic activities at equilibrium raised by the power according to the stoichiometry. In this study the negative logarithm to the base 10 of the Ksp is used (pKsp).

Solubility is the propensity for a solute to dissolve in a solvent and arrive at an end point where the potential energy of the system is at its lowest (Smith, 2015). pKsp is a function of the amount of dissolved solid in solution at equilibrium. **Table 1** shows published pKsp values for bulk enamel, and for HAp, which are within the range 110–126. This range suggests uncertainties in the precise value, and as to whether the solubility of bulk enamel is similar to that of HAp, and, if it is influenced by chemical inclusions. The range also suggests incongruent dissolution behavior of both enamel and hydroxyapatite. However, the range in the measured pKsp values of both enamel and HAp also suggests that the values may also be dependent on the choice of experimental protocol, such as the types of materials used (e.g., whether powdered or bulk samples); the methodology; and the analysis/calculations used to calculate the pKsp value.

Conventional methods of the measurement of solubility product of enamel use chemical equilibrium conditions, with the concentration of solute in the solution at saturation determined by an analytical procedure (Chen et al., 2004; Brittain, 2014). In this study, the aim was to develop a method to measure the rate of bulk enamel demineralization at increasing calcium concentrations in the demineralizing solution (and therefore increasing degrees of saturation) until dissolution stopped and equilibrium achieved. No chemical analyses of solutions was required.

The dissolution rate of enamel can be expressed as a function of the degree of saturation with respect to enamel (Margolis and Moreno, 1985, 1992):

$$R = k\bar{A}(C_{eq} - C_b)^n \quad (3)$$

where;
R = rate;
k = rate constant;
$\bar{A}$ = specific surface area of dissolving surface;
C_{eq} = equilibrium concentration of solvent;
C_b = undersaturated concentration of solvent;
n = integer.

Equation (3) indicates that the addition and/or presence of ionizable solutes will influence the rate (Berner, 1978). It is therefore important to ensure that all ionic concentrations are accounted for and controlled. Previous studies have highlighted that caution is required to ensure that the monitoring device used to measure dissolution rates is sensitive enough to identify the point at which equilibrium is reached, and must not mistake extremely low rates that are undetectable for the condition of equilibrium (Zhang et al., 2000).

In this study, a real-time methodology scanning microradiography (SMR) was used to accurately measure the rate of bulk enamel mineral loss in demineralizing solutions that contained increasing concentration of calcium. The calcium concentration at which the rate ceased (i.e., equilibrium) was then compared with calculated results of degree of saturation at a range solubility products of hydroxyapatite. These values were calculated using a ionic speciation program (Chemist) incorporating the chemical conditions used in the SMR experiment, to calculate the different species that would be present in the dissolution media. The SMR methodology provides a precise means of measuring real-time dissolution of enamel blocks under controlled conditions that simulate caries. Further, the methodology is directly quantitative achieved using an X-ray photon counting system with minimum error (for a

TABLE 1 | Published $pKsp_{Enamel/HAp}$ values with references and summary of methodologies.

pKsp	References	Substrate and method
106–116	Patel and Brown, 1975	Human powdered enamel. pH range 4.5–7.8. Measured the amounts dissolved to calculate Ksp.
110 (*Apparent* solubility product 116)	Zhang et al., 2000	Contact Microradiography assessed the demineralization of sections of enamel in lactic acid solutions ranging pH 5–5.07 over a range of DS_{en} values (0.28–0.79) that were based on a $pKsp_{Enamel}$ of 110. Suggest that enamel may have an *apparent* solubility product of 116 based on experimental findings.
116	Shellis et al., 1993	Enamel powder equilibrated with 4 or 17 mM of H_3PO_4 at 37°C. Amounts dissolved were measured and used to calculate the ion activity product at equilibrium = Ksp.
117	Colvers, 2006	HAp Ksp cited in special feature article
118	McDowell et al., 1977	4 g synthetic hydroxyapatite. Ion concentrations at equilibrium then measured. Ksp determined as a function of temperature.
Enamel: 117.6 HAp: 121.82 (Pooled from pH 4.5–5.5)	Shellis and Wilson, 2004	Powdered synthetic HAp. Premolar enamel powder. 5 mg equilibrated with acetic buffers at pH 4.5, 5.0 (0.15 M) 5.5 (0.2 M) in a range of degrees of saturation (range of pI_{HA}) at 37°C. Mass fraction dissolved plotted against pI_{HA} to give distribution curves at each pH. No statistical difference in pH differences.
126	Fan and Darvell, 2007	Solid HAP titrated with KCl solutions at pH 3.2, 3.6, and 4.1 at 37°C. Dissolution monitored using a semiconductor-diode laser scattering system that peaked each time solid was added and disappeared when all solid dissolved. Same solution was adjusted to a decreasing pH using 1M HCl.

full description of SMR and calculation of statistical errors of the photon counting system see Anderson et al., 1998).

For the solubility product to be accurately calculated, all phases and ion-pairs present during dissolution need to be accounted for. Chemical speciation of a solution describes the chemical form and concentrations of each species present, and can be derived using the thermodynamic principals of mass balance (Quinn and Taylor, 1992). Speciation software can be used to calculate the chemical speciation of complex systems. In this study, we describe a novel kinetic method to measure the *apparent*-$pKsp_{BEnamel}$ under conditions relevant to caries, in conjunction with a speciation program so that the *apparent*-$pKsp_{BEnamel}$ value could be calculated at conditions of pH = 4.0 and 25°C. The rate of demineralization of natural unaltered surfaces of human permanent enamel blocks was measured using SMR to determine the effective solubility in an inorganic caries-like demineralizing solution with a decreasing degree of undersaturation with respect to HAp.

MATERIALS AND METHODS

Scanning Microradiography

SMR is an X-ray absorption technique that enables the monitoring of mineral loss (and eventually gain once equilibrium is surpassed) in thin sections of enamel samples during demin/remineralization studies (Anderson et al., 1998). Developed to overcome some of the limitations of conventional (contact) microradiography which required samples to be in contact with a photographic film, SMR can measure mineral changes in real time as solutions can be circulated through SMR cells, within which samples are mounted, at a controlled rate simulating salivary flow.

In this study, the integrated mode of SMR (**Figure 1**) was used whereby the direction of acid attack was parallel to a 15 μm diameter X-ray beam so that changes in the projected mineral mass from the surface could be measured as mineral was lost from the surface and receded to the enamel dentine junction (Anderson and Elliott, 2000). The X-ray generator was operated

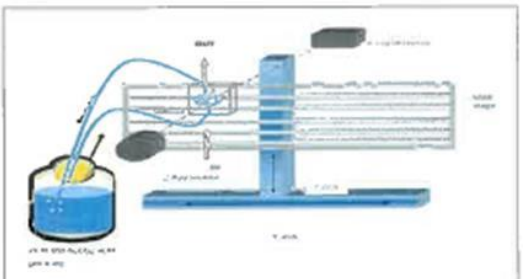

FIGURE 1 | Schematic diagram of SMR experimental set up showing X-rays parallel to the direction of acid attack and perpendicular to the enamel surface.

at a maximum voltage of 41 kV and a current of 0.7 mA. The transmitted X-ray intensity for energies selected at 22.1 keV at each point was measured and the mass of absorbing mineral determined. Since demineralization is nearly linear with time under constant chemical conditions (Elliott et al., 1994; Wang et al., 2006), the rate of projected mineral mass loss of the same enamel sample at decreasing degrees of undersaturation with respect to HAp could be measured (Margolis et al., 1999).

Enamel Sample Preparation for SMR

Eleven different permanent enamel blocks were prepared from teeth extracted for orthodontic purposes, with the roots removed and discarded and stored in methylated ethanol solution at room temperature were analyzed. Teeth were cut parallel to the tooth face into 2 mm enamel blocks with the natural buccal surfaces intact using a diamond cutting saw (Microslice 2, Malvern Instruments, UK). Ethical approval was granted by Queen Mary Research Ethics Committee (QMREC 2011/99).

The enamel blocks were mounted in SMR cells with the natural surfaces exposed (**Figure 2**). Each was scanned with X-ray Microtomography (XMT) (Elliott et al., 1994) to identify caries free (unaffected) areas suitable for analysis with SMR. The

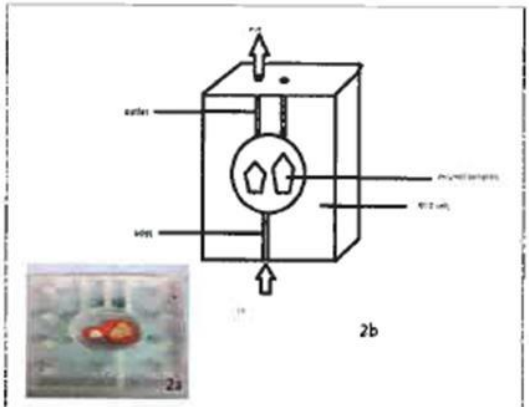

FIGURE 2 | (a,b) A photo and schematic diagram of human enamel blocks in an SMR cell with figure (b) showing the flow of acid into and out of the cell.

SMR cells were then mounted on the XY stage of the SMR apparatus. The samples were initially immersed in deionized water circulated using a peristaltic pump as previously described in Mishra et al. (2009) for 48 h in order to ensure the samples were fully hydrated prior to the commencement of the dissolution experiment. The temperature was maintained at 25.0 ± 1.0°C throughout the experiment, as solubility is highly dependent on temperature.

Calculation of Integrated Mineral Mass Using SMR

The mineral mass of enamel was calculated using the mass absorption coefficient (μ_m) of pure hydroxyapatite as previously described in Anderson et al. (1993), for AgKα radiation at 22.1 keV (4.69 cm^2 g^{-1}). The integrated mineral mass per unit area (m) at each data point is:

$$m = \frac{1}{\mu_m} \ln \frac{No}{N} \quad (4)$$

where;

μ_m is mass attenuation coefficient of HAp for AgKα radiation at 22.1 keV.

N_0 is number of incident photons.

N is number of transmitted photons.

Identification of SMR Scanning Points

Before the dissolution experiment, SMR area scans were carried out in order to locate the samples on the XY stage, and to select the coordinates of ~5 points suitable for measuring mineral mass changes as identified using XMT (see section Enamel Sample Preparation for SMR). The selected points were located horizontally across the buccal enamel surface from distal to mesial.

Preparation of Demineralization Solution

2.0 L of pH = 4.0 acetic acid 0.1 M (Anderson et al., 2004) was prepared using 12 g of pure acetic acid, diluted with deionized water and adjusted to a pH of 4.0 with a 1.0 M stock solution of KOH using a pH meter (Orion-pH/ISE meter Model 710).

Calculation of Demineralization Rates

Mean demineralization rates were calculated using linear regression from the projected mineral mass curves obtained from SMR analysis of selected points on the enamel surface (**Figure 3**). The rate of mineral loss was determined from the gradient in units of grams per unit exposed area per hour. Typical times between successive data points on the same sample was about 10 min.

Calculation of Equilibrium Conditions

Thermodynamic equilibrium was assumed to be when demineralization rate was zero. The calcium concentration at thermodynamic equilibrium was determined by plotting demineralization rates against calcium concentration (**Figure 6**) and determining the x-intercept (calcium concentration) from the line equation of the polynomial regression curve (of order 2) using MATLAB (MathWorks).

Preparation of Calcium and Phosphate Increments

0.66 g increments of $CaCl_2$ and 0.822 g increments of K_2HPO_4 were weighed so that any additions of each increment into the 2.0 L of acetic acid solution would give a concentration of 3.0 mM calcium and 1.8 mM phosphate (Ca/P 1.67).

The concentration of calcium and phosphate in the demineralizing solution was increased incrementally by 3.0 mM calcium and 1.8 mM phosphate, respectively (Ca/P 1.67) every 48 h. Steps were taken to ensure pH was maintained constant throughout. The rate of demineralization of the enamel sample was measured at each increase in calcium/phosphate concentration increment using SMR.

CALCULATION OF DEGREE OF SATURATION OF DEMINERALIZING SOLUTIONS USED

An ionic speciation program, Chemist (MicroMath, Missouri, USA) was used to calculate the degree of saturation with respect to hydroxyapatite (DS_{HAp}) for a solution at pH = 4.0 in a range of solutions with increasing calcium concentrations identical to those used in the SMR measurements. This calculation was repeated for a range of pKsp values from 116 to 126, and the degree of saturation as a function of calcium concentration was then plotted for each pKsp value (**Figure 4**). The calcium concentration at equilibrium (i.e., when the saturation was 1) was determined from each plot, and then these were then plotted for each pKsp value (**Figure 5**). The corresponding calcium concentration required to halt demineralization from the SMR data (**Figure 3**) was then used to determine the pKsp for the calcium concentration required to reach equilibrium (**Figure 7**).

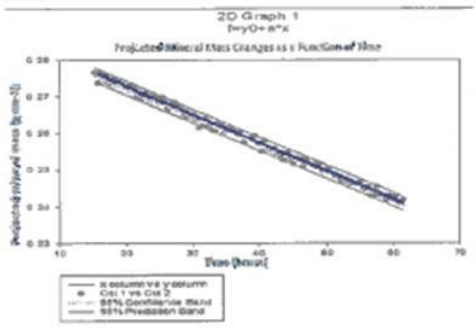

FIGURE 3 | Typical SMR showing the linear changes in projected mineral mass of enamel with time and the 95% confidence intervals ($p \leq 0.0001$) in 0.1 M acetic acid solution at pH = 4.0.

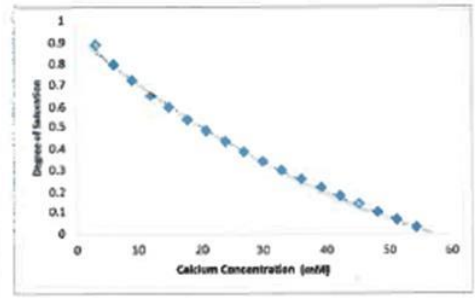

FIGURE 4 | A typical Chemist plot for a pKsp of 118 showing thermodynamic equilibrium is reached at 57 mM of calcium at the x-intercept, under pH = 4.0 at 25°C conditions. The degree of saturation with respect to HAp was calculated based on the conditions and calcium and phosphate concentrations used in the SMR experiment.

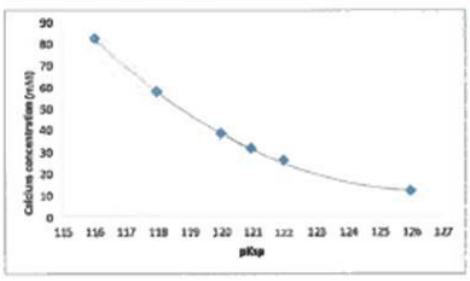

FIGURE 5 | Calcium and phosphate concentration (mM) in equilibrium with HAp as a function of the pKsp assumed for HAp, assuming pH = 4.0, 0.1 M acetic acid, and 25°C as calculated by Chemist.

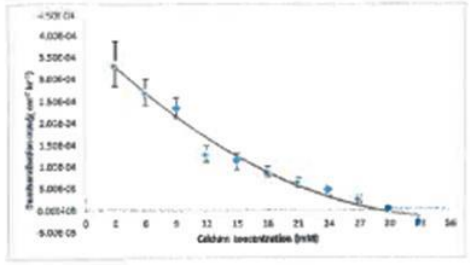

FIGURE 6 | Enamel demineralization rate as a function of increasing calcium concentration at pH = 4.0 and 25°C based on results from the SMR experiment. Rate is zero at a calcium concentration of 30 mM calculated using MATLAB from the x-intercept of the regression curve ($R^2 = 0.98$).

RESULTS

Enamel Demineralization Rate As a Function of Increasing Calcium Concentration

Figure 3 shows a typical plot of mineral mass changes of bulk enamel with time during demineralization with 0.1 M acetic acid at pH = 4.0 at 25°C (confidence intervals of 95%, $p \leq 0.0001$). Similar results showing a linear rate of mineral loss with time were obtained at each incremental additional calcium concentration. Mean enamel demineralization rates were calculated from a total of 33 points on 11 different permanent enamel blocks (see section Calculation of Demineralization Rates for calculation of demineralization rates procedure).

The mean demineralization rates were then plotted as a function of calcium concentration (**Figure 6**), which showed a decreasing, but non-linear, trend (SE ranged from $\pm$ 2.90 $\times$ 10^{-06} to $\pm$ 1.09 $\times$ 10^{-05}). This result shows that under the conditions used, the calcium concentration required to achieve thermodynamic equilibrium was 30 mM as determined from the horizontal intercept (regression curve $R^2 = 0.98$), calculated using MATLAB.

Identifying the pKsp of Bulk Enamel using Ion Speciation Software

Data fitting of the SMR data shows that calcium concentration required for demineralization of bulk enamel to cease (at conditions of pH = 4.0 and 25°C), i.e. that equilibrium is achieved is 30 mM. under the same conditions. Fitting to the speciation software data suggests a pKsp of 121 corresponds to a calcium concentration of 30 mM to reach thermodynamic equilibrium for pH = 4.0 and 25°C conditions. This result suggests that the $pKsp_{BEnamel}$ is 121 (**Figure 7**).

DISCUSSION

It is important to measure the solubility of enamel under caries like conditions using a precise measuring system in order to

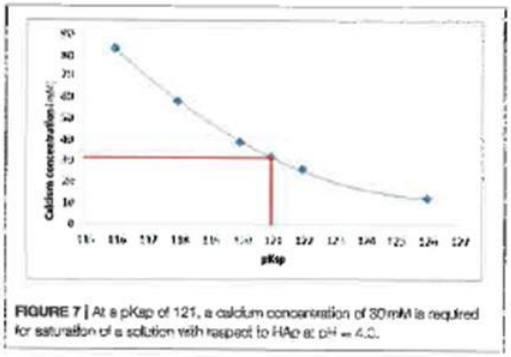

FIGURE 7 | At a pKsp of 121, a calcium concentration of 30 mM is required for saturation of a solution with respect to HAp at pH = 4.0.

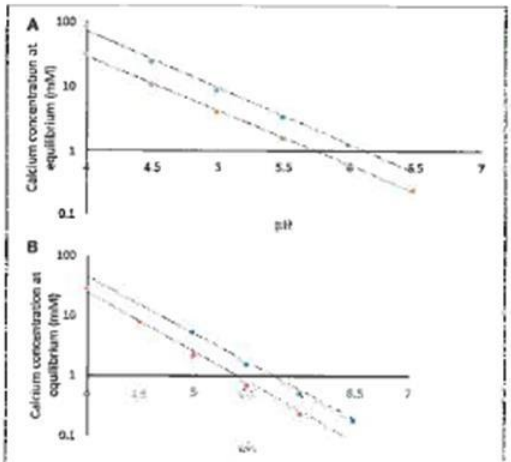

FIGURE 8 | (A) Calculated calcium concentration required for equilibrium at pKsp values of 116 (blue) and 121 (red) for a demineralization solution of 100 mmol/L acetic acid. **(B)** Calculated calcium concentration required for equilibrium at pKsp values of 116 (blue) and 121 (red) with only that acid or base required for pH condition.

accurately derive the solubility product. This information is relevant to the development of our understanding of caries and erosion and to develop preventative measures such as to screen anticaries agents.

The SMR data showed that the bulk human enamel demineralization at pH = 4.0 was reduced to zero at a calcium concentration of 30 mM. Correlation with the speciation software calculations shows this corresponds to a pKsp value of 121. **Figures 4, 6** show a consistency between the speciation software of degree of saturation (proportional to chemical driving force) and the SMR kinetic data, indicating that the method was appropriate.

Figure 6 shows that the decrease in demineralization rate was non-linear (rather than linear as would be expected from simple first-order dissolution kinetics) similar to that obtained from speciation calculations for all pKsp values **(Figure 4)**. This is consistent with what would be predicted for the calcium phosphate ternary system (Lenist et al., 1990).

As discussed earlier it is important to account for all possible phase transformations, and equilibria, as a lack of information on the resulting equilibria results in imperfect calculations (Pan and Darvell, 2007). Ion speciation programs rely on databases that report experimental results for speciation constants as well as the methods and conditions of the experiments reported (VanBriesen et al., 2010). The similarities observed in the data from the SMR method and the speciation software **(Figures 4, 6** respectively) confirm the methodology. The small standard errors **(Figure 6)** also indicate that there was little variation in the demineralization rates between samples.

The *apparent*-$pKsp_{HEnamel}$ value of 121 measured in this study is higher than many previously reported values (see **Table 1**), and higher than many values reported for pure HAp. As mentioned above, the methodology may influence the values reported for enamel and hydroxyapatite (Dorozhkin, 2012, Liu et al., 2013).

How does this impact on the clinical situation? We have used the speciation software to model the equilibrium conditions as a function of pH for the pKSp values under the conditions used in the experiment. **Figure 8A** shows the calcium concentration required for equilibrium under the conditions used, including acid concentration and temperature (plotted on a log scale) for a pKSp value of 116 (blue), and for pKsp of 121 (red). This shows that at pH 4.0, the calcium concentration required for equilibrium for a pKSp = 116 would be 85 mM, whereas for pKSp = 121 this would only be 31 mmol/L. However, let us consider a calcium concentration of 1 mmol/L, cited as the value of free calcium concentration in saliva (Lagerlof, 1983). Then, from **Figure 8A**, this would suggest that the saturation would occur only at pH above 6.0. This is often called the "critical pH" (Dawes, 2003). However, using a value of pKSp of 121, then this would suggest a much lower "critical pH" (at a calcium concentration of 1 mM). Of course, these calculations were performed with an acid concentration of 0.1 M, which is high for oral conditions. **Figure 8B** is a repeat of this calculation, but with no fixed acetic concentration (and is therefore not necessarily repeatable in a laboratory), but represents the opposite extreme with a zero acetic concentration. This reduces the critical pH value, assuming a free calcium ion concentration of 1.0 mM (Lagerlof, 1983). The oral environment acid concentration is likely to be somewhere between these extremes, but this calculation confirms that a pKSp value of 116 is too low, and that is likely to be nearer to 121, otherwise there would be insufficient calcium in the oral environment to prevent enamel being undersaturated. It is also likely that other factors including salivary proteins (Kosoric et al., 2010) also play in role in the protective function of enamel, and will modify the apparent solubility product.

Whilst these results provide an insight into the dynamics of enamel dissolution under pH = 4.0 conditions at 25°C, the

result is for bulk enamel only, and based on an *in vitro* design, and so it is important to acknowledge that any conclusions made are limited to these conditions only. For instance, further similar SMR studies are required to determine the effect pH (Ito et al., 1996). An increase in dissolution rate is observed when pH is reduced (Gao et al., 2001). Furthermore, published data on the effect of pH on the solubility product of enamel is contradictory, e.g., Shellis and Wilson (2004) found no statistical difference in the solubility product of powdered enamel at different pH values between 4.5 and 5.5 whereas the earlier studies of Patel and Brown (1975) reported lower solubility product values of 106–116 over a pH range of 4.5–7.6. The inconsistency in results is in spite of both experiments using powdered enamel as the substrate which again highlights the advantage of using bulk enamel as the substrate rather than powdered. Such measurements will also confirm or otherwise the marked change in slope of the solubility isotherm for HAp at around pH 3.9 as reported by Pan and Darvell (2009a,b).

Also, further similar SMR studies are required to study the influence of different ionic substitutions on both enamel and HAp powder, including carbonate, Mg^{2+}, F^-, etc. would provide significant further information on the chemistry of demineralization process. Also, similar studies are required too for a comparison of bulk enamel values with values obtained for powdered hydroxyapatite, similar to the studies reported in **Table 1.**

Further, the physical and chemical heterogeneities within enamel should not be ignored (Arends and Jongebloed, 1977; Zhang et al., 2000; Bechtle et al., 2012). For example, demineralization rates of prismatic, interprismatic and aprismatic enamel are not the same due to differences between the organization of crystals, the presence of more soluble material, and the porosity (Avery et al., 1961; Boyde, 1967; Shellis, 1996; Shellis and Dibdin, 2000). On a chemical compositional level, enamel is a substituted calcium hydroxyapatite (Neel et al., 2016). Its composition varies with ions such as F^-, CO_3^{2-} and Mg^{2+} replacing OH^-, PO_4^{3-} and Ca^{2+} within the stoichiometry allegedly altering the solubility of enamel (Aoba, 1997; Elliott, 2003; West and Joiner, 2014; Liu et al., 2016). Thus, the site of source material may be a critical factor. Further solubility measurements are also needed to investigate the influence of the structural or chemical heterogeneities of enamel on the demineralization rate. As the enamel is etched away and moves toward the enamel dentine junction there are changes in demineralization rate resulting from gradients in ionic substitutions within enamel structure (Anderson and Elliott, 2000). In addition, within enamel, the processes of demineralization and remineralization may not be co-localized, with ions diffusing in different directions (Anderson and Elliott, 1992).

In conclusion, the SMR method described here provides greater insight into bulk enamel dissolution by measuring the *effect* of calcium concentration on the dissolution kinetics of bulk enamel demineralization under standardized caries-like conditions. The measured $pKsp_{BEnamel}$ value of ~121 is similar to that reported by Shellis and Wilson (2004) for pure HAp, and is in agreement with recent suggestions that $pKsp_{BEnamel}$ is higher than that reported previously in literature, and may be much closer to the value for pure HAp. However, further similar kinetic studies will be needed to measure enamel solubility at a range of pH conditions, temperatures, and, for example, the influence of salivary proteins, in order to replicate the changing conditions of the oral environment.

ETHICS STATEMENT

Written informed consent was obtained from patients who agreed to give their teeth anonymously for research. Ethical approval was granted to use that pool of teeth by Queen Mary Research Ethics Committee (QMREC 2011/99). The site license is in the name of the author FW.

AUTHOR CONTRIBUTIONS

LH, contribution toward the conception and design of the work. Acquisition, interpretation and analysis of all data. Drafting and revising the work and ensuring the integrity and accuracy of the work. FW, contributions include the interpretation and analysis of data. Revising work and ensuring the integrity and accuracy of the work. RL, contributions include the interpretation and analysis of data. Revising work and ensuring the integrity and accuracy of the work. PA, contributions include the design and conception of the work. Interpretation and analysis of data. Drafting and revising the work and ensuring the integrity and accuracy of the work.

FUNDING

LH is the recipient of a PhD studentship from BBSRC (grant number BB/I.502091/1).

ACKNOWLEDGMENTS

This study was supported by the Biotechnology and Biological Sciences Research Council and GlaxoSmithKline. The authors are thankful to the staff and students in the Dental Physical Sciences Unit at Queen Mary University of London.

REFERENCES

Anderson, P., Bollet-Quivogne, F. R. G., Dowker, S. E. P., and Elliott, J. C. (2004). Demineralization in enamel and hydroxyapatite aggregates at increasing ionic strengths. *Arch. Oral Biol.* 49, 199–207. doi: 10.1016/j.archoralbio.2003.10.001

Anderson, P., and Elliott, J. C. (1992). Subsurface demineralization in dental enamel and other permeable solids during acid dissolution. *J. Dent. Res.* 71, 1473–1481. doi: 10.1177/00220345920710080301

Anderson, P., and Elliott, J. C. (2000). Rates of mineral loss in human enamel during *in vitro* demineralization perpendicular and parallel to the natural surface. *Caries Res.* 34, 33–40. doi: 10.1159/000016567

Anderson, P., Levinkind, M., and Elliott, J. C. (1998). Scanning microradiographic studies of rates of *in vitro* demineralization in human and bovine dental enamel. *Arch. Oral Biol.* 43, 649–656. doi: 10.1016/S0003-9969(98)00052-1

Aoba, T. (1997). The effect of fluoride on apatite structure and growth. *Crit. Rev. Oral Biol. Med.* 8, 136–153. doi: 10.1177/10454411970080020301

Arends, J. K. (1981). "Mechanism of dental caries," in *Biological Mineralisation and Demineralisation, Life Sciences Research Report 23, Dahlem Konferenzen Berlin*, ed Nancollas (Berlin; Heidelberg; New York, NY: Springer-Verlag), 303–327.

Arends, J. K., and Jongebloed, W. L. (1977). Dislocations and dissolution in apatites: theoretical considerations. *Caries Res.* 11, 186–188. doi: 10.1159/000262266

Avery, J. K., Visser, R. L., and Knapp, D. E. (1961). The pattern of the mineralization of enamel. *J. Dent. Res.* 40, 1004–1019. doi: 10.1177/00220345610400050101

Bechtle, S., Ozcoban, H., Lilleodden, E. T., Huber, N., Schreyer, A., Swain, M. V., et al. (2012). Hierarchical flexural strength of enamel: transition from brittle to damage-tolerant behaviour. *J. R. Soc. Interface* 9, 1265–1274. doi: 10.1098/rsif.2011.0498

Berner, R. A. (1978). Rate control of mineral dissolution under earth surface conditions. *Am. J. Sci.* 278, 1235–1252. doi: 10.2475/ajs.278.9.1235

Borutta, A., Wagner, M., and Kneist, S. (2010). Early childhood caries: a multifactorial disease. *OHDMBSC.* 9, 32–38.

Boyde, A. (1967). The development of enamel structure. *Proc. R. Soc. Med.* 60, 923–928.

Brittain, H. G. (2014). Thermodynamic vs. kinetic solubility: knowing which is which. *Am. Pharmaceut. Rev.* 17, 10–15.

Brunton, P. (2014). Summary of: continuing development of an oral health score for clinical audit. *Br. Dent. J.* 216, 526–527. doi: 10.1038/sj.bdj.2014.380

Chen, Z. F., Darvell, B. W., and Leung, V. W. H. (2004). Hydroxyapatite solubility in simple inorganic solutions. *Arch. Oral Biol.* 49, 359–367. doi: 10.1016/j.archoralbio.2003.12.004

Dawes, C. (2003). What is the critical pH and why does a tooth dissolve in acid? *J. Can. Dent. Assoc.* 69, 722–724.

DeVoe, H. (2016). *Thermodynamics and Chemistry, 2nd Edn. Version 8.* Maryland, MD; Pearson Education, Inc.

Dorozhkin, S. V. (2012). Dissolution mechanism of calcium apatites in acids: a review of literature. *World. J. Methodol.* 2, 1–17. doi: 10.5662/wjm.v2.i1.1

Elliott, J. C. (ed.). (2003). "Structure and chemistry of the apatites and other calcium orthophosphates," in *Studies in Inorganic Chemistry*, Vol. 18 (London, UK: Elsevier), 259–295.

Elliott, J. C., Anderson, P., Gao, X. J., Wong, F. S. L., Davis, G. R., and Dowker, S. E. P. (1994). Application of scanning microradiography and X-Ray microtomography to studies of bones and teeth. *J. X-ray Sci. Technol.* 4, 102–111.

Gao, X. J., Fan, Y., Kent, R. L. Jr., Van Houte, J., and Margolis, H. C. (2001). Association of caries activity with the composition of dental plaque fluid. *J. Dent. Res.* 80, 1834–1839. doi: 10.1177/00220345010800091201

Gibbs, J. W. (1873). A method of geometrical representation of the thermodynamic properties of substances by means of surfaces. *Trans. Conn. Acad. Arts Sci.* 2, 382–404.

Hobdell, M. H., Oliveira, E. R., Bautista, R., Myburgh, N. G., Lalloo, R., Narendran, S., et al. (2003). Oral diseases and socio-economic status (SES). *Br. Dent. J.* 194, 91–96. doi: 10.1038/sj.bdj.4809882

Ito, A., Maekawa, K., Tsutsumi, S., Kawaki, F., and Tetsuki, T. (1996). Solubility product of OH-carbonated hydroxyapatite. *J. Biomed. Mater. Res.* 36, 522–528. doi: 10.1002/(SICI)1097-4636(19970915)36:4<522::AID-JBM13>3.0.CO;2-C

Keyes, P. H. (1962). Recent advances in dental caries research. *Int. Dent. J.* 12, 443–464.

Kosoric, J., Hector, M. P., and Anderson, P. (2010). The influence of proteins on demineralization kinetics of hydroxyapatite aggregates. *J. Biomed. Mater. Res. A* 94, 972–977. doi: 10.1002/jbm.a.32759

Lagerlof, F. (1983). Effects of flow-rate and pH on calcium-phosphate saturation in human-parotid saliva. *Caries Res.* 17, 403–411. doi: 10.1159/000260694

Lalloo, R., and Myburgh, N. G. (1999). Dental caries, socio-economic development and national oral health policies. *Int. Dent. J.* 49, 196–202. doi: 10.1111/j.1875-595X.1999.tb00522.x

Lenist, D. G., Anderson, P., and Elliott, J. C. (1990). Diffusion coefficients for the ternary system $Ca(OH)_2$-H_3PO_4-Water. *J. Chem. Soc. Faraday Trans.* 86, 3093–3095. doi: 10.1039/FT9908603093

Leung, V. W. H., and Darvell, B. W. (1991). Calcium phosphate system in saliva-like media. *J. Chem. Soc. Faraday Trans.* 87, 1759–1766. doi: 10.1039/ft9918701759

Liu, Q., Chen, Z., Pan, H., Darvell, B. W., and Mainilinna, J. P. (2016). Effect of magnesium on the solubility of hydroxyapatite. *Eur. J. Inorg. Chem.* 2016, 5623–5629. doi: 10.1002/ejic.201601056

Liu, Q., Huang, S., Mainilinna, P. J., Chen, Z., and Pan, H. (2013). Insight into biological apatite: physiological properties and preparation approaches. *Biol. Med. Res. Int.* 2013, 1–13. doi: 10.1155/2013.929748

Local Government Authority Report (2015). *Tackling Poor Oral Health in Children, Local Governments Public Health Role.* London, UK: Public Health England.

Margolis, H. C., and Moreno, E. C. (1985). Kinetic and thermodynamic aspects of enamel demineralization. *Caries Res.* 19, 22–35. doi: 10.1159/000260826

Margolis, H. C., and Moreno, E. C. (1992). Kinetics of hydroxyapatite dissolution in acetic, lactic, and phosphoric acid solutions. *Calcif. Tissue Int.* 50, 137–143. doi: 10.1007/BF00298791

Margolis, H. C., Zhang, Y. P., Lee, C. Y., Kent, R. L. Jr., and Moreno, E. C. (1999). Kinetics of enamel demineralisation *in vitro*. *J. Dent. Res.* 78, 1326–1335. doi: 10.1177/00220345990780070701

McDowell, H., Gregory, T. M., and Brown, W. E. (1977). Solubility of $Ca_5(PO_4)_3OH$ in the system $Ca(OH)_2$- H_3PO_4- H_2O at 5, 15, 25, and 37°C. *J. Res. Natl. Bur. Stand. A Phys. Chem.* 81A, 273–281. doi: 10.6028/jres.081A.017

Mishra, S., Thomas, H. F., Fearne, J. M., Boyde, A., and Anderson, P. (2009). Comparison of demineralisation rates in pre- and postnatal enamel and at the neonatal line. *Arch. Oral Biol.* 54, 101–106. doi: 10.1016/j.archoralbio.2008.09.013

Nancollas, G. H. (2005). A new model for nanoscale enamel dissolution. *J. Phys. Chem. B* 109, 999–1005. doi: 10.1021/jp046431d

Noel, E. A. A., Aljabo, A., Strange, A., Ibrahim, S., Coathup, M., Young, A. M., et al. (2016). Demineralization-remineralization dynamics in teeth and bone. *Int. J. Nanomedicine* 11, 4743–4763. doi: 10.2147/IJN.S107624

Pan, H. B., and Darvell, B., W (2009a). Calcium phosphate solubility: the need for re-evaluation. *Cryst. Growth Des.* 4, 639–645. doi: 10.1021/cg801118v

Pan, H. B., and Darvell, B. W. (2007). Solubility of hydroxyapatite by solid titration at pH 3–4. *Arch. Oral Biol.* 52, 618–624. doi: 10.1016/j.archoralbio.2006.12.007

Pan, H. B., and Darvell, B. W. (2009b). Solid titration of octacalcium phosphate. *Caries Res.* 43, 322–330. doi: 10.1159/000226231

Patel, P. R., and Brown, W. P. (1975). Thermodynamic solubility product of human tooth enamel, powdered sample. *J. Dent. Res.* 54, 728–736. doi: 10.1177/00220345750540040601

Quinn, G. W., and Taylor, D. M. (1992). NSPEC: a chemical speciation program for personal computers. *Analyst* 117, 689–691. doi: 10.1039/an9921700689

Robinson, C., Kirkham, J., Brookes, S. J., and Shore, R. C. (1995). "Chemistry of mature enamel," in *Dental Enamel: Formation to Destruction*, eds C. Robinson, J. Kirkham, and S. J. Brookes (Leeds: CRC Press), Chapter 8, 167–191.

Shellis, R. P. (1996). A scanning electron microscopic study of solubility variations in human enamel and dentine. *Arch. Oral Biol.* 41, 673–684. doi: 10.1016/0003-9969(96)00040-9

Shellis, R., and Dibdin, G. (2000). "Enamel microporosity and its functional implications," in *Development, Function and Evolution of Teeth*, eds M. Teaford, M. Meredith Smith, and M. Ferguson (Cambridge: Cambridge University Press), 242–251. doi: 10.1017/CBO9780511542626.017

Shellis, R. P., Wahab, F. K., and Heywood, B. R. (1993). The Hydroxyapatite Ion Activity Product in Acid Solutions Equilibrated with Human Enamel. *Caries Res.* 27, 365–372. doi: 10.1159/000262566

Shellis, R. P., and Wilson, R. M. (2004). Apparent solubility distributions of hydroxyapatite and enamel apatite. *Adv. Colloid Interface Sci.* 278, 325–332. doi: 10.1016/j.jcis.2004.06.016

Smith, B. T. (2015). *Remington Education: Physical Pharmacy, 1st Edn.* London, UK: Pharmaceutical Press.

VanBriesen, J. M., Small, M., Weber, C., and Wilson, J. (2010). "Modelling chemical speciation: thermodynamics, kinetics and uncertainty," in *Modelling of Pollutants in Complex Environmental Systems*, ed G. Hanrahan (St. Albans: ILM Publications), 133–149.

Wang, L. J., Tang, R., Bonstein, T., Bush, P., and Nancollas, G. H. (2006). Enamel demineralization in primary and permanent teeth. *J. Dent. Res.* 85, 359–363. doi: 10.1177/154405910608500415

West, N., and Joiner, A. (2014). Enamel mineral loss. *J. Dent.* 42, 2–11. doi: 10.1016/S0300-5712(14)50002-4

Zhang, Y. P., Kent, R. L. Jr., and Margolis, H. C. (2000). Enamel demineralization under driving forces found in dental plaque fluid. *Eur. J. Oral Sci.* 108, 207–213. doi: 10.1034/j.1600-0722.2000.108003207.x

Conflict of Interest Statement: Author RL is employed by GlaxoSmithKline and LH is the recipient of a studentship from BBSRC and stipend from GlaxoSmithKline.

The other authors declare that the research was conducted in the absence of any commercial or financial relationships that could be construed as a potential conflict of interest.

Appendix B

Enamel dissolution, a novel method of the apparent enamel solubility

Hassanali L, Lynch R, Anderson P.

Enamel dissolution is significantly influenced by its solubility. However, there has been, and remains, significant debate within the literature about the value of the solubility of enamel. Is it similar to the solubility of hydroxyapatite, or is it influenced by chemical inclusions in enamel, are there gradients in solubility. Just to add to the complexity, bulk hydroxyapatite itself has deceptive solubility properties, which depend on surface energy, pH, to name but a few. Several methodologies have been reported which purport to measure the solubility product of enamel (and or hydroxyapatite), but the values also seem to be methodology dependent.

In this paper, we report a method to measure the effective solubility of enamel. In this method, the rate of enamel dissolution is measured as a function of degree of saturation with respect to hydroxyapatite. Enamel slabs were demineralised, and the rate of demineralisation measured at increasing calcium concentrations, until the rate drops to zero, and then beyond. It assumed that at the point at which the rate is zero, the enamel is in thermodynamic equilibrium with the demineralising solution, and therefore the effective solubility product can be determined.

Scanning microradiography was used to measure the rate of mineral loss in slabs of enamel in a constant pH demin solution at pH=4.0 for 48h. Calcium was then added to the demin. solution, decreasing the rate of demin as the degree of saturation was reduce, and the dissolution rate re-measured. This was repeated until the rate of demin. was zero, and then continued.

The rate of demineralisation decreased from 5.22×10^{-4} g cm^{-2} and 8.53×10^{-4} g cm^{-2} (SE 6.83×10^{-5} & 4.53×10^{-5}, respectively) dropping to zero at a calcium concentration of 31.5 mmol l^{-1} for permanent and deciduous enamel, respectively.

The apparent solubility product is calculated to be 121, which is considerably lower than that previously reported for enamel, and much closed to the lower end of the spectrum of values reported for hydroxyapatite.

Enamel 9, 2016 Leeds, U.K

Appendix C

Queen Mary University of London — Dental Physical Sciences Unit — Barts and The London School of Medicine and Dentistry

ENAMEL DISSOLUTION: NOVEL KINETIC METHOD TO MEASURE APPARENT ENAMEL SOLUBILITY

L. Hassanali*, F. S. L. Wong*, R. J. M Lynch**, P. Anderson*

Introduction

Enamel dissolution is significantly influenced by its solubility. However, there remains significant debate within the literature about the value of the solubility product (pKsp) of bulk enamel. Several methodologies have been reported which measure the pKsp of enamel (and or hydroxyapatite). However, the values seem to be methodology dependent. The published range of solubility values for enamel range between 110 and 126 (See Table 1).

We report a method to measure the effective solubility of bulk enamel under caries-like conditions at pH 4.0. The rate of enamel dissolution was measured as a function of degree of (under-) saturation with respect to hydroxyapatite. The premise is that when the rate is zero, the enamel is in thermodynamic equilibrium with the demineralising solution, and therefore the effective solubility product (pKsp) can be determined.

Objectives

To quantitatively measure the demineralisation rate of bulk enamel at caries relevant pH conditions using Scanning Microradiography (SMR).
To monitor the variation in demineralisation rate of bulk enamel at decreasing undersaturation.
To measure the effective solubility product (pKsp) of bulk enamel at pH=4.0

Method

2mm enamel blocks with the natural buccal surfaces exposed were located in SMR cells and exposed to circulating 2L 0.1M Acetic acid pH 4.0.

SMR was used to measure the decrease in enamel mineral mass during demineralisation at 5 points on each sample. Demineralisation rates (g cm^{-2} hr^{-1}) were calculated from a linear regression curve of projected mineral mass (g cm^{-2}) plotted against demineralisation time (hours). Changes in demineralisation rate were monitored after each increase of 3mmol L^{-1} increments of calcium (and phosphate at Ca:P 1.67 ratio) added every 48 hours to the demineralising solution.

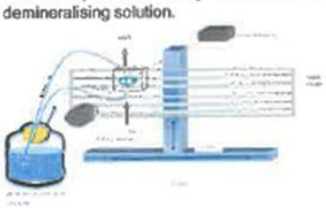

The demineralisation rates at each calcium concentration were compared with calculated solubility (pKsp) values between 116 and 126 and their respective undersaturation levels (0-1) over the same calcium concentrations. Theoretical solubility values were calculated using the program Chemist, and compared with the measured data..

Darvell et al. 2004
McDowell et al, 1977
Dawes, 2003
Margolis and Moreno, 1992

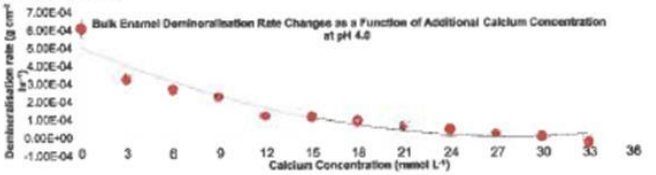

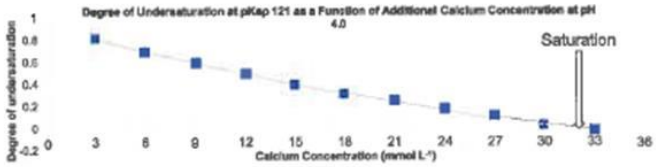

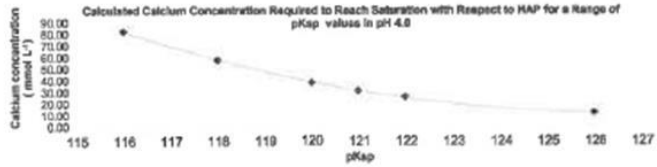

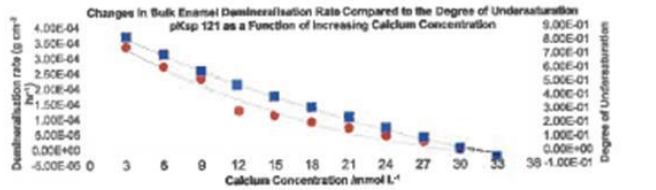

Comparing the SMR demineralisation to the degree of undersaturation with respect to HAP for a range of HAP pKsp values (116 – 126) suggests that enamel has an effective solubility of 121.

Results

The demineralisation rate at a zero Ca^{2+} concentration was 6.111×10^{-4} g cm^{-2} hr^{-1}.
Demineralisation is reduced to zero at 31.5 mmol L^{-1} Ca and 18.86mmol L^{-1} P, and precipitation commences thereafter in pH 4.0 conditions.

Conclusion

This technique provides a method of measuring the effective pKsp of bulk enamel at caries relevant condition. This shows that the effective solubility (pKsp) of enamel is 121 under the caries-like conditions studied.

*Queen Mary University of London, Dental Physical Science unit, 2nd floor Barcroft Building, Mile end, E1 4NS
**GSK Waybridge

Enamel 9, 2016 Leeds, U.K

www.dental.qmul.ac.uk — BBSRC — GSK

CONTROL ID: 2314939

TITLE: Comparing the Demineralisation Rates of Deciduous and Permanent Enamel.

Objectives: GA dental extractions for children in the UK are increasing. The causes are many-fold. Although there are many studies on the physical chemistry underlying the aetiology of demineralisation in human permanent enamel (PE), data relating specifically to deciduous enamel (DE) are relatively scarce. The overall aim is to understand the differentiating demineralisation characrteristics of PE and DE. The objectives of this study were to use scanning microradiography (SMR) to; establish DE baseline demineralisation rates; measure the effect of increasing the calcium and phosphate ion concentration in the demineralising solution on DE rates; and to establish whether a statistically significant difference exists between the demineralisation rates of DE and PE.

Methods: Pairs of PE and DE 2mm slabs with natural surfaces exposed were mounted into 3 SMR cells. 18 points on DE and 13 points on PE slabs were analysed using SMR. Samples were initially immersed in deionised water for 48h; then demineralising solution (acetic acid pH 4.0) was circulated for 48h. Real-time SMR was used to measure the rate of mineral loss at each point. Then, 0.5mmol l^{-1} calcium ions and 0.3mmol l^{-1} phosphate ions were added to the demineralising solutions, and mineral loss rates re-measured. Thereinafter; 1mmol l^{-1} calcium ions and 0.6mmol l^{-1} phosphate ions were sequentially added to the demineralising solution every 48h and the rates of mineral loss measured continuously using SMR.

Results: The mean baseline demineralisation rates were not significantly different ($p<0.05\%$) at 3.96×10^{-4} gcm^{-2} hr^{-1} (DE) and 4.54×10^{-4} g cm^{-2} hr^{-1} (PE). The demineralisation rate in DE and PE decreased as the calcium ion concentration was increased, and both followed similar trends.

Conclusions: These results show that DE demineralises slower than PE but this was not significant ($p<0.05\%$). Increasing the calcium and phosphate ion concentrations in the demineralising solution reduces the PE and DE demineralisation rates, and both follow similar trends.

AUTHORS (FIRST NAME INITIAL LAST NAME): L. Hassanali[4], F. Wong[2], R. J. Lynch[1], P. Anderson[3]

AUTHORS/INSTITUTIONS: R.J. Lynch, Oral Healthcare, GlaxoSmithKline, Weybridge, UNITED KINGDOM|F. Wong, Centre for Oral Growth and Development, Institute of Dentistry, QMUL, London, London, UNITED KINGDOM|P. Anderson, QMUL, London, London, UNITED KINGDOM|L. Hassanali, Dental Physical Science, Queen Mary University, London, London, UNITED KINGDOM|

PRESENTER: linda Hassanali

PRESENTER (E-MAIL ONLY): linda.hass@hotmail.co.uk

PREFERRED PRESENTATION TYPE: Oral

Support: Yes

Support Funding Agency/Grant Number: GSK and BBSRC Case Award, BB/L502091/1

AWARDS:

Appendix E

#2803

Queen Mary University of London

Barts and The London School of Medicine and Dentistry

Institute of Dentistry

Histological structures of deciduous and permanent enamel compared using Confocal Laser Scanning Microscopy and Rhodamine B dye

L. Hassanali*, F. S. L. Wong*, B. Padidar***, R. J. M. Lynch**, P. Anderson*

*Queen Mary University of London, Dental Physical Science unit, 2nd floor Bancroft Building, Mile end, E1 4NS
**GDH, St Georges Avenue, Weybridge, KT13 0DE
***Kingston University, School of Life Sciences, London, UK

Introduction

Caries is the most common oral disease affecting children. If unsuccessfully treated, cases can often lead to the extraction of childrens' teeth, a procedure that is on the increase in the UK, yet caries is largely preventable (LGA, 2016).

Enamel demineralisation is influenced by microstructural features within enamel, for example, demineralisation is faster in interprismatic enamel than in prismatic regions (Boyde, 1967; Shellis and Dibdin, 2000; Shellis. 1996). However, little is known about the similarities and differences between deciduous enamel (DE) and permanent enamel (PE) microstructures. Confocal Laser Scanning Microscopy (CLSM (Figure 1)) was used to image features within DE and PE soaked in Rhodamine B fluorescent dye so that quantitative measurements of the dimensions of microstructural features could be made using Image J software.

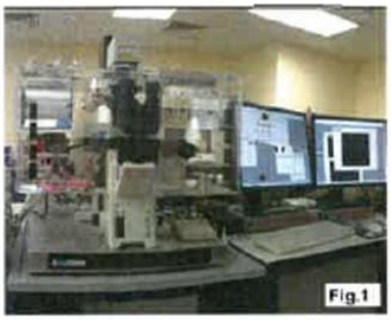

Fig.1

Objectives

- To quantitatively measure the microstructural features within DE and PE using Confocal Laser Scanning Microscopy.
- To quantitatively assess and highlight differences between DE and PE microstructure.

Methods

2mm thick sections of sound DE and PE with polished surfaces were soaked in 100ml of 0.1mmol L^{-1} Rhodamine B dye for 5 days (Figure 2).
Sections were mounted on glass slides and coated with 1 drop of Zeiss Immersol 518 N immersion oil.

CLSM images were obtained from; outer, inner, and EDJ enamel of DE and PE.
CLSM images were analysed using Image J to quantitatively compare prism structures in both enamel types.

Fig.2

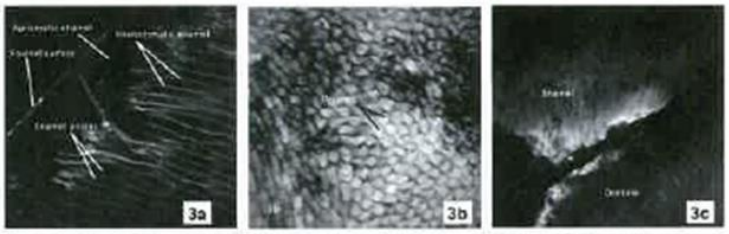

3a 3b 3c

Figures 3 a-c: CLSM images of Rhodamine B dye penetration of deciduous enamel showing outer, inner and EDJ regions, respectively.

4a 4b 4c

Figures 4 a-c: CLSM images of Rhodamine B dye penetration of permanent enamel showing outer, inner and EDJ regions, respectively.

Results

Rhodamine B penetrated both DE and PE up to depths of 61µm, primarily along the interprismatic regions where porosity is greater (Figures 3a-c & 4a-c).

Comparisons between DE and PE revealed significant differences between; outer, inner and EDJ prism widths (Table 1).

Table 1: Prism widths from outer, inner and EDJ enamel and aprismatic and interprismatic widths.

Outer	5.51 (± 0.13)	6.3 (± 0.2)
Inner	5.5 (± 0.18)	4.8 (± 0.17)
EDJ	5.26 (± 0.1)	2.76 (± 0.15)
Aprismatic thickness	23.6 (± 1.0)	5.3 (± 0.16)
Interprismatic thickness	0.48 (± 0.02)	0.47 (± 0.02)

No significant difference between interprismatic widths was observed.

Discussion/Conclusion

Rhodamine B penetrates DE and PE along interprismatic boundaries. No significant differences between DE and PE interprismatic widths in bulk enamel. No significant difference within DE prism widths between outer, middle and EDJ but significant differences within PE. Significantly greater aprismatic thickness in DE. This suggests a protective function for DE.

References: Public Health England. Local Government Association (2016) Tackling poor oral health in children - local government's public health role
Boyde A. (1967) The development of enamel structure. Proc R Soc Med 1(60): 1023-1026
Shellis R.P. and Dibdin G.H. (2000) Enamel microporosity and its functional implications. In Development, Function and Evolution of Teeth eds Teaford, Meredith Smith and Ferguson. M (Eds.) Units I. Development, Function and Evolution of Teeth. Cambridge Cambridge University Press, 242-251
Shellis R. P. (1998) A scanning electron microscope study of soluble elements in human enamel and dentine. Arch Oral Biology. 43: 475-484

Poster for IADR 2017, San Francisco, U.S.A

www.dental.qmul.ac.uk
l.hassanali@qmul.ac.uk

BBSRC

Histological structures of deciduous and permanent enamel compared using Confocal Laser Scanning Microscopy and Rhodamine B dye

L. Hassanali[a], F.S.L. Wong[a], B. Padidar[b], R.J.M. Lynch[c], P. Anderson[a]

[a]Queen Mary University of London, Dental Physical Sciences department, London, UK
[b]Kingston University, School of Life Sciences, London, UK
[c]GlaxoSmithKline, Weybridge, Surry, UK

Objectives: GA extractions of childrens' teeth are increasing. Quantitative research of differences between deciduous enamel (DE) and permanent enamel (PE) is required to provide information to formulate prevention treatment plans. Enamel pore structure can be studied using Confocal Light Scanning Microscopy (CLSM) using Rhodamine B fluorescent dye which penetrates pores within the structure. This method examines differences in structure between DE and PE.

Method: 2mm thick sections of sound DE and PE with polished surfaces were soaked in 100ml of 0.1mM rhodamine B solution for 5 days. The sections were mounted onto glass slides and viewed using an Olympus ix81 CLSM with laser excitation at 543nm matching Rhodamine B excitation wavelength. CLSM images were obtained from; outer, inner, and EDJ enamel of DE and PE, and were analysed using ImageJ to compare prism structures in both enamel types.

Results: Rhodamine B penetrated both DE and PE up to depths of 61µm, primarily along the interprismatic regions where porosity is greater. Comparisons between DE and PE revealed significant differences between; outer (DE 5.51±0.13µm, PE 6.3 ±0.2µm); inner (DE 5.5±0.18µm, PE 4.8±0.17µm); and EDJ (DE 5.26 ±0.1µm, PE 2.78 ± 0.15µm) prism widths. The DE aprismatic mean thickness (23.6µm) was greater than the PE mean thickness (5.3µm). No significant difference between interprismatic widths was observed.

Conclusion: Rhodamine B penetrates DE and PE along interprismatic boundaries enabling CLSM images for quantitative analysis of histological structures. The significantly greater aprismatic thickness in DE suggests a compensatory protective function for DE.

Abstract for IADR conference 2017 San Francisco, U.S.A

Appendix F

Excel spreadsheet of SMR data of DE and PE demineralisation rates as a function of calcium concentration (mM) with standard deviations and standard errors.

CALCIUM CONCENTRATION (mM)	DE DEMINERALISATION RATE (g cm-3 hr-1)	sd	se
0	0.000673889	0.00042122	7.02029E-05
3	0.000401182	0.00015016	4.52757E-05
6	0.000275945	0.00015695	4.73212E-05
9	0.000232291	0.00011921	3.59422E-05
12	0.00017	0.00010834	3.26672E-05
15	0.00017	6.8131E-05	2.05422E-05
18	0.000147918	6.1455E-05	1.85294E-05
21	0.000122364	6.5219E-05	1.96641E-05
24	0.000112769	3.8674E-05	1.16608E-05
27	7.62561E-05	5.2432E-05	1.5809E-05
30	0.00005	1.8317E-05	8.19146E-06
33	-0.00001736	4.056E-05	1.81389E-05

CALCIUM CONCENTRATION (mM)	PE DEMINERALISATION RATE (g cm-3 hr-1)	sd	se
0	6.11E-04	2.88E-04	5.01E-05
3	3.34E-04	9.83E-05	2.96E-05
6	2.70E-04	7.58E-05	2.28E-05
9	2.34E-04	6.19E-05	1.87E-05
12	1.29E-04	6.16E-05	1.86E-05
15	1.12E-04	3.63E-05	1.09E-05
18	8.89E-05	3.64E-05	1.10E-05
21	6.47E-05	2.36E-05	7.12E-06
24	4.29E-05	2.64E-05	7.96E-06
27	2.55E-05	1.79E-05	5.39E-06
30	1.00E-06	2.24E-06	1.00E-06
33	-2.91E-05	7.66E-06	2.90E-06

Appendix G

Excel spreadsheet of SMR data showing baseline demineralisation rates of DE and PE. T-test (*p=0.05*) was not significant.

	ALL DEMIN DATA START TO APRIL 2016:	
	DECIDUOUS	PERMANENT
1	0.000625	0.00056
2	0.000521	0.00054
3	0.000601	0.000407
4	0.000835	0.0004
5	0.0006	0.0004
6	0.0006	0.0004
7	0.0002	0.0004
8	0.0002	0.0006
9	0.0001	0.0004
10	0.0001	0.0004
11	0.0001	0.0004
12	0.0006	0.0004
13	0.0006	0.0006
14	0.0002	0.0015
15	0.0002	0.0012
16	0.0001	0.001
17	0.0001	0.001
18	0.0001	0.0009
19	0.0009	0.0008
20	0.001	0.0006
21	0.0011	0.0008
22	0.0013	0.001
23	0.0014	0.000667
24	0.0016	0.000516
25	0.0012	0.000578
26	0.0007	0.000722
27	0.00098	0.000734
28	0.000949	0.000282
29	0.000879	0.000143
30	0.000877	0.000376
31	0.00137	0.000382
32	0.00089	0.00046
33	0.00073	0.0006
34	0.00068	
35	0.000467	
36	0.000856	
Mean	**0.000673889**	**0.000611121**

Deciduous demin mean	permanent demin mean	T TEST NOT SIGNIFICANTLY DIFFERENT
6.74E-04	**6.11E-04**	0.531110264
sd and se	sd and se	
4.21E-04	2.88E-04	
7.02E-05	**5.01E-05**	

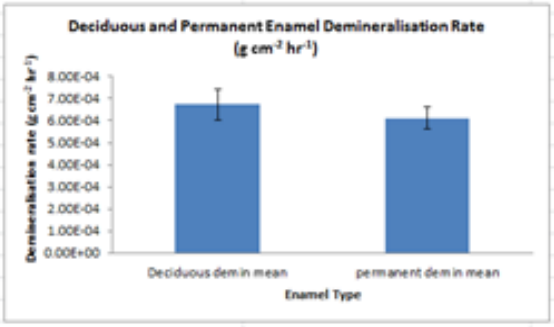

Appendix H

Excel spreadsheet sample of XMT data of DE and PE showing t test (*p=0.05*) result of no significant difference in mineral concentrations.

	Total Deciduous mineral concentration (g cm^{-3})	DE	SD	SE	Total Permanent mean min concentration (g cm^{-3})	PE	SD	SE	
1									
2	2.647306667	2.492312	0.26789	0.00773	2.701333333	2.47748829	0.27992	0.00748	
3	2.784828845			0.00748	2.869569672				
4	2.809386667				2.934797417				t test
5	2.819210065				2.947235707				0.15770212
6	2.826576601				2.946055224				There is NO significant difference
7	2.809386667				2.947939404				
8	2.794652244				2.95970236				
9	2.771322179				2.959028377				
10	2.709928976				2.956961857				
11	2.504872113				2.969610851				
12	2.261752113				2.95034224				
13	2.323146667				2.931846211				
14	2.740814671				2.923272179				
15	2.821854671				2.937482543				
16	2.832243999				2.925760107				
17	2.809386667				2.913433923				
18	2.840556001				2.938718403				
19	2.8364				2.94290682				
20	2.807309341				2.944396605				
21	2.793802675				2.91656882				
22	2.702371996				2.880349343				
23	2.634838663				2.916553963				
24	2.469642675				2.873420423				
25	2.203663992				2.873870195				
26	2.579773333				2.896695111				
27	2.809386667				2.890525265				
28	2.879557852				2.868810597				
29	2.849906667				2.865605465				
30	2.844391895				2.836231167				
57	2.890426667				2.486265329				
58	2.8671952				2.87692				
59	2.787776				2.989850591				
60	2.579773333				3.004857848				
61	2.242106667				3.023805				
62	2.692328439				3.021741181				
63	2.845404895				3.034310485				
64	2.86679				2.991726667				
65	2.863413333				2.966401667				
66	2.87692				2.975968439				
67	2.8364				2.959648333				
68	2.834148439				2.936949029				
69	2.854408439				2.926444895				
70	2.812763333				2.903933333				
71	2.723844895				2.895491667				
72	2.553885105				2.88705				
73	2.30964				2.844841667				
74	2.256364304				2.851407257				
75	2.515241181				2.870542152				
76	2.596656667				2.880296667				
77	2.630798819				2.887987363				
78	2.666815696				2.890426667				
79	2.667566667				2.81614				
80	2.667942152				2.849906667				
81	2.693829029				2.735475485				
82	2.711463333				2.458213333				
83	2.690078228				2.647548436				
84	2.625546076				2.921298855				
85	2.51224				3.013433231				
86	2.525746667				2.990762291				
87	2.800030599				2.972913231				
88	2.872135939				2.983526769				
89	2.890848075				2.964713333				
90	2.900556667				2.986903436				
91	2.903722629				2.984731564				
92	2.87692				2.958924376				
93	2.847444401				2.923951564				
94	2.849906667				2.911651043				
95	2.807276925				2.9402325				
96	2.791659167				2.951206667				
97	2.790251772				2.936011667				
98	2.799256667				2.91744				
99	2.814451667				2.915389688				
100	2.793910728				2.906345624				
101	2.753460963				2.906465833				
102	2.813888439				2.874989897				
103	2.768373673				2.848218333				
104	2.776464167				2.88705				
105	2.784835599				2.850509064				
106	2.776745105				2.847976564				
107	2.801578463				2.824219688				
108	2.814732605				2.778996667				
109	2.762394272				2.816019791				
110	2.59328				2.809386667				
111	2.336364291				2.676652601				
112	2.761976916				2.936526271				
113	2.847722639				2.961880985				
114	2.878574567				2.96264006				

115	2.902937892	2.937636519
116	2.88931912	2.945578439
117	2.854708287	2.920180503
118	2.873612217	2.887813127
119	2.864152148	2.892872724
120	2.819472095	2.924144709
121	2.850757587	2.919083761
122	2.8245479	2.936470893
123	2.829799292	2.885325199
124	2.797614256	2.902555653
125	2.779979952	2.887460603
126	2.819054739	2.871114835
127	2.826860241	2.844608001
128	2.791992781	2.851916459
129	2.775933355	2.842935876
130	2.760578976	2.848796419
131	2.766585391	2.866463139
132	2.774600247	2.859801651
133	2.782132915	2.850735976
134	2.772994304	2.807769919
135	2.749514315	2.818353743
136	2.75102436	2.820870035
137	2.730337549	2.805465681
138	2.654629981	2.824650551
139	2.444706667	2.815922543
140	2.18808	2.72332894
141	2.712052224	2.768866667
142	2.880615424	2.927501116
143	2.930363179	2.984146725
144	2.892630955	2.988969956
145	2.893668267	2.957133392
146	2.893538603	2.93735558
147	2.863413333	2.930120059
148	2.863413333	2.954583333
149	2.840592469	2.951344435
150	2.8266752	2.944453333
151	2.813449472	2.941145551
152	2.783453867	2.937148928
153	2.783064875	2.923228957
154	2.783367424	2.938113304
155	2.7845344	2.903933333
156	2.796701205	2.912341233
157	2.813168533	2.896215624
158	2.783994133	2.909240103
159	2.751880683	2.891528811
160	2.748336533	2.83743326
161	2.748142037	2.875265433
162	2.777705429	2.90731
163	2.758774485	2.886843348
164	2.720329109	2.880090015
165	2.660813333	2.888496564
166	2.323146667	2.919232335
167	2.747967801	2.876093392
168	2.890871036	2.850664391
169	2.858911561	2.768866667
170	2.925333296	2.367594405
171	2.929501453	2.765007812
172	2.921941772	2.861897885
173	2.914438819	2.890977739
174	2.892205495	2.905035477
175	2.867915105	2.900487783
176	2.847961707	2.84653
177	2.827284351	2.844117709
178	2.864414177	2.843291101
179	2.876475631	2.865481204
180	2.829951917	2.8650679
181	2.815890127	2.831162115
182	2.775814496	2.828544523
183	2.728013052	2.8364
184	2.710338228	2.796706608
185	2.728512799	2.765283348
186	2.759861772	2.743645668
187	2.756360844	2.795328928
188	2.703834768	2.818070103
189	2.684269011	2.800289927
190	2.693329283	2.77562
191	2.699777365	2.774380088
192	2.681101697	2.766661028
193	2.620293333	2.771898913
194	2.282626667	2.780236579
195	2.722754907	2.769831043
196	2.871124289	2.76617884
197	2.916086632	2.768866667
198	2.917133399	2.75536
199	2.912461443	2.864762649
200	2.87623116	2.905700005
201	2.851208709	2.906502301

Appendix I

Excel spreadsheet of CLSM data of DE and PE with t test values (*p=0.05*) and descriptive summary comparing microstructural features within both enamel types. Standard deviations (sd) and standard errors (se) given.

	A	B	C	D	E	F	G	H	I	J	K	L	M
1								Enamel region					
2	Sample number	DE top prism width	sd	se	PE top prism width	sd	se	DE aprismatic length	sd	se	PE aprismatic length	sd	se
3	1	5.15	0.398	0.126	7	0.6356	0.201	28.24	3.332	1.054	4.71	0.513581109	0.162
4	2	5.94			6.34			25.34			5.91		
5	3	4.95			6.29			22.06			5.11		
6	4	5.53			6.64			23.84			5.63		
7	5	6.14			6.31			30.16			5.63		
8	6	5.55			6.54			21.31			5.5		
9	7	5.35			5.48			20.64			4.62		
10	8	5.35			7.41			20.67			4.89		
11	9	5.15			5.99			21.22			6.16		
12	10	5.98			5.31			22.31			5.23		
13	**mean**	**5.509**			**6.331**			**23.579**			**5.339**		
14	**% difference**				**12.98**						**77.4**		
15	**t.test**	t.test			0.012469181			t.test			3.09937E-08		
16													
17													
18					summary								
19		aprismatic regions:			significant difference with deciduous being 77.4% thicker. DE range = 20.64-30.16, PE 4.64-6.16								
20		outer prisms			significant difference with DE being 12.98% smaller in width								
21		inner prisms			significant difference with DE being 12.44% smaller								
22		edj prisms			significant difference with DE being 47.2% wider								
23		interprismatic			no significant difference								

	N	O	P	Q	R	S	T	U	V	W	X	Y	Z	AA	AB	AC	AD	AE	AF
	DE middle	sd	se	PE middle	sd	se	DE EDJ	sd	se	PE EDJ	sd	se	DE inter prismatic	sd	se	PE inter prismatic	sd	se	
	6.03	0.591	0.187	4.64	0.563	0.178	5.56	0.353	0.112	2.26	0.492	0.156	0.44	0.087	0.028	0.44	0.06685	0.02114	
	5.83			3.77			5.18			3.2			0.45			0.45			
	4.97			5.21			5.74			2.86			0.44			0.52			
	5.28			4.76			5.58			2.86			0.42			0.42			
	4.79			4.75			5.58			2.86			0.44			0.44			
	4.87			4.55			5.18			2.21			0.44			0.59			
	5.6			5.21			4.57			3.02			0.59			0.59			
	5.58			4.95			4.97			3.76			0.44			0.42			
	6.73			4.56			5.16			2.57			0.63			0.44			
	5.53			5.94			5.15			2.21			0.63			0.45			
	5.521			**4.834**			**5.267**			**2.781**			0.4			0.4			
				12.44						**47.2**			**0.48364**			**0.46909**			
	t.test			0.039255			t.test			1.0328E-06			t. test			0.63216			